DOE/ER/40492--T1

U.C. DAVIS HIGH ENERGY PARTICLE PHYSICS RESEARCH TECHNICAL PROGRESS REPORT - 1990

MASTER

DISCLAIMER

Contents:

Reprints removed for separate processing

TASK A

The area of responsibility of the UCD group for the H1 detector at the Hera accelerator at the DESY laboratory in Hamburg is the construction, and operation of the analog readout for a calorimeter built into the iron return yoke of the H1 magnet. The yoke is a calorimeter when instrumented. That is, there are planes of streamer tubes interspersed within the layers of the return yoke iron. The purpose is to measure the "tail" of the hadronic shower if it is not fully contained within the liquid argon calorimeter; hence the name "tail catcher". In designing the readout, our intentions were to utilize, as much as possible, electronics that is common with that of other members of the collaboration; thus, the shaper and sample-and-hold circuits are identical to those used for the liquid argon. However, the signals from the streamer tubes are larger and faster than those from the liquid argon, so additional integration is provided at the front end. The ADC system is a multiplexed ADC system developed jointly between the French and German parts of the collaboration. The ADC is controlled by a Data Signal Processor (DSP), which does tasks such as pedestal subtraction and also, more importantly, reads out channels surrounding a single channel above a certain threshold. Since one of the multiplexers is located on the board containing the shaper and sample-and-hold circuit, some control signals have to be supplied by the ADC board in VMEbus to the front end board. For the liquid argon readout, this front end board is located as close as possible to the calorimeter, with the first stage multiplexing done there so as to reduce the number of cables brought out. Due to space constraints this forces the board to be very compact, and elaborate water cooling has to be performed in order to keep the heat problem under control. We do not have these space constraints for the tail catcher electronics, so we have mounted 128 channels on a double width fastbus sized board (the "superboard"), making use of the fastbus mechanics but not the fastbus protocol.

The superboard contains line receiver, shaper, sample-and-hold, and control cards. The design is completed, and prototypes are under test. This densely packed and rather complicated six-layer board was designed on UCD's Mac II CAD/CAM computer. Each board can handle 128 channels of analog input signal, so a total of forty boards will be required for the full H1 detector. Our CAD tape was sent to a local vendor who has supplied us with three boards; a second-source

vendor supplied two additional boards. The first vendor's boards are being tested and so far have been found to be satisfactory. There are no shorts, line breaks, etc., in the power system. The line receiver and shaper units have been tested to the output stage. The 16-1 and 8-1 multiplexers also function as required, as does the sample-and-hold "poly", which steps the readout through the 128 channels. In order to test the board's sample-and-hold function, a home-made sequencer has been built that will simulate the actual sequencer signals. This is being used to test the board's functions as completely as possible at UCD. The next step is to take the board to CERN at the end of June, where the Saclay people have the complete calorimeter electronics system under test. The analog board will be put into this chain to make sure that there are no problems that do not show up in the UCD tests. Once checked out at CERN, the board will be taken to DESY (mid July) and used to check out the tailcatcher module that is being prepared for beam tests. The beam tests will take place at CERN starting at the end of July, 1989, and continuing intermittently throughout the rest of the year. The early periods will be devoted to the tail-catcher, which will then be used in the calibration runs of the liquid argon calorimeter components through December, 1989.

Testing should have confirmed the design by the end of August, at which point the orders for the superboard PC board can be let. The line receivers can also be ordered at that time. Both components will have arrived before the end of 1989. The componenets that are being taking from the Liquid Argon Calorimeter (LAC) electronics must be ordered as part of the calorimeter order to reduce costs. These orders go out in 1989, some commitments having already been made. Since we cannot chage this part of the system in any case, there is no reason to wait for the August tests to be completed. Assembly of the PC boards and component cards will take place toward the beginning of 1990 and checkout of the superboards will go on during the next month or two. Finished crates of superboards will be sent to Aachen/DESY for use in checkout of the tailcatcher modules and eventually installed at the H1 detector sometime near the end of 1990.

Computing

The VAX 8600 was installed in the Fall of 1987 and continues to serve us well. Between AMY and E653 it is nearly 100% utilized, and the theorists, whose use was not considered in our computer proposal of some years ago, have also found it to be very valuable. (They alone could saturate the CPU time, if allowed.)

One serious bottleneck that showed up last year continues to be a problem and that is disk space. The 8600 is the heart of our computing capability; it stores our program libraries and our frequently-used data bases. Each of the several components that are drawn upon for each of the analysis topics (mu-mu and tau-tau asymmetry, heavy lepton search, K-zero, etc.) of the different experiments here (AMY, E653, H1) requires fast access to these files. Work stations fetch the libraries and data files through the local area network. Our inability to store the files for the topics currently being worked on is an impediment to our analysis work. A 456 Mbyte disk would increase the productivity significantly.

TASK C

Maturing of AMY

The AMY detector rolled in on November 1986, exactly two years after its formal proposal (TRISTAN-EXP-03, NOV. 1984). Physics data taking started in January 1987. Only $4.3M from the U.S. has been spent on the whole detector (together with 1 B Yen from Japan). AMY is the last TRISTAN experiment to get approved, yet initially it was one of the only two experiments taking data and the first paper was published after one year of data taking. This is the "AMY miracle."

During the last year AMY made an impact in High Energy Physics. Using the R value measured, we found that the all-important mass of the intermediate boson Z is somewhat lower than what was directly measured by UA1 and UA2.

"Measurements of the e^+e^- Total Hadronic Cross Section and a Determination of M_Z and $\Lambda_{\overline{MS}}$", Phys. Lett. B218,499 (1989).

The recently commissioned Stanford Linear Collider so far seems to support the lower mass. This is some feat as we are still 30 GeV below the Z peak. This illustrates the value of doing an experiment in the very valley of the cross section and the power of the interference effect.

We have accumulated enough data to be useful for the study of QCD effects. The first paper in this area, on its non-abelian nature, was published.

"Experimental Evidence for the Non-Abelian Nature of QCD from a Study of Multi-Jet Events in e^+e^- Annihilations", Phys.Rev. Lett. 62:1713 (1989).

With these, AMY is now a mature experiment. A comprehensive program is underway. At the General meeting of the American Physical Society at Baltimore, Kaori Maeshima of U.C. Davis gave an invited talk: *"Recent Results from TRISTAN"*.

In addition we contributed 10 talks:

Measurement of Charged Particle Multiplicity in e^+e^- Interactions at W = 50 to 57 GeV. Hongwei Zheng, U. of Rochester.

Forward-Backward Charge Asymmetry in e^+e^- Hadrons. David D. Stuart, UC Davis.

Experimental Evidence for the Non-Abelian Nature of QCD. S. Schnetzer, Rutgers U.

A Study of Properties of Multi-Jets Produced in High Energy e^+e^- Annihilations. Young-Kee Kim, U. of Rochester.

A Determination of QCD Parameters from a Study of Multi-Jet Events Produced in e^+e^- Annihilations from $\sqrt{s} = 50$ to 57 GeV. I.H. Park, Rutgers U.

Search for Heavy Leptons, SUSY Particles in e^+e^- Interactions up to $\sqrt{S}$ = 60 GeV. John R. Smith, UC Davis.

Search for the b' Quark. Sarah C. Eno, U. of Rochester.

Search for Mono-Jet Production at e^+e^- Annihilations at $\sqrt{S}$ = 55.5 GeV. E. Low, VPI and S.U.

A Search for Charged Scalar Production in e^+e^- Annihilations from $\sqrt{S}$ = 50 to 57 GeV. J. Vinson, Rutgers U.

Experimental Studies of Tagged $e^+e^-e^+e^-$ and $e^+e^-\mu^+\mu^-$ Events. Yiu-Hung M. Ho, U. of Rochester.

These are the physics topics we are pursuing currently and in the near future. Long term physics goals will be discussed in a later section.

U.C. Davis Contributions to AMY Hardware and Upgrade.

The U.C. Davis group played a crucial role in the construction of the electromagnetic shower detector by making its cathode-readout boards and read-out boards for the Endcap calorimeter in the AMY upgrade. UC Davis also helped to build, install, and operate the Inner Tracking Chamber (ITCh), made of "straw" tubes, and again the straw-type vertex chamber in the AMY upgrade. .

The construction of the "plotted" circuit boards for the electromagnetic shower detector involved the drawing and etching of over 200, 8'x4' double sided boards. Each layer was adjusted so that the pads lined up in exact tower geometry - to do

this, 80 different patterns had to be drawn. The purpose of exact tower geometry is to provide best possible angular resolution and angular separation between showers with a finite number of electronic readout channels. The method of fabrication of the "plotted" circuit boards is that of drawing with acid resistant ink on a large board. It is unique in the world. This ability to produce boards of such high quality is now again applied to the AMY upgrade.

The search for a phenomenon may depend on the hermicity of the detector. To improve this aspect, we upgraded the endcap region. The new endcap calorimeter makes use of gas-filled plastic tubes. Pickup pads on the surfaces provide readout signals in addition to those from the wires running the length of the tubes. UCD fabricated the large PC boards that held the pickup pads for the shower counter and will do the same for the endcap calorimeter. "Printing" of the designs onto the G-10 PC boards as well as the etching would be done at UCD.

The inner tracking chamber is a high precision drift chamber utilizing minimum material. It consists of polycarbonate tubes arranged to form a four-layer closed-packed array of drift cells. Each layer consists of 144 tubes. Tube technology was chosen for its cylindrically symmetric cathode structure as well as its strength. This device is the least accessible of the entire AMY detector. It must be insensitive to wire breakage. Individual tubes provide isolation between adjacent sense wires, thereby eliminating the possibility of losing the use of large segments of the chamber due to one broken wire.

An important function of the inner tracking chamber is to provide a charge track trigger. This trigger processor was designed and built by UCD. The trigger processor counts different types of track segments in the ITCh, the total number of hits, and assigns a topology number to each event. The trigger decision is made using this information. Track segments are identified by analysing the hits in a twelve tube cluster. The hits in a cluster are used to address a fast memory (4096 by 4 bits). The four outputs are used to signify different track types. The important part of this sophisticated trigger is its ease of programmability for the

various track patterns and associated parameters, its continuous monitoring ability, and its ability to simulate the trigger by Monte Carlo events.

The AMY charged particle tracking system includes the Inner Tracking Chamber (ITC) and the Central Drift Chamber (CDC). Both these detectors measure the position of the track in the $r-\phi$ plane exceedingly well (around 180 microns globally in the CDC, and 80 microns in the ITC). Even though these charged particles are measured well, the capabilities of the AMY detector need to be and are in the process of being substantially improved. For example, the CDC Z-coordinate is poorly measured, and the ITC has none at all. The areas of interest include: track recognition, track extrapolation, momentum measurement, reconstructed mass resolution, and secondary vertex finding. Monte Carlo studies indicate that all of these areas can be enhanced with the following modifications to the central tracking system:

1) Reduction of the beam pipe radius.

2) Reduction in the amount of material in front of the first tracking layer by changing the beam pipe from Aluminum (2% of a radiation length) to Beryllium (0.3% R.L.).

3) Enhancing the $r-\phi$ resolution to 50-100 microns.

4) Increasing the resolution in z with the addition of several measurements of $\sim$ 6mm.

We (UCD and KEK) are currently constructing the new vertex chamber for the AMY detector to be installed just outside of the new smaller diameter beam pipe. The outer radius of the current AMY beam pipe is 12.5 cm, thickness of 2mm aluminum. The new beam pipe wil be 5 cm in radius, 1mm beryllium material.

It is extremely useful to be able to determine the vertex region accurately, and for that we need high accuracy position measurements. We are aiming to produce a chamber with $r-\phi$ resolution of less than 50 μm, and z-resolution of approximately 1%. The chamber will be a straw chamber type, and 65 cm long. The cross section view of the straw chamber is shown in Figure 1. The inner tube starts 5.2 cm from

the beam center line. It is a 4-layer chamber similar to the ITC (Inner Tracking Chamber, already in existence at AMY).

The primary responsibility of U.C. Davis for this chamber is to design the front end electronics (from the chamber wire to just in front of ADC/TDC). For the z-read-out, we are going to use the charge division method. We have constructed a test chamber with 36 straws, and have been testing for the optimum performance. To obtain better than 50 μm resolution, we need to pressurize the chamber gas to more than 2 atm for the chamber gas commonly used (e.g., CO_2, Ar-Ethane). To fit all the electronics in near the end of the chamber, in the gas can, the electronics design has to be not only optimized for the best performance, but also very small. Actually, to have the most front end of the electronics as close as possible is essential for the good performance (high resolution), because we need to keep the signal travelling distance very short. in order to prevent the degrading of the signal and to minimize the pick up noise before getting to the preamps. The electronics design is closely related to the design of end-plates and gas can. The design of electronics, mechanical parts, is almost in final form. Figure 2 shows the side view of the straw chamber end region; Figure 3a,b shows the layout of the high voltage card and preamps in actual size. Out from the chamber, the signal goes to the preamp cards, then into the postamp module. There, the signal from both ends of the wire is shaped and fed into ADC for the Z measurement, and also, separately, both ends of the signal will be summed over linearly, then discriminated and fed into the TDC module for $R-\phi$ measurement. Currently we are manufacturing all the prototype electronics at U.C. Davis. We shall perform the beam test at KEK at the end of June with the test chamber and the prototype electronics.

In the second phase a delay-line technique will be applied for the Z read-out. The tubes are manufactured by spirally winding a conductive strip into a tube. This spiral cathode forms a delay line. The goal is to measure the time difference between the arrival of pulses on the two ends of the cathode to measure the z coordinate. A time difference of 100 picoseconds yields a z measurement of 1 mm.

The delay line concept will be tested and the time difference resolution measured.

AMY Analysis in U.S. and the role of U.C. Davis

While the majority of the AMY analysis is still carried out on site at KEK on the FACOM machine, a significant amount has been shifted to the United States. U.C. Davis is taking an important role in developing the U.S. analysis capability, due to both its strength in analysis and its geographic location.

The U.C. Davis group was quite successful in building its VAX-CPU power based on a cluster of three MicroVax 3200's. The tau-pair production analysis carried out at U.C. Davis was the first complete analysis in which a major part was done in the U.S. The analysis being done primarily at U.C. Davis now includes the jet charge F/B asymmetry and Higgs search in the tau decay mode. A data distribution procedure was established. For the U.S. collaborators to contribute significantly to physics analysis it is very important for them to obtain the data as fast as possible. We now routinely transmit some selected events through the trans-Pacific link to U.C. Davs, which in turn distributes them to other U.S. institutions. This proves to be very useful for people working on a special analysis topic to make feedback to the running of the experiment. We have a University of California 56K baud link between LBL and U.C. Davis. With the anticipated upgrade of the trans-Pacific link to 56K baud in the Summer of 1989, a significant fraction of the data can be distributed in the U.S. within a day after they are taken. U.C. Davis is designated by the collaboration as the data center in the U.S. Even with the fast trans-Pacific link, not all data, especially the Monte Carlo simulated data, can be shipped through computer links. We have just acquired a dual EXABYTE tape unit. It immediately became a very important work horse. The medium, an 8mm videa cassette cartridge can pack 10 tapes worth of data (2.3 giga-byte). Thus it solved our old problem of delay caused by international shipping. There are so much data packed on the tape, that we often have to use it directly instead of off-loading onto a disk. More EXABYTE units can definitely improve the productivity of the system.

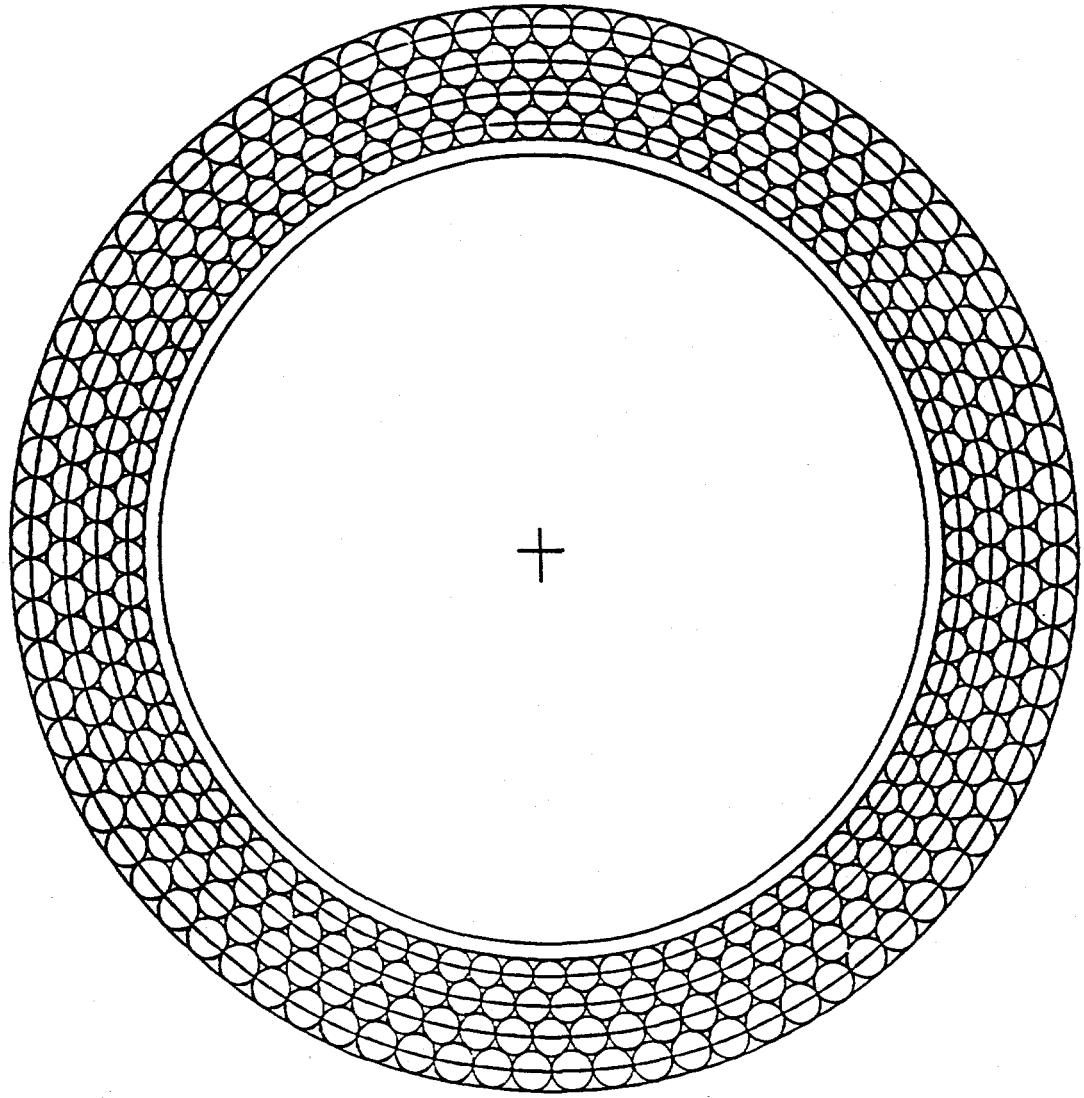

VTX Chamber Cross Sectional View

Scale 1:1

Fig. 1

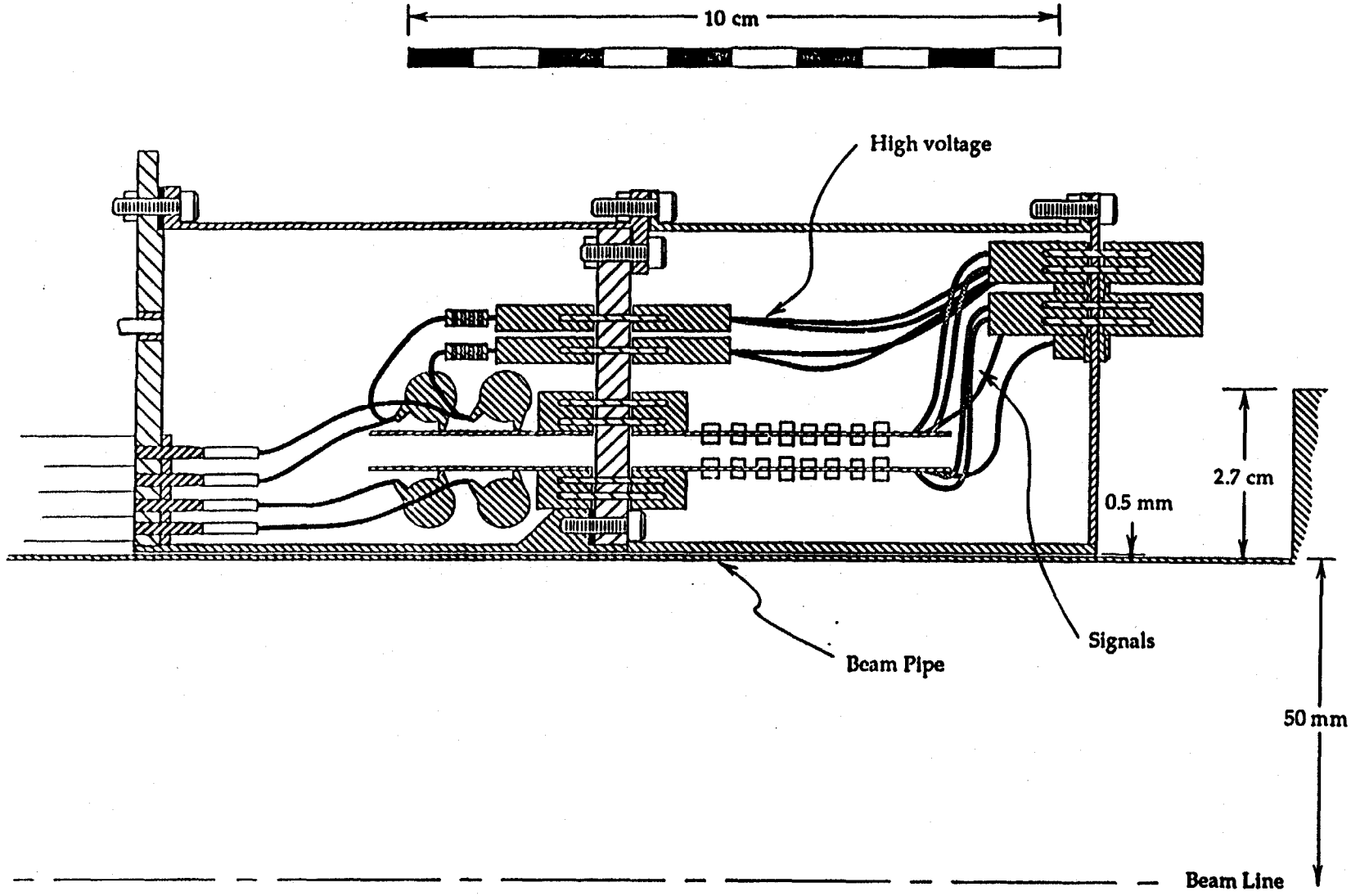

Straw Chamber with Preamps
Side View Detail
Scale 1:1

Fig. 2

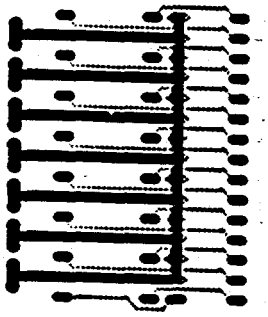

High Voltage card

figure 3a

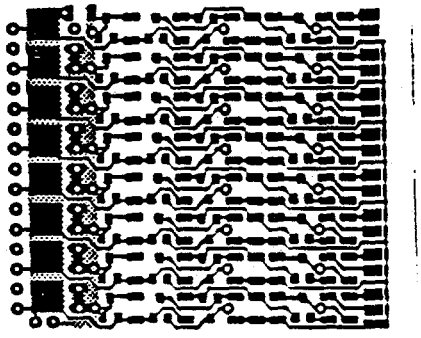

preamp card

figure 3b

TASK D

The Research Program at FERMILAB.

The current research effort at Fermilab, is the outgrowth of a sabbatical (1977-78) spent by Principal Investigator P. Yager at the laboratory in collaboration with MSU, UCSD and Carleton University working on E383, the inclusive production of K^0 from Hydrogen in a K^- beam. Follow-on experiments, using much the same apparatus, culminated in E663, where the polarization of inclusively produced Λ's and anti-Λ's was measured in $\bar{p}p$, K^-p and pp reactions. This latter experiment led to the dissertation of UC Davis student S.A. Gourlay. The conversion of the M4 underground beam to a CDF test facility prevented further exploitation of the neutral particle spectrometer. Although task D did not yet exist at this time, this work was the natural precendent, and the University provided a certain amount of support - sabbatical leave, some travel and an 800 BPI tape drive and controller for the on-line data-acquisition computer. In 1982, a collaboration was formed with Ohio State University, Oklahoma University, Carnegie-Mellon University, a variety of institutions in Japan and Korea and UC Davis. This collaboration submitted a proposal (Appendix A) to study hadronic production of charm and beauty in a hybrid emulsion spectrometer, and more or less coincident with the approval of E653, Task D was funded in February 1983.

Since this beginning, the task has been almost exclusively devoted to the Charm and Beauty production and decay experiments in the hybrid emulsion spectrometer. A large (3 meter x 3 meter, 12 double sided chambers) muon spectrometer and associated electronics was built under the direction of J. Volk and P. Yager. The latter spent a full year, calendar year 1984, of sabbatical leave in residence at Fermi, covering the test-run period where at least one module of each type of equipment was tested. The UC Davis LSI 11/23 computer was used to record data and evaluate module performance during this test-run. Two graduate students were devoted exclusively to this experiment since January 1, 1984 with one, Mokhtarani, graduating Dec. 1988. The second student, V. Paolone, interrupted

his thesis work to replace J. Volk as a Research Physicist for the second run, but has now virtually finished his dissertation. A third graduate student, J. Wilcox was added in January 1987, devoted to the second run and its analysis. University support has included purchase of a printronix 600 line per minute printer and almost half of the Micro-VAX II that served as the "On-line brain" during the second run. Sabbatical leave was taken by Yager in residence at Fermilab during the Fall quarter, 1987.

Originally, the E653-FNAL Agreement called for three fixed target-running periods to expose the complete volume of emulsion. However, we were fortunate enough to take 6 10^6 triggers during the first actual running period, which ended in August 1985. The improvements to the experiment made on the basis of the first run included general up-grades of the whole spectrometer, data acquisition system and beam-line. When the second fixed-target run started in June, 1987, the smooth start-up and greatly improved reliability of all of the sub-systems in the experiment, including the muon spectrometer, allowed us to take the remaining 9.6 10^6 triggers by November 1, with three months remaining in the fixed-target period. Part of the remaining time was devoted to recording test data for the proposed all-electronic experiment, P780. Although the E653 group remains convinced that 780 was a viable and important experiment, well suited to the existing spectrometer with only minor changes, the PAC rejected our proposal in December 1987, and again at the review of our appeal in May 1988. Although the opportunity to pursue production of heavy flavor is not forthcoming in an all-electronic configuration of the E653 spectrometer as originally anticipated, negotiations immediatly started to join one of the other fixed-target heavy flavor experiments for the forthcoming running period. Among those considered by the several E653 groups were P791 and E687. Some of our colleagues have joined the former and UC Davis has formally joined E687.

The first run electronic data analysis, which must precede the visual scanning of the emulsion by our colleagues in Japan, was completed in the Fall of 1987. The innovative scanning methods of the emulsion groups were new to this experiment

and required a certain amount of refinement and shake-down. The success rate on finding the vertices in the emulsion on the basis of the electronic analysis is 95%, far more successful than has ever been achieved with these hybrid techniques.

Preliminary results from the first run were presented at the DPF meeting in Storrs, Connecticut, August 1988. Among the four presentations by E653 were two by the UC Davis graduate students. One was on all electronic results and the second was on pair production of charm and production characteristics. The ability to see both produced charm particles is the unique feature of emulsion targets, compensating somewhat for the labor intensive scanning procedures. Using an A dependance of between $A^{2/3}$ and A^1 and a 20 micro barn cross section per nucleon, consistent with the WA75 results, we expect an ultimate yield of 1400 charm pairs. Furthermore, the high resolution and visual capability of the emulsion will allow us to see any unusual or unexpected short-lived phenomena that would be obliterated in most all-electronic experiments, where even observation of both members of the pair is rare. One also has the potential to directly measure the $D_s \rightarrow \tau$ branching ratio by careful scanning of the "kink" type charm candidates that initially appear to be $D \rightarrow \mu$, but through our careful measurement it turns out to be $D \rightarrow \tau \rightarrow \mu$, with a barely perceptible kink on the "D" track.

The 1987 run, as noted above, was remarkably successful. The beam was changed to deliver 600 GeV pions, since B production calculations indicate that their cross section would increase at least a factor of 3 over that for 900 GeV protons due primarily to the anti-quark content of the π. The electronic data analysis for the second run is proceeding smoothly. Extensive Monte Carlo work has been done to find methods of selection enhancing the probability of finding the B-pairs. At this time, the scanning results from the first run are almost complete, and the data reduction part through the second run is 25% complete. Predictions will be sent to the emulsion groups in Japan within a month, when their scanning of the first run is completed. In addition to the new beam, three larger (9 x 9 cm) microstrip detectors were added to the downstream end of the vertex SSD system for increased acceptance. Nagoya University provided 3 high resolution

(12.5 micron pitch) detectors for the up-stream part of the vertex SSD system to improve the resolution extrapolating back into the emulsion. A moving emulsion "tape", essentially a roll of film passing between the bulk of the emulsion and the micro-strip detectors, was installed and worked successfully during the run.

The muon system was improved by the addition of more steel to reduce the punch-through confusion in the upstream arm. One of the OSU vector drift chambers was inserted in the absorbing steel to facilitate the link between the triggering muon and the corresponding spectrometer track. The 12 UC Davis muon chambers were all reworked with improved amplifiers and better field shaping. The net result exceeded our wildest expectations. The muon tracks are clear clean and easy to reconstruct with a good muon track on virtually every trigger. Multi-muon events present no problem in the second run data.

Modifications to the data acquisition system both in FastBus Memories and in the VAX/LSI on-line system plus the increased spill of the Tevatron for the second run greatly sped up the data logging. Improved diagnostics were run on the UC Davis Micro VAX II, insuring that all systems were properly functioning. It should be noted that the VAX/LSI on-line program was entirely saturated reading FastBus, building events and writing tape, so that the Micro VAX was absolutely essential to our operation. An interesting sidelight on this particular computer is that it arrived at Receiving at 1:30 PM on a Friday and that by 4:00 PM that day we had brought it to the experiment, unpacked it, assembled it and had it running. By 5:00PM it was on the DecNet and running some of our monitor programs!

All Electronic production of Heavy Flavors.

UC Davis, in participating in E653, always intended to follow the hybrid experimental program with all-electronic running in the same detector. Although the PAC and the lab did not choose to approve our proposal, P780, the interest in this type of physics remains very strong and several other opportunities have arisen for Davis to participate in one of the several Experiments or proposals. The two experimental programs most seriously investigated were P791 in the Tagged

Photon Lab and E687 in the Wide Band Photon beam (p-West). We have joined the latter experiment. The UC Davis Micro Vax was installed at the experiment in the Fall of 1988. Additional disk and EXABYTE 8mm cartridge tape drives were added and the system was upgraded to VMS 5.1. This computer is serving at the boot-node for the local VAX cluster for E687 and has been in extensive use since Spring of 1989. Apart from general participation and data analysis, UCD expects to develop and refine a high transverse mass on-line trigger. Commitments to E653 and teaching has prevented full participation until July 1989. At this time, Yager will spend the next six months at Fermilab, preparing for the fixed target run, now scheduled for January 1990. A graduate student will be devoted to this experiment, several are under consideration and Paolone will shift from E653 to E687 as a Research Physicist. The E687 proposal is appended, B.

Future Plans, The B-Collider work group.

Beginning in Spring, 1987, we have been participating in a B-Collider Work Group, meeting roughly every other month, exploring the design and feasability of a "B Factory" at the Tevatron. A letter of intent was passed to the Lab and to the PAC. A working group of experimenters from UC Davis, Yale, Penn, OSU, Princeton, Florida, Northeastern, I.I.T. , Oklahoma, Fermilab and other institutions is convening at the Snowmass D.P.F. working meeting to pursue this prospect to the proposal stage. One exciting prospect of our proposal is the possibility that a p-p capability is being considered at Fermilab, which would greatly benefit Beauty production factories with the increased luminosity and short interaction region. Appendix C contains our letter of December 9, 1987 to Fermilab Director L. Lederman, and Appendix D is the proposal submitted January 1989, which has been partially approved.

APPENDIX A

"A PROPOSAL TO MEASURE CHARM AND B DECAYS VIA HADRONIC PRODUCTION IN A HYBRID EMULSION SPECTROMETER"

Spokesperson: Neville W. Reay
Dept. of Physics, Ohio State
Univ., Columbus, Ohio 43210
614-422-7436, FTS 8-940-7436

E653

A PROPOSAL TO MEASURE CHARM AND B DECAYS VIA HADRONIC PRODUCTION IN A HYBRID EMULSION SPECTROMETER

N. Ushida
Aichi University of Education, Kariya, Japan

W. Ko, R. Lander, P. Yager
Department of Physics, University of California, Davis, California

R. Edelstein, C. Forsyth, R. Lipton, J. Russ
Department of Physics, Carnegie-Mellon University, Pittsburgh, Pennsylvania

S. Pordes
Fermi National Accelerator Laboratory, Batavia, Illinois

T. Ando, G. Fujioka, H. Fukushima, Y. Takahashi, C. Yokoyama
Physics Department, Kobe University, Kobe, Japan

Y. Homma, Y. Tsuzuki
Faculty of Liberal Arts, Kobe University, Kobe, Japan

S.Y. Bahk, C.O. Kim, J.N. Park, J.S. Song
Korea University, Seoul, Korea

H. Fuchi, K. Hoshino, K. Niu, K. Niwa, H. Shibuya, Y. Yanagisawa
Department of Physics, Nagoya University, Nagoya, Japan

J. Dunlea, J. Kalen, S. Kuramata, N. Reay,
K. Reibel, R. Sidwell, N. Stanton
Department of Physics, Ohio State University, Columbus, Ohio

K. Moriyama, H. Shibata
Faculty of Sciences, Okayama University, Okayama, Japan

G. Kalbfleisch, P. Skubic
Department of Physics and Astronomy, University of Oklahoma, Norman, Oklahoma

M. Chikawa, T. Hara, O. Kusumoto, Y. Noguchi, T. Okusawa, T. Omori, M. Teranaka
Osaka City University, Osaka, Japan

J.-Y. Harnois, C. D. J. Hebert, J. Hebert, B. McLeod
Department of Physics, University of Ottawa, Ottawa, Ontario, Canada

H. Okabe, J. Yokota
Science Education Institute of Osaka Prefecture, Osaka, Japan

S. Tasaka
Institute for Cosmic Ray Research, University of Tokyo, Tanashi, Tokyo, Japan

J. Kimura, Y. Maeda
Yokohama National University, Yokohama, Japan

May, 1982

Table of Contents

Table of Contents continued

List of Figures

A. Summary of the Experiment

We propose an experiment which employs a hybrid emulsion spectrometer to measure lifetimes and decay properties of beauty particles (B) and charmed particles (C) produced by interactions of high energy hadrons. Emulsion is the highest resolution detector (by more than an order of magnitude) for observing short lifetimes, and the electronic detection system is needed to select events, locate them within the emulsion and provide information about decay products.

A similar technique has proven successful in measuring the lifetimes [1,2;3] of neutrino-produced charmed particles (Fermilab Experiment 531). We believe that the experience therein gained will permit us to switch to hadronic production, where there are more beauty and charmed particles to be found.

The key to this experiment is a new form of solid-state detector which we are developing. With this detector as part of the hybrid emulsion system we should be able to obtain, in a four-month run with modest beam, 15,000 charmed-particle decays, and based on a 50 nanobarn cross section, about 200 B decays. Nearly 30 tau decays should also be observed.

Completing the development work on the new detector will require a year, so that data taking could begin late in 1983. Since the technique we propose has many novel features, we request "shakedown" running on whatever machine (conventional or Tevatron) exists at that time.

B. Physics Motivation

We wish simultaneously to search for B-particle decays and to make a high statistics measurement of charm decays.

The latter measurement provides an acceptable and secure motivation for the experiment. A $\pm$ 10% knowledge of lifetimes permits conversion of branching ratios into absolute partial decay rates without loss of precision. A current experiment [1,2,3] shows hints of two neutral lifetimes and the possible existence of weakly decaying neutral charmed baryons. Definitive studies of these effects, plus the possibility of observing sequential F $\rightarrow$ tau $\rightarrow$ other lepton decays, creates interest in a high statistics charm measurement. Observation of visible decay lengths also provides a relatively background-free sample of charmed particles for studying decay modes and production dynamics.

Of even greater interest than these charm measurements, however, is the opportunity to measure the lifetime of particles (B) carrying the b quark, for which strong evidence now exists [4], and to search for other new phenomena which may be associated with lifetimes down to 10^{-15} sec. This experiment will have a sensitivity of 4 events/nanobarn for detecting such interesting events. Should B-particles be produced at this level, their sequential B $\rightarrow$ charm $\rightarrow$ strange decays should be topologically striking and relatively background-free once the secondary and tertiary vertices are identified.

Measurement of B lifetimes and relative branching ratios into charm would, in the "standard" Kobayashi-Maskawa six-quark model [5], permit determination of the extended Cabibbo angles θ_2 and θ_3. In the approximation of small θ_1 and CP-violating phase δ, we may write

$$\sin \theta_1 = s_1, \quad \cos \theta_1 = \cos \theta_2 = \cos \theta_3 = 1$$

If we also assume the ratio,

$$\frac{(B \to \text{charm} + X)}{(B \to \text{no charm})} = \left| \frac{s_3 + s_2 e^{i\delta}}{s_1 s_3} \right|^2 >> 1 ,$$

then, $$\tau_B = \left(\frac{M_c}{M_B} \right)^5 \frac{1}{\left| s_3 + s_2 e^{i\delta} \right|^2} \tau_{charm}$$

The θ_i are given in terms of quark mass ratios by many of the higher symmetry models which predict proton decay [6], and charm lifetimes are 10^{-13} to 10^{-12} seconds [1,2,3]:

$$\tau_B = \left(\frac{1.9 \text{ GeV}}{5.3 \text{ GeV}} \right)^5 (10 - 100) \ (10^{-13} \text{ to } 10^{-12} \text{ seconds})$$

$$\tau_B = 5 \times 10^{-15} \text{ to } 5 \times 10^{-13} \text{ seconds}$$

If the Higgs particle comes from a single multiplet, its couplings are flavor diagonal, and its existence would have no effect on the B lifetime. However, if there are multiple Higgs doublets, in general the charged Higgs could couple $B \to H^- + (\text{charm})$. If $M_B > M_{H^-} + M_C$, the B lifetime could be considerably shortened.

A recent theoretical preprint [7] uses CESR data and a conventional six-quark model to set bounds on the B lifetime in terms of the ratio $\tau (b \to u) / \tau (b \to c)$. Recent CLEO data [8] on this ratio then may be used to set an upper limit of 1.3×10^{-13} seconds for the B lifetime. If the B lifetime turns out to be much shorter than expected, it may be that the b quark (and perhaps the tau lepton) are not conventional. In this case, theoretical predictions have even more freedom, and information obtained on B decays could prove

to be even more exciting.

C. Description of the Experiment

1. Design Motivation

The apparatus is a hybrid emulsion spectrometer similar in concept but technically more demanding than the one used successfully in Experiment 531, and it will be operated in a charged hadron rather than in a neutrino beam. Given a reasonable track density ($1000/mm^2$), we can obtain 2.8×10^8 interactions in 100 liters of emulsion, and will rapidly check the emulsion for an interesting subset of 61,000 predicted secondary vertices.

Reducing secondary interactions leads to an emulsion design in which many thin modules 10 cm x 20 cm x 1.5 cm are sequentially exposed in hourly intervals. Each module will be mounted on a precision stage which moves during the beam spill, exposing strips of emulsion.

The design of the spectrometer is motivated by the following requirements:

1) Finding events in the emulsion quickly and efficiently;

2) Large acceptance;

3) Identification and momentum analysis of decay products;

4) Good reconstruction efficiency for the expected high multiplicity, highly collimated events;

5) Minimum path for pion and kaon muonic decays (since our selection criteria depend on $B\bar{B}$ and $C\bar{C}$ muonic decays);

6) Ability to resolve secondary vertices electronically.

2. Solid-State Detectors

It is very difficult to satisfy the above design criteria with existing technology. Drift chambers, for example, fall short of the position resolution required for beam tagging and decay vertex resolution by factors of 10. Even worse, they can achieve track pair resolution no better than 2 mm, so that tracks more closely spaced than this are lost. Since projected angles between tracks of < 1.0 mrad occur with appreciable probability in hadron interactions at 350 to 800 GeV, it is impossible to place drift chambers close to the emulsion target without incurring unacceptable reconstruction losses. Yet, high resolution detectors close to the emulsion target are essential if the apparatus is to be kept short and secondary vertices are to be reconstructed.

We have, therefore, produced a spectrometer design which relies on the rapidly evolving technology of position-sensitive silicon detectors, and are well into a program of prototyping and testing. Details of our progress and a photomicrograph of our prototype with 40 micron strip spacing are given in Appendix I.

Briefly, the detectors are thin silicon wafers onto which are deposited strips with a center-to-center spacing of 40 microns, as shown in fig. 1. When they are reversed-biased, the ionized electrons resulting from charged-particle passage are collected on individual strips, as shown in the figure. In the region of highest track density individual strips will be read out, and resistive interpolation [9] (with taps every 3-10 strips) will be employed in regions with lower track density. For the spectrometer, we have assumed detectors with the following characteristics: 6 cm diameter active area, 0.3 mm thickness, position resolution of at least $\pm 40/\sqrt{12}$ ($= \pm 12$) microns, two-track separation of 40 microns, and the ability to function in magnetic fields

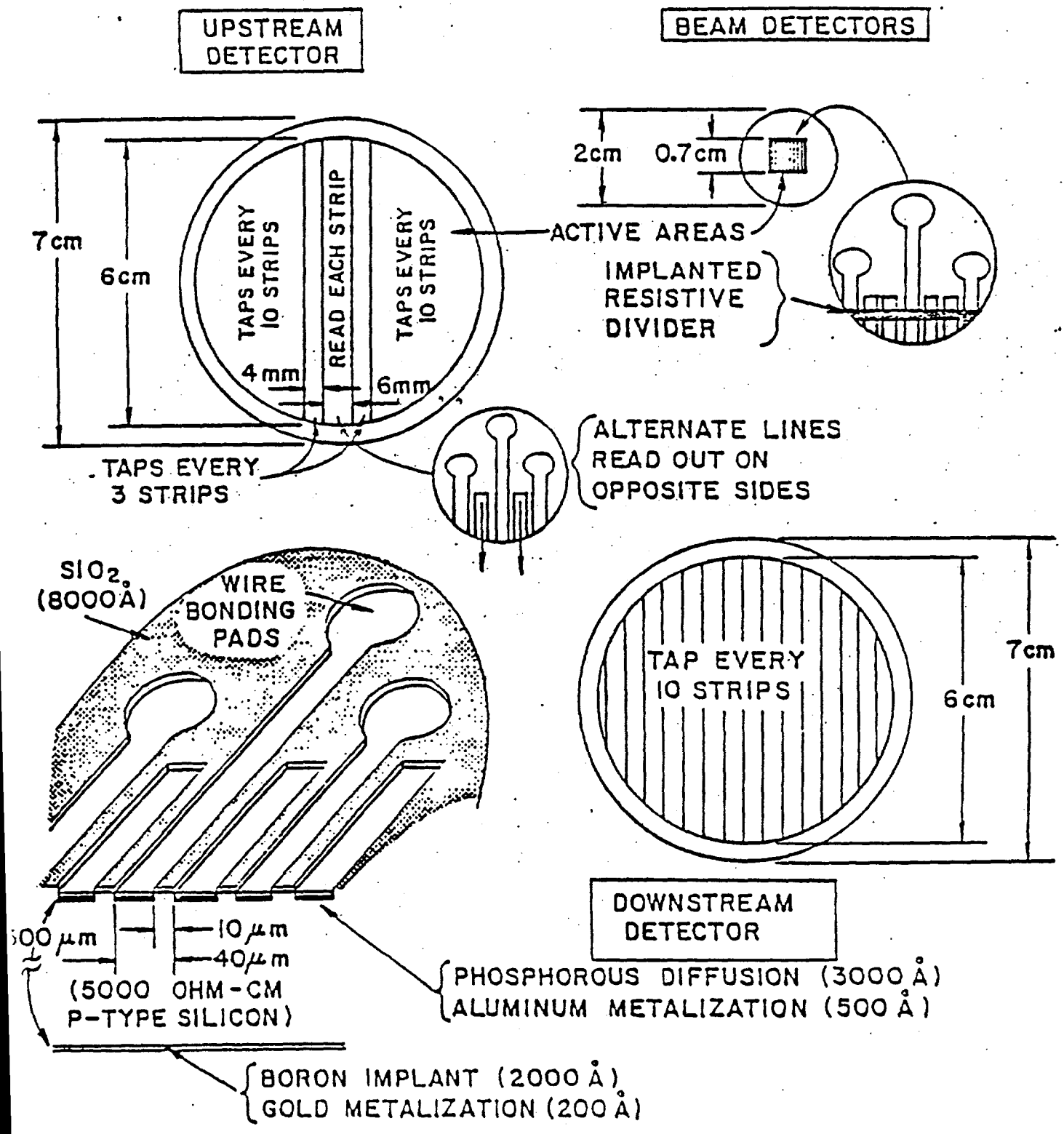

SILICON SOLID STATE DETECTORS

Figure 1.

up to 0.7 Tesla.

These requirements are all achievable using "old fashioned" solid state technology.

3. Discussion of Apparatus

A schematic elevation view of the experiment is shown in fig. 2 , and an enlarged view of the charged particle spectrometer is given in fig. 3. Note that the total length of the apparatus between the emulsion target and the upstream side of the calorimeter is less than 3.5 m. The major components are the beam and beam detectors, emulsion target, vertex detector, charged-particle spectrometer, charged-particle identifiers, gamma detector, neutral hadron detector, muon identifier, and trigger counters.

a. Beam and Beam Detectors. We require a hadron beam of about 5 x 10^4 /second with a small (3 mm x 3 mm) focus and a halo integrated over 10 cm x 20 cm which is less than about 7% of the beam intensity. The momentum spread of the beam is relatively unimportant. For B production at 400 GeV, a pion beam would be preferred. For charm production at any energy and B production at Tevatron energies, a proton beam is preferred, as the spot size and halo requirement are more easily satisfied. Possible locations are discussed in Appendix II . The beam coordinates (angles) will be determined to $\pm$6 microns ($\pm$ 7 microradians) by sets of small silicon detectors as shown in fig. 2. The relative positions of all electronic detectors will be calibrated continuously on the high momentum beam tracks.

b. Emulsion. Nuclear emulsion is the only detector which can observe

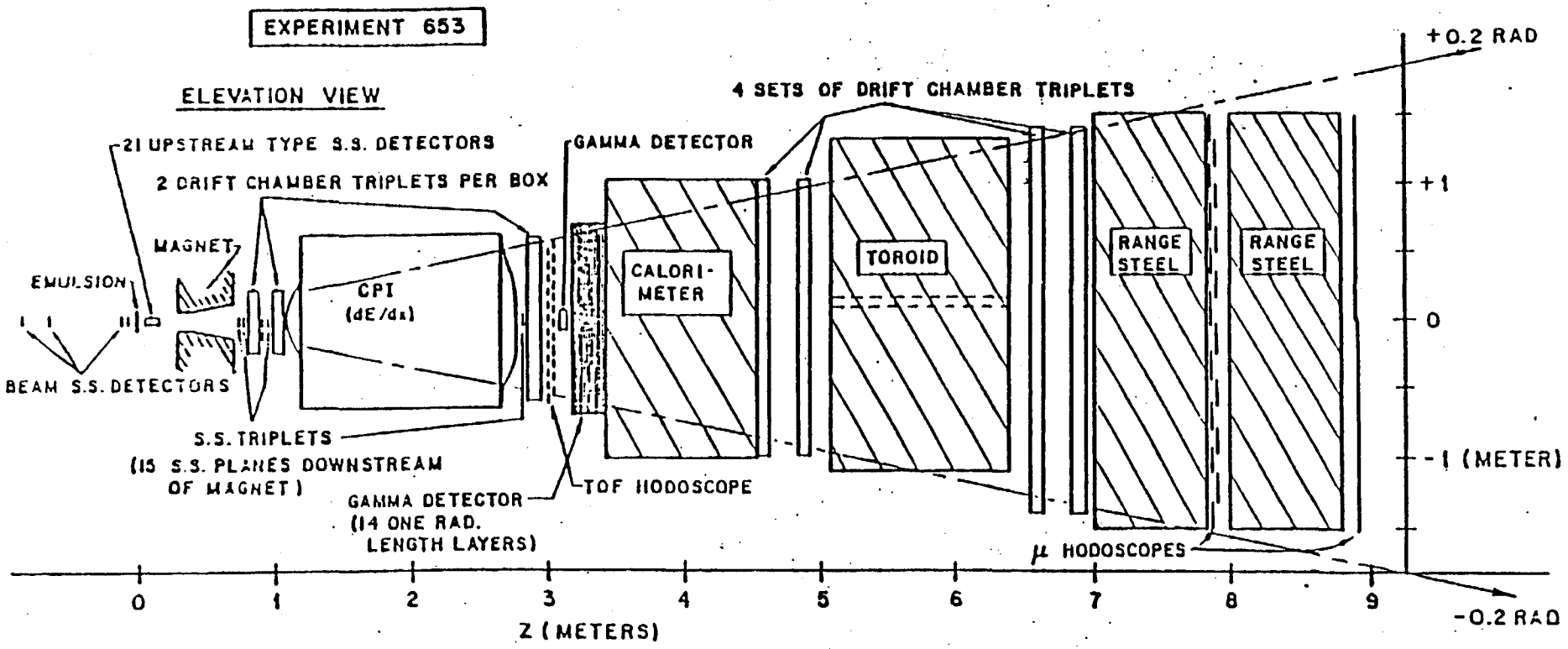
EXPERIMENT 653
ELEVATION VIEW
21 UPSTREAM TYPE S.S. DETECTORS
2 DRIFT CHAMBER TRIPLETS PER BOX
GAMMA DETECTOR
4 SETS OF DRIFT CHAMBER TRIPLETS
+0.2 RAD
MAGNET
EMULSION
CPI
(dE/dx)
CALORI-
METER
TOROID
RANGE
STEEL
RANGE
STEEL
+1
0
-1 (METER)
BEAM S.S. DETECTORS
S.S. TRIPLETS
(15 S.S. PLANES DOWNSTREAM
OF MAGNET)
GAMMA DETECTOR
(14 ONE RAD.
LENGTH LAYERS)
TOF HODOSCOPE
μ HODOSCOPES
0
1
2
3
4
5
6
7
8
9
Z (METERS)
-0.2 RAD

Figure 2.

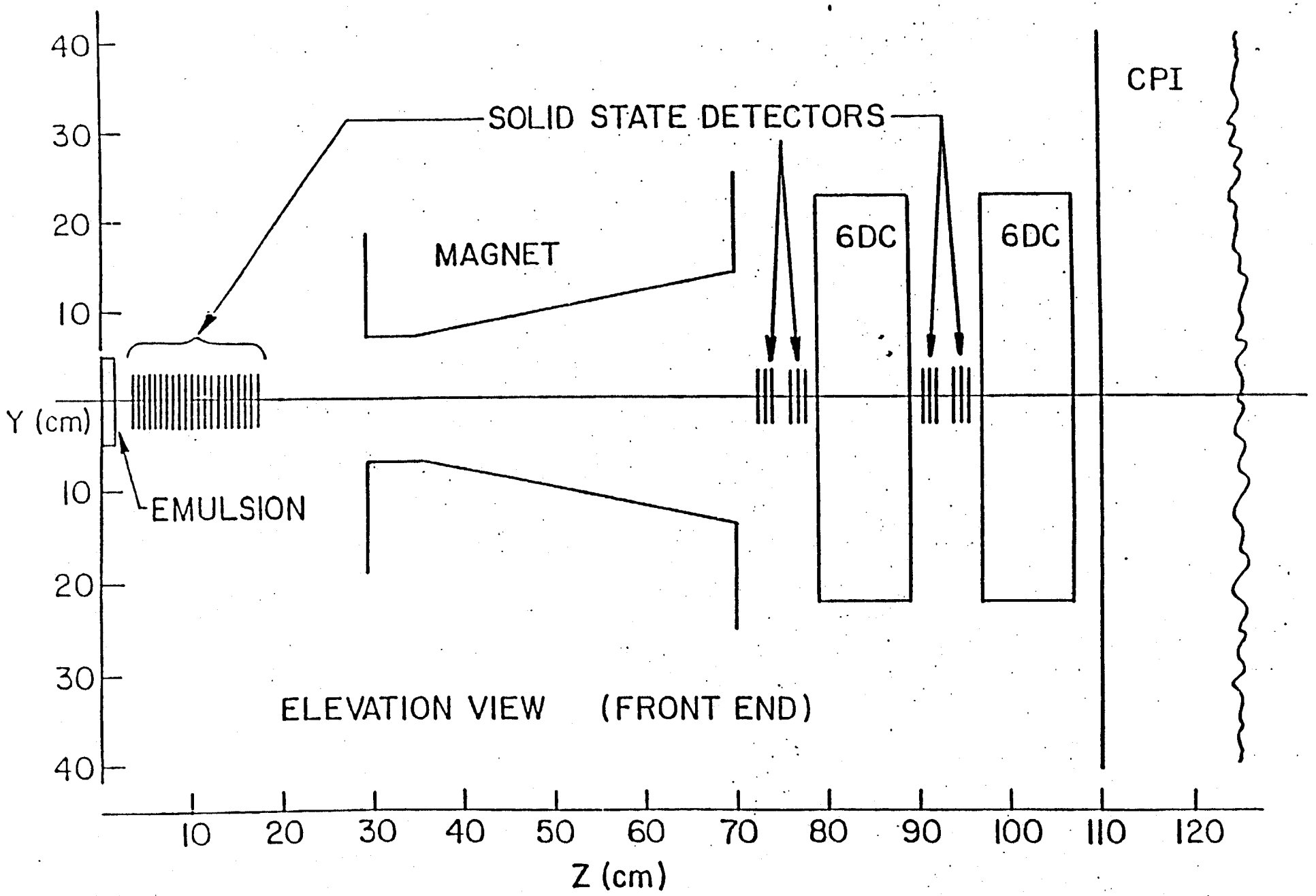
SOLID STATE DETECTORS
CPI
MAGNET
6DC
6DC
EMULSION
ELEVATION VIEW (FRONT END)
Y (cm)
Z (cm)
40
30
20
10
10
20
30
40
10
20
30
40
50
60
70
80
90
100
110
120

Figure 3.

short-lived particles with lifetimes down to 10^{-15} sec with high efficiency. In this experiment we will use as much emulsion as possible and as high a track density as tolerable to get good sensitivity to rare events. The pouring facility built at Fermilab for E531 can produce 32 liters of emulsion modules per month, so that an exposure of 100 liters is well within our capability. Maximum track density is a slightly subjective number, but the Nagoya group has experience from E531 with densities of 225/ mm^2, and from NA-19 at CERN with densities of up to 10,000/ mm^2. The maximum reasonable intensity appears to be about 1000/mm^2, which will give 2.8×10^8 interactions in 100 liters.

Historically, a serious drawback to the use of nuclear emulsion in studying rare processes has been the limited number of events which can be examined under the microscope. A breakthrough of this limitation has been made by the Nagoya group, who have developed a microscope with a TV monitor and computer-controlled digitized stage. This system has already shown its power in analyzing E531 neutrino interactions, and has been extended to handle 6,000 fully-measured events for the second E531 exposure; good progress is being made toward the goal of 10,000 measured events per year. Furthermore, the techniques described below, which take advantage of the excellent resolution of the silicon detectors, make it possible to eliminate uninteresting events quickly, so that the scanning rate should approach 40,000 events per year.

Fig. 4 is a schematic drawing of the emulsion mounting stage and a module of the "vertical" type, in which the sheets are mounted perpendicular to the beam. The emulsion volume is divided into modules 10 cm x 20 cm in area by 1.5 cm thick. This thickness, 0.04 interaction lengths, is a compromise which provides sufficient fiducial volume to observe decays and minimize edge losses, while also keeping secondary interactions and gamma conversions to

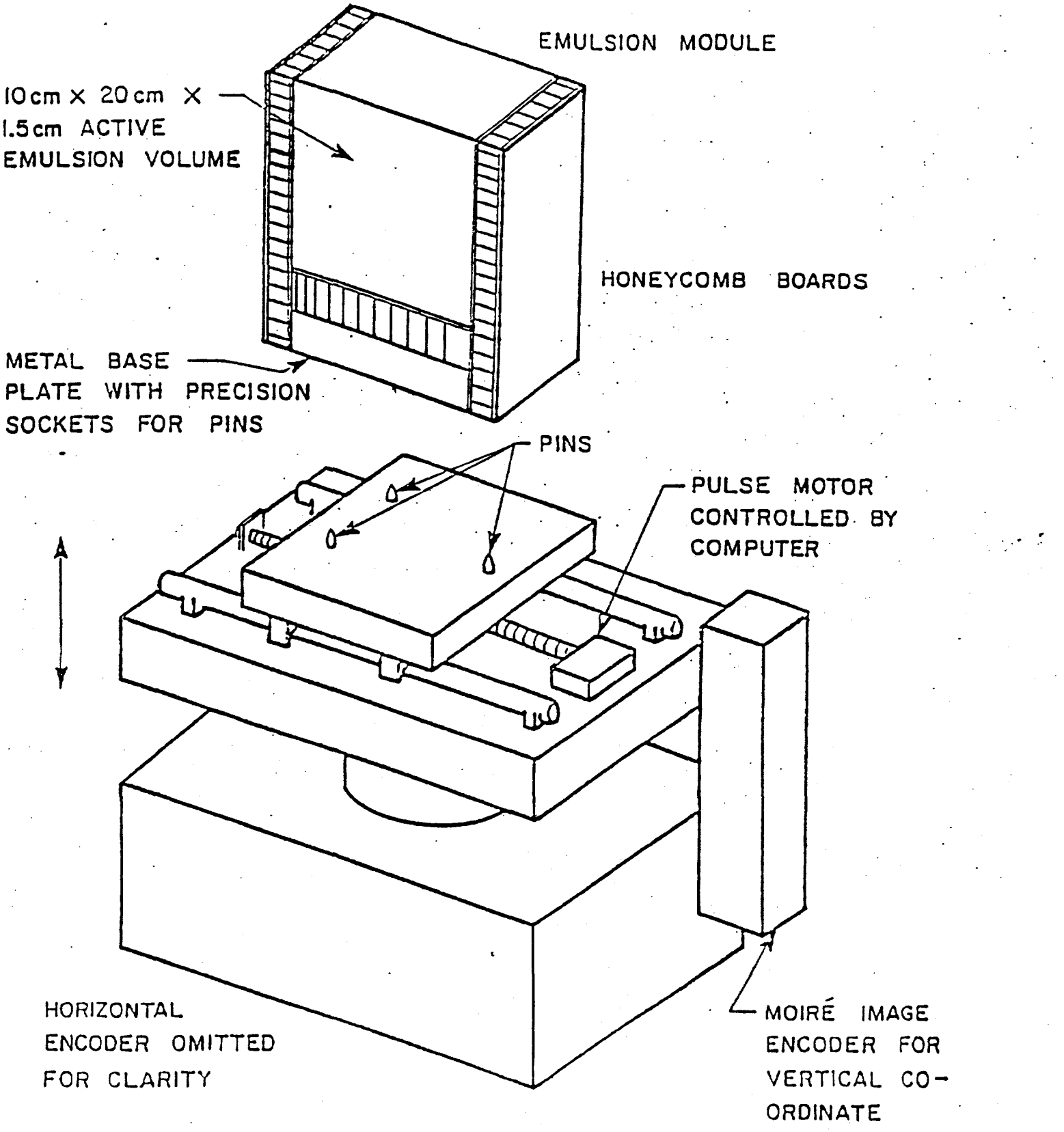

SCHEMATIC DRAWING OF EMULSION STAND

Figure 4.

a tolerable level. Each module contains 40 10 cm x 10 cm x 0.73 mm sheets of plastic- backed emulsion.

In order to maintain the desired track density with a 3 mm x 3 mm beam spot of optimum intensity, it is necessary to have the emulsion mounted on a precision microscope-type stage which moves continuously during the beam pulse, uniformly exposing a band 10 cm high x 3 mm wide. This stage is driven by computer controlled motors, and its position is monitored with standard Moire image encoders which digitally record the position of the stage at each event with 1 micron accuracy. In E531 the individual emulsion sheets were registered with each other mechanically to $\pm$ 50 microns. Improving this tolerance will substantially reduce the time required to follow tracks from one sheet to another. To do this, we will use the heavy-ion technique already tested successfully by the Nagoya group. The assembled modules will be exposed to a low-intensity heavy ion beam (2 GeV/nucleon Ne, few/cm^2) which provides easily-recognized local fiducials. Relative sheet registration will then be limited mainly by the mechanical stability of the package between exposures, which should be held to a few microns.

The solid state detectors will be able to locate vertices to better than $\pm$ 10 microns in the plane of the emulsion sheets and to $\pm$ 0.2 mm along the beam direction. This defines a scanning volume 1000 times smaller than we used in E531, and means that a predicted vertex will certainly fall within one microscope field of view (100 microns x 100 microns at high power), and within $\pm$ 1 emulsion sheets. Finding a predicted primary or secondary vertex under these circumstances will take approximately 4 minutes. As discussed in section D, we intend to select events with charm decays by reconstructing and resolving the secondary vertices with the solid-state detectors. Because

of this very short time required to find a predicted vertex in the emulsion, these electronic predictions of a decay can be quickly verified. Most vertices from secondary interactions will have dark nuclear breakup tracks and can be immediately rejected. Primary vertices will be even easier to find because one has the additional option of scanning along a beam track. B selection does not rely on electronic prediction of a B-decay secondary vertex. However, if the B lifetime is less than the charm lifetime as expected, most B decays will occur in the same emulsion sheet and microscope field of view as the primary vertex, and can be found simply by varying the depth of focus of the microscope.

In order to use the high precision of the emulsion and the solid state detectors the two systems must be registered with each other to an accuracy small compared with the transverse distance between interactions. This was done to $\pm$ 50 microns with the thicker modules and drift chambers of E531 using the fiducial sheet technique [1,2,3]. In this experiment we will expose four 10 cm x 3 mm bands in each module at 1/20 normal intensity (comparable to the integrated beam halo), during which the spectrometer will run with a total interaction trigger. The interactions in these low-intensity bands can be unambiguously identified by both position and event topology; once found, they provide local calibration good to the 6 micron accuracy of the beam detectors.

c. Vertex Detector. The vertex detector locates events in the emulsion, and also plays a key role in event selection by reconstructing more than half of the secondary vertices from charm decay. It consists of 21 silicon strip detectors spaced 0.7 cm apart, with 7 detectors measuring each of 3 projections rotated 60 degrees from each other (x,u,v). Each silicon wafer (fig. 1) has

an active area of 6.0 cm diameter and is only 0.3 mm thick to reduce multiple scattering. In the central 0.6 cm band of each detector every strip is read out separately to maintain 40 micron track pair resolution in the region of high track density. On either side of this central band the charge interpolation technique [9] is used, with pulse height information being read out from taps every 3 to 10 strips, thus preserving the spatial resolution of ±12 microns but relaxing the track pair resolution where it is not needed.

We have studied the track pair resolution performance of this system by generating Monte Carlo events which contain a $B\bar{B}$ pair cascading through $D\bar{D}$ and contributing 10 charged particles, together with an additional (typically) 10 "ordinary" tracks distributed like hadronic interactions at an energy equal to that left over from the $B\bar{B}$ pair. It was then asked what fraction of the charged tracks from B or D decay was compromised by shadowing from the 20 other tracks. It was found that such a track was shadowed (by another track hitting the same or an adjacent strip) in 2 or more views only 4% of the time, and in all 3 views only 0.5% of the time. Shadowing of a track in only one of three views should not present a serious problem since the ionization is being measured, thus signaling the presence of two overlapping tracks.

This reliable performance at high track density is an enormous improvement over drift chamber technology, in which electronic dead time leads to missing or grossly shifted hits for nearby tracks. In areas of high track density drift chamber discriminators refire at regular intervals equal to the minimum track separation so that a hit may not lie on any true track, as shown below:

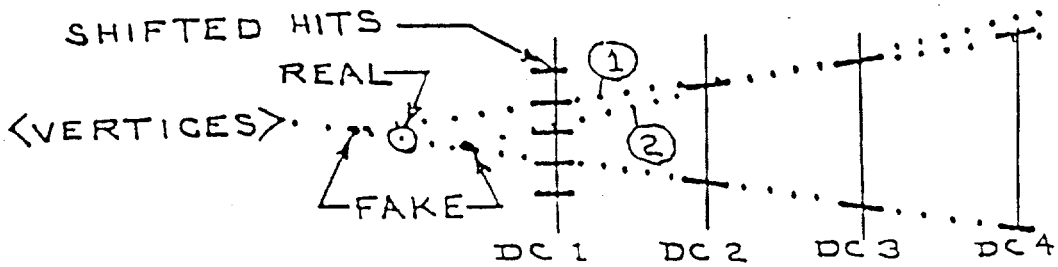

Note that in this example neither hit adjacent to the track in DC 1 is real, so both tracks 1 and 2 are incorrect. From our experience with the drift chambers in E531 it has become evident that most spurious secondary vertices are generated by this effect.

The silicon strip detectors do not refire, have a two-track resolution 50 times better than drift chambers, and reveal multiple tracks by ionization. We believe that this improved performance will allow reliable reconstruction of secondary vertices with a very low percentage of fakes, so that resolving vertices will be limited only by the 12 micron measurement accuracy and multiple scattering. As discussed in Section D, this ability to recognize charm decays with an electronic detector is an enormous advantage in efficient selection of events to be looked at in the emulsion.

d. Charged Particle Spectrometer. In order to achieve maximum aperture and minimum depth we have designed the spectrometer around the small iron magnet shown schematically in fig. 3 and discussed in more detail in Appendix III. This magnet has a pole-piece depth of only 40 cm and allows a vertical (horizontal) aperture from the target of $\pm$200 (240) mrad. By having the pole pieces open vertically outward a transverse kick of 0.20 GeV/c is obtained with a maximum field of 1.7 Tesla; a kick of 0.30 GeV/c seems quite feasible (Appendix III).

The directions of charged particles downstream of the magnet are measured by silicon detectors at small angles and by drift chambers similar to those used in E531 at larger angles (fig. 3). Pairs of drift chamber xuv triplets located 84, 102 and 290 cm from the target cover the full magnet exit aperture. Tracks within 30 mrad of the beam are picked up by two pairs of silicon detector

triplets which cover the region in which the track pair resolution of the drift chambers is inadequate. An additional silicon triplet at 283 cm gives a very long lever arm for very stiff tracks. If one uses the rule of thumb that tracks from B and C decay have transverse momenta around 1 GeV/c, this small-angle system catches tracks above about 80 GeV/c. All downstream silicon detectors are 6 cm in diameter and use charge-interpolation readout with taps every 10 strips.

The momentum resolution of the spectrometer is shown in fig. 5; it is dominated at all but the highest momenta by the constant multiple scattering contribution of $\pm 2\%$, and is still only $\pm 5\%$ at 300 GeV/c.

It is clear that to use the excellent resolution of silicon detectors to full advantage we must build stable mounting hardware and monitor the alignment carefully. Our experience with the much larger apparatus in E531 was that drift chamber positions could be held stable to ± 25 microns over 1-week intervals, and that absolute survey discrepancies between the drift chambers and the emulsion fiducial sheet were ± 50 microns [2]. In addition, we will now have the powerful survey tool of stiff beam tracks passing through the central regions of all the high resolution devices.

e. Charged Particle Identification. Identification of charged particles will use two complementary techniques familiar to us from E531: dE/dx in $Ar-CO_2$ to distinguish particles in the momentum range 5-30 GeV/c, and time of flight for softer tracks.

Even with an 800 GeV/c beam more than 20% of the charged tracks from charm decays have $p < 5$ GeV/c. More than 80% of these soft tracks can be cleanly

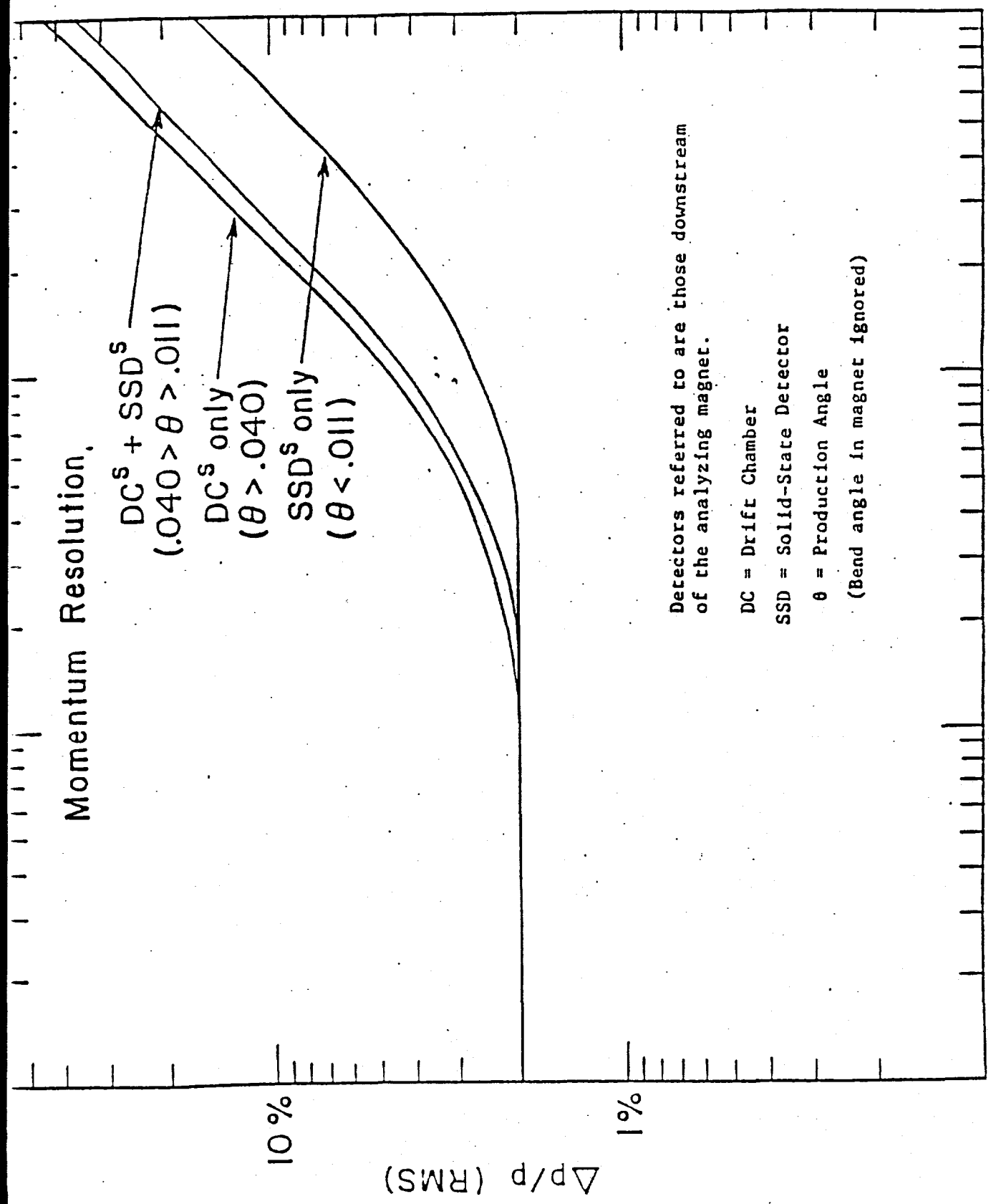
Momentum Resolution
DC^s + SSD^s
(.040 > θ > .011)
DC^s only
(θ > .040)
SSD^s only
(θ < .011)
Detectors referred to are those downstream
of the analyzing magnet.
DC = Drift Chamber
SSD = Solid-State Detector
θ = Production Angle
(Bend angle in magnet ignored)
10 %
1%
Δp/p (RMS)
10
100
P (GeV/c)

Figure 5.

identified in the TOF system over a 3 m flight path for a time resolution of ±65 (±95) picosec for the case of single (multiple) tracks crossing a scintillator. This resolution is a reasonable extrapolation from that achieved in E531 (±100, ±150 picosec) with much larger scintillators. For this experiment, the downstream hodoscope will consist of a bank of 30 Pilot F scintillators 1.4 m long x 4.0 cm wide x 2.5 cm thick, viewed at both ends by phototubes of modest quality. A start time resolution of ±30 picosec is easily obtained with 3 small beam counters upstream of the target.

The dE/dx charged particle identifier (CPI) will identify at least 60% of the B,C decay tracks in the momentum range 5-30 GeV/c. Since the requirement of a short spectrometer limits the available length to 1.5 m, it is necessary to run the chamber at a pressure of 3 atm absolute, and to sample ionization every 1.0 cm along the tracks in order to obtain the necessary resolution. The empirically determined [10] resolution is

$$\sigma_{Emp}\ (FWHM) = .96\ N^{-.46}\ (xP)^{-.32}$$

where N=number of samples, x=sample size in cm, and P is the absolute pressure in atm. For a CPI with 150 1.0 cm samples at 3 atm a resolution of ± 3.4% is reached, allowing a 3 S.D. separation of pions and K's at 30 GeV/c.

The proposed design of the CPI consists of two cells, one on either side of the beam axis, allowing the beam and the unresolvable forward jet from hadronic events to pass through a region with no electric field. Ionization from tracks outside this 10 mrad region is collected on 150 sense wires in each cell. The expected track pair resolution is 6 mm, and the necessary sampling clock speed is around 40 MHz. Possible readout and compaction schemes are discussed in Section 3j.

f. Gamma Detector. The design of the electromagnetic shower detector for electron identification and gamma detection is shaped by the same concerns about high track density which motivated the spectrometer design. A similar solution was chosen: conventional technology at large angles, and solid state detectors at small angles. Ideally, the detector should measure both conversion position and energy for each incoming electron or photon; since fully developed showers are likely to overlap, we have emphasized getting conversion points early in the shower development.

- The detector is located 3.1 m from the target and has an active area of 1.4 m x 1.4 m. The conventional portion consists of alternating layers of lead converter and extruded aluminum proportional ionization chambers (EPIC). A similar device has been used successfully in the second run of E531. The EPIC tubes will have a cross sectional area of 1 cm x 1 cm, and will be run at a pressure of 10 atm. To measure accurate and unambiguous conversion points the first three sections of the detector will each consist of a 1.5 radiation length (r.l.) converter followed by three crossed planes (xuv) of EPIC tubes. The remaining 9.0 r.l. will consist of 1.0 r.l. converters each followed by one EPIC plane (x or u or v). Tubes in this section will be ganged longitudinally, with all corresponding wires from each projection summed and read out in common. The number of data lines for this conventional detector is 1320. Because of sharing of shower ionization between adjacent tubes we expect a position resolution of $< \pm 1.5$ mm. An energy resolution of $\delta E/E = 0.30/\sqrt{E}$ has been achieved by similar devices using multiwire proportional chambers at 1 atm with 1 r.l. sampling [11]. The factor 10 increase in pressure should improve this value to $0.20/\sqrt{E}$.

Masking of one shower by another grows rapidly more serious at small angles. Beyond 3 cm from the beam, however, monte carlo studies based on bubble chamber events [12] indicate that 98% of the showers will be separated by 2 or more tube spacings in this conventional detector.

One third of the gammas from pi zero decay are less are less than 3 cm from the beam at 3.1 m. The conversion points (and a rough measure of the energy) of these small angle showers will be obtained by a miniature gamma detector placed just upstream of the conventional one. This detector, 6 cm in diameter, will consist of alternating layers of tungsten and silicon wafers with 1 mm strip spacing, using a pattern of radiators and rotated planes similar to that in the large detector. Because the wafers are so thin the device is quite dense, and the shower spread is small. To estimate this shower size the monte carlo program "EGS" was used to generate electron-induced showers. Ten slabs of lead [13] 5.6 mm thick, each followed by an empty space of 3.0 mm represented the detector. Fig. 6 shows the average number of charged particle crossings (from 10 showers) vs. transverse position at the exits of converters 1,3,5 and 9 for incident 25 GeV electrons. At the third space the ionization density is down a factor of 10 from its central value only 0.35 mm from the shower center. These calculations indicate that it should be possible to determine conversion positions to a few hundred microns with such a detector, and to resolve conversion points of showers $\geq$1 mm apart. The losses from masking in this detector will be about 13%, thus maintaining the efficiency

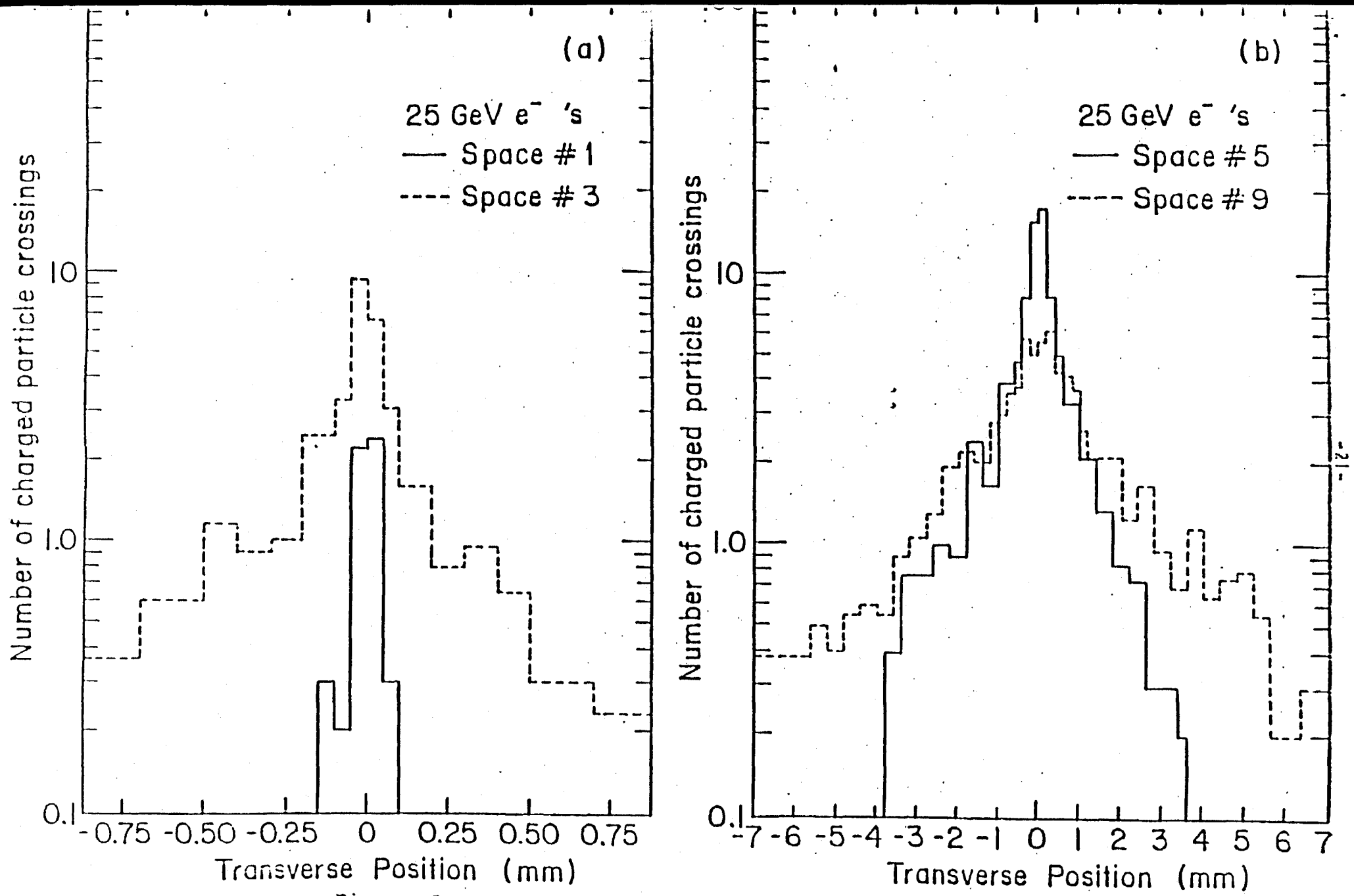

Figure 6. Shower development in the gamma detector after 1,3,5,9 radiation lengths.

of the two complementary detectors at 93%.

g. Hadron Calorimeter. The primary purpose of the hadron calorimeter is to measure the conversion points and energies of neutral hadrons (K^o,Λ^o,n). The position resolution achievable [14] is < $\pm$10 mm, or $\pm$4 mrad at 3.8 m. This angular error makes a smaller contribution to the overall mass resolution than the expected energy measurement error of about $0.7/\sqrt{E}$ for the energies of interest (5-35 GeV).

The proposed detector (fig. 2) consists of alternate layers of iron plates 5 cm thick x 2.4 m high x 3 m wide, and planes of EPIC tubes 1 cm^2 in cross sectional area, operated at atmospheric pressure. The first seven gaps in the iron will be instrumented with pairs of EPIC planes at right angles, with the planes in alternate gaps rotated 45 degrees to give stereo information. The EPIC tubes in these gaps will be ganged transversely as follows: every wire read out for angles < 60 mrad, adjacent tubes added in pairs for angles between 60 and 120 mrad, and adjacent groups of 4 tubes added for angles from 120 to 240 mrad. The final 9 gaps in the calorimeter steel will be instrumented with one EPIC plane each, with alternate planes rotated by 90 degrees. These planes will be ganged transversely like those in the first 7 gaps, and will also be ganged longitudinally, with all x and all y planes in these last 9 gaps read out in common. In all, 1280 amplifiers are required.

The major difficulty in finding neutral hadrons is separating them from the charged hadron background. Monte carlo calculations indicate [15] that showers produced by 30 GeV hadrons typically have transverse size < 20 mm at a depth of 0.5 collision lengths. We have estimated the masking loss contribution to the detection efficiency by using "boosted" [12] bubble chamber data to

generate charged hadron hits on the front face of the calorimeter. A successful identification is assumed if no other tracks have hits within one wire spacing in any direction. The resulting efficiency is shown in fig. 7 as a function of polar angle θ. On the same plot is shown the K^o angular distribution expected from $B \to D(5\pi)$, with $D \to K^o(3\pi)$. We find that more than 80% of the K^o can be resolved under the assumptions above, and 65% with the more restrictive requirement of two wire spacings between showers.

h. Muon Detector. The muon detector has two functions: to reduce the hadron flux enough to give a manageable trigger rate, and to determine from the reconstructed event whether a given track which has traversed the detector is indeed a muon. The first objective is simply accomplished by requiring enough range of iron; 5 GeV of range should be sufficient (see Section D and Appendix V).

To meet the second objective it is essential to track the muon candidate from the emulsion through the spectrometer, hadron calorimeter and absorber with frequent sampling of position and ionization in the iron to look for evidence of hadronic interaction. It is also very important to make a second momentum measurement after several interaction lengths of iron to be sure that no large energy loss has occurred, and that the correct muon candidate has been tracked through the region of dense hadron showers.

The frequent sampling is performed in the EPIC chambers of the calorimeter. The second momentum measurement is done with a square iron toroid (similar to those in E613) 1.3 m deep and 2.5 m on a side. Assuming low carbon steel (1010 or equivalent), a current of 1000 Amp and 100 turns, one obtains reasonable saturation and a nearly constant magnetic field of 2.0 T. On either

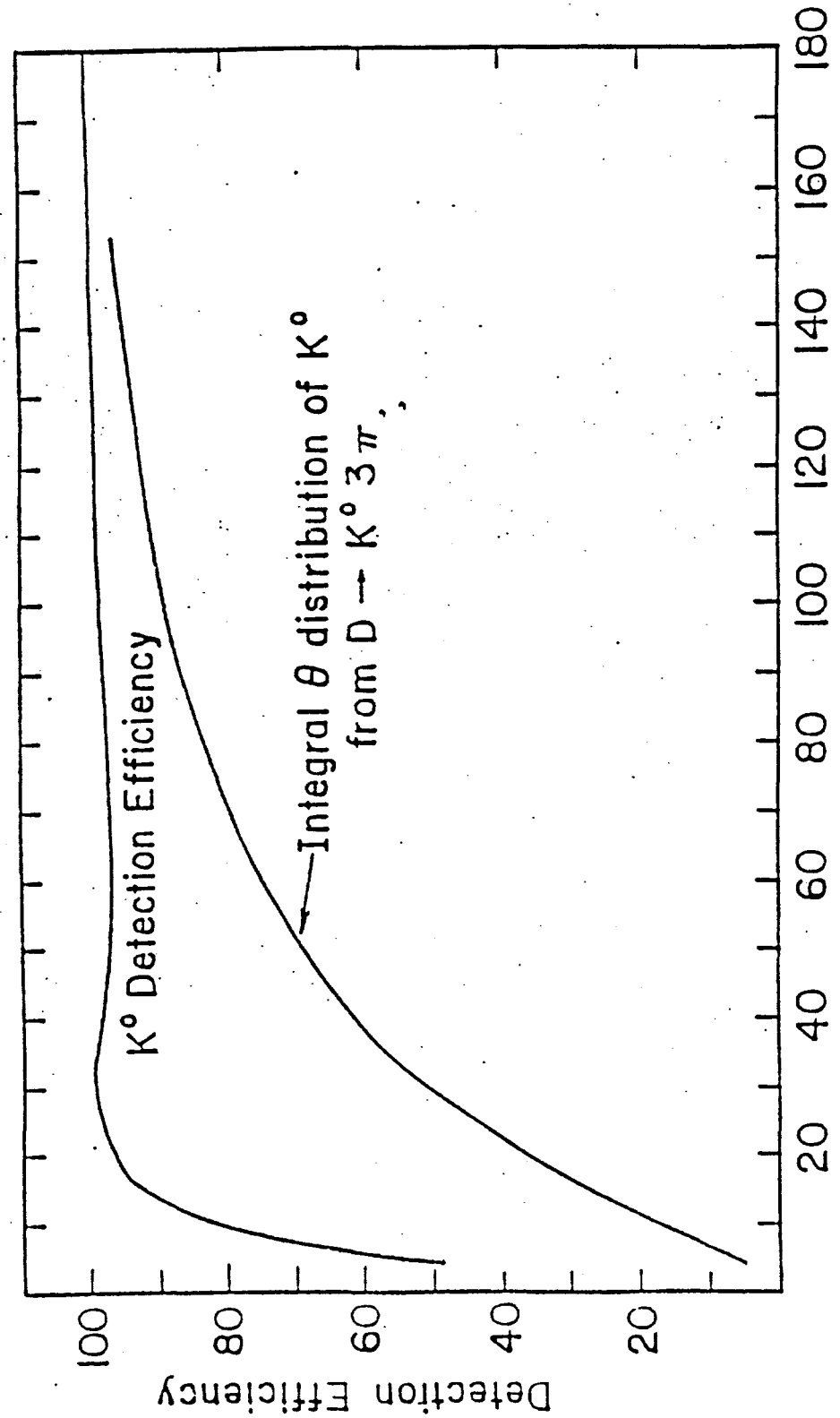
Integral θ distribution (K°) %
Detection Efficiency
100
80
60
40
20
K° Detection Efficiency
Integral θ distribution of K°
from D → K° 3π
20
40
60
80
100
120
140
160
180
θ (mrad)

Figure 7.

side of the toroid are 2 xuv triplets of EPIC chambers instrumented for drift chamber readout using surplus electronics from E531. This system will have a resolution

$$\delta p/p = \left[(.19)^2 + (.01p)^2\right]^{\frac{1}{2}}, \quad (p \text{ in GeV/c})$$

where the first term is the multiple scattering contribution and the second comes from the ± 0.5 mm resolution of the chambers. Downstream of the toroid are two identical modules, each consisting of 0.8 m of steel followed by banks of scintillators (as in E531) to complete the range requirement. Muons of 2.8 GeV will penetrate the toroid, and the downstream absorbers transmit 4.0 and 5.2 GeV respectively.

i. Trigger Counters. Since non-zero data from all events from each spill will be stored in a fast buffer memory, we are studying a variety of triggers, many of which require fast processing before recording on tape. Although several techniques appear promising, we present here only the simplest muon trigger, which should be able to lower the rate of recorded events to about 13 per second. This trigger requires a non-halo beam particle to interact in the emulsion, giving rise to a tagged muon stiffer than 5 GeV. The following sketch qualitatively indicates counter locations:

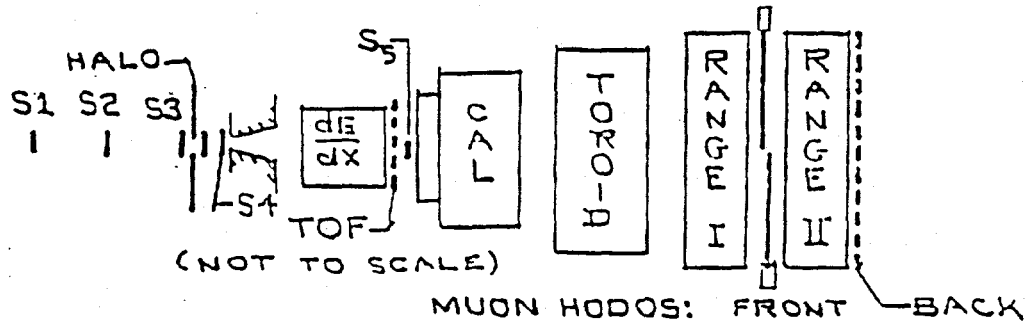

The trigger will consist of

$$\text{Trigger} = (\text{Beam}) \cdot (\text{Interaction}) \cdot (\text{Muon})$$

with components as listed below:

$$\text{Beam} = S1 \cdot S2 \cdot S3 \cdot \overline{\text{Halo}}$$

$$\text{Interaction} = (S4 \geqslant 3 \text{ in pulse height}) \cdot (\geqslant 2 \text{ TOF paddles})$$

$$\text{Muon} = \mu_1 \cdot \mu_2$$

(Note that the TOF hodoscope will have a small hole for non-interacting beam, and also that the muon counters may need shielding against slow neutrons.)

j. Data recording. In this experiment it will be necesary to record information from 9500 solid state detector lines, 520 lines of multi-hit drift chamber wires, 2600 lines of EPIC chambers in the gamma detector and hadron calorimeter, and 300 lines of dE/dx chamber wires. In a 20 second Tevatron spill perhaps 260 events may be recorded. The sheer volume of data necessitates some processing prior to recording on tape, a large amount of buffer storage and use of high density magnetic tape drives.

The solid state detectors (SSD) will be multiplexed in a fashion similar to the proposed Droege system for the Colliding Detector Facility, in which outputs of addressable amplifiers are recorded only if they exceed "table look-up" thresholds. In this way the SSD data should be reduced to typically 1500 2-byte words per event with efficient packing.

The drift chamber multi-hit system already exists and provides efficiently-packed data which will contribute perhaps another 500 words. EPIC chambers may be recorded either with the LeCroy 2280 processor and 12-bit, 48-fold 2282B ADC's, or alternatively with the Droege system. We expect typically 1000 2-byte

words from channels over threshold. More compact recording schemes involving extraction of moments are under study.

The dE/dx chamber in E531 uses CCD pulse height storage and sequential digitization. With the advent of stable flash encoders and inexpensive digital memory it appears feasible to devote an encoder and memory chip to each of the 300 sense wires. We are investigating algorithms to extract the arrival time and integral pulse height of each resolved track from the many time samples of ionization per track obtained from each wire. By compressing time and pulse height information into a single word, the information content from a single event should be reduced to typically 3000 2-byte words.

Such a system may be extended in a natural fashion to encompass more sophisticated trigger processing in the future.

From the above considerations, it is necessary to record (1500+500+1000+3000) = 6000 words per event, or 1.6M words per Tevatron spill. We are developing a fast memory system to buffer several events to smooth ...stical fluctuations in data arrival and permit a more uniform rate of permanent data recording.

The exposure of each emulsion module will require approximately one hour. During this time about one 2400 foot reel of 6250 byte/inch data tape will be written. The system is thus well-matched to high density recording, but we will require at least two such high density drives to avoid reliability problems such as have been experienced by E516.

D. Event Rates and Background

The event rates for $C\bar{C}$ and $B\bar{B}$ pairs have been calculated assuming respective cross sections of 25 microbarns and 50 nanobarns per pair per target nucleon at 800 GeV. (If recently reported preliminary results [16] from CERN are verified, there is a leading particle contribution to B production at the level of a few microbarns, and to charm production at the 100 microbarn level.) To obtain the total number of interactions we use the measured [17] mean free path (MFP) of high energy protons in emulsion, 36 cm, corresponding to a total interaction cross section of 12.1 millibarns per nucleon. For 100 liters of emulsion exposed to a beam track density of 1000 per square millimeter we have:

$$\begin{aligned}
\#\text{int.} &= (\text{thickness/MFP})(\text{tracks/area})(\text{area}) \\
&= (\text{volume})(\text{tracks/area})/(\text{MFP}) \\
&= (10^5 \ \text{cm}^3)(10^5/\text{cm}^2)/(36\ \text{cm}) \\
&= 2.8 \times 10^8 \ \text{interactions}
\end{aligned}$$

The number of charm and beauty pairs present in the emulsion is then

$$\begin{aligned}
\#\ \text{charm pairs} &= (2.8\times10^8)(25\ \text{microbn})/(12.1\ \text{millibn}) \\
&= 5.8 \times 10^5 \ \text{pairs} \\
\#\ \text{beauty pairs} &= (2.8\times10^8)(50\ \text{nanobn})/(12.1\ \text{millibn}) \\
&= 1150 \ \text{pairs}
\end{aligned}$$

The key to success in this experiment is selection criteria for emulsion scanning which have a high efficiency for finding these charm and beauty events.

All of our selection criteria require a muon from charm or beauty decay. We have calculated distributions in lab momentum p and transverse momentum p_T of these muons with a production model in which charm or beauty pairs result

from decay of a heavy parent of mass M which is centrally produced with a distribution

$$d\sigma/dxdp_T = (1-|x|)^n p_T e^{-bp_T}$$

where for charm (beauty) M=4.23 (11.10) GeV, n=4.0 (3.0), b=2.0 (1.0) GeV^{-1}. Four-body decays such as $B \rightarrow D\pi\mu\nu$, $D \rightarrow K\pi\mu\nu$ generate the muons. Integral muon distributions vs. p_T from this monte carlo calculation are shown in fig. 8 for muons from direct B decay, and from directly-produced and B-cascade D's.

Estimation of background depends on reliable calculation of the number of muons from pi and K decay. This calculation, described in Appendix IV, is based on particle production data from the ISR [18] at energies bracketing 800 GeV lab equivalent; it has been checked successfully against an independent approach which starts from a tape of measured 360 GeV bubble chamber events [12]. The resulting muon fluxes from pi,K per interaction per meter of flight path are shown in figs. 9 ,10. The effective decay path of the apparatus is 3.5 meters. We believe that most of the muons from K decay, and some from pion decay as well, can be eliminated offline by comparison of the track slopes perpendicular to the spectrometer bend plane upstream and downstream of the magnet, and by comparison of the momenta determined by the spectrometer and by the toroid. Therefore only the pion contribution from fig. 9 has been used in the background estimates below.

The electronic trigger will require an interaction in the emulsion, plus a muon of more than 5 GeV/c by range. This should reduce the modest interaction rate of 600/sec to a recordable level of about 13/sec. Offline, three types of selection will be performed on reconstructed events to obtain the sample

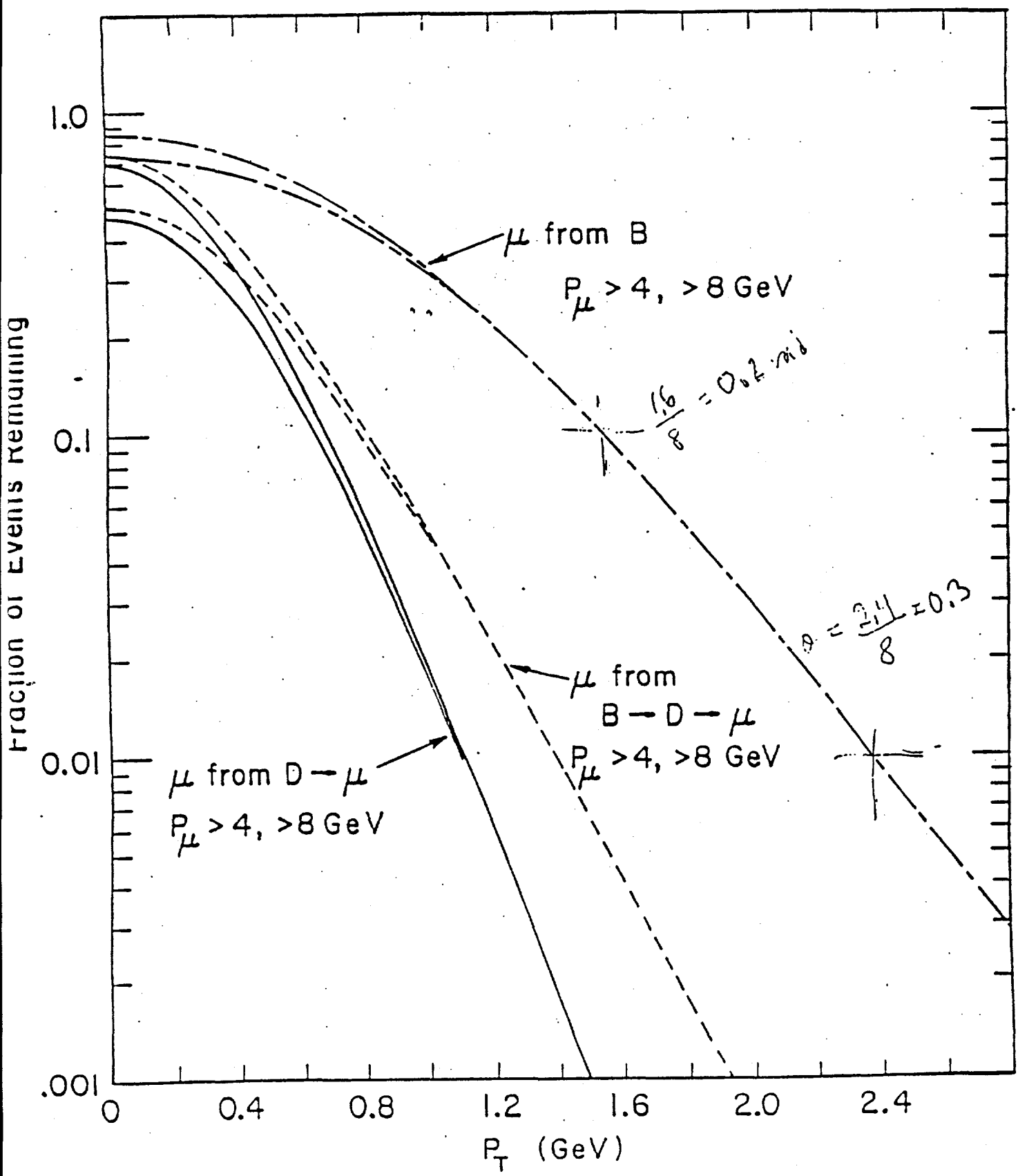
Fraction of Events Remaining
1.0
0.1
0.01
.001
0
0.4
0.8
1.2
1.6
2.0
2.4
P_T (GeV)
μ from B
$P_\mu > 4, > 8$ GeV
μ from B − D − μ
$P_\mu > 4, > 8$ GeV
μ from D − μ
$P_\mu > 4, > 8$ GeV

Figure 8.

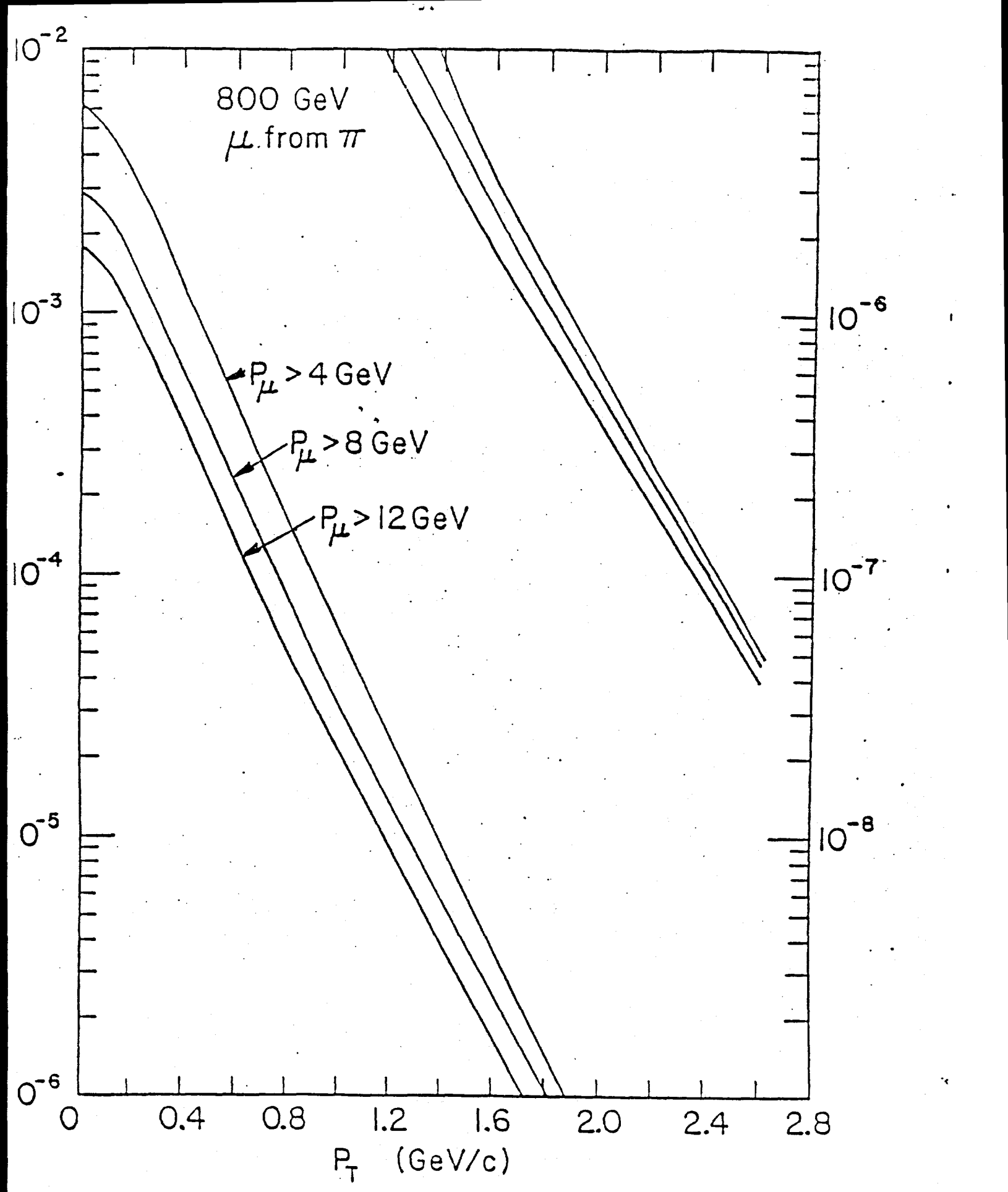

Figure 9. Muons from pion decay, per interaction

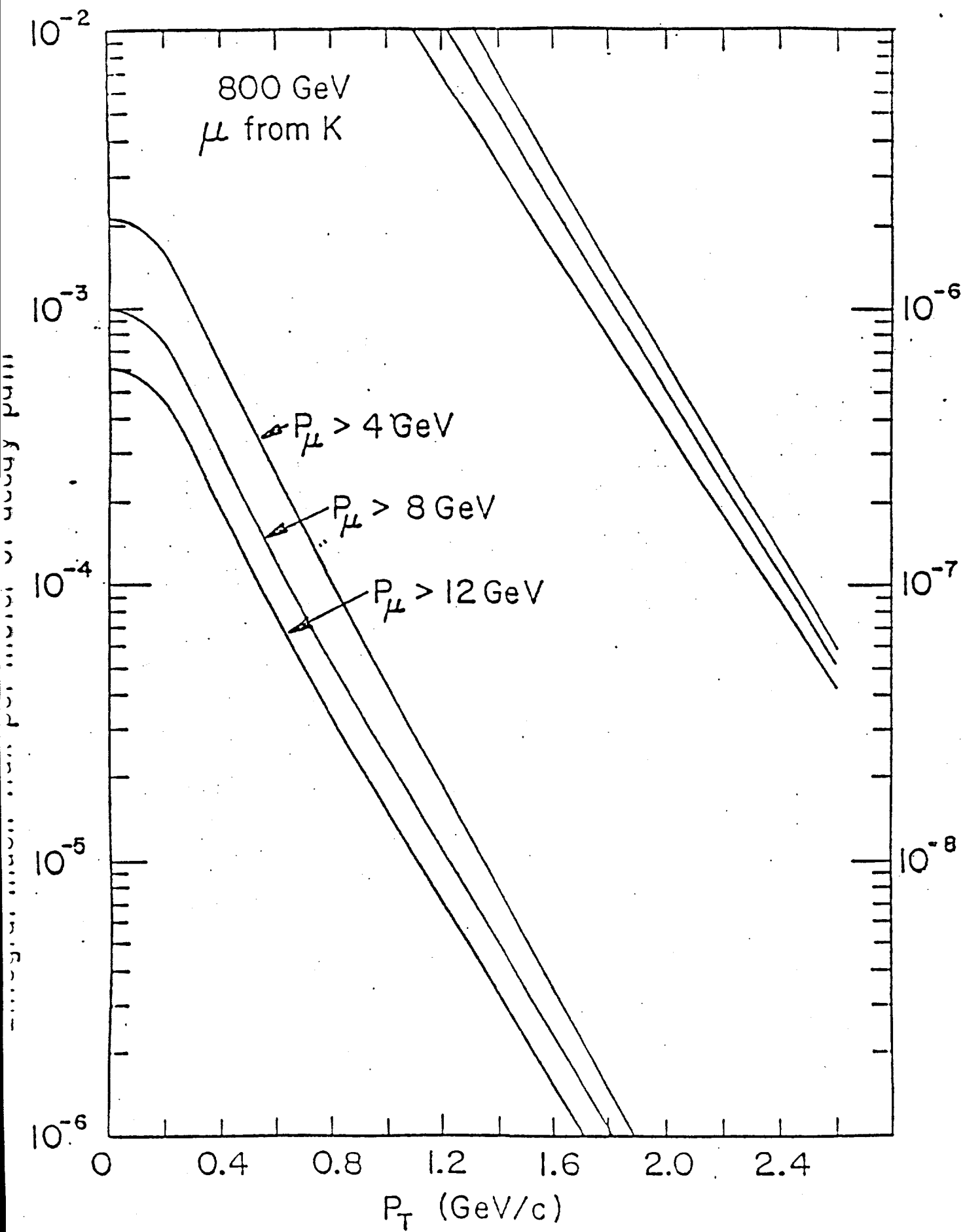

Figure 10. Muons from kaon decay.

to be scanned in the emulsion:

1. Charm Selection. We will capitalize on the excellent resolution of the silicon detectors by requiring an electronically-reconstructed secondary vertex from which a muon of $p > 8$, $p_T > 0.2$ GeV/c emerges. This requirement will pick up not only directly-produced charm, but charm from B decays as well. As shown in fig. 8 , this weak muon cut has an acceptance of 40% (45%) for muons from directly-produced (B-cascade) charm.

We have tested the ability of the vertex detector to resolve secondary vertices with a monte carlo program which simulates multiple scattering in the emulsion and in the silicon detectors, and which generates random measurement errors of ±12 microns at each detector. Multiprong decay vertices can be located to ±7.5 microns in the transverse coordinate and ±220 microns along the parent direction.

Table 1 summarizes the effects of branching ratios and vertex reconstruction cuts on each charmed species. A secondary vertex cut at 4 standard deviations still retains 76% of charged D's and at least half of the others. The abundance-weighted total efficiency for this selection is 0.041 (0.051) for direct (B-cascade) charm.

The yield of directly-produced charm is

$$\begin{pmatrix}\text{Found}\\ \text{charm}\\ \text{pairs}\end{pmatrix} = \begin{pmatrix}\text{Events}\\ \text{in}\\ \text{emulsion}\end{pmatrix}\begin{pmatrix}\text{Muon}\\ \text{cut}\\ \text{survivors}\end{pmatrix}\begin{pmatrix}\text{BR and}\\ \text{vertex}\\ \text{cuts}\end{pmatrix}\begin{pmatrix}\text{Scan}\\ \text{success}\end{pmatrix}$$

$$= (5.8 \times 10^5)(0.40)(2)(0.041)(0.8)$$

$$= 15{,}000 \text{ found charm pairs}$$

The factor of 2 comes from 2 chances of semileptonic decay per pair. The lifetime measurement of one charmed particle per pair is unbiased by this event selection.

Table 1. Data and Assumptions for $C\bar{C}$ Event Selection

Particle	$D^{\pm}$	D^0	F	Λ_c	
Lifetime (10^{-13} sec) (a)	9.5	3.2	2.0	1.8	
BR to μ	0.20	0.07	-0.04	-0.04	
2 - 6 prongs (b)	0.52	0.93	- 0.5	- 0.5	
Fraction passing vertex cut of 4 S.D.	0.76	0.59	0.5	0.5	
Product of BR, prong and vertex cuts	0.079	0.038	0.010	0.010	
Relative Abundance in $C\bar{C}$ Production (c)	0.20	0.60	0.10	0.10	
Contribution to finding $C\bar{C}$ pairs	0.016	0.023	0.001	0.001	Total .041
Relative Abundance in $B\bar{B}$ decays (d)	0.33	0.67	0	0	
Contribution to finding $B\bar{B}$ pairs	0.026	0.025	0	0	Total .051
Contribution if no BR to μ required	0.13	0.37	0	0	Total 0.50

(a) From refs. 2, 3
(b) From ref. 19
(c) Assumes $D^*/D = 3.0$
(d) Assumes $D^*/D = 1.0$

We will also obtain a measurement of the tau lifetime. Assuming 3% of the F's decay to taus, and assuming 10% of the charm sample is F's, we expect 45 taus. This number is reduced to 28 by the smaller efficiency for finding single-prong kinks in the emulsion, as measured in E-531.

The yield of B pairs found from their charm decays is similarly found to be:

$$\text{B pairs found} = (1.15 \times 10^{3})(0.45)(2)(0.051)(0.8)$$

$$= 42 \text{ pairs or } 84 \text{ B particles}$$

where 100% decay of beauty to charm has been assumed. Note that both B-particles in the pair are available for unbiased lifetime measurement.

The main background to real charm decays comes from secondary interactions in the emulsion from which one of the outgoing particles has decayed to give the tagged muon. Calculation of this background is discussed in Appendix IV. The probability of a secondary interaction is 0.165, and the chance of a muon from such an interaction passing the p, p_T and multiplicity cuts is found to be 0.13 times that of a muon from the primary vertex, which is (fig. 9) 1.55×10^{-3} per meter per interaction. The background rate is then

$$BG = (0.165)(.13)(.00155 /m)(3.5 m)(2.8 \times 10^{8} \text{ interactions})$$

$$= 32{,}600 \text{ secondary vertices.}$$

As discussed in the emulsion section, searching the emulsion for a secondary vertex can be limited to one or two sheets and a single microscope field of view, allowing us to look for more than 60,000 such secondary vertices if necessary. Of those resulting from nuclear interactions, 95% can be immediately rejected by the presence of dark tracks from nuclear breakup or recoil [20].

2. $B\bar{B}$ Selection Using a Single Muon with Large Transverse Momentum. This

is the standard type of trigger proposed by many groups. We will require a muon with $p > 8$, $p_T > 1.3$ GeV/c. From fig. 8 ,the fraction of surviving muonic B decays is 0.18. Taking 11% for the BR of B to muons, we have

$$\text{B pairs found} = (1.15 \times 10^3)(2)(0.11)(0.18)(0.8)$$

$$= 36 \text{ pairs, or } 72 \text{ decays.}$$

Each found pair contributes one completely unbiased lifetime measurement and one restricted only in that it is a semileptonic decay.

From fig. 9 , the background is

$$\# \text{ BG} = (2.8 \times 10^8 \text{ int.})(8.5 \times 10^{-6} \text{ muons/m/int})(3.5\text{m})$$

$$= 8300.$$

If the background is unexpectedly high we can, according to figs. 8 and 9, obtain an additional factor of 2.4 rejection at the cost of a factor 1.5 in signal reduction by increasing the p_T cut from 1.3 to 1.5. However, we point out that using a single criterion to cut deeply into both signal and background leads to rate and background estimates which are very model-dependent. For example, our model of muons from B decay gives $(2)(0.11)(0.030)=0.0067$ B pairs surviving the cut of $p > 10$, $p_T > 2$ GeV/c used in Proposal 694. The model used in that proposal obtains 0.022 for this fraction of survivors. Furthermore, our muon background model gives twice as many muons from an 11 m decay path as their model. Model dependence of the very high-p_T tails has thus introduced a discrepancy of a factor 7 in signal to BG, with our model predicting a signal to background of only 1/1000 for the geometry and cuts of that proposed experiment.

We therefore believe it is desirable to avoid relying too heavily on model-dependent selection criteria, especially those which depend totally on a single criterion. For this reason we are investigating a third event selection

Table 2. Summary of Selection Criteria.

SELECTION	FOUND CHARM DECAYS	FOUND B DECAYS	NUMBER TO BE PARTIALLY SCANNED	NUMBER TO BE FULLY SCANNED
Muon with $p > 8$, $p_T > 0.2$ Plus a Secondary Vertex Containing the Muon	15,000 (- 30 taus)	84	47,600*	17,000
Muon with $p > 8$, $p_T > 1.3$	—	72†	—	8,300
Muon with $p > 8, 0.7 < p_T < 1.3$ Plus a Secondary Vertex With no Muon	—	72†	13,000	1,000
TOTAL	15,000	200††	60,600	26,300

* Includes both signal and background

† Half are semileptonic

†† The sum has been corrected for double counting

which loosens the p_T requirement but requires in addition a non-muonic secondary vertex.

3. Selection Using a Muon of Moderate Transverse Momentum with a Nonmuonic Secondary Vertex. Reducing the muon p_T cut from 1.3 to 0.7 would increase the B yield 170% over that of selection 2, while increasing the background a factor of 15. Most of this additional background can be eliminated if it is feasible to reconstruct secondary vertices reliably without requiring a muon from a secondary vertex candidate. From Table 1, the fraction of B-cascade charm surviving the prong and vertex cuts, but without the charm muonic branching ratio, is 0.50. We estimate the number of secondary interactions with the right prong number and visible energy to be about 0.5, giving a rejection factor of (0.165)(0.5)=0.08 beyond the muon cut. It is thus reasonable to expect a yield of B's about equal to that of selection 2, with a background of about 13,000 additional events to scan for decay vertices as in selection 1.

Table 2 summarizes the criteria, yield, and background for each of the selection methods.

E. Identification and Reconstruction of Decays

In order to be used to full advantage in studying charm and beauty decays, an apparatus with a high resolution vertex detector must do more than merely see secondary vertices. It must also be able to distinguish decays from interactions, determine the charge of a decaying particle (nontrivial for short decay distances), and reconstruct and identify its species.

As discussed in Section D, the probability of secondary interactions in

the emulsion is about 17% per event. Of these interactions 5% will have no visible nuclear breakup or recoil and a prong number consistent with a decay [20]. The background of fake single charm decays is thus 0.9%. For 50K event candidates containing 15K charm pairs this background is only 3% of the charm signal, and may be further reduced by other considerations such as visible mass. This source of background is also negligible for beauty decays via charm. In the case of B decays without a subsequent cascade, one also has the strong constraint that the visible mass of the decay must be large, so that only for the very small subset of unconstrained beauty decays without charm cascades is there any significant background.

An interesting problem for detectors with resolution appreciably coarser than emulsion is determining the number of prongs emitted by the decay, and thus its charge and species. There are two reasons for this difficulty. First, when an unseen decay vertex must be deduced by measurement, as happens for decay distances so short as to be barely resolvable, forward-going tracks are often ambiguous in their origin. This familiar problem need not be elaborated. A more serious difficulty arises from the expectation that much of charm production is via resonances such as D*. In the particular case of $D^{*+} \rightarrow D^{o}\pi^{+}$, or of $\Sigma_c \rightarrow \Lambda_c \pi^{+}$, the pion is emitted at a very small angle to the direction of the charmed decay product, typically < 5 mrad at Tevatron energies. Since the average decay distance for such events is about 1 mm, the resolution needed to distinguish the decay vertex from the accompanying pion is 5 microns, easy for emulsion but very difficult for other techniques. If the decay vertex is not resolved from the pion the D^{o} looks like a charged decay, and a Λ_c looks like the decay of a doubly charged object.

An important consideration in fitting events is that more than 90% of

the decays throw off one or more neutral hadrons. To obtain unambiguous assignment of these neutrals to a vertex it is necessary not only to detect them in the spectrometer with reasonable efficiency and precision, but also to know with some accuracy the missing transverse momentum at the decay vertex, which is typically 300 MeV for each neutral. In this experiment (as in E531) we will be able to constrain the direction of the decaying particle because the transverse coordinates of both primary and secondary vertices are measured to $\pm$0.4 microns in the emulsion. Thus for a charmed particle with a typical momentum of 70 GeV/c and decay distance of 1 mm, we can constrain p_T to 0.040 GeV/c. In the case of the proposed streamer chamber or NaI detector experiments, the resolution is about $\pm$20 microns in <u>one</u> transverse coordinate, giving 1.4 GeV/c P_T resolution in that projection and no information at all in the other projection. Thus while most decays in the emulsion can be fit with no combinatorial background, this is definitely not the case for detectors in which only one view is available. We note that in the case of LEBC, which has approximately the same resolution as other proposed Fermilab experiments, only one pair decay has so far been fit from a May,1980 exposure of 600K interactions.

We have made monte carlo studies of the mass resolution and acceptance of our spectrometer for $B\bar{B}$ and $C\bar{C}$ events obeying the production model of Section D. Results for the "typical" decays $B \to D\pi^{\pm}\pi^{\pm}\pi^{\pm}\pi^{o}\pi^{o}$ and $D \to K\pi^{\pm}\pi^{\pm}\pi^{o}$ are shown in fig. 11. A decay is considered to be within the acceptance of the spectrometer if <u>all</u> secondary products, including gammas from pi zero decay, lie within a cone of half-angle 200 mrad. The integrated acceptance for B (charm) is 73% (64%), and is > 90% for Feynman x > 0. For most events the mass resolution is better than 1.2%.

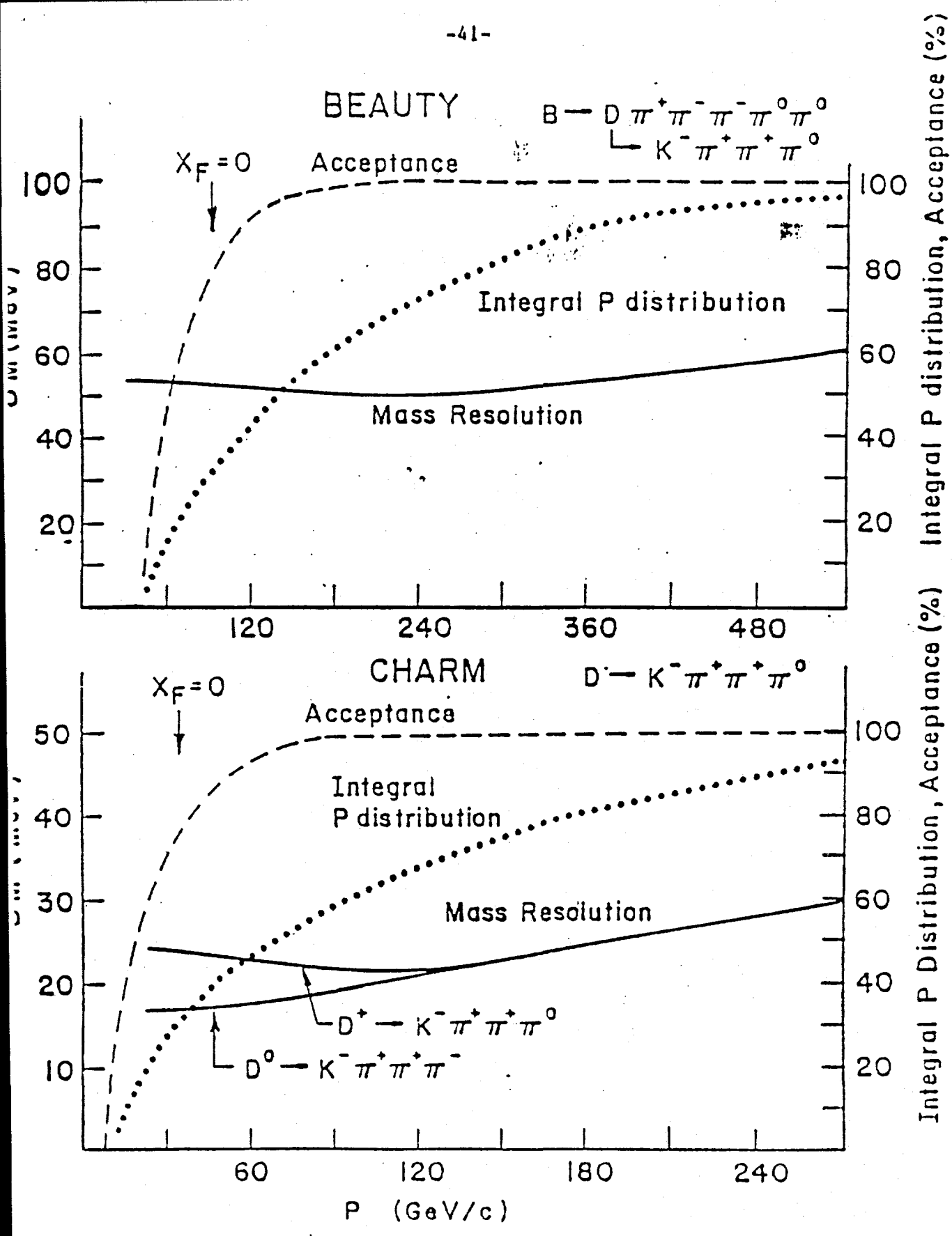
BEAUTY
B — D π⁺π⁻π⁻π⁰π⁰
└ K⁻π⁺π⁺π⁰
X_F = 0
Acceptance
Integral P distribution
Mass Resolution
100
80
60
40
20
120
240
360
480
CHARM
D⁻ — K⁻π⁺π⁺π⁰
X_F = 0
Acceptance
Integral
P distribution
Mass Resolution
D⁺ — K⁻π⁺π⁺π⁰
D⁰ — K⁻π⁺π⁺π⁻
50
40
30
20
10
60
120
180
240
P (GeV/c)
Integral P Distribution, Acceptance (%)

Figure 11.

In addition to those events completely contained in the spectrometer, we can expect to recover events with one or more charged tracks at lab angles > 200 mrad. These slow tracks, typically 1 GeV/c, can be momentum-analyzed by measuring ionization and multiple scattering in the emulsion. The expected mass resolution for charm and beauty decays in this category is about 80 and 190 MeV respectively, and including them increases the acceptance to 80% of all decays.

The acceptance in fig. 11 does not include effects of "pattern recognition" losses such as masking of charged or neutral particles by nearby tracks. These losses are 2% for charged tracks, 7% for gammas, and 30% for long-lived neutral hadrons. Even when these losses are folded in, we still expect more than 65% of all non-leptonic charm decays, perhaps 50% of beauty decays, to be fully constrained, with a negligible (< 5%) fraction of decays having ambiguous fits from combinatorial background. For comparison the fraction of fully constrained non-leptonic multiprong decays in E531 is 54%.

The next question to consider is what fraction of charm decays has the species uniquely identified. We take 5% as an acceptable level of feedthrough. In general, the identification is unambiguous if one or more of the following is true: (a) the resolution in the calculated mass is small; (b) some or all of the decay products are identified by TOF, dE/dx or some other means; or (c) the particle comes from the decay of a resonance such as D* or F*.

If the mass resolution is sufficiently good, no particle identification is necessary to distinguish species because only one kinematic fitting hypothesis is tenable. We have studied the possible ambiguous interpretation of D^+ decays, using for concreteness the $K^-\pi^+\pi^+$ mode and asking how often it could pass for $F \to KK\pi$ or $\Lambda_c \to Kp\pi$. We find that for the 1/3 of events which have

mass resolution better than 10 MeV, only 30% of the generated D's are ambiguous with the F hypothesis, and only 12% are ambiguous with Λ_c. Overall, we find 30% of the events will be cleanly identified even in the absence of particle identification.

However, more than 90% of the charged decay products of charm and beauty have momenta less than 40 GeV/c, and roughly 65% of these can be identified to better than 2 standard deviations by TOF or dE/dx. The majority of charged tracks will be identified for 50% of beauty decays and 75% of charm decays.

The final handle on identifying decays comes from resonance production (D^*, F^*, Λ_c^*,Σ_c). The mass resolution for $D^0\pi^+$, $\Lambda_c\pi^+$ and $D^+\pi^0$ will be of order 2 MeV. We estimate that the backgrounds under the resonance effective mass peaks will be << 5%; it is zero for the 18 D^0 decays from E531. Assuming half of charm production to go via resonances, we have 45% of D^0 and Λ_c and 30% of D^+, unambiguously tagged by this criterion alone.

To summarize, we estimate that 85% of all constrained and about half of unconstrained charm decays can be identified by one or (usually) more than one of the above methods.

CHARM PAIR CORRELATIONS IN HADRONICALLY PRODUCED EVENTS[1]

VITTORIO PAOLONE[2]
Department of Physics, University of California, Davis
Davis, California 95616

Abstract

Preliminary results of charm pair correlations in 800 Gev proton-emulsion interactions at the FNAL fixed target experiment E653 are presented. Specifically the transverse Φ_T distributions of the $c\bar{c}$ system will be discussed and compared with the results of other experiments conducted at lower $\sqrt{s}$ energies.

1 Introduction

The inclusive cross section $\sigma(pN \rightarrow c\bar{c}X)$ for the production of charm is supposedly dominated by the partonic subprocess of gluon-gluon fusion. In the center of mass of the two gluon system the $c\bar{c}$ pair would be produced back-to-back. In the lab frame Φ_T is defined as the angle between the c and the $\bar{c}$ in the plane whose normal is parallel to the incident beam direction. This distribution is a Lorentz invariant and should be strongly peaked at 180 degrees with smearing due to the intrinsic P_t distribution of the internal partons.

2 Azimuthal Angle Distribution

In 1985 the E653 collaboration recorded 5.6×10^6 triggers to tape from 800 Gev proton on emulsion interactions. Only a $\sim 5 \times 10^4$ event subsample based on offline trigger requirements was further scrutinized. Presently $\sim 10\%$ of the emulsion has been completely scanned with ~ 60 charm pair candidates found so far. Approximately 5% of the 1985 data sample has been reanalyzed integrating both the emulsion and spectrometer information.

Presented (figure 1) is a preliminary distribution of the azimuthal angle Φ_T for 30 charm pairs from the 1985 E653 data run. Only pairs where both decays were multiprong or one multiprong and one high P_t kink ($P_t > 350$ Mev) were included. The azimuthal angle should be insensitive to both the dressing mechanisms of the

[1]Work supported by the Department of energy, contract DE-AM03-76ER70191
[2]Representing the E653 Collaboration (See last page)

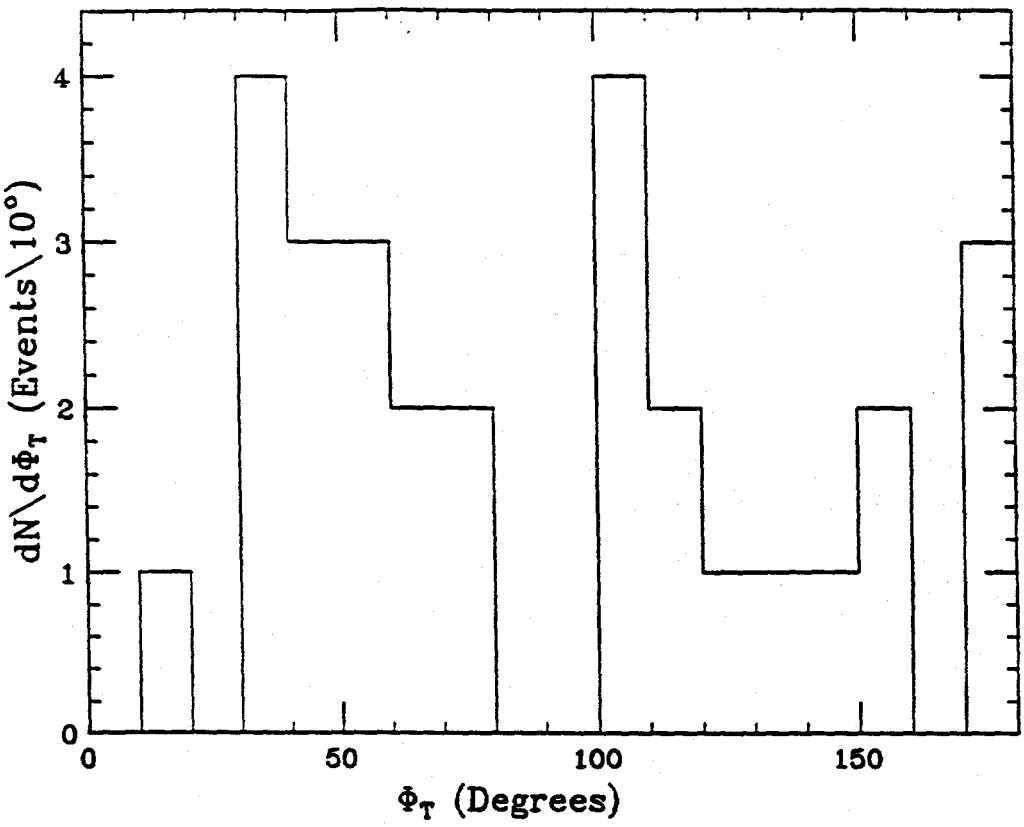

Figure 1: Φ_T Distribution

$c\bar{c}$, and the scanning and reconstruction inefficiencies. As shown in figure 1 no obvious peak can be seen at 180 degrees and also the distribution seems to be equally populated over entire range from 0° to 180°. Typical error on Φ_T is $\sim 15°$.

Comparing the E653 results with NA 27[3] at 360 Gev/c $\pi^- p$ interactions, and assuming the NA 27 distribution is correct, we should expect 21 ± 3 in the bins for $\Phi_T > 90°$. Seen are 14 entries which is only a $\sim 2\sigma$ effect. More statistics are needed to confirm or reject any discrepancies between the two experiments.

[3]LEBC-EHS Collab., M. Aguilar-Benitez et al., Phys. Lett. 164B(1985) 404.

List of E653 Collaborators

N. USHIDA
Aichi University of Education, Kariya 448, JAPAN

R.L. LANDER, A. MOKHTARANI†, V.S. PAOLONE, J.T. VOLK† , P.M. YAGER
University of California (Davis), Davis, CA 95616, USA

R.M. EDELSTEIN, A.P. FREYBERGER, D.B. GIBAUT, R J. LIPTON,
W.R. NICHOLS, D.M. POTTER, J.R. RUSS, Y. ZHANG
Carnegie-Mellon University, Pittsburgh, PA 15213, USA

J.Y. KIM, M.Y. PAC
Chonnam National University, Kwangju 500-070, KOREA

B.R. BALLER, R.J. STEFANSKI
Fermi National Accelerator Laboratory, Batavia, IL 60510, USA

S. TASAKA, K. NAKAZAWA
Gifu University, Gifu 501-11, JAPAN

Y.S. CHOI, D.C. KIM, I.G. PARK, J.S. SONG
Gueongsang National University, Jinju 660-300, KOREA

M. CHIKAWA
Kinki University, Kowakae, Higashi-Osaka 577, JAPAN

T. ABE, T. HARA,T. FUJII, G. FUJIOKA, K. FUJIWARA, H. FUKUSHIMA,
Y. TAKAHASHI, K. TARUMA, Y. TSUZUKI, C. YOKOYAMA
Kobe University, Rokkodai-cho Nada-ku, Kobe 657, JAPAN

J.H. CHO, J.S. KANG, C.O. KIM, K.Y. KIM, J.C. LEE, S.B. LEE, I.T. LIM, K.S. SIM
Korea University, Seoul 136-701, KOREA

Y. ISOKANE, Y, TSUNEOKA
Nagoya Institute of Technology, Nagoya 466, JAPAN

S. AOKI, K. HOSHINO, H. KITAMURA, M. KOBAYASHI, K. KODAMA,
M. MIYANISHI, K. NAKAMURA, M. NAKAMURA, Y. NAKAMURA, S. NAKANISHI,
K. NIU, K. NIWA, H. TAJIMA
Nagoya University, Nagoya 464-01, JAPAN

J.M. DUNLEA‡, S.G. FREDERIKSEN, S. KURAMATA, B.G. LUNDBERG†,
G.A. OLEYNIK†, N.W. REAY, K. REIBEL, C.J. RUSH, R.A. SIDWELL,
N.R. STANTON
Ohio State University, Columbus, OH 43210, USA

K. MORIYAMA, T. SHIBATA
Okayama University, Tsushimanaka, Okayama 700, JAPAN

T.S. JAFFERY, G.R. KALBFLEISCH, P.L. SKUBIC, J.M. SNOW,
S.E. WILLIS*, W.Y. YUAN
University of Oklahoma, Norman, OK 73019, USA

O. KUSUMOTO, T. OKUSAWA, M. TERANAKA, T. WATANABE, J. YAMATO
Osaka City University, Sugimoto Sumiyoshi-ku, Osaka 558, JAPAN

H. OKABE, J. YOKOTA
Science Education Institute of Osaka Prefecture, Karita, Sumiyoshi-ku, Osaka 558, JAPAN

T. ISHIGAMI, M. KAZUNO, M. KOBAYASHI, F. MINAKAWA,
H. SHIBUYA, S. WATANABE
Toho University, Funabashi 274, JAPAN

Y. SATO, I. TEZUKA
Utsunomiya University, Utsunomiya 350, JAPAN

S.Y. BAHK, S.K. KIM
Wonkwang University, Iri 570-180, KOREA

† Present Address: Fermilab National Accelerator Laboratory, P.O. Box 500, Batavia, Il 60510 U.S.A.
‡ Present Address: Univ. of Rochester, Rochester, NY 14627
* Present Address: Northern Illinois University, DeKalb, Il 60115 U.S.A.

APPENDIX B

E687: "High Energy Photo Production of States Containing Heavy Quarks and Other Rare Phenomena"

E687 Proposal

PROPOSAL SUMMARY

We propose to study the photoproduction of states containing heavy quarks, charm and beauty, using a multiparticle spectrometer. The apparatus is similar to that used in E87 and E401, but is upgraded to have a much larger acceptance, better γ and π^o reconstruction capabilities, and a prompt decay vertex detector. To achieve high sensitivity to low cross sections, the experiment must run in a wide band photon beam, preferably the new beam proposed for the Proton East area.

The experiment has two phases:

1. A 500 hour run with a thick target (1 interaction length) and a beam dump. This phase will produce a large sample of dimuon decays of T's and J/ψ's with energies up to 450 GeV and will measure the size of beauty photoproduction through the detection of multimuon final states.
2. A 1500 hour run with an open geometry and a 10% interaction length target. We will collect very large samples (> 10^6) of charmed particle events and will search for specific B-meson and B-baryon final states.

The power of the spectrometer and the flexibility of the trigger scheme we employ enables us to do sensitive searches for completely new phenomena with less bias than other experiments.

This proposal is a logical extension of experiments carried out by members of this group over the past 6 years. In particular, the new spectrometer is designed so that we can take advantage of the powerful and efficient techniques we have used to reconstruct complicated multiparticle final states.

INTRODUCTION

Photons are known to couple to heavy quarks (charm, beauty, etc.) and other new phenomena. In order to take maximum advantage of the Tevatron capability to explore new regions of physics, it is vital to have a versatile multi-particle high rate spectrometer, with quick analysis capability, placed in a high intensity, high energy photon beam.

We propose the construction of such a spectrometer, capable of detailed characterization of the complex final states that will be produced by the interaction of high energy photons and hadrons available at the Tevatron. We would use this spectrometer initially to study photoproduction reactions at energies from 200 to 500 GeV. This energy and intensity regime, which is crucial to our proposed program, is available only in broad band photon beams.

Our basic strategy is to subject a large number of events to very detailed on-line analysis before deciding to record them. This approach allows us to achieve very high cross section sensitivity with smaller biases than other experiments.

This proposal is a logical extension of experiments conducted by members of the group over the last six years. These experiments successfully observed and studied three aspects of charmed photoproduction: J/ψ;[1] D-meson[2] and charmed baryon production[3] (fig. 1). The program is continuing through 1982 with a study of charm production by neutrons, E400.[4] Many of the techniques used in the present detector and the data analysis will be carried over to the proposed detector.

5. muon identifier,

6. a sophisticated triggering scheme and data acquisition system based on hardware which has already been used in experiments by a subset of this group,

7. a prompt decay vertex detector which is being developed for E400.

Section III describes the properties of the beam we require for this experiment. It has been our experience that the techniques that succeed in the study of photoproduction reactions can be extended (sometimes with some difficulty) to the study of hadro-production. We therefore would like this detector to be located in a beam line which can supply either photons or incident hadrons. The new beam proposed for Proton East[5] seems to have ideal properties.

Section IV summarizes the event rates for some of the states we intend to study. For example, the total yield of $\psi(2\bar{2})$, $T(2\bar{2})$, like sign dimuons, and trimuons (from beauty) detected in this experiment will be 2.0×10^5, 250, 5100 and 1200, respectively.

Section V discusses the cost of the experiment, the time scale for construction, the division of responsibilities, and the manpower.

the experiment must provide a sufficiently detailed characterization of the events to allow the separation of elastic and inelastic production. The most natural way to accomplish these goals is to measure the reactions

$$\gamma + p \to \psi + x \quad (\psi \to \mu^+\mu^-)$$

and

$$\gamma + p \to \psi + x \quad (\psi \to e^+e^-).$$

These two decay modes constitute 14% of all ψ-decays and are easy to trigger on. Part of this measurement should be done using a liquid hydrogen target. A simple recoil spectrometer, such as used in E401, capable of measuring the azimuthal and polar angle is sufficient to decide on the elastic or inelastic nature of the event at the target vertex. The elastic events can be used to find the total ψ-nucleon cross section by measuring $d\sigma/dt$ $(t = 0)$ and using the optical theorem. Finally, the ψ signal provides an excellent calibration for a new spectrometer.

The photo-production of the ψ' has been barely observed at low energy. The higher yields that we can achieve should allow us to observe several hundred examples of $\psi' \to \mu^+\mu^-$, e^+e^-, $\psi\pi^+\pi^-$. Detailed comparisons of the ψ and ψ' cross sections will be quite interesting.

T-production

T-production confronts the same physics as ψ-production except that the mass and charge of the constituent quark are now different. Even though the cross section is very small, by running at the high intensities and energies available in a wide band beam a few hundred examples of $T \to \mu^+\mu^-$, e^+e^- can be obtained. This sample is roughly the size of the earliest ψ-photoproduction samples at Fermilab from which much was learned. In particular, the order of the cross section would provide a check of production models of

Charm production

Much has been learned about charm from measurements at e^+e^- machines, in photon beams and in hadron beams. Several powerful detectors, including Mark III and the Fermilab Tagged Photon Lab spectrometer, will have results before this experiment will run. Nevertheless, information on charm has been extracted only slowly. It is our thesis that the study of charm is a much easier task than the study of beauty and is therefore worth doing carefully. Given the complexity of beauty spectroscopy, we may well have to rely on our knowledge of charm to learn how heavy quarks behave. We present here a partial list of open questions which could be answered by the large accumulation of charmed events - of the order of several million - that we can achieve. We are confident that many of the answers will still be unknown at the time we begin this experiment and that new questions will arise as new results come in. A list of topics which this experiment could investigate are:

F-decay modes (including those involving τ's) D_S

Decay modes of charmed baryons Λ_c, Σ_c, and Σ_c^*

Masses and decay modes of baryons bearing both charm and strangeness

Lifetime measurements

Cabibbo suppressed hadronic decays

Cabibbo suppressed semi-leptonic decays

Better limits on possible violations of the "standard theory" of weak decays of charmed particles

Details of production mechanisms

Rare decays

Exotic four-quark charmed mesons

for new physics. We will be sensitive to a wide variety of new phenomena in an unbiased fashion, avoiding dependence on any specific production mechanism.

Downstream of M2 are located additional Cerenkov counters, proportional chambers, an electromagnetic calorimeter, a hadrometer, and a muon detector. These are described in more detail below.

There are two separate phases of this experiment. The first uses a thick, segmented target and a beam dump. The physics objectives of this part of the experiment are prompt dimuon and multimuon production. The target and dump arrangement is shown in fig. 5. The second phase is an open geometry experiment with a 10% interaction length target. For this phase, we would use a thin beryllium target. Finally, we will have available the liquid hydrogen target used in E401 to make a brief measurement of ψ production on protons since we feel that the topic of elastic ψ-photoproduction needs additional investigation.

$\gamma p \to \psi p$

Tracking system

The tracking system is based on 5 sets of multiwire proportional chambers, P0-P4, which measure tracks which are not swept out by M1. Pattern recognition will be done using the wire hit information only, with drift time being used to provide higher resolution in track fitting. Two additional upstream sets of chambers, P-2 and P-1, will extend the acceptance down to particles of momentum 1GeV/c. Details on the sizes, wire spacings, and numbers of wires in the chamber system are given in Table II. (Additional tracking information will come from the prompt decay vertex detector described below.)

The first chamber, P-2 will be located directly upstream of M1. This chamber will have 3 planes, x, v, and u. The next chamber, P-1, will be placed inside of M1. It also will have 3 planes, x, v, and u. These planes will measure the non-bend view (x) and $\pm 11^{\circ}$

For our previous experiments, (E87, E401, and E400) we have developed such a set of tracking routines which work very well in conjunction with our present chamber system. We can routinely reconstruct a hundred complex events per second on the Cyber 175, and have also adapted these routines for use in the M7. The program is based on using only the hit information for pattern recognition (i.e., using the chambers as proportional chambers); higher precision is obtained by incorporating drift time information at a later stage after the tracks have been identified. The routines find projections in each of three different views, and then match up the projections to find tracks. They move sequentially through different categories of tracks, (tracks going all the way through the spectrometer, tracks going through the first magnet only, etc.) eliminating the hits on the found tracks at each stage.

The proposed experiment will use extensions of these same techniques. We will still use the chambers as proportional chambers to do the pattern recognition, and have adjusted the wire spacings in the various planes accordingly. However, we expect to obtain even better drift information than we have in the past and thus achieve resolutions of 200μm or better when we fit the tracks. Moreover, the addition of a fourth view will provide an additional constraint on the tracks, and will allow us to deal with higher multiplicities. Finally, the information from the small chamber near the target will provide a powerful constraint in the later stages of the pattern recognition.

mirrors present very little material to the particles passing through the spectrometer. C3 is a counter that has been used in E87 and E401, and is being upgraded for E400. It uses spherical mirrors to reflect light directly onto photomultiplier tubes.

This system allows complete particle identification for momenta from 10 to 40 GeV/c. Between 4 and 10 GeV/c, one can separate pions from Kaons and protons. Identification of protons extends up to 75 GeV/c. For some phases of the program, it might be useful to extend the particle identification to even higher momenta. One way to accomplish this would be to fill C3 with pure helium. The resulting threshold momenta would be 18, 63, 110 GeV/c for π, K, and p, respectively.

Photon-Electron identifier

Two electromagnetic shower counters are required to identify photons, π^0's and electrons. The acceptance of the neutral detector is matched to the acceptance for the charged particles. One shower counter will be immediately downstream of P2 and upstream of M2, and the second shower counter will be placed behind P4.

In order to cover the entire charged particle acceptance, the shower counters must be able to withstand megacycles of 100 GeV electrons. Presently, we plan lead-scintillator sandwich shower counters with high spatial resolution. The expected energy resolution is $15\%/\sqrt{E}$. The ½" thick scintillator strips will be placed after each radiation length of lead and will be read out by wave shifter bars. Two wave bars will be used for each set of strips to longitudinally divide the counter and to aid in the identification of electrons. A position resolution fo 4mm is obtained by measuring the energy deposited in 2½mm scintillator strips. The strips are

a neutron or K_L^O identifier. However, the calorimeter was still quite useful in electron and muon identification. For this Tevatron experiment we want the additional capability of identifying neutral hadrons. To accomplish this goal, the detector must be more finely divided.

The new detector's configuration will have 5" wide strips, horizontal and vertical. Parallel strips at the same level, but different layers, will be read together by wave shifter bars. The hadrometer will be divided in two longitudinally to observe shower development. A diagram is shown in figure 8.

Alternatively, the calorimeter currently being used by E609 might be reconfigured to match our required dimensions.

Muon detection

As with the electromagnetic detectors, there are two separate regions of muon detection, depending on whether the muon passes through the aperture of M2 or not.

Muons passing through the aperture of M2 (±45mr) are identified by their ability to penetrate the electromagnetic detector, the hadrometer, and two blocks of iron at the end of the spectrometer. There is one block of 6' x 8' x 2', followed by a 2' gap, then a 6' x 8' x 6' block. The gap between the blocks contains an array of scintillation counters and two planes of proportional tubes, one with horizontal wires and one with vertical wires. After the last block, there is another set of X-Y proportional planes and a scintillation hodoscope. The proportional tubes give a ½" cell size (1" half-lapped square tubes). Their purpose is to permit the reconstruction of muon trajectories for the higher level triggers. The scintillation counters are used in the lower level triggers.

buffer during a spill with a deadtime of about 6%. This system has run smoothly through two experiments, E87 and E401. The data is leisurely copied through the on-line computer to magnetic tape between spills.

For E400 we are rearranging the system to cut the cycle time to 500ns. By running four systems in parallel we will gain a factor of four in speed. This will allow us to increase the buffer size by a factor of eight to half a megaword without increasing our deadtime.

In the Tevatron era, with a 10-second spill, we will be able to continue this approach. The only change we need to make is in the on-line computer software. By treating the memory as a ring buffer, we can copy the data to magnetic disk during the spill without increasing the deadtime. The inter-spill period is also longer, though not by the same factor of ten. At 1600bpi, 45 inch per second tape speed, and 45% loss to inter-record gaps, we wrote our 64K words to tape in about 4 seconds. Using a 6250bpi drive and increasing the record length (to decrease the fraction of tape lost to inter-record gaps), but leaving the tape speed the same, would allow us to read 0.5Mwords in 5.4 sec in E400, or 5.Mw in 54 sec at the Tevatron. Thus, we could record the entire data set on tape if we wanted to. A faster tape drive would ease the crunch a bit. However, at 5.Mw per minute and about 60Mw per tape we would be changing tapes every 12 minutes. We have no intention of writing five tapes per hour, although the data acquisition system could handle the rate with a readout deadtime of only 6% during the spill.

Triggering scheme

The power of our triggering scheme lies in its essentially unlimited flexibility, which gives us tremendous latitude in adjusting the acceptance criteria. Any knowledge gained from our experience or from other experiments can be directly incorporated in the trigger. Early stages of the trigger apply very loose cuts, while later stages, in which the full processing power of the M7[8] is brought to bear on large numbers of events, permit us to apply in the trigger many of the cuts which are usually applied to the data off-line.

The primary trigger will be a simple cabled trigger, sensitive to much of the total cross section. We will run with MHz rate at this level. Second level triggers allow us to impose somewhat more detailed criteria. For example, we will be able to ask for a muon, signaled by a detector deep in some steel; a heavy particle, signalled by a scintillator firing without corresponding Cerenkov light; or an electron, signalled by energy in an electromagnetic shower counter. Additional cuts at this level can include rough multiplicity requirements.

The tertiary trigger decisions will be made by the M7 trigger processor. The M7 is a stored program computer which will have access to a subset of the event record directly through interfaces to the experiment. We have demonstrated in E401 and through simulation of E400 that a 50μsec calculation in the M7 can refine the straight hardware triggers of the lower levels. Simple pattern recognition is the most probable application. We can crudely match bend angles with Cerenkov cells to improve the heavy particle triggers. We can calculate dimuon masses or single muon transverse momenta to select more exciting events of those categories. Strike-shower correlations can help distinguish electron and photon showers.

The typical minimum projected angle between tracks which will be detected in the spectrometer is greater than 10mr. These tracks will usually be separated by more than four wires when they reach the first plane of the high resolution detector. With the help of the downstream chambers P$\bar{0}$, P1, and P2, which can resolve projected angles as small as 2mr, we believe we can resolve tracks with projected angles as small as 4mr in the high resolution chamber.

A vertex detector can be made to separate the primary production vertex from a decay vertex if the transverse measurement, L, of these vertices is less than speed of light, c, times the mean lifetime, τ, of the decaying particle, that is $L \lesssim c\tau$. The $c\tau$ values of interest are D^o = 30μm, F^+ = 60μm, τ^- = 60μm, Λ^+ = 60-90μm, and D^+ = 300μm. The transverse location of the primary production vertex or the decay vertex will be measured to 60μm in our detector. Such a measurement is quite adequate to distinguish the D^+ decays from the "tagged" charm events. But, the measurement is marginal for the F^+, Λ^+, and τ^-, and not sufficient for the D^o.

During E-400 we will gain experience in using these chambers. Following E-400 we will evaluate the performance and consider possible upgrades. It does seem possible to improve the resolution by a factor of (2-4) by using the minidrift system we presently use for our downstream MWPC and by adding 1% Xenon to the chamber to lengthen the drift time. These upgrades would allow a separation of the D^o F^+, Λ_c^+, or τ^- decay vertex from the primary vertex and would provide additional sensitivity for the observation of beauty decays. Another possible use of the chamber would be to incorporate it into the trigger. Our E7 trigger processor could read out the wire information and search for events in which there were two vertices. This scheme would provide a unique way of separating charm and beauty decays from the background

small demand on proton intensity ($<<10^{12}$ protons/pulse). It should be possible to debug the detector using negative pions. Finally, the spectrometer we propose is very powerful and it makes sense to locate it in an area where it can be used in several different kinds of incident particles. (The proposed beam can be operated as a π^-, p, n, γ or e^- beam.)

For the photon beam intensity, we used the number given in the beam design report:

# of photons of energy $E_\gamma > 200$ GeV = 4.5×10^7/pulse.

The acceptances were calculated by assuming that the b and c quarks are excited by a gluon-fusion or diffractive-like mechanism (fig. 2). The essential characteristic of this kind of production is the creation of a fast-forward pair of heavy-quark-bearing particles that have essentially the total energy of the incident photon. The invariant mass of the pair is strongly peaked toward the production threshold. These properties are characteristic of the charm events observed in E87.

The acceptances quoted in Tables IV and V are based on the requirement that the track reach the proportional chamber station P2. In fact, we expect that it will be possible to reconstruct tracks that are swept out of the acceptance before they reach P2, but pass through P-2, P-1, and P0. This lowers the momentum cut-off of the spectrometer to $\sim$ 1 GeV/c and increases all acceptances to virtually 100%.

The rates projected in Tables IV and V clearly demonstrate that large samples of ψ's, D's and Λ_c's will be obtained. Thousands of events will be observed in any decay mode whose branching fraction is $\gtrsim$ 0.1%. Experiment 87 was able to observe significant signals (fig. 1) despite the presence of large backgrounds from hadron contamination in the old broad band beam. The absence of this contamination in the new beam will result in extremely favorable signal to background ratios. Similarly, the event yield calculations show that large samples of Υ and multilepton events will be obtained to study the general characteristics of b-quark excitation.

If it turns out that the B lifetime is $\sim 2 \times 10^{-13}$ then our chances of directly observing the sequential decays in the prompt vertex detector are excellent and this should allow us to overcome even the most severe backgrounds. If any decay mode with a particularly striking signature, for example the much discussed $\psi K\pi$ mode, is substantial this would also improve our chances.

TABLE I: DETECTOR GEOMETRY

Device	Z position	Transverse dimension
Target	0	
P-2	24"	4" x 4"
Front M1	36"	24" x 48"
P-1	66"	16" x 40"
Back M1	96"	
P0	116"	30" x 60"
P1	186"	40" x 60"
P2	266"	60" x 90"
Front M2	330"	36" x 36"
Back M2	402"	
P3	420"	40" x 60"
P4	600"	60" x 90"

$P_{\perp}$ M1 = 1.0 GeV

$P_{\perp}$ M2 = 0.5 GeV

Division of responsibilities

Fermilab would provide:

1) the two magnets, power supplies, shield plates, stands,
2) muon steel (all of which can come from the present setup),
3) calorimeter steel (existing hadrometer steel can be used),
4) liquid hydrogen target and refrigerator (existing E401 target),
5) on-line computer,
6) some PREP electronics in addition to PREP electronics already assigned to E400.
7) some support structures for the electromagnetic calorimeters,
8) calibration dipole (AN421) from existing experiment.

The experimenters will provide all detectors described in Section II of this proposal together with support electronics and cabling. The experimenters will provide all special computer interfacing and memory extensions external to the online computer system.

Costs

The costs of the various detectors are summarized in Table VI. As can be seen, extensive use will be made of existing equipment developed in our previous and current experiments. The major expenditures are for the new multi-wire proportional chamber system and for the new shower counters.

TABLE III: CERENKOV PROPERTIES

Counter	Radiator material	Length	Threshold momenta π/K/p	Photo-electron yield (B = 1)	Number of cells
C0	Isobutane	10"	2.5/9.0/17.0	8.8	30*
C1	N_2	60"	5.75/21/39	9.6	30*
C2	20%N_2 + 80%He	80"	10.8/38.7/73.4	4.0	30*
C3	20%N_2 + 80%He	170"	10.8/38.7/73.4	8.5	30
C3**	He	170"	16.5/59/112	3.6	

* 1 or 2 cells may consist of densely packed clusters of 3/4" PMT's as shown in fig. 6.

** Alternative use for high momentum tracks.

TABLE V

EVENT YIELD (Open Geometry Phase)

Final State	Cross Section/ Nucleon	Total Event Rate/Pulse	Total Event Yield (1500 hours)	Acceptance*
Total hadronic final states	120μb	3×10^4	2.7×10^9	--
Total charm	1μb	250	2.25×10^7	90% (3-4 trk)
Total charmed mesons	670nb	170	1.5×10^7	90% (3-4 trk)
Charmed baryons	330nb	80	0.75×10^7	90% (3-4 trk)
Total Υ	30nb	7.5	6.75×10^5	--
$\Upsilon \to \mu^+\mu^-$	4.2/nb	1.0	9.0×10^4	95%
Total B	2.5nb	0.63	5.6×10^4	60% (6 trk)
Total T	70pb	0.017	1600	--
$T \to \mu^+\mu^-$ **	5pb	0.00119	110	70%
Total trimuons from B's	16.8pb	0.0042	375	80%
Total quadrimuons	0.46pb	0.0001	10	50%
Total like-sign dimuons	70pb	0.017	1600	85%

* Lower limit. Does not include classes of tracks which are reconstructed in less than 5 chambers.

** Integrated mass resolution on the T is 70 Mev (σ).

FIGURE CAPTIONS

1. Representative results on charm particle production by photons from E87 and E401.

   a. Charmed Baryon production

   b. D-meson production

   c. J/ψ production

2. Gluon fusion model production for bare beauty and upsilon production as a function of photon energy.

3. Preliminary results on the energy dependence of J/ψ photoproduction from E401.

4. Layout of proposed experiment (open geometry configuration).

5. Layout of target region for dump configuration.

6. Cerenkov counter cell arrangement to be used in regions of highest track density.

7. Electromagnetic shower counter.

8. Hadrometer.

9. Prompt decay vertex detector.

10. Photon spectrum of proposed wide band beam.

FIGURE 2a.
GLUON FUSION MODEL PREDICTION FOR BEAUTY PRODUCTION

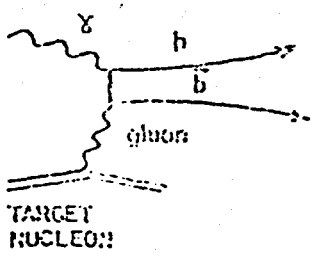

FIGURE 2b

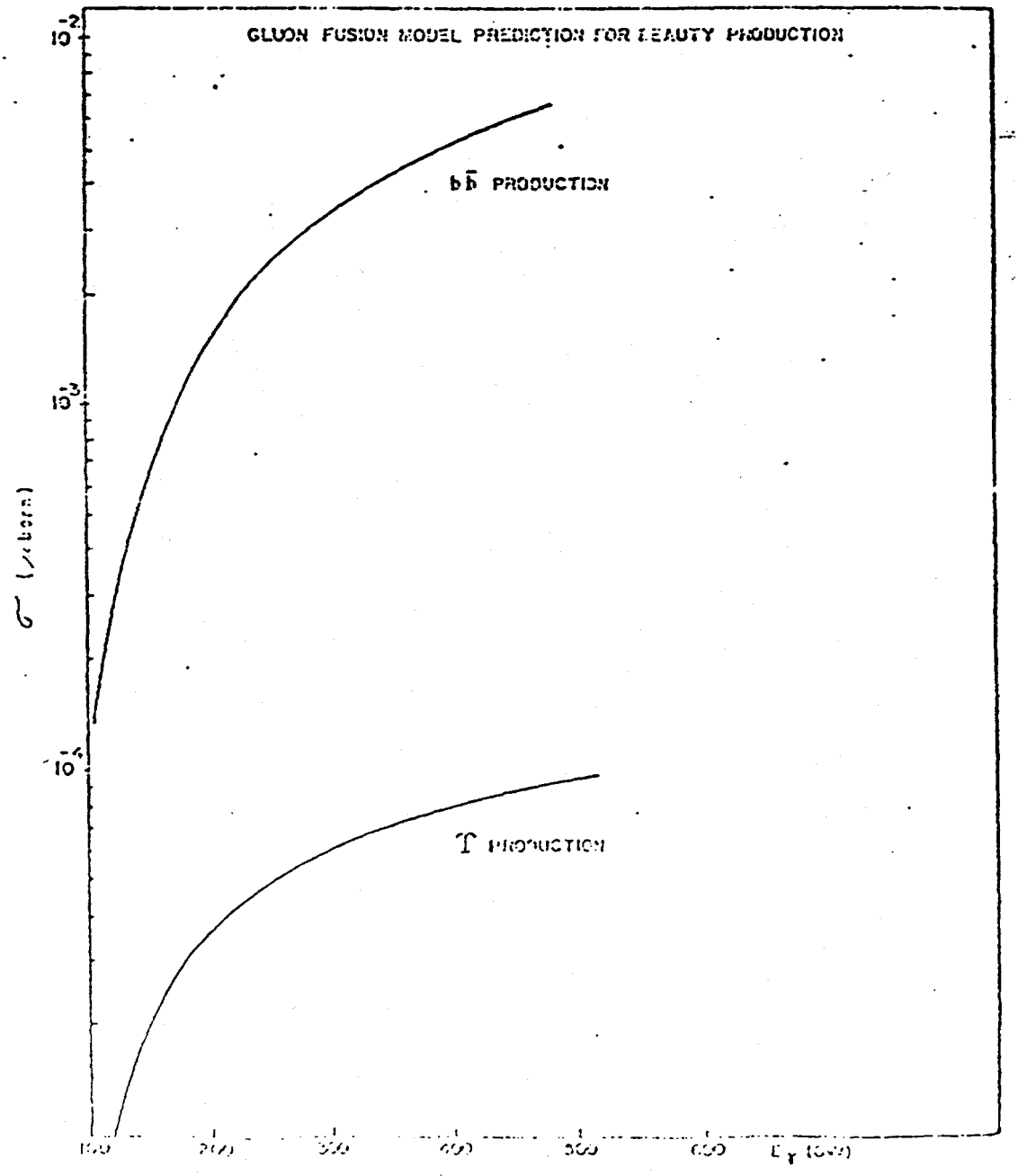

FIGURE 4

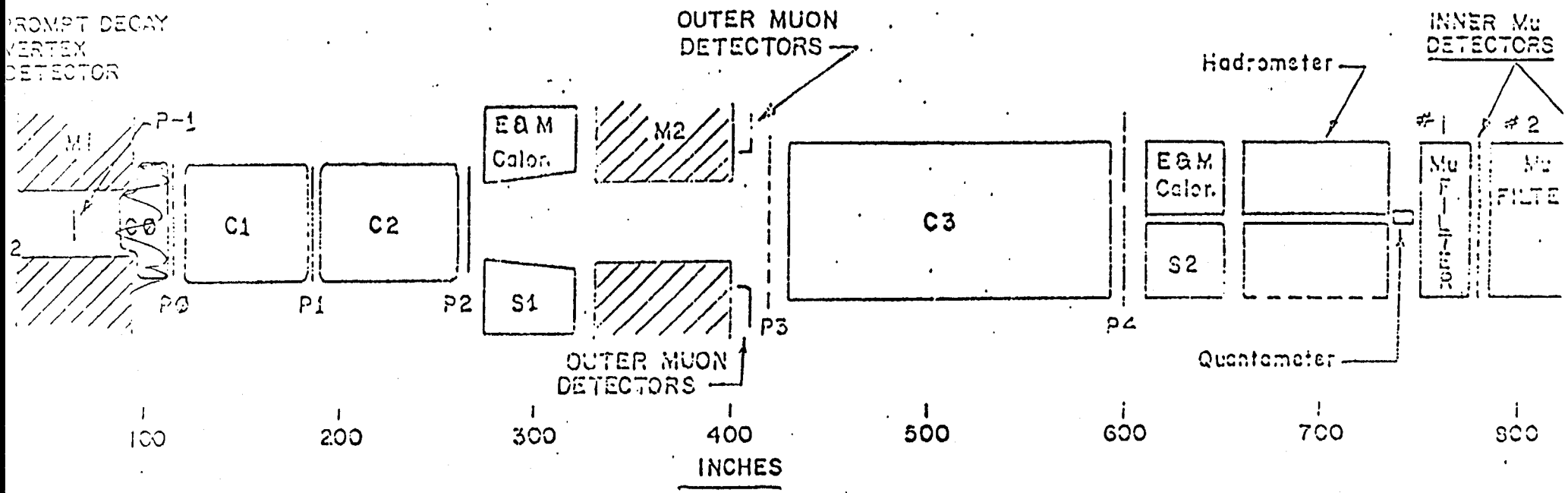
PROMPT DECAY
VERTEX
DETECTOR
OUTER MUON
DETECTORS
INNER Mu
DETECTORS
Hadrometer
M1
P-1
E & M
Calor.
M2
C1
C2
C3
E & M
Calor.
S2
S1
P0
P1
P2
P3
P4
OUTER MUON
DETECTORS
Quantometer
#1
#2
100
200
300
400
500
600
700
800
INCHES

FIGURE 6

CERENKOV COUNTER CELL LAYOUT

FOR HIGHEST DENSITY REGION

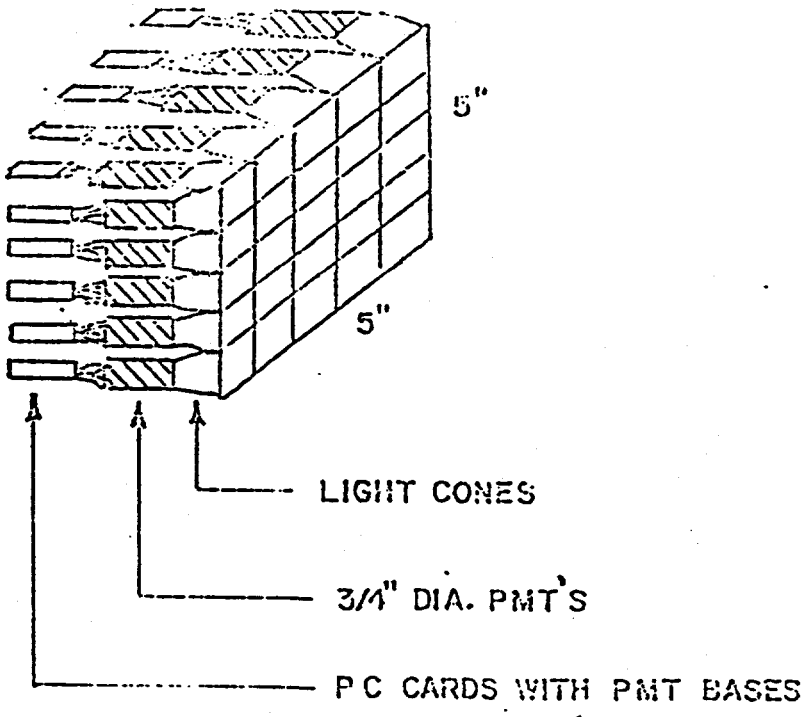

FIGURE 3

HADRON CALORIMETER

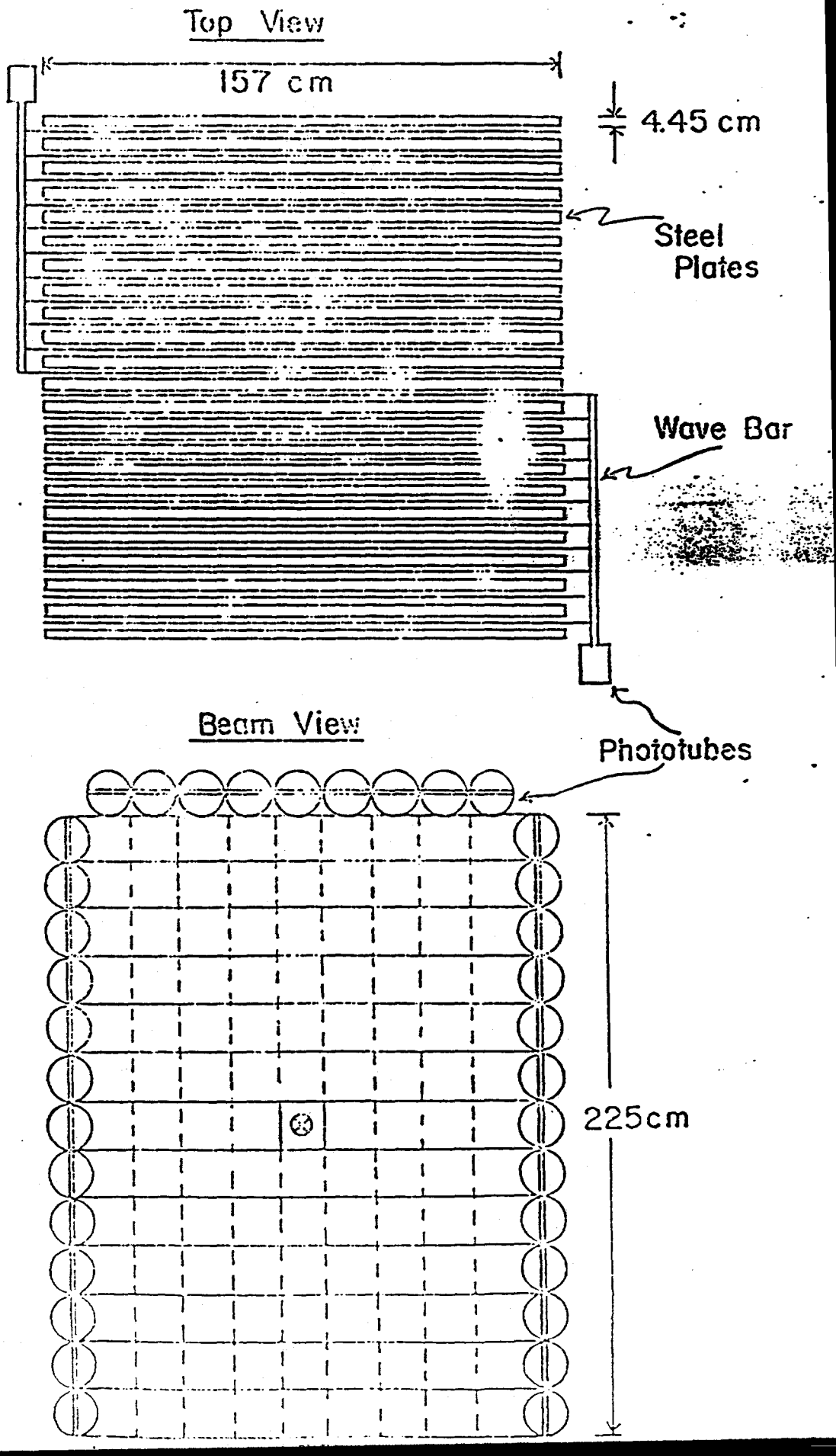

FIGURE 10

PHOTON FLUX:

NEW BROAD BAND BREMSTRAHLUNG BEAM
(30% RADIATOR)

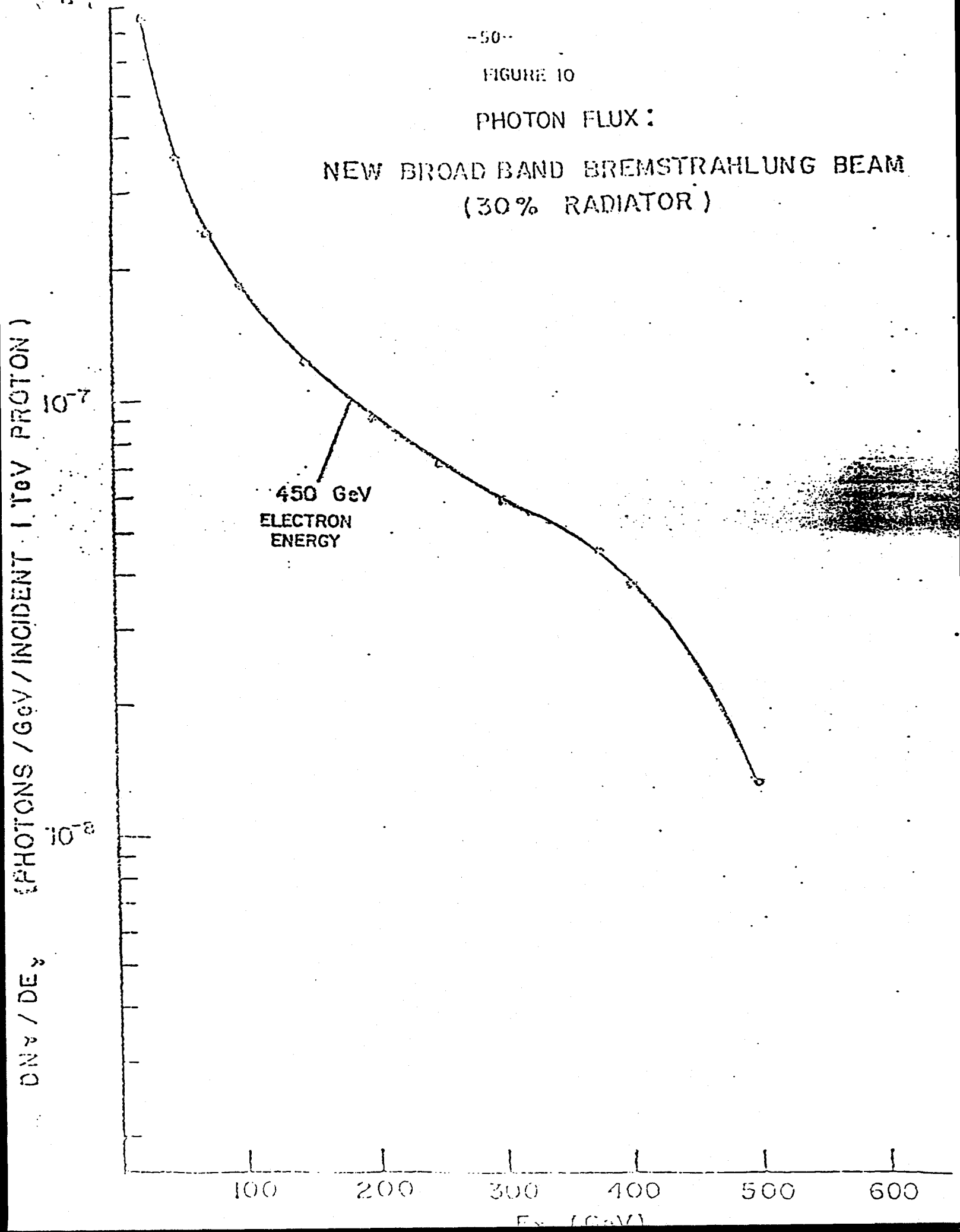

APPENDIX C

B-Collider Letter of Intent and Responses

Letter of Intent for the BCD

A Bottom Collider Detector for the Fermilab Tevatron

H. Castro, B. Gomez, F. Rivera, J.-C. Sanabria, *Universidad de los Andes*
P. Yager, *University of California, Davis*
E. Barsotti, M. Bowden, S. Childress, P. Lebrun, J. Morfin, L.A. Roberts,
R. Stefanski, L. Stutte, C. Swoboda *Fermilab*
P. Avery, J. Yelton, *University of Florida*
K. Lau, *University of Houston*
R. Burnstein, H. Rubin, *Illinois Institute of Technology*
E. McCliment, Y. Onel, *University of Iowa*
G. Alverson, W. Faissler, D. Garelick, M. Glaubman, I. Leedom, S. Reucroft,
D. Kaplan, *Northeastern University*
S. E. Willis, *Northern Illinois University*
S. Fredricksen, N. W. Reay, C. Rush, R. A. Sidwell, N. Stanton,
Ohio State University
G. R. Kalbfleisch, P. Skubic, J. Snow, *University of Oklahoma*
N. S. Lockyer, *University of Pennsylvania*
D. Judd, D. Wagoner, *Prairie View A&M University*
K. T. McDonald, *Princeton University*
A. Lopez, *Universidad de Puerto Rico*
B. Hoeneisen, *Universidad San Francisco de Quito*
S. Dhawan, P. E. Karchin, W. Ross, A. J. Slaughter, *Yale University*

(October 7, 1988)

Abstract

A dedicated B physics experiment is proposed for the Fermilab Tevatron p-$\bar{p}$ Collider. The goal is to study the full range of physics associated with 10^{10} produced $B\bar{B}$ pairs per year. This corresponds to a run of 10^7 sec at an average luminosity of 10^{31} cm^{-2}sec^{-1}, with a $\sigma_{B\bar{B}} \sim 45$ μbarns and a ratio of 1 $B\bar{B}$ pair/1000 inelastic events. Since B decay products have typical P_T's of only a few GeV/c, this physics is not accessible to a conventional p-$\bar{p}$ detector. The proposed B detector employs a cyclotron-style dipole magnet and emphasizes charged-particle tracking, vertexing, particle identification, mass resolution, and a flexible trigger system. There is no hadron calorimetry or muon system. The detector design envisions upgrades for higher luminosities and is compatible with a p-p collider at Fermilab. We anticipate first data collection in 1994. This detector is very similar to the central part of the SSC B spectrometer presented at Snowmass '88.

Contents

List of Figures

List of Tables

1 Introduction

The Tevatron p-$\bar{p}$ collider, already performing beyond expectations, could produce up to 10^{11} $B\bar{B}$ pairs per year by 1994, thus making it a unique B facility. We propose to construct a powerful detector to study this sample of $B\bar{B}$ pairs, with the opportunity to make major contributions to our understanding of the standard model and beyond. It will likely take 10-15 years to explore this rich area of physics, as in the case of the K system. The proposed program will measure a spectrum of physics quantities leading towards a thorough study of CP violation in the B system and the best possible determination of the elements of the K-M matrix. A natural evolution is to continue this program at the SSC.

The task before us is sufficiently different from the goals of the existing or planned detectors that a new effort is needed. A great deal of effort has gone into the study of whether this experiment is feasible and competitive with other approaches. After more than two years of meetings, workshops, seminars, conferences and study groups, we feel very strongly that this experiment can be built and will play a major role in the particle physics program of the 1990's.[1,2,3,4,5,6] The experimental techniques and technologies required are essentially available. The next step is to begin a realistic engineering design which will capitalize on the existing technology but remain flexible to take advantage of advances in technology which are sure to come over the next several years. We are submitting the Letter at this time to elicit the support of the Laboratory in this endeavor and to be considered in the planning for the Tevatron Upgrade.

While the physics potential in the B system is great, the technical challenge to harvest it is formidable, and it will require considerable lead time to meet this challenge. We believe it is vital that a dedicated team of physicists begin full-time work now on a detector which could take data in 1994. The upgraded Tevatron provides the best opportunity for a combined program of major new physics measurements in the 1990's, and of detector development for B physics in the SSC era.

The prospects for eventual expansion of the B physics program are considerable. Factor-of-ten improvements are possible in (at least) two directions. The detector could be made to operate at a luminosity of 10^{32} rather than 10^{31} $\mathrm{cm}^{-2}\mathrm{sec}^{-1}$; and the experiment could be moved to the SSC where the B cross section is ten times larger.

This Letter outlines the physics of interest, the conceptual design of the detector, and its impact on the accelerator.

2 Brief Summary of Bottom Physics Goals

We propose a physics program to study the B system in complete and thorough detail. Many important measurements will be made on the way to the major goal for this program, CP violation in the B system. The richness of this program will likely require efforts beyond the initial experiment proposed here.

The experiment is designed to study B-decay modes useful for direct measurement of the elements of the K-M matrix. These measurements, if made with sufficient accuracy, will overconstrain the standard model and thereby probe possible physics beyond the standard model. For example, with precise measurements of the K-M matrix parameters one can learn about the Yukawa couplings of the Higgs sector.[10,11,12,13,14]

Here we list what can be studied with a sample of 10^{10} B's (and $\bar{B}$'s) from a p-$\bar{p}$ collider. This might be obtained in a run of 10^7 seconds at an average luminosity of 10^{31} cm^{-2}sec^{-1}, assuming $\sigma_{B\bar{B}} \sim 45$ μbarns.[7,8,9] The signal-to-noise ratio is ~ 1 $B\bar{B}$ pair/1000 inelastic events. We suppose the efficiency for reconstruction, including the invariant mass, of an all-charged decay of a B is 30%. The trigger efficiency is taken to be 20% if a particle/antiparticle tag is not required, and 3% if the tag is required. We would measure:

- the production cross section for B_d and B_s mesons, and B baryons.
- rapidity distributions for the above states.
- lifetimes for the above states.[16]
- branching ratios of $B \rightarrow$ all-charged modes that have a branching ratio $\tilde{>}$ 10^{-7}.[17]
- branching ratios of the charmless decay modes that have all-charged final states.[18]
- branching ratios of CP eigenstates, obtaining a sample of several hundred decays from modes with branching ratios of 10^{-5} or larger.
- gluon structure functions at low x from the longitudinal-momentum distribution of B production.[25]
- mixing in the B_d and B_s systems. The relative amount of mixing is predicted by the standard model.[19,20,21]
- the upper limit or rate for rare decays such as $B \rightarrow e^+e^-$ or $B \rightarrow Ke^+e^-$ as a signal for new physics.

- the strongest signals for CP violation in the B system, as discussed further below.

The experimentally accessible signal of CP violation in the B system is an asymmetry of the form

$$A = \frac{\Gamma(B \to f) - \Gamma(\bar{B} \to \bar{f})}{\Gamma(B \to f) + \Gamma(\bar{B} \to \bar{f})}.$$

Such asymmetries are expected to be in the range 0.05–0.30 for some favorable modes.[14,15] If the final state f is a CP eigenstate the relation between the measured asymmetry and the K-M matrix involves no knowledge of strong interactions (unlike all measures of CP violation in the K system, see [10] and references therein). But in this case, $f = \bar{f}$, so the identification of the parent B as a particle or an antiparticle must come from a tag based on the reconstruction of the other B in the event.

As examples we consider three modes, $f = K^+\pi^-$, $\pi^+\pi^-$, and ψK_S, of which the $K^+\pi^-$ decay is 'self-tagging,' while the other two are CP eigenstates and require a tag on the second B. The table lists the size of the CP asymmetry needed to produce a 3-σ effect in the proposed experiment, for the branching ratios and efficiencies also stated. The assumed branching ratio, Γ, for the ψK_S decay includes factors of 0.07 for $\psi \to e^+e^-$ and 0.3 for detection of the decay $K_S \to \pi^+\pi^-$. Of the 10^{10} B's produced only about 4×10^9 are B^0 or $\bar{B}^0$.

f	Γ	ϵ	$N_{\rm recon}$	A for 3 σ
$K^+\pi^-$	10^{-5}	0.06	2400	0.06
$\pi^+\pi^-$	5×10^{-5}	0.01	2000	0.07
ψK_S	10^{-5}	0.01	400	0.15

Table 1: The CP violation asymmetry needed for a 3-σ signal in various B-decay modes. ϵ is the assumed reconstruction $\times$ trigger efficiency. The number of reconstructed events is for a run of 10^7 sec at an average luminosity of 10^{31} cm^{-2}sec^{-1}, in which 4×10^9 B^0 and $\bar{B}^0$ mesons would be produced.

The information to be gained from B decays to CP eigenstates is conveniently characterized on a triangle, as advocated by Bjorken. An overconstrained determination of the K-M matrix consists of measuring the interior angles of this triangle. Each angle can be directly inferred from an asymmetry measurement. Thus a thorough study involves determination of the asymmetries in several decay modes in each of three classes of decays, all to CP eigenstates. A general-purpose B detector is certainly required for such a study.

3 Comparison to Other Approaches

3.1 e^+e^- machines

The main advantage of the Tevatron Collider and the SSC over existing and proposed e^+e^- machines is the larger B cross section at a hadron collider. The Lorentz boost of $B\bar{B}$ pairs produced at hadron colliders is also an important advantage over conventional $\Upsilon(4s)$ machines, as this permits reconstruction of the secondary decay vertex. However, e^+e^- machines have the advantage of much better signal-to-noise. The issue for the hadron machines is the experimental effficiency. The issue for e^+e^- machines is accelerator technology.

The key experimental technique which should permit extraction of the weaker B signal at a hadron collider is the reconstruction of the secondary decay vertex in a silicon vertex detector. In the case of charm physics, once this technique matured, experiments at hadron machines matched and now surpass those at e^+e^- machines.

The $B\bar{B}$ cross section at the $\Upsilon(4s)$ is about 1 nb, $\sim 45{,}000$ times less than at the Tevatron. On the Z, the $B\bar{B}$ cross section is about 5 nb. At a luminosity of 10^{32} $cm^{-2}sec^{-1}$, it is unlikely that present-day e^+e^- machines will observe CP violation.

Even assuming a 100% reconstruction efficiency for B's at an e^+e^- machine compared with 1% at a hadron collider, it would require a luminosity 500 times greater at the e^+e^- collider than at the Tevatron collider to produce an equal sample of reconstructed B's. Compared to the SSC, a luminosity 5000 times greater is required at the e^+e^- machines.

The prospects of studying CP violation have stimulated many proposals for high-luminosity e^+e^- machines. Amaldi and Coignet,[40] and Cline[41] have suggested symmetric linear colliders with luminosities of 10^{34} $cm^{-2}sec^{-1}$. Other ambitious approaches have been put forward by PSI, KEK, and SLAC.[42,43,44] More recently, SLAC and DESY have been studying the option of asymmetric collisions, yielding a boosted $\Upsilon(4s)$. With a luminosity of 10^{34} $cm^{-2}sec^{-1}$, the number of produced $B\bar{B}$ pairs per year will be on the order of 10^8. Even with 100% reconstruction efficiency, this sample would be only comparable to that obtainable in the first-generation experiment proposed here for the Tevatron. As yet, there is no realistic design for such a machine, which would probably be built only after the SSC.

LEP and SLC have powerful detectors, low-multiplicity events, and, since the B's come from Z decay, they are boosted which allows secondary vertex detection. If their luminosity approaches 10^{33} $cm^{-2}sec^{-1}$, they would be quite competitive with the BCD. However, it is unlikely they will produce enough events to address CP violation in the neutral B system. Even at 10^7 Z^0's produced per year this is less $B\bar{B}$'s than CESR produces now.

3.2 Fixed Target Experiments at Hadron Machines

The bottom cross section is $\sim$ 1000 times larger at the Tevatron collider than at fixed-target energies. Furthermore, the ratio of bottom to total cross section is about 3000 times larger at the collider. These advantages will permit a hadron-collider experiment to explore a much greater range of phenomena in the B system compared to a fixed-target experiment which must focus on very specific issues. Although fixed-target photoproduction yields a better $\sigma_{B\bar{B}}/\sigma_{\rm tot}$ than hadroproduction, the size of $\sigma_{B\bar{B}}$ is down by several orders of magnitude. Recent reviews on this subject have been given by Bjorken,[22] Garbincius,[24] and Sandweiss and Cox.[23]

3.3 Other Hadron Colliders

UA1 at the CERN $Sp\bar{p}S$ collider has already observed a large $B\bar{B}$ cross section. However the $B\bar{B}$ cross section is about a factor of 5 lower than at the Tevatron, and with the upgraded luminosity the Tevatron production of B's will exceed the CERN production by at least an order of magnitude.

A workshop held at BNL this summer explored the possibility of a bottom experiment in the proposed RHIC machine, running in a $p\bar{p}$ mode. Again the cross section is about a factor of 5 lower, but here the anticipated luminosity could be $> 10^{32}$ cm^{-2}sec^{-1}.

4 Detector Overview

The experiment is shown in figure 1. The design is driven by the need for large angular acceptance, good momentum resolution for low-momentum tracks, precision vertexing, and particle identification. Calorimetry is not important except for electron identification. The basic character of the detector is "central" with greater emphasis on the angular region $2° < \theta < 30°$ than in present detectors designed for W and Z physics. The main design considerations are listed here and greater detail is provided in subsequent sections.

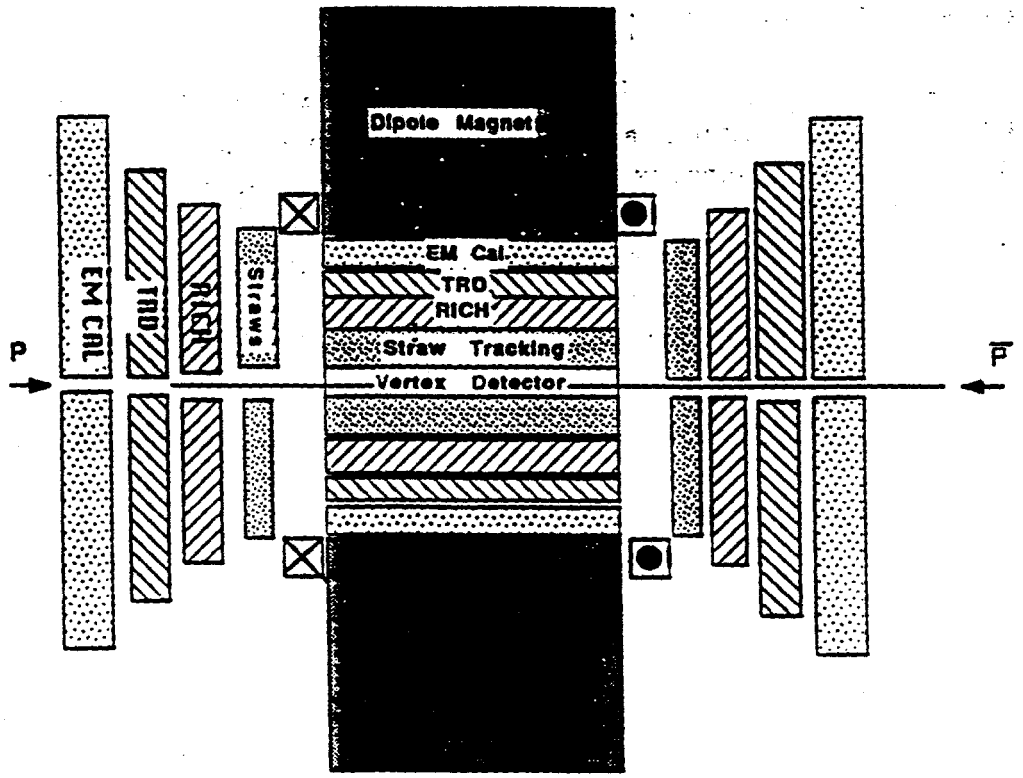

Figure 1: Overview of BCD detector.

- A dipole magnet is chosen to optimize the detection of tracks produced between $2° < \theta < 178°$ (pseudorapidity: $-4 > \eta > 4$). The kinematics of $B\bar{B}$ production are such that both forward and central tracks must be measured well in order to have a high geometric acceptance, while transverse momenta greater than 5 GeV/c are seldom of interest.[6] A dipole magnetic field oriented perpendicular to the beams is the best and simplest solution.

The magnet design calls for circular pole tips of 4-m diameter, separated by a 4-m gap.

- Even for small-angle high-momentum tracks, good momentum measurement can be obtained with a field of one Tesla in the dipole-magnet spectrometer. A low-field, large-diameter magnet is preferable for pattern recognition of low-momentum tracks.

- The gap size of 4 m permits a tracking system with 75-100 samples per track, the minimum acceptable number in a high-multiplicity event, while still accomodating the EM calorimeter, TRD, and RICH counters inside the coil.

- The vertex detector is designed to find the secondary vertices of the B particles with high efficiency, thereby reducing the combinatoric background. Also the ability to measure the time evolution of the states is particularly important for CP studies. Extensive Monte Carlo simulations[45] indicate that 3–D vertex reconstruction is necessary to achieve good pattern recognition, and that the system should have a worst-case impact-parameter resolution of < 20 μm. All tracks should intersect at least 3 planes with an angle of incidence $< 45°$. These requirements, along with the size of the intersection region, led to a hybrid design of barrels and planes using double-sided silicon. The detector is located outside the beam pipe, at 1.5-cm radius, to minimize effects of multiple scattering. Studies of this design, where tracking efficiencies were 100%, gave an efficiency for finding B vertices of $\sim 45\%$. A preliminary mechanical model of this detector design has been constructed.

- The vertex detector relies on the gas tracking system for most of the pattern recognition. The tracking system is designed for efficient and rapid 3–D pattern recognition of tracks over the full angular range. There are 75-100 hits along each track. The technology used is thin straw tubes arranged in superlayers. Straw tubes provide a measurement error of 40 μm per hit. Such high precision will allow a mass resolution of 20 MeV/c^2 and an extrapolation error into the silicon vertex detector of 50 μm. Good mass resolution is desirable to separate B_d and B_s, and to set a narrow mass window around the B as a rejection against combinatoric background.

- Particle identification is important in reducing the combinatoric background, especially for modes such as $B \to K\pi$ and $B \to p\bar{p}$. Electron identification is required for triggering and tagging the particle-antiparticle nature of the B. The design incorporates TRD's, RICH counters and an electromagnetic calorimeter over the full detector acceptance and for the full momentum range of the B decay products.

- The trigger and data acquisition system is designed to handle a luminosity of 10^{32} $cm^{-2}sec^{-1}$ and data-flow rates of GigaBytes per second. The trigger philosophy is to assemble the full event as soon as possible and pass it to a numeric processor where a variety of trigger algorithms can be implemented. The system is based on the latest communications-industry technology, which represents a new approach for high-energy-physics experiments and is suitable for SSC data rates.

5 Detector

5.1 Dipole Magnet

The dipole magnet for the BCD should have circular poles tips of 4-m diameter, a 4-m high gap, and a field strength of one Tesla. The large gap accomodates tracking and particle identification systems inside the magnetic field, while the circular pole tips maintain a field symmetry that simplifies the tracking algorithms. The magnet design and steel arrangement is shown in figure 2.

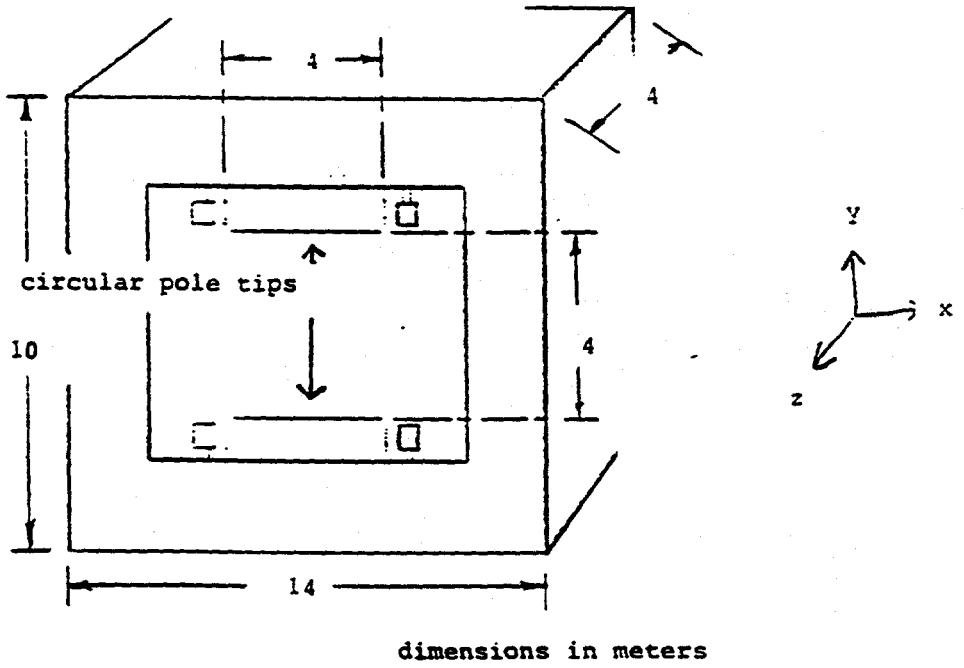

Figure 2: Dipole-magnet design and steel arrangement.

A comparison has been made with existing magnets that might be available on a time scale adequate for the Bottom Collider Detector. These are the CCM (Chicago Cyclotron Magnet), the MFTF (Magnet Fusion Test Facility) magnet, the Fifteen Foot Bubble Chamber Magnet, and the Berkeley 184" Cyclotron magnet.

The CCM would be an ideal magnet for the B Collider, if its gap were opened from the present 1 m to the needed 4 m. It will utilized in the muon-physics program for several years. If it should become available, the cost of moving it to a new facility would be around $750k.

The MFTF magnet has been turned on only once so this is a virtually new magnet. Only the superconducting coils of the MFTF magnet would be of use at

the Bottom Collider Detector. The BCD project would have to pay the cost of building the magnet yoke. Four of the existing ten coils could be used to achieve a 1-Tesla field. The cost of transport and installation are roughly estimated as $500k.

The Fifteen Foot Bubble Chamber Magnet has not been considered seriously for this project because it is being sought for an experiment at Gran Sasso. As for the MFTF magnet, a steel yoke would have to be built to incorporate the existing coils.

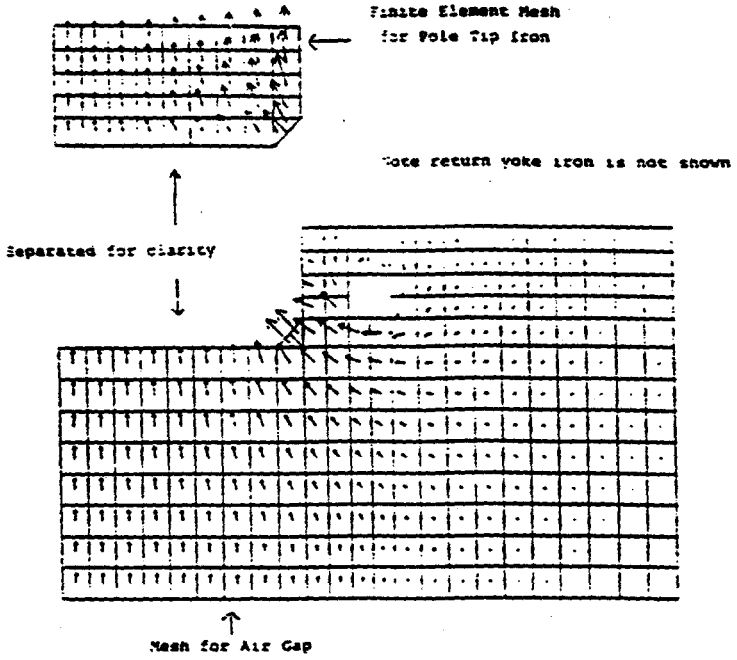

Figure 3: The vectors in each mesh element show the magnitude and direction of the magnetic-field flux density, for one quadrant of the magnet. At the center the value is about 1.14 Tesla, and near the corner of the pole it is about 3 Tesla (use of a B-H table in the ANSYS simulation would reduce this). The plots for the air region and the pole have been separated for clarity.

An attempt had been made to acquire the Berkeley 184″ Cyclotron Magnet for the Bottom Collider Detector. This was not possible because the magnet plates are only two inches thick (too many plates, too much rigging cost), they are mildly radioactive, and they are welded together into a yoke that also supports the crane at the Berkeley Cyclotron Building. The estimated cost of the procurement of this steel exceeds $1M, and was considered excessive. The copper magnet coils from the cyclotron are not considered useful because they are oil cooled and radioactive.

5.1.1 Design of a New Dipole Magnet

We are presently pursuing the design of a new dipole magnet. A study using the ANSYS finite-element analysis program is underway to explore several design issues.

As detailed in the Detector Overview section, the magnet-gap size is driven by the need for good momentum resolution and electron identification. This requires a long lever arm for tracking, and placement of the detector elements inside of the magnet. At present, the magnet modeling uses an overall dimension of $14 \times 10 \times 4$ meters for the yoke. The pole tips are 2 meters in radius. The weight of the magnet is estimated to be 3000 tons. With a 1-Tesla central field, the stored magnetic energy is 100 MJoule. A cost estimate is included in section 10.

Shown in figure 3 is the field map for this design. The $\int B\,dl$ from the magnet center outwards is typically 3 Tesla-meters, as seen in figure 4. With this, a momentum resolution of 1% or better can be achieved for all tracks with P_T less than 4 GeV/c.

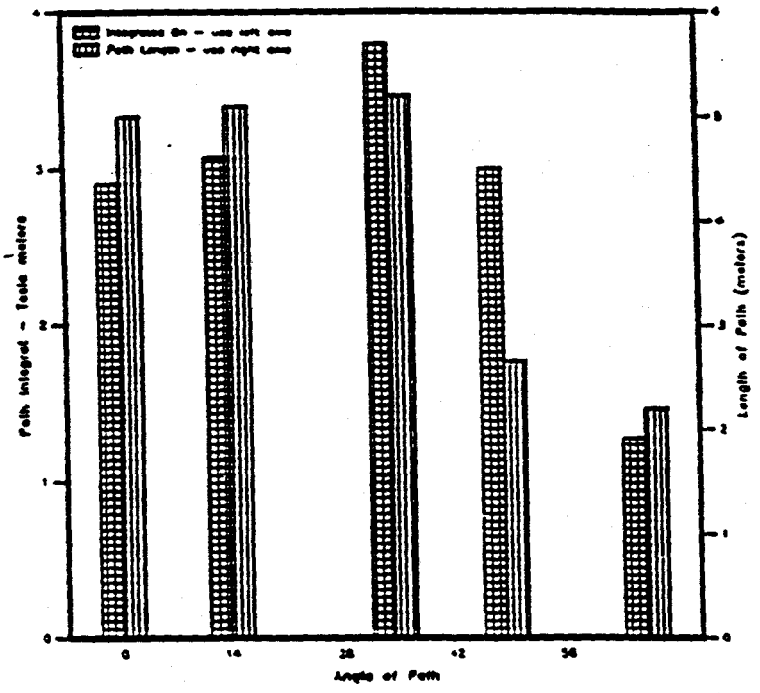

Figure 4: Shown here is the integral of the component of the magnetic field perpendicular to lines emanating from the magnet center at various angles with respect to the horizontal symmetry plane. The path length available is also shown.

An important physics issue relates to the transverse length of the iron yoke. The azimuthal symmetry of the field is destroyed by the presence of the vertical

return iron. By locating the iron further from the coils the field symmetry can be maintained. This results in a simpler field map and simpler track finding, which will be critical for the fast-tracking trigger of the experiment. The ANSYS simulation indicates that the vertical iron yoke should be about 3 m back from the pole tips to insure good field symmetry, while a minimal configuration with only 1-m spacing would cause considerable field distortion. The extra 2 m of steel in the horizontal yoke pieces adds a relatively small increment to the cost of the magnet.

Another important issue is the size and weight of the largest piece of the magnet. The coils are the largest pieces, about 5 meters in diameter including insulation. The weight of the largest steel piece would be limited to about 30 tons. In addition, we intend to bolt the magnet steel together allowing easy dismantling (for possible relocation at the SSC).

5.2 Silicon Vertex Detector

5.2.1 Introduction

The vertex detector is essential in extracting the B signal in a high-multiplicity environment. The clear association of tracks with a secondary vertex suppresses the otherwise overwhelming combinatoric backgrounds.

The lifetime, $c\tau$, of bottom mesons is about 360 μm. Secondary vertices must be reconstructable when their separation from the primary vertex is of this scale. We propose a microvertex detector based on silicon-strip detectors. Alternative vertex detectors utilizing the silicon-drift technique are also under consideration. Multiple scattering of charged particles and conversion of photons in the silicon detectors is a non-negligible problem. As a consequence we plan to use 200-μm-thick silicon, with double-sided readout.

The difficulty for precision vertexing in a collider experiment is that the secondary tracks emerge into the full 4π laboratory solid angle At present, tracking with silicon-strip detectors has been implemented only in geometries with near-normal-incidence tracks. However, because the interaction region in a hadron collider is spatially extended, there is no plausible geometrical arrangement of silicon planes which does not have some tracks at 45° incidence.

Figure 5 presents the angle of incidence (degrees from normal) on the silicon vertex detector for decay products of bottom mesons.

We anticipate that development of silicon detector technology will permit its use for 45°-incident tracks. A normally incident track will traverse the 200-μm thickness of a silicon detector giving a signal of 200 μm $\times$ 80 electron-hole pairs/μm = 24000 electrons. We plan to use 50-μm strip width, so that a 45° track would cross 70 μm of silicon per strip. The signal is then 70 μm $\times$ 80 electron-hole pairs/μm = 5600 electrons. It appears likely that VLSI readout chips for the silicon-strip detectors

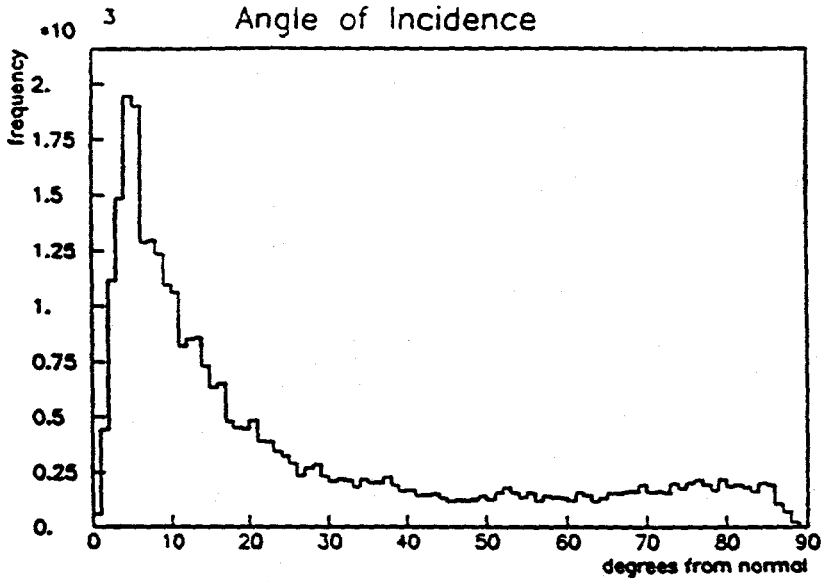

Figure 5: Angle of incidence upon the silicon vertex detector for bottom meson decay products (degrees from normal).

will achieve noise figures of 1000 electrons, which is entirely adequate. Indeed, if this noise level can be maintained even tracks with $\sim 0°$ incidence should be detectable, as these would yield about 4000 electrons.

5.2.2 Detector Geometry

The proposed detector geometry that has evolved over the past year is shown in figure 6.

The silicon vertex detector is logically segmented into two regions. The "central" region covers most of the interaction region with a combined geometry of equally-spaced silicon planes and three segmented barrels. The "rapidity-spaced" region covers the outer limits of the interaction region with silicon planes covering equal intervals in pseudorapidity. All silicon elements lie outside the beryllium beam pipe.

The beryllium beam pipe has radius 1.3 cm and thickness 400 μm. All (double-sided) silicon elements are of 200 μm thickness and have a strip pitch of 50 μm. Each disk has an inner radius of 1.5 cm and an outer radius of 13.5 cm. The detector consists of thirty-one parallel silicon disks and three segmented silicon barrels. The barrels have strips in z and ϕ directions, while the planes have strips in the x and y directions. The total length of the vertex detector is approximately 210 cm.

The central region of the vertex detector contains twenty-one planes with an

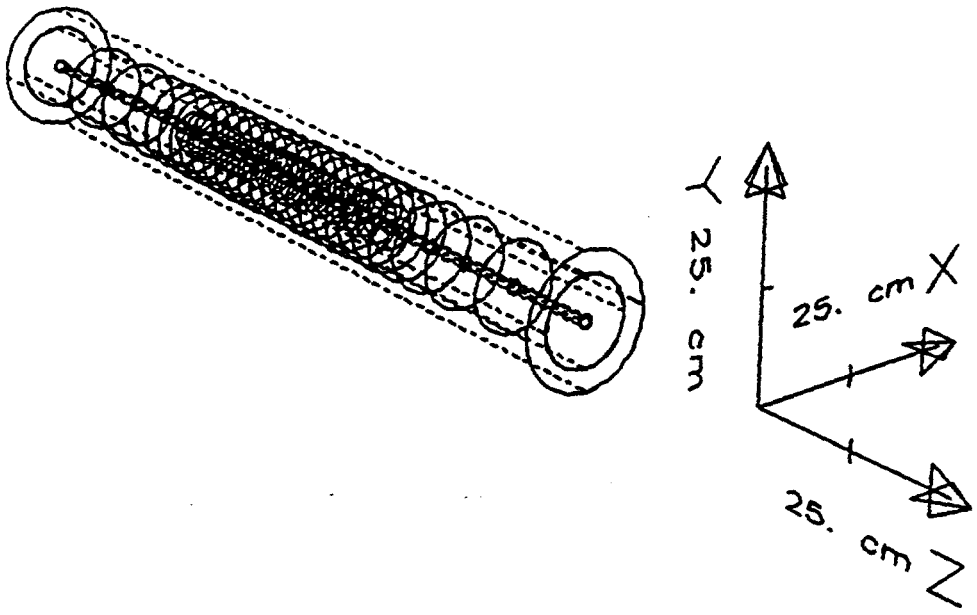

Figure 6: BCD Silicon Vertex Detector

interdisk spacing of 4 cm. The barrel segments are placed in the interdisk volumes and extend to the disk edges of the neighboring planes. The inner barrel radius is 1.5 cm; the middle silicon barrel radius is 5.0 cm; the outer silicon barrel radius is 10.0 cm. The central region extends from the center of the interaction region to $z = \pm 40$ cm.

The rapidity-spaced region is abutted to the central region and covers the outer limits of the interaction region. Silicon planes are placed every one-third unit of pseudorapidity, with the $\eta = 3$ planes equivalenced to the outer planes of the central region. Five rapidity-spaced planes extend from the ends of the central region.

This detector combines the features of the planar and barrel silicon geometries. Planes provide effective detector surfaces for particles traveling into the forward and backward regions, while barrels provide effective detector surfaces for radially-moving particles. The outer radius of the silicon planes has been chosen to be twice the interplane distance to guarantee three hits for all particles in the central region. Since the planes and barrels present relatively perpendicular surfaces to the particle tracks, this provides that all tracks that pass through the body of the detector will have three acceptable hits.

Figure 7 presents a scatterplot of hits per track versus B pseudorapidity for $B \rightarrow \pi^+\pi^-$. Hits are required to pass the cluster cut (see next section). (A shorter silicon vertex detector, designed for a shorter interaction region, was used in this study. Results for the long interaction region are expected to be similar.)

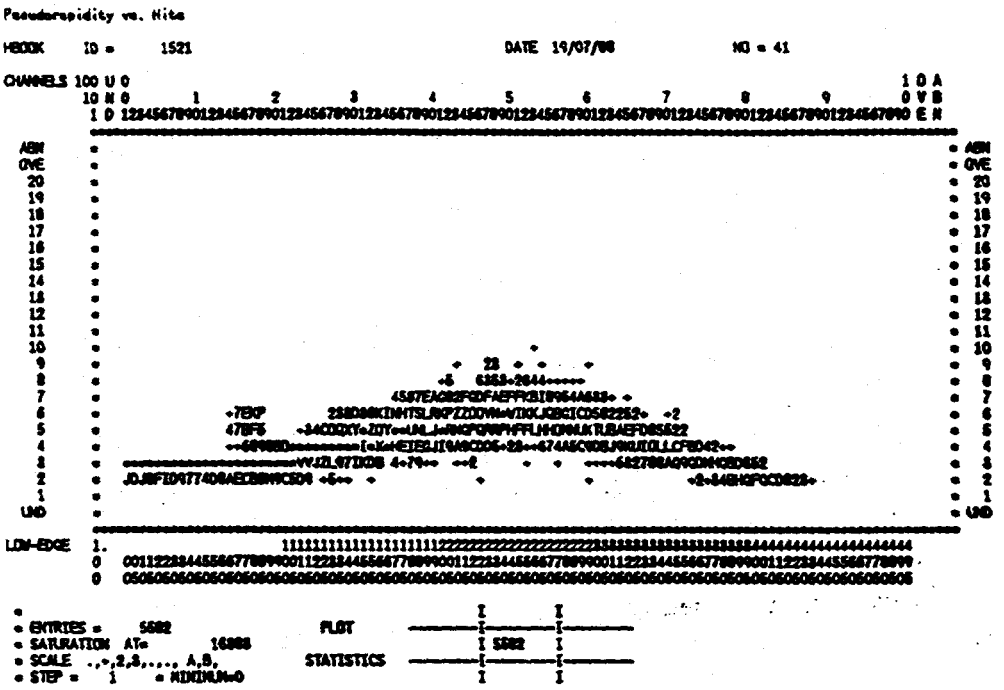

Figure 7: Pseudorapidity of the B meson versus the number of valid hits per track in $B \rightarrow \pi^+\pi^-$. Valid hits are those that pass the required cluster cut.

A model of the vertex detector has been built to address mechanical design issues.

5.2.3 Simulation of Vertex Detector Performance

PYTHIA 5.1 was used as the event generator for the simulation of the above design. Bottom meson events were generated for a p-$\bar{p}$ collider with 2 TeV center-of-mass energy. The minimum invariant mass of the hard-scattering parton subsystem was set at $10.5\,\mathrm{GeV/c^2}$; the minimum allowed transverse momentum was $0.0\,\mathrm{GeV/c}$. Decays of secondary particles were prohibited in the PYTHIA event generation—all particle decays were handled by GEANT3.

Bottom mesons only were selected from among the full PYTHIA–generated event for entry into GEANT3. Our objective was to determine whether reconstruction of bottom mesons would be possible using this vertex detector—one should first check that reconstruction is possible without any extraneous particles. Simulations were run using two decay modes: $B_d^o \rightarrow \pi^+\pi^-$ and $B_d^o \rightarrow \psi K_s^o$ ($\psi \rightarrow e^+e^-$). No magnetic field was present in the simulations, this being a preliminary design study.

Analysis was performed using GEANT3's knowledge of the particle decay. No

pattern recognition was used; the GEANT3 particle-decay chain was followed to identify descendents of each bottom meson. Both of the chosen decay modes allow a simple trigger—both provide two prompt, charged particles. Bottom meson events were accepted if both charged-particle tracks had at least two hits in the silicon detectors.

A cluster-size cut was imposed on the particle hits in the silicon detectors. The cluster size is defined to be the number of adjacent silicon strips which are fired by the passage of a single-particle track. Large cluster sizes present possible problems with signal size, hit location and pattern recognition. Hits with cluster sizes greater than four strips were rejected.

Particle tracks were defined by the first two (valid) hits on the track. Cuts on the vertex resolution were imposed on the quantity $S/\Delta S$, where S represents the distance of flight of the bottom meson and ΔS represents the three-dimensional distance between the reconstructed decay vertex and the true (Monte Carlo) decay vertex. $S/\Delta S > 5$ was the imposed cut. Figure 8 shows a scatterplot of S versus ΔS and the applied cut.

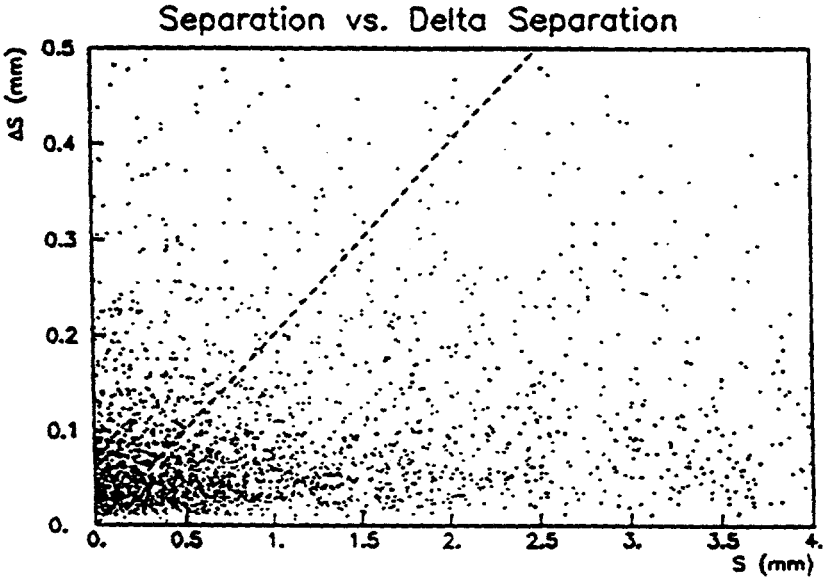

Figure 8: Scatterplot of separation S vs. delta separation ΔS for simulated $B \rightarrow \psi K_s$ events. The region below the dashed line contains events that satisfy the cut $S/\Delta S > 5$. Events with small S are predominantly produced in the central region, where the lower B momentum leads to a lower fraction of events surviving the cut.

Simulations were performed taking the the Tevatron interaction region to be a

Gaussian distribution of events with $\sigma = 35\,\text{cm}$. Vertex-detector acceptance as a function of the applied cuts can be seen in Table 2. Results are shown for both of the decay modes $B_d^\circ \to \pi^+\pi^-$ and $B_d^\circ \to \psi K_S^\circ$. Application of cuts is cumulative down through the rows of the table.

cuts	$B_d^\circ \to \pi^+\pi^-$	$B_d^\circ \to \psi K_S^\circ$
geometry cut	0.768	0.775
cluster cut	0.751	0.763
vertex cut	0.466	0.449

Table 2: Vertex-Detector Acceptance—interaction region with Gaussian distribution, $\sigma = 35\,\text{cm}$.

Figure 9 presents the accepted-pseudorapidity distributions for bottom mesons in the BCD silicon vertex detector. All cuts (geometry, cluster size, and vertex) have been imposed on this distribution. The distribution is for the decay mode $B_d^\circ \to \pi^+\pi^-$; the distribution for the decay mode $B_d^\circ \to \psi K_S^\circ$ is virtually identical.

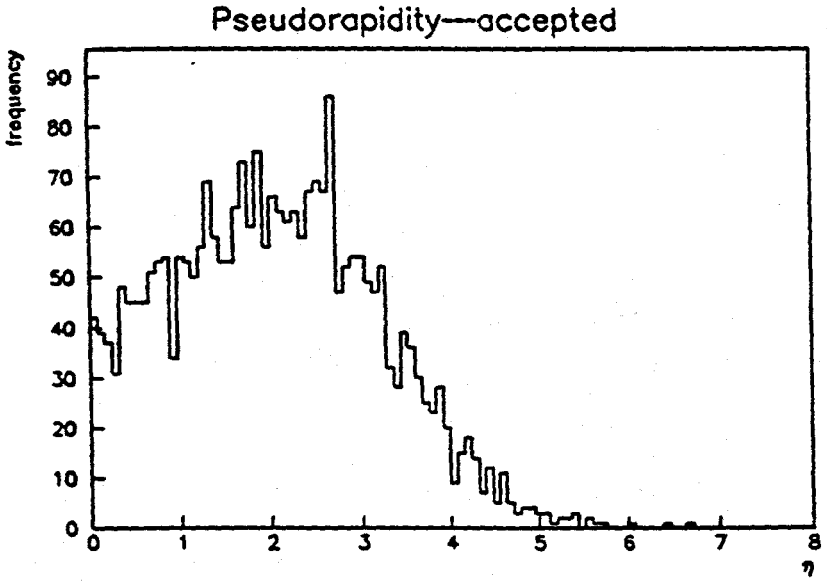

Figure 9: Pseudorapidity of accepted B mesons

5.2.4 Silicon–Straw Tube Matching Studies

General Character of Silicon Hit Distributions

Because a track has typically only three hits in silicon planes, the task of pattern recognition must be accomplished using information from the straw-tube chambers as well. Here we consider how well the silicon-hit information can be matched to a track as found in the straw-tube system. Difficulties arise when two or more tracks give closely spaced hits in the silicon planes all of which are potential matches to a track found in the straw-tube chambers. However, we find this confusion to occur in less than 2% of all tracks, using the simulation described below.

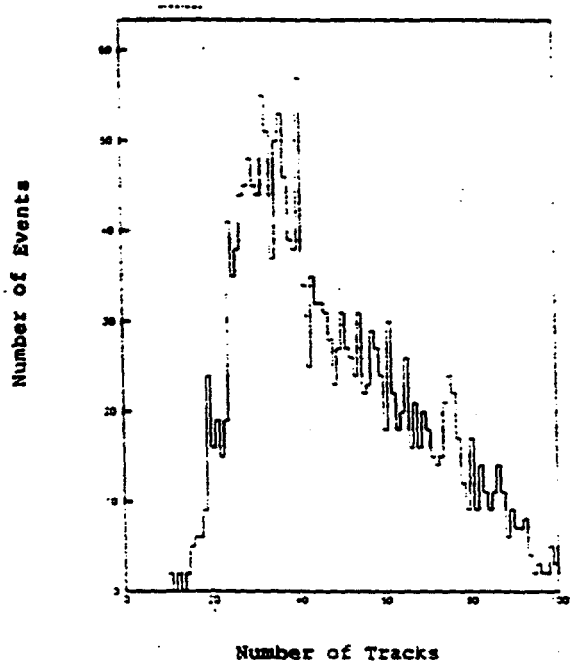

Figure 10: Multiplicity of tracks that strike the silicon vertex detector.

We studied simulated hit distributions in the silicon microstrip vertex detector by considering all the tracks generated in events containing the decay $B^0 \to \pi^+\pi^-$. The effects of decaying particles, photon conversions, multiple scattering in the detectors, *etc.*, are included. The charged-track multiplicity per event seen by the vertex detector is histogrammed in figure 10. The most probable number of tracks is 35 with a long tail on the high side. The number of strips fired per track, assuming a discriminator cut at 5% of minimum ionizing, is shown for the inner barrel detectors in figure 11a and for the planar detectors in figure 11b. The large number of strips fired per track in the barrel detectors is due to the cases where a small-angle track passes through many z-measuring strips. This condition is common since the distribution of track angles in space is highly peaked at small angles. This forward-

peaked distribution also results in relatively few multi-hit tracks seen in the planar detectors.

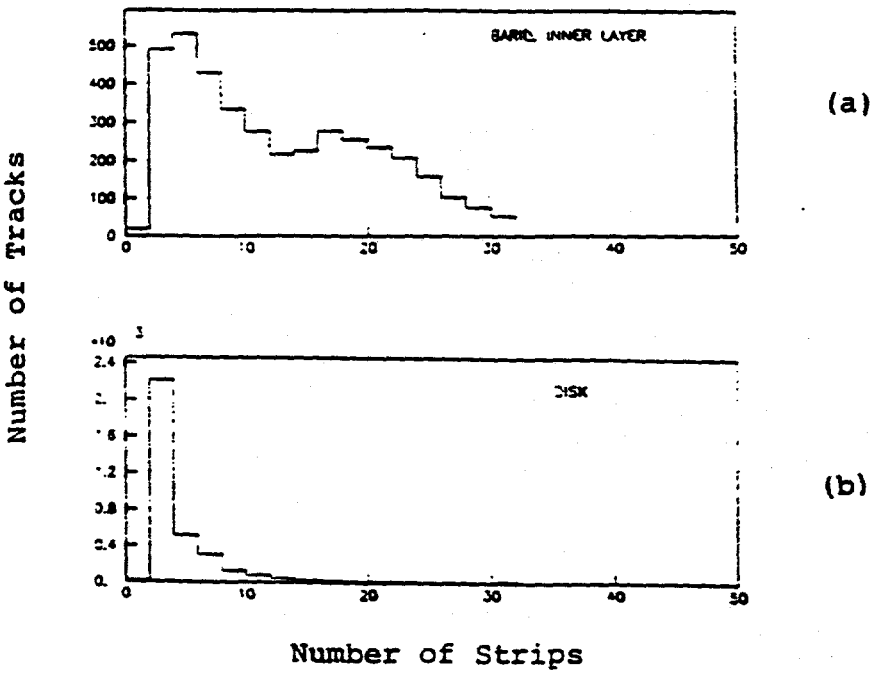

Figure 11: The number of silicon strips fired per track, with a discriminator cut at 5% of minimum ionizing. (a) Barrel silicon: (b) planar silicon.

The distribution of path length traversed through a single strip is shown in figure 12a for the inner barrel and figure 12b for the planes. The peaks at 200 μm are due to tracks at normal incidence to the detector, whereas the peaks at 50 μm are due tracks at grazing incidence and orthogonal to the strips. Hits due to path lengths much less than 200 μm could be suppressed by placing the discriminator cut above the 50-μm peak. This option will be explored in future studies. The very large path lengths are due to grazing-incidence tracks travelling along the length of a single strip. These very long path lengths are not disadvantageous to pattern recognition since they result in only one strip firing.

Effective Spatial Resolution of the Silicon Strips

The resolution of the silicon strips is affected by the number of silicon hits that can be associated with a given track found in the straw-tube system. If only one track passed through the window defined by the straw-tube track, then the silicon coordinate is given either by the single-strip coordinate or by the mean coordinate

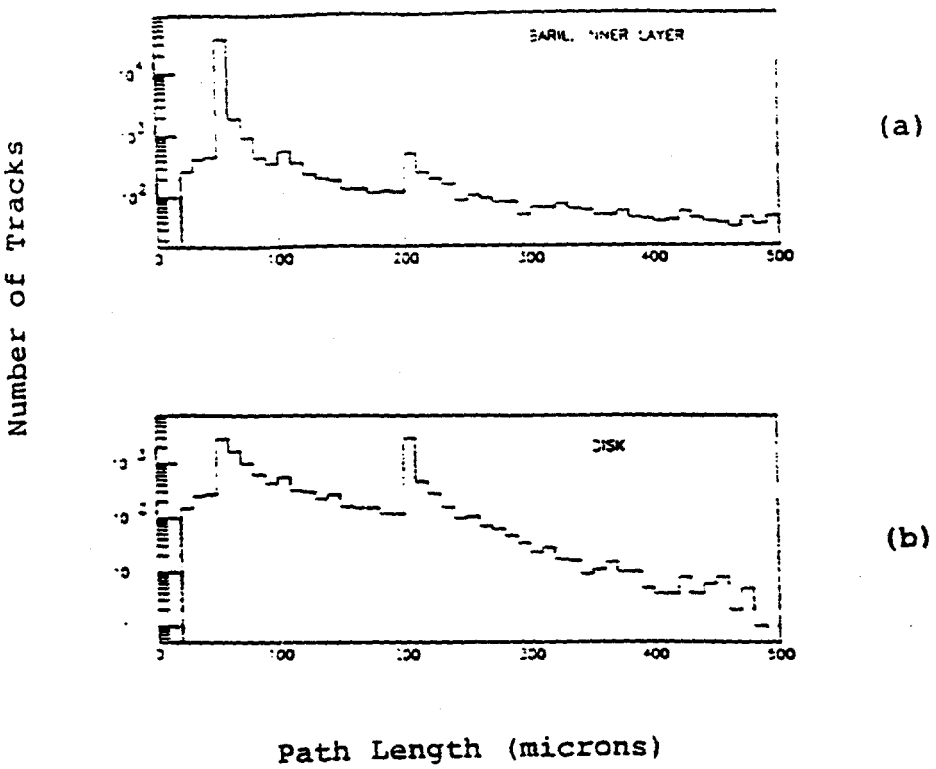

Figure 12: Distributions of path length in individual silicon strips. (a) Barrel silicon; (b) planar silicon.

if more than one strip has fired. The resolution in this case is illustrated by the histograms in figures 13a-c of the difference in position between the mean strip coordinate and the true (Monte Carlo) position of the track at the silicon detector. For the ϕ-measuring barrel strips and for the planar detectors the resolution is essentially due to the single-strip width of 50 μm. However for the z-measuring barrel strips, the residual distribution is widened due to tracks with multiple-hit patterns. Most of these tracks, however, will also be measured with better accuracy in the planar detectors.

If more than one track has passed through the window defined by the straw-tube track, then we do not know which silicon hit to assign to the track. One simple algorithm is to take the average of the hit coordinates within the window. The residuals in this case are shown in figures 13d-f for a search window of 150 μm, corresponding to a ± 1.5-σ cut for a 50-μm pointing resolution. The main effect is to enhance the non-Gaussian tails of the residual distribution. The fraction of search windows containing more than one track is 1.6% for the inner barrel and 1.4% for the planar disks. These fractions could be reduced if the strip lengths were decreased from the 5 cm assumed in this study.

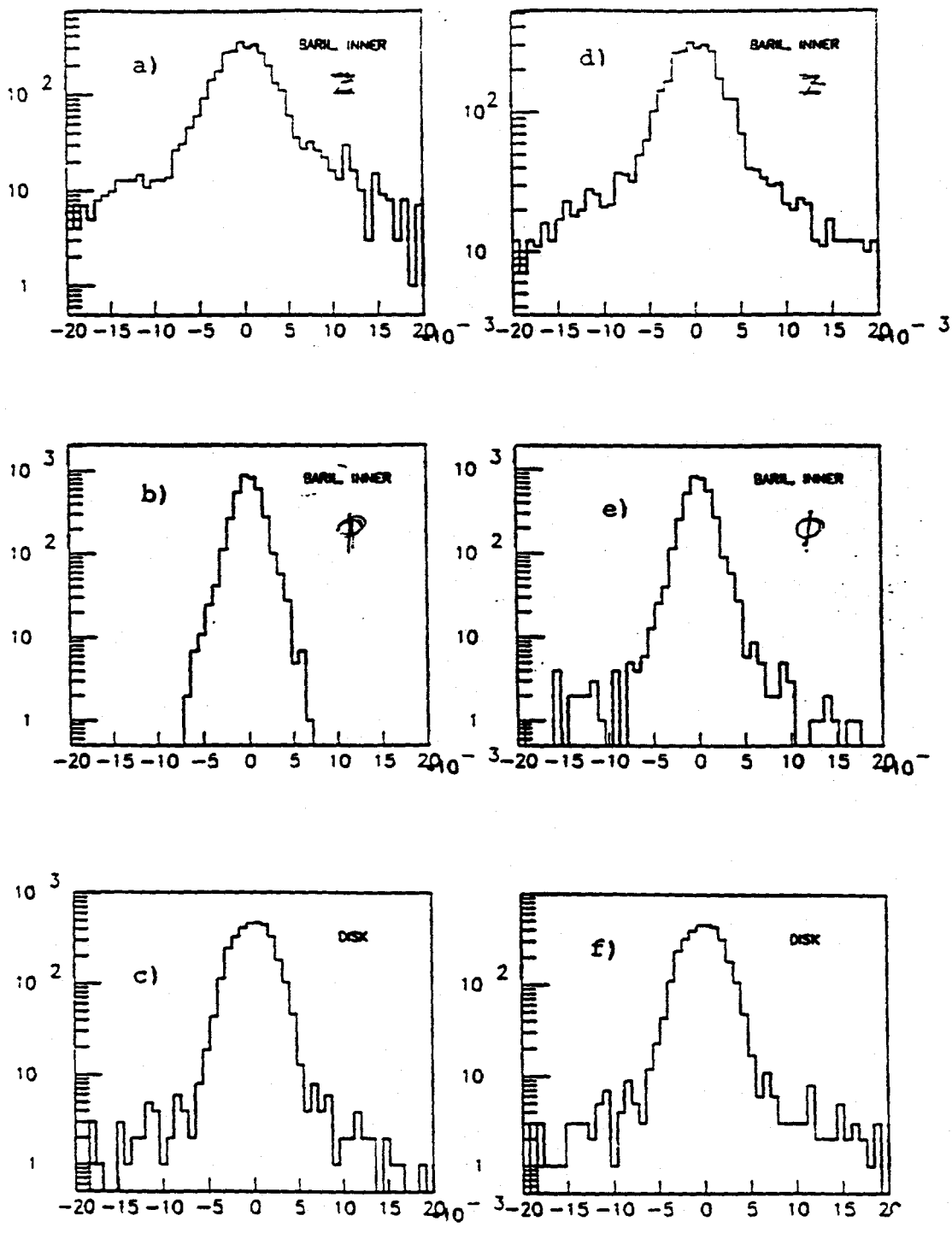

Figure 13: (a-c) Residuals between measured silicon hit positions and Monte Carlo generated positions; (d-e) Residuals based on the means of all hits in the silicon within a window defined by a track found in the straw-tube system.

5.3 Silicon Vertex Detector: Devices

Our present design uses the currently available double-sided silicon microstrip detectors. However, there is a world-wide effort to develop high-rate, high resolution pixel detectors. We plan to take advantage of these new devices as they become available. Below we discuss the microstrip detectors and two future possibilities.

5.3.1 Double Sided Microstrip Detector

We will use "double-sided" silicon microstrip detectors with the cathode strips oriented orthogonally to the anode strips, providing both an x and y measurement with a single silicon wafer. Such devices with dimensions 5 cm by 5 cm by 300 microns and 50-micron-pitch readout have been fabricated and tested.[46] An important feature is that capacitors integrated on the silicon couple the anode (high voltage) strips to the first-stage VLSI amplifiers. This type of detector will be used in the ALEPH and DELPHI experiments at LEP. A commercial manufacturer producing doubled-sided, capacitively-coupled detectors is Messerschmitt Buelkow Blohm (MBB) GmbH, Munich.

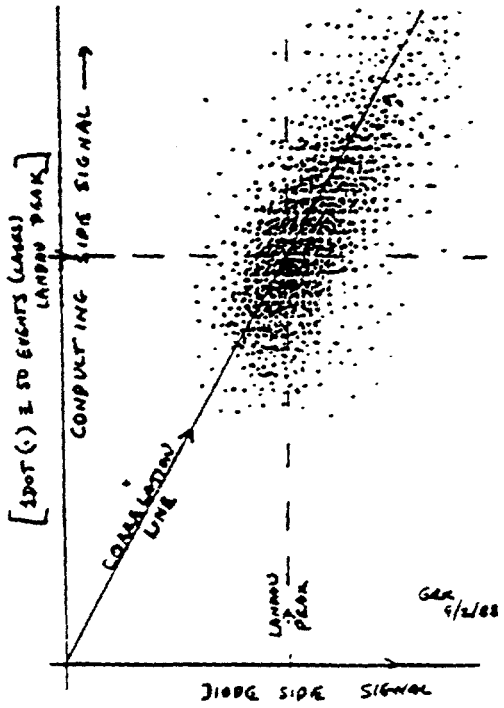

Figure 14: Observed correlation of pulse heights collected on opposite faces of a doubled-sided silicon strip detector.

Tests have been made on a double-sided wafer by the University of Oklahoma

group[60] to study the correlation of the pulse heights in the anode and cathode strips. If more than one track penetrates the silicon wafer, then it may be possible to pair the x and y hits since the pulse heights will be the same in x and y for a given track. The pulse heights for different tracks will vary according to the Landau distribution. Figure 14 shows the correlation of pulse heights observed on opposite sides of a silicon detector. This technique appears promising and makes the double-sided microstrip detector a quasi-pixel device.

5.3.2 Silicon Pixel Detectors

Silicon Detectors based on pixels rather than strips offer two potential advantages for a collider experiment. Each hit is recorded as an unambiguous space point, which clarifies pattern recognition and speeds use of the detector information in a trigger. Also, as the capacitance of a pixel is quite low, very small charges can be detected, and the active thickness of the silicon can be less than for a strip detector. When the detector thickness is comparable to or less than the pixel width the problem of angled tracks is largely removed.

We are investigating[61] the multianode silicon drift chamber of E. Gatti and P. Rehak, which implements 'virtual pixels' by recording the history of ionization electrons drifting towards a relatively small number of anode pads. Other promising techniques are those pursued by Parker *et al.*, by Shapiro *et al.*, and by Nygren *et al.*, who consider devices with true silicon pixels each with its own readout.

5.4 Tracking

Multiple scattering in and instrumentation costs of the silicon microstrip detectors (SMD's) do not allow a number of planes sufficient to reconstruct most tracks in three-dimensional space. The vertex detector must therefore be regarded as a precise vernier which improves the pointing accuracy of tracks reconstructed unambiguously in three dimensions by a larger tracking system consisting mainly of wire chambers.

This outer-tracking system must be able to reconstruct curved tracks coming from an arbitrary origin in a dipole magnetic field. This is a more difficult problem than that commonly encountered in collider detectors using a solenoidal field, in which the tracks in the azimuthal view are circles coming from a single, well-defined beam-intersection point. The tracking system must also measure momentum to an accuracy of $\pm 1\%$ in a 1.0-T dipole magnetic field, must deal with interaction rates of 5–10 MHz, and cannot have massive support structures such as end plates which would interfere with the nearly 4π electron trigger which will surround it.

Tracking designs based on straw tubes have several attractive advantages for this experiment. They require no massive mechanical supports, their small drift distance allows high rates, and the damage due to broken wires is very localized. However,

the support is distributed in the walls of the straws, which are a potentially large source of multiple scattering. The wall thicknesses must be reduced substantially below those now in common use if this design approach is to be viable.

DeSalvo[56] has proposed a design for an SSC central-tracking detector which is based on a large number of straws of 3.0-mm diameter and 30-μm wall thickness, pressurized to 3–4 atm. In addition to improving the resolution of the straws to 30–40 μm, pressurization adds to the rigidity and allows the reduction in diameter which leads to thinner walls. A "superlayer" of 8 rows of such tubes (figure 15) contains only 3.4×10^{-3} radiation lengths, resolves left-right ambiguities locally, and provides both a vector with 2-mrad pointing accuracy and an estimate of curvature. The multiple scattering in eight such superlayers induces a momentum resolution of 0.6% when distributed along 0.75 m in a 1.0-T field. The tracking design described here is based in large part on straws which are assumed to meet these specifications.

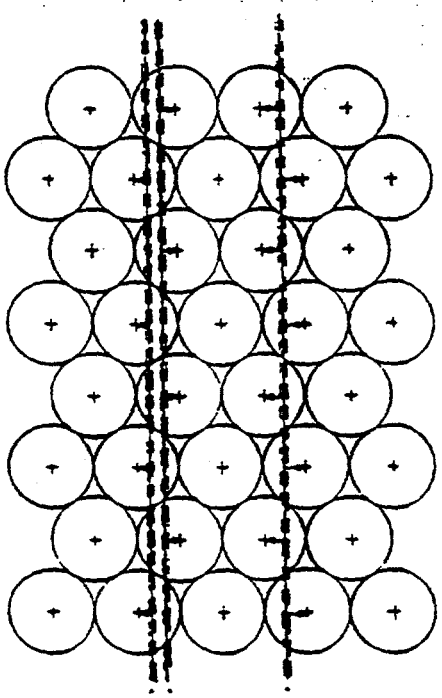

Figure 15: A "superlayer" of 8 rows of straw tubes.

The maximum radiation exposure which wire chambers can tolerate limits how close to the beam the straws can be placed, and leads in turn to a hybrid system with additional microstrip detectors for small-angle coverage. A conservative limit on the safe total multiplied charge in a wire chamber is[57] 0.1 Coul/cm per 10^7 sec at a gain of 10^5. The charged-particle flux into a normal area element Δa at a

perpendicular distance $r_\perp$ from the beam is well-approximated by[58]

$$(dN/da)\Delta a = (H/2\pi)(\sigma_{\rm inel} \cdot L)/r_\perp^2 \qquad (1)$$

where $H = dN/d\eta$ near pseudorapidity $\eta = 0$, $\sigma_{\rm inel}$ is the inelastic cross section, and L is the luminosity. For the Tevatron, $H \approx 4.0$, $\sigma_{\rm inel} = 40$ mbarns, giving $r_{\perp \rm min} \approx$ 6-8 cm for 3-mm straws at $\mathcal{L} = 1\text{-}2 \times 10^{32}$ cm^{-2}sec^{-1}. For an SSC detector it is estimated[58] that $H \approx 7.0$, $\sigma_{\rm inel} = 100$ mbarns, resulting in $r_{\perp \rm min}$ twice as large at the same luminosity.

A conceptual outer-tracking design using both straws and SMD's to cover pseudorapidities η out to 5.0 is shown in figures 16 and 17. It contains approximately 2×10^5 straws, plus an additional 10^5 SMD strips with 50-μm pitch located outside of the vertex detector.

Figure 16 shows the straw-tube panels and SMD's in a plan view section through the median plane of the central portion of one quadrant of the tracking system. Each straw-tube panel is a superlayer of eight rows of 3-mm thin-walled straws. In figure 16, the dipole magnetic field is perpendicular to the page and parallel to the wires in the x straw tube panels, which measure position in the bend plane. The u and v straw tubes are oriented at $\pm 14°$ to the x axis to provide information for the nonbend plane and to resolve the stereo ambiguity. Straw orientations with a large component of the magnetic field perpendicular to the wires are avoided because the effects of the Lorentz force are more difficult to deal with in reconstruction. Gas and voltage feeds and signal readouts of all straws are at the ends ± 80 cm above and below the plane of figure 16. The straw-tube x panels are arranged in an "egg-crate" pattern (with x panels both perpendicular to and parallel to the beams) to facilitate reconstruction of small-radius curved tracks.

Tracks in the forward and backward directions are reconstructed by u-x-v triplets of straw-tube superlayers and/or xy-uu' doublets of SMD's with double-sided readout, spaced approximately logarithmically along the beam direction z out to ± 320 cm from the interaction point. (Three straw-tube triplets and four SMD doublets are located beyond the largest z included in figure 16.) Because no straws are closer than 8 cm to the beam, tracks with pseudorapidity $\eta \leq 2$ are reconstructed by a combination of straws and SMD's; those with $\eta > 2$ are reconstructed almost entirely with the SMD's. In reconstructing tracks with this hybrid system it is therefore better to use straws and SMD's interchangeably in the same projection, which requires that the orientation of SMD strips be parallel to the straw-tube wires. In this design the x and u orientations of the straws and SMD's are identical. The SMD's have no v projection, but have instead additional large-angle stereo y and u' projections (perpendicular to x and u, respectively) to further resolve confusion among very small-angle tracks.

Figure 17 shows a section of the tracking system through the center of the detector and perpendicular to the beams. In this view the magnetic field and the x wires

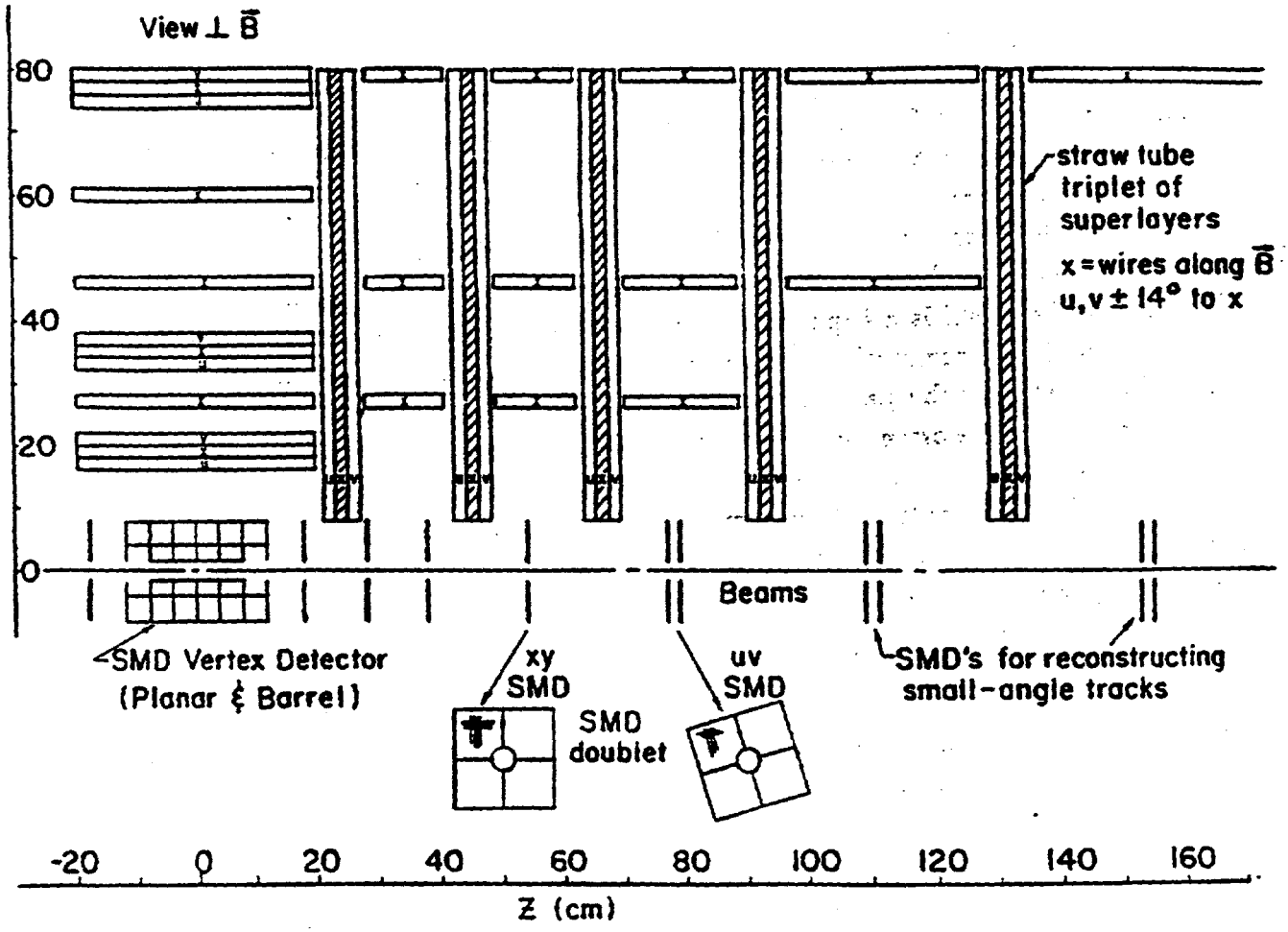

Figure 16: Plan view section through the median plane of one quadrant of the tracking system, showing the location of straw-tube panels and silicon microstrip detectors. The dipole magnetic field and the wires in the x straws are perpendicular to the page.

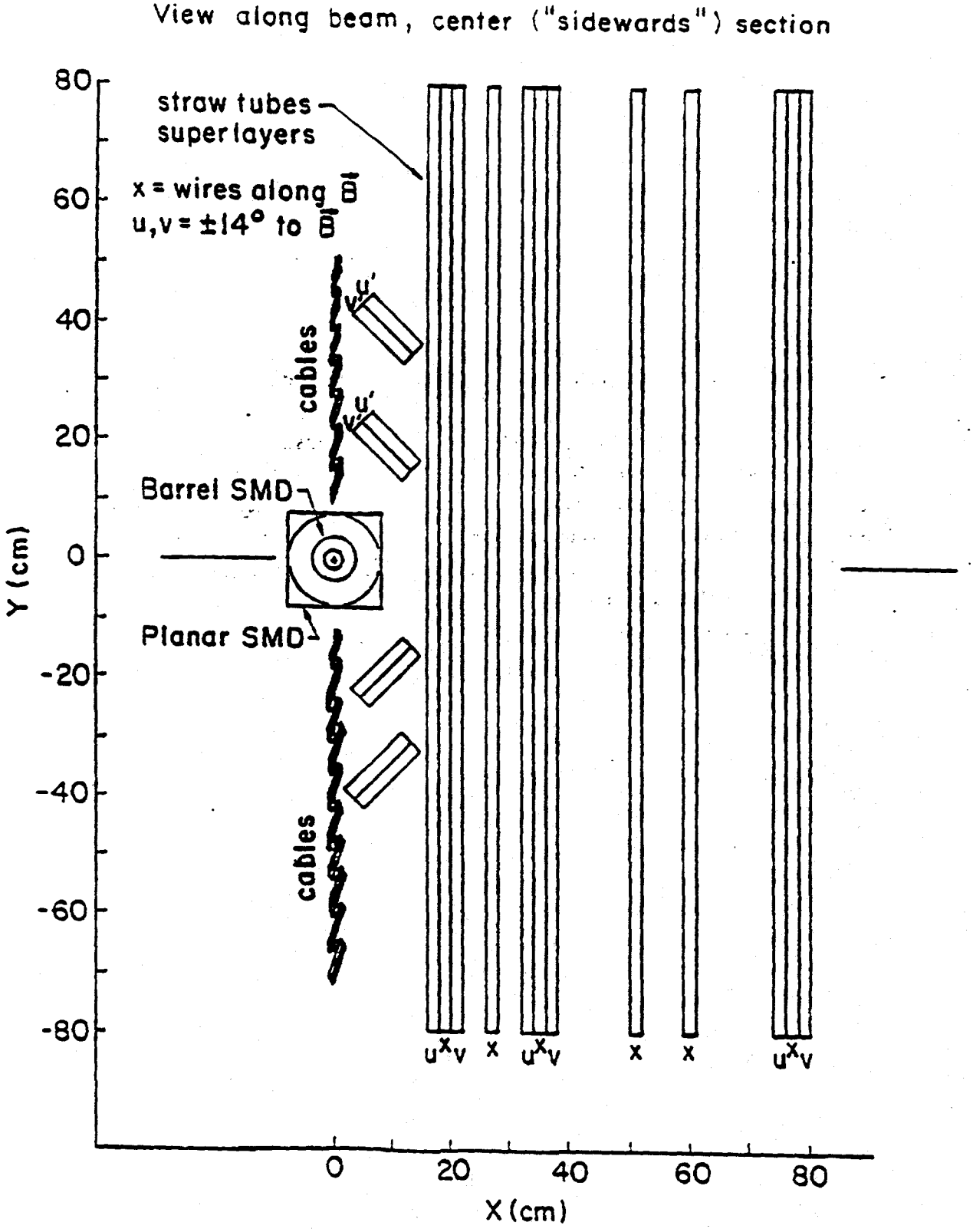

Figure 17: Section of the tracking system through the center of the detector and perpendicular to the beams. In this view the magnetic field and the wires in the x straws are vertical.

are vertical. Although the track density in this small-η region is low, it can be seen that the allowed large dip angles of $\approx 70°$ present difficulties, solved satisfactorily in this design, in obtaining a sufficient number of samples in each projection on tracks with large dip angle, and in extrapolating such tracks back to the vertex detector.

An estimate of the hit occupancy of straws and SMD strips can be made using equation (1). In the worst case of 3-mm straws 8 cm from the beam the occupancy is about 6%, while for a 50-μm SMD strip at 1.5 cm from the beam the occupancy is less than 1%.

The next step in designing the tracking system is to confront realistic simulated events in the detector with an actual trackfinding algorithm to determine whether the system has an adequate number of samples in each projection, and whether there is sufficient information to combine projections into three-dimensional tracks with high efficiency and small number of fakes. Work on such a trackfinding program is well underway. It is designed to deal with configurations of N superlayers of up to M samples each, provided only that all detectors in a projection are in the same rectangular coordinate system, and can find tracks of uniform curvature from an unspecified origin. On a longer timescale, a prototyping effort must be established to show that the very thin-walled straws on which this design is based can actually be built with the expected mechanical and electrical properties.

5.5 RICH Counters

The use of a ring-imaging Čerenkov counter (RICH) offers a means of π-K-p identification for transverse momenta up to about 4 GeV/c, as suitable for products from B decay. Low-momentum hadrons in the central region can be identified in a time-of-flight system described in a later subsection. In principle, a RICH counter can contribute to e-π separation, although this requires a somewhat different detector configuration than that proposed for hadron identification.

The detector is divided into two angular regions: forward, with $2° < \theta < 30°$; and central, with $\theta > 30°$. Then identification of of particles with transverse momenta up to 4 GeV/c implies the forward detector must operate with momenta up to 120 GeV/c, while the central detector must deal with momenta up to 8 GeV/c. The central region could be covered with a single RICH counter using a liquid radiator, such as C_6F_{14}, with a threshold of $\gamma_t = 2$. The forward region would require two counters: one with the same radiator as in the central detector to cover the lower momenta; and another with a gaseous radiator such as C_5F_{12} with threshold $\gamma_t = 17$. Table 3 summarizes the ranges of particle momenta and corresponding γ's over which the RICH counters should operate.

The space avalilable for the RICH counters permits a thickness of approximately 25 cm for the liquid counters, and 1 m for the gaseous counter. Complete coverage

	P (GeV/c) at $\gamma_t = 2$	γ at $P = 8$ GeV/c	P (GeV/c) at $\gamma_t = 17$	γ at $P = 120$ GeV/c
π	0.3	56	2.5	840
K	1	16	8.5	240
p	2	8	17	120

Table 3: Ranges of momenta and γ which should be covered by the RICH counters. $\gamma_t = 2$ for liquid C_6F_{14}, and $\gamma_t = 17$ for gaseous C_5F_{12}.

of the momentum ranges given in the table would require a position resolution of about 1 mm for detector of the Čerenkov photons. In turn this would require about 10^7 detector pixel elements. In the initial implementation we plan to use a wire-chamber detector with readout of cathode pads of size 8 mm × 8 mm, similar to that used in experiment E-665. For this about 10^6 elements are read out. The lower position resolution implies that π-K separation would be available only up to about 2.5-GeV/c transverse momentum.

The wire-chamber gas must be sensitive to UV photons for the detector to have reasonable efficiency. While most RICH counters to date use TMAE as the photo-sensitive vapor component, this must be heated to 70°C for optimal performance, and it is subject to radiation damage at relatively low doses. We prefer to use TEA, which functions at room temperature and is much less sensitive to radiation than TMAE. If TEA is used, then the windows between the radiator volume and the wire-chamber detector must be of CaF, which is somewhat more expensive than the quartz window suitable for TMAE. The quantum efficiency for TEA is lower than that for TMAE, in part because it is sensitive over a smaller range of wavelengths. However, because the optical dispersion of TEA is less than for TMAE the former has greater resolving power for the Čerenkov rings. The stated thicknesses of the radiators yield about 15 photoelectrons per Čerenkov ring with TEA.

An SSC R&D proposal[35] has been submitted by several members of the BCD collaboration to study the methods of triggering with fast RICH input. The results of this study will influence the option of electron identification via the RICH counters.

Preliminary cost estimates are based on the RICH counters of E-665 and SLD, and are summarized in section 10.

5.6 Time-of-Flight Counters

Particle identification in the central detector will be accomplished through the use of several devices. A time-of-flight system will be used to identify charged hadrons of momenta up to a few GeV/c, which complements the capability of the RICH

counters at higher momenta.

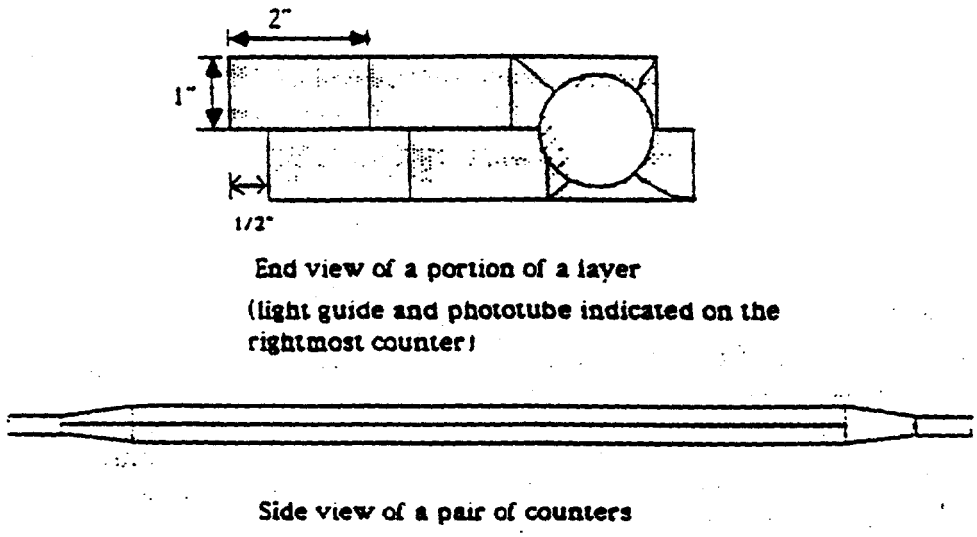

Figure 18: End and side views of the time-of-flight counters.

The system will be located 2 m from the beam, a distance constrained by the magnet-gap height. It will consist of two layers of $1'' \times 2''$ scintillator, staggered by $\frac{1}{2}''$, for a total of 640 scintillators. The scintillator will be chosen to have a fast rise time and long attenuation length. Adiabatic light guides will connect a set of two scintillators, ganged in depth (see figure 18) to two 2" photomultiplier tubes, one on each end. The phototubes must either operate in the magnetic field, or be located outside it.

The p.m. signals will be split, with part of the signal going to an ADC and part to a TDC. The ADC pulse height will be used to correct the TDC time, yielding a measurement which is better than that achievable using rise-time-compensated discriminators. The TDC's need to have a 50-ps least count. The stop time as measured by each tube will be combined to yield a single measurement for each track. Using this method, it should be possible to achieve a timing resolution of 70 ps per track. For counters at the 2-m distance, this allows a 1-σ separation of K's from protons at momenta up to 8 GeV/c, and π's from K's up to 4 GeV/c.

5.7 Transition-Radiation Detectors (TRD's)

Separation of e's from charged pions will be aided by multiple layers of thin-sampling TRD's.[38] The combination of tracking information with the transition-radiation

signal should permit an online pion-rejection factor of 50 in the TRD. The utility of the TRD's at small production angles needs further study.[39]

5.8 Electromagnetic Calorimeter

The calorimeter functions primarily to aid in electron identification, rather than providing a precision energy measurement. As such, position resolution is more critical. We thus have the option to use a sampling calorimeter (as opposed to total absorption in BGO or lead glass, *etc.*).

The calorimeter should have tower geometry, with three longitudinal samplings per tower. This feature should permit an online rejection factor of several hundred for charged π's. The transverse size of the towers should be sufficient that the energy measurement is of only a single particle with 99% probability, leading to a tower count of 10^4 given an average multiplicity of 100. A position-sensitive detector will be placed between the first and second layers of each tower to reject overlaps of a charged pion with a photon from π^0 decay. For this a two-track resolution of about 1 cm is desirable.

The particular form of the electromagnetic calorimeter is not specified at this time.

6 Front-End Electronics

6.1 Introduction

The front-end electronics will be in the form of custom integrated circuits, permitting low-cost and low-power readout of the large number of detector elements of the Bottom Collider Detector. All of the various chips proposed here are straightforward extrapolations or reconfigurations of presently available devices.

The front-end electronics should operate at a collider interaction rate of up to 5 MHz. Many of the readout signals are to be used in the first-level trigger, and all of the signals must be buffered during the 1-2 μs formation time of this trigger. VLSI chips (Bipolar and CMOS as appropriate) are mounted directly on the detector elements in order to amplify, shape, store and sparsify the signals. The basic module is a small number of high-channel-density ASIC's covering a relatively small physical area, tied together on a low-mass printed-circuit board. As this board serves many detector channels, the number of cables or optical fibers to the outside world is small.

Here we discuss the individual systems.

6.2 Silicon Strip Front End Electronics

6.2.1 General Considerations

The compact configuration of silicon planes will require local signal processing with a high degree of multiplexing. The signal processing speed must be compatible with the 2.5-MHz interaction rate at $\mathcal{L} = 5 \times 10^{31}$ cm^{-2}sec^{-1}. Analog and/or digital delay must be provided to allow time for a trigger decision to be made. Finally, the readout time must be minimized by use of sparsification. The first generation of suitable low-power "microplex" integrated-circuit readout electronics partially meets these goals and probably will be suitable for $\mathcal{L} < 10^{31}$ cm^{-2}sec^{-1}. The exact limitations will be established by testing. For $\mathcal{L} > 10^{31}$ cm^{-2}sec^{-1}, we will employ the chips currently under development for the SSC. The currently existing devices include the MPI CAMEX,[48,49] the LBL SVX[50] and the RAL MXI.[51] Below we comment briefly on the known properties of these CMOS chips.

MPI CAMEX

The 64- and 128-channel CAMEX chips were developed at the Max Planck Institute (Munich) for the ALEPH experiment at LEP. These chips are now being made commercially by ELMOS, Duisburg, Fed. Rep. Germany. The 64-channel chip has a power dissipation of about 120 mW and has been operated with a sampling time of 133 ns with a noise figure of 275 + 30 C_D[pF] electrons r.m.s., where C_D is the single-strip capacitance. The dependence of noise on readout speed has not been

measured. Radiation damage measurements have been made with a Co^{60} source and a broad-band x-ray source with a maximum energy of 200 KeV. The tolerance is not known for minimum ionizing particles and slow neutrons.

LBL SVX

The SVX chip was developed by Lawrence Berkeley Lab for the CDF detector at Fermilab. It has 128 channels with both analog and digital circuitry, and a total power dissipation of about 200 mW. The analog section provides up to two pairs of double-correlated samples, and in addition there is a comparator (discriminator) with a setable threshold. The readout has a fast-scan feature which selects only those channels with signal above threshold, and, if desired, the neighboring channels. In the fast-scan mode, channels not requiring readout take up no time in the readout cycle.

MXI

This chip was developed by Rutherford Appleton Lab for the DELPHI experiment at LEP and is a CMOS version of the Stanford Microplex[52] chip used in FNAL E-665[53] and Mark II at SLC. The RAL chip has 128 channels and dissipates 55 mW per chip. There are two storage capacitors per channel allowing a single pair of correlated samples. Radiation damage has been studied using a Co^{60} γ source.

6.2.2 New Devices

The current generation of VLSI silicon-strip readouts do not allow for a trigger delay. This problem is being addressed by the silicon strip readout system being developed by Seiden *et al.* at U. C. Santa Cruz. In their approach, an analog amplifier and comparator chip (AACC) provides a fast (15-ns rise time) signal that is digitized to 1 bit (yes or no). The bits are stored in a level-1 memory that is 64 cells deep and is clocked at the bunch-crossing rate of the accelerator. This is followed by a 16-cell-deep level-2 memory.

Another approach is to employ an analog pipeline for a trigger delay. Such a VLSI device with 10-MHz clock speed is being developed for the ZEUS calorimeter at HERA by a DESY-Fraunhoffer-Madrid-Nevis collaboration.

Other considerations are described briefly below.

- A possible feature for the front-end electronics is a pulse-height sum with a separate threshold used to reject greater-than-minimum-and nuclear interactions.

- It is important to note that driving the signal off the chip is very power consuming. The data readout would be over a few (10-100) optical fibers. Overall power-cost per channel probably can be kept to 1-3 mW/channel. With 10^5 channels, this is still considerable heat to dissipate.

- Bonding techniques such as indium bump bonding or tab bonding may make possible the connection of the CMOS chip to the detector strips at these high densities.

- We estimate about \$20/chip plus \$30 for packaging or about \$0.50/channel.

6.3 Straw Tubes

We take as our model the TVC chip set developed at U. Penn for the SSC (see figure 19). The bipolar amplifier/shaper/discriminator could be used directly and the CMOS TVC/analog store could be used but with a slower clock, typically 5-10 MHz.

The system would consist of the preamp/shaper/discriminator followed by the TVC/analog store/ADC/readout control chip. The bipolar chip will have four channels and the CMOS chip will have 8 channels. In addition the system would need a data-collection chip (digital CMOS) for every 8-32 TVC chips. Total power costs would be about 20 mW per channel. A possible arrangement would have a thin printed-circuit board mounted on the ends of 128 straws, with 32 bipolar chips, 16 CMOS TVC chips, and one data-collection chip, in addition to discharge protection and bypass and coupling capacitors for the straws. The cost would be about \$2-3 for the bipolar chip/channel, \$1-2 for CMOS, \$0.25 for the data chip and \$0.50 for mounting, for a total of $<$ \$6/channel.

It will be useful to include segment-finding electronics for some of the superlayers. This should be possible by adding a CMOS digital-logic chip in parallel to the CMOS TVC chip. Found segments would then be shipped to the trigger system. The increase in power cost should be only about 10% assuming a high level of multiplexing.

6.4 RICH Counter

A readout system identical to that for the silicon strip detector is planned for this system. The RICH counter will have pad sensors whose signals will be similar in magnitude and shape to the signals from silicon strips. While the electronics for this detector will be identical to the silicon system, the mounting problems and power-density problems are much different. Individual pads will have to feed in over a fairly large area to a single CMOS chip: small groups of these front-end chips would then feed into a local data-collection chip and thence out to the data-acquisition system. The relatively low density of connections will keep the per channel cost much less than in the silicon case ($<$ \$0.25/channel).

DRIFT CHAMBER ELECTRONICS

TIME MEASUREMENT

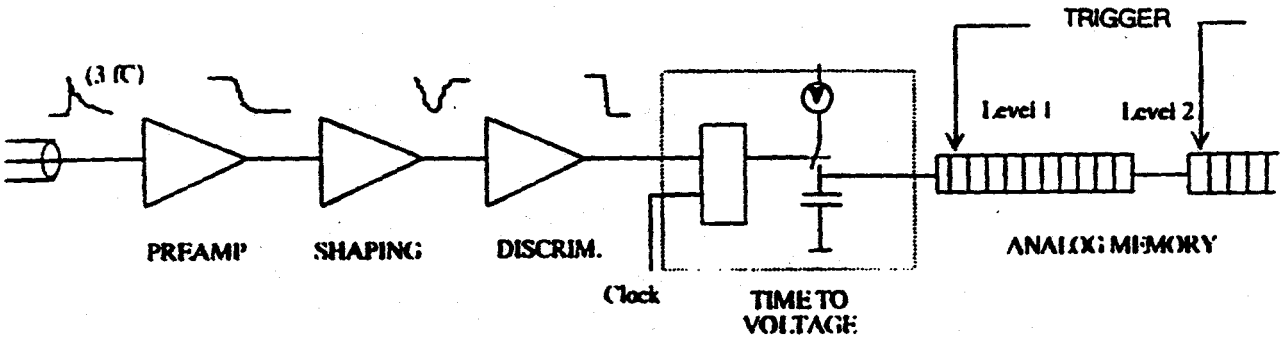

REQUIREMENTS:

TIME RESOLUTION:	< 0.5 ns
DOUBLE PULSE RESOLUTION:	20-30 ns
MEMORY STORAGE:	1 us
ENC:	700-1000 e-
POWER:	< 10-15 mW
RADIATION HARD:	1-10 Mrad
SIZE:	< 1 sq. cm/channel

Figure 19: Block Diagram of SSC chip set

6.5 TRD

The TRD detector will have many separate layers of wire-chamber detectors, The electronics must sense clusters on individual wires, but the linking and majority logic to find tracks would be done outside the detector. While the silicon-detector CMOS system would be appropriate in terms of signal handling, the relatively low density, linear arrangement of wires would probably argue for the development of a lower-channel-count CMOS device that could be more easily tied to the chamber. For the lower-channel-count device (*e.g.*, 8–16 channels), the effective power per channel would go up slightly because of the increased output-drive requirements. The cost in dollars however, would scale almost directly with TRD area and should be equivalent to the RICH-counter costs per channel.

6.6 EM Calorimeter

The calorimeter would use a readout system similar to that of the straw tubes in the sense that a bipolar front end would feed a CMOS delay-and-encode section. However, the calorimeter requires charge measurement over a large dynamic range and may or may not require an acurate time measurement. Thus the bipolar chip will necessarily require rather more power (for the dynamic range) and the CMOS chip will require more area for storage capacitors (high- and low-charge ranges). In addition the calorimeter will serve as one of the primary triggering detectors and must provide fast signals out of the detector to the central triggering system. These signals will require > 40 mW per output, but the trigger outputs will be sums of local channels so that the total power burden is not greatly increased. If a suitable clustering algorithm can be defined and tested, it is possible to imagine shipping only cluster position and size information to the trigger system, greatly reducing the burden on and increasing the power of the trigger. We estimate that the total power requirement per channel would be about 30 mW and the cost per channel would rise slightly to $< \$7$. Mounting and cooling is least restrictive in this region and we anticipate no major problems for the calorimeter system.

6.7 Development Costs

The purely digital CMOS chips are amenable to commercial design and production, but the analog bipolar and mixed analog/digital CMOS chips will require careful simulation and design. Each of the analog designs will require about three to four months of an expert engineer's time to develop and an additional foundry cost of order \$25K per chip (per run). Digital CMOS designs can be handled commercially for order \$40K per chip with only block-level schematics provided to the foundry.

6.8 Chips to be developed

1. CMOS preamp/discriminator/delay/encode - 128 channels.
2. CMOS data-collection fiber driver, all digital, possible to design and fabricate commercially.
3. Bipolar preamp/shaper/discriminator - 4 channels, after the design of Newcomer, *et al.* - should need little work.
4. CMOS TVC analog-store/encode - 8 channels, Penn/Leuven design - may need only to be appropriately packaged.
5. CMOS preamp/discriminator/delay/encode - 8 chan, a subset of design 1.
6. Bipolar high-dynamic-range preamp/shaper/discriminator - 4 channels, variation of 3.
7. CMOS TVC Charge analog-store/encode - 4 channels, variation of 4.
8. Clustering and trigger-driving chip, analog CMOS, perhaps based on neural-net work at Penn.

7 Trigger and Data Acquisition

7.1 Introduction

We propose a trigger architecture in which a first-level hardware trigger is followed by a software trigger implemented in an online array (farm) of numeric processors. The philospohy of this approach is that any trigger decision which uses digital information should be made in commercial, programmable processors.

The first-level trigger should reduce the rate by a factor of 50 in a 1-2 μsec decision time, so that even at a luminosity of 10^{32} cm^{-2}sec^{-1}, for which the interaction rate is 5 MHz, at most 100 kHz of events are presented to the numeric processors. The data from the various detector components can be organized into event records at a 100 kHz rate via the "barrel-switch" technology of the telephone industry. The numeric processors, perhaps 2000 in total, each are the equivalent of 30-50 VAX 780's. The archival event rate will be about 1 kHz, which can be accomodated by video-cassette tape drives.

Two types of first-level triggers will be implemented. A simple trigger is based on a requirement of 1 or 2 tracks above a mimimum-P_T cut of 2-3 GeV/c. More ambitious is a trigger on an electron above a mimimum-P_T cut of only 1-1.5 GeV/c, which would also provide a tag on the triggering B as particle or antiparticle.

Each of these first-level triggers is then completed in the numeric processors. The topology trigger is followed by a requirement of a reconstructed secondary vertex, while some aspects of the electron trigger can only be implemented with the power of the numeric processors.

7.2 Triggers

7.2.1 Topology Trigger

The B mass, as well as its typical production transverse momentum, are large compared to the average transverse momentum of particles from p-$\bar{p}$ collisions. Hence a "stiff-track" trigger will be enriched with B's.

Figures 20a and 21a show the number of tracks having transverse momenta above a given value in events containing a $B \to \pi^+\pi^-$ decay, and any B decay, respectively. For comparison, figure 20b shows the same distributions for all events (according to an ISAJET model) not containing a B, while figure 21b shows these distributions for all events.

We infer from figure 21b that with a requirement of 1 track above $P_T = 3$ GeV/c, a factor of 50 reduction in the trigger rate can be obtained. Then the efficiency for the $B \to \pi^+\pi^-$ decay is still 90%, as seen in figure 20a. Also, the efficiency for all B decays remains about 25%, as seen in figure 21a.

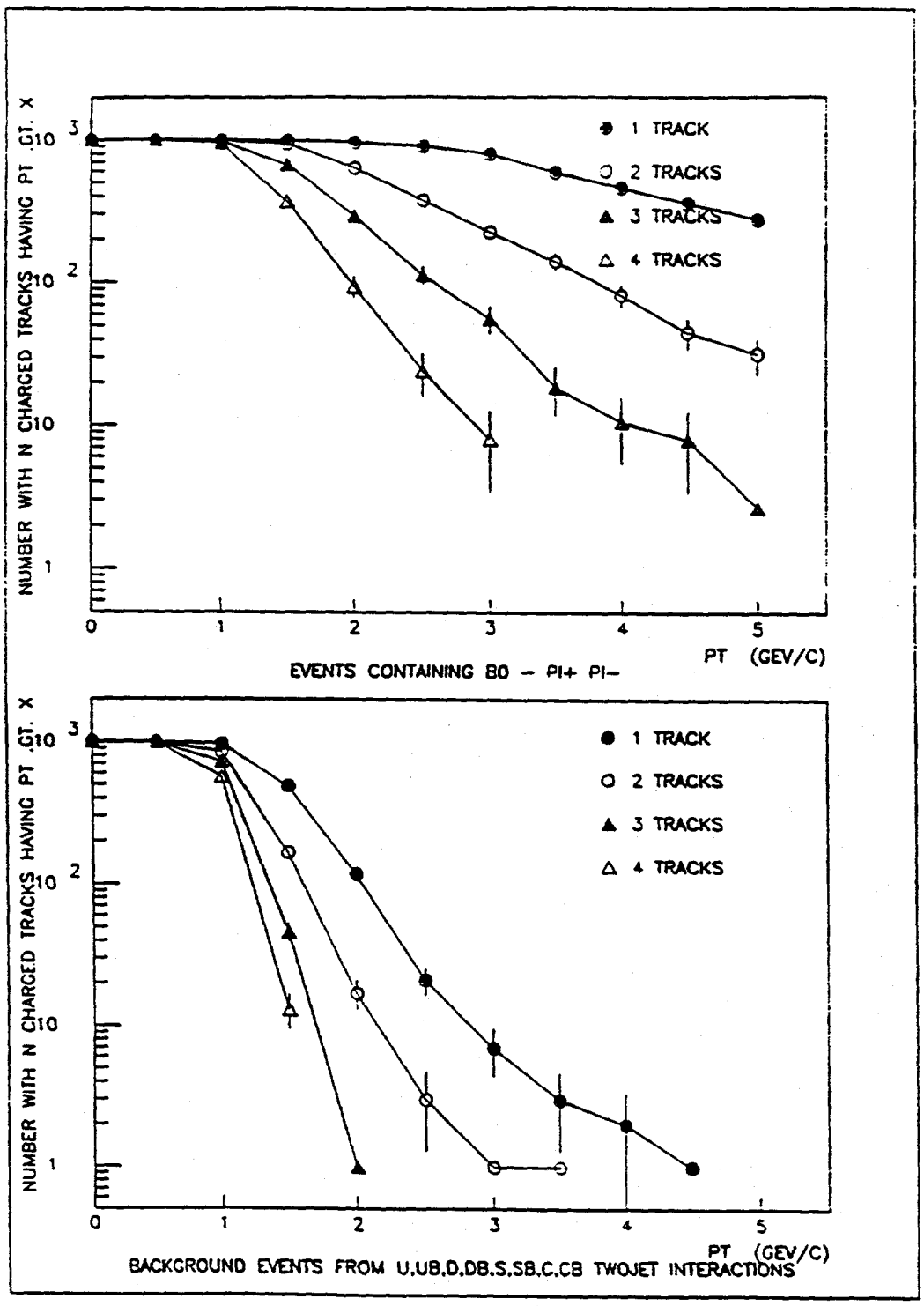

Figure 20: (a) The number of charged tracks above a given P_T for events containing a $B \to \pi^+\pi^-$ decay, according to an ISAJET simulation; (b) the same for events without any B's.

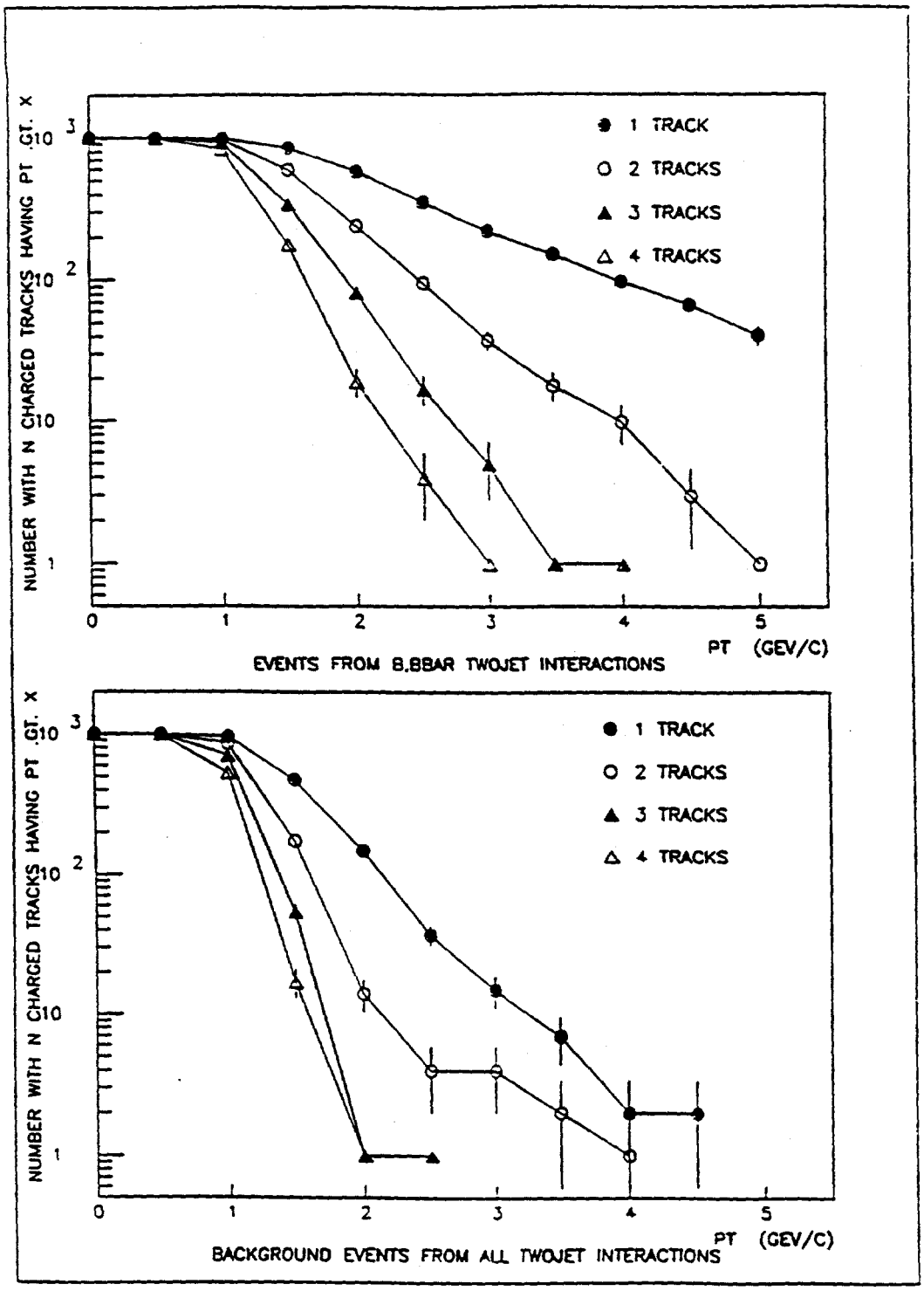

Figure 21: (a) The number of charged tracks above a given P_T for event containing a B decay; (b) the same for all events.

A trigger requiring two tracks both above a P_T cut might be less vulnerable to fake tracks; for a 2-track cut at 2 GeV/c a factor of 50 enhancement can also be obtained, but with only about 70% efficiency for the $B \rightarrow \pi^+\pi^-$ decay, and 30% efficiency for all B decays.

The events surviving the topology trigger are then fed to the processor farm, where an additional factor of 100 reduction in rate is desired. This could be attained if a secondary-vertex-finding algorithm can be implemented online. Simulations of the necessary algorithms on fast numeric processors[35] will be performed in the coming months to evaluate this trigger strategy.

7.2.2 Electron Trigger

Another signature of a B meson which appears suitable as a trigger for the Bottom Collider Detector is a moderate-transverse-momentum electron from a semileptonic decay. As indicated in figure 22 (based on an ISAJET calculation) about 50% of semileptonic B decays yield an electron with $P_T > 1$ GeV/c. The semileptonic branching fraction is 12%, and either B of a $B\bar{B}$ pair is suitable for triggering. Thus a trigger cut of $P_T > 1$ GeV/c on electrons could yield a 12% triggering efficiency for $B\bar{B}$ pairs. If the efficiency of electron identification, including eventual offline reconstruction of a secondary vertex for the $B \rightarrow eX$ decay, is 25% an overall trigger efficiency of 3% could be achieved.

This is a formidable goal at a luminosity of 10^{32} cm^{-2}sec^{-1}, as the electrons must be identified amidst a 5-MHz interaction rate yielding a 500-MHz total rate of particles in the detector. The rate of prompt electrons which would satisfy this trigger is 1-2 kHz.

Only part of the electron trigger could be implemented in the front-end analog logic. The signals from the electromagnetic calorimeter would be combined into candidate clusters. The longitudinal energy distribution within a cluster can provide a rejection factor of over > 100 against charged pions. A pad chamber immediately preceding the calorimeter insures that the cluster is due to a charged particle. Events passing these cuts must be passed into the numeric processors to reject converted photons, Dalitz decays, and $\pi^{\pm}$-π^0 overlaps.

In the rest of this section estimates are given as to the rates of various classes of fake-electron events.

Sources of Electrons

A summary of the rate of electrons from various sources as a function of transverse momentum is shown in figure 22. Prompt electrons derive from direct electronic bottom and charm decay, e^+e^- decays of vector mesons, and Dalitz decays of pseudoscalar mesons. Fake-electron triggers will derive from misidentified $\pi^{\pm}$'s, including $\pi^{\pm}$-π^0 overlaps. A hint of the severity of the fake-electron problem is given

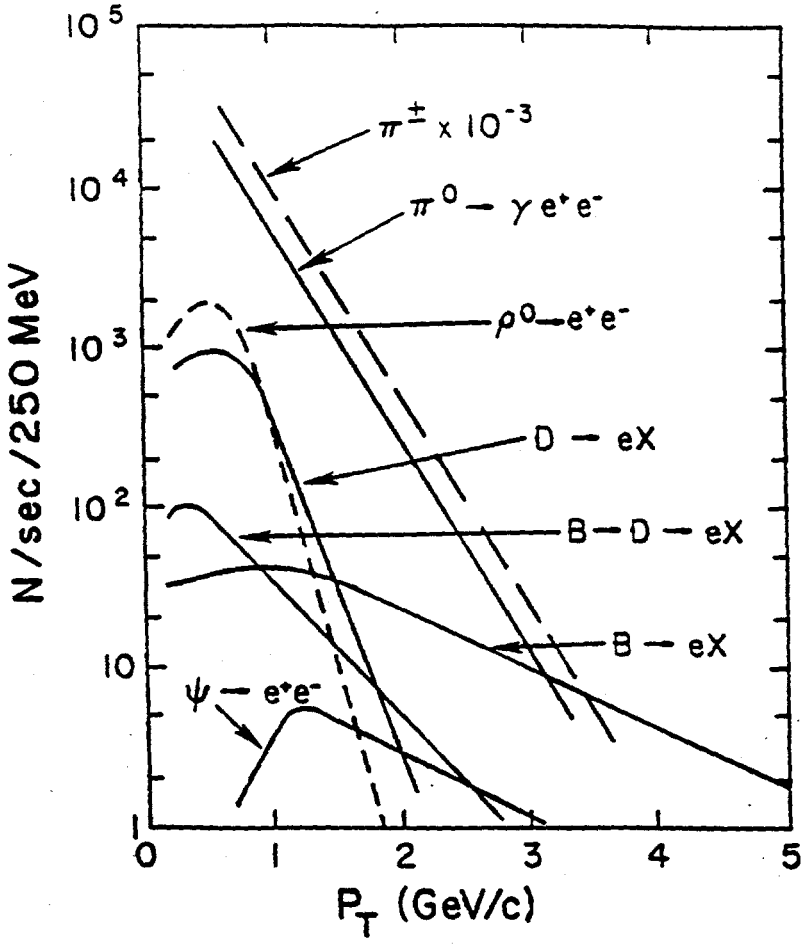

Figure 22: The rate of electrons per 250-MeV/c bin from various sources in p-$\bar{p}$ collisions at $\sqrt{s} = 2$ TeV and luminosity 10^{32} cm^{-2}sec^{-1}.

by the spectrum for $\pi^{\pm}$, also sketched in figure 22.

The present philosophy is to pass all prompt electrons to the offline event-processing stage (supposing the fake-electron triggers can be sufficiently suppressed). With a trigger cut of $P_T > 1$ GeV/c a substantial fraction of the prompt electrons are from B decay, and there is no need to distinguish among the various sources of prompt electrons in the trigger.

Misidentified Hadrons

The rate of charged π's into the detector is about 300 MHz: 60 charged pions per event times the 5-MHz interaction rate. Of these about 15 MHz have transverse momentum above 1 GeV/c and so are potential fake triggers if misidentified as electrons. The online π-e rejection must be greater than 10^4 to reduce fake electron triggers to a 'mere' 1 kHz.

Three types of detectors could contribute to π-e separation: the transition-radiation detectors, the electromagnetic calorimeter, and the RICH counter (at least for low-momentum particles). We suppose that a multi-layer system of tracking

TRD's can yield a rejection factor of 50, but this would be achieved only in the numeric processors. The RICH counter might yield a factor of 5 rejection, most likely also in the numeric processors.

The electromagnetic calorimeter is configured with three longitudinal samples. Comparison of the relative pulse heights in these three layers could yield a factor of 50-100 rejection against pions in a hardware trigger. A match of the shower energy with the charged-track's momentum will be made in the numeric processors; only interactions leading to $\pi^{\pm}$-π^0 charge exchange will survive this E/P cut. The overall rejection factor from the electromagnetic calorimeter is greater than 500. The combined rejection factor from the three detector could then be 10^5, corresponding to a trigger rate of 150/sec from misidentified hadrons.

Overlaps of $\pi^{\pm}$ and γ's from π^0's

A fake-electron trigger is generated if the momentum of a charged pion matches the energy of a π^0 whose shower overlaps the charged-pion track in the electron calorimeter. The TRD and RICH detectors still provide rejection of the charged pion, so the rate of dangerous charged pions is 0.01×15 MHz $= 150$ kHz. Further rejection is obtained by spatially resolving the charged track from the π^0 shower in the electron calorimeter.

A study of the overlap problem was made with the ISAJET Monte Carlo program. Initially, an 'overlap' was defined as a charged pion whose separation from a neutral pion was $|\Delta\eta| < 0.1$ and $|\Delta\phi| < 0.2$. It was found that about 7% of charged pions with $P_T > 1$ GeV/c had such an overlap. These overlaps are dangerous only if the E/P cut is also satisfied. Assuming the electron calorimeter has energy resolution for photons of $\sigma_E = 0.15\sqrt{E}$ the statistical significance of the E/P cut in standard deviations is

$$S.D. = \frac{|E-P|}{0.15\sqrt{E}}.$$

A cut requiring a 2σ separation of E of the π^0 from the P of the $\pi^{\pm}$ yields a rejection factor of 15. The rate of overlaps satisfying the combined trigger cuts is then less than 1 kHz.

The definition of overlap used above is satisfied by a pair of pions whose separation is less than 10 cm at 1-m radius from the beamline. However, two particles should be resolvable in the electron calorimeter if their separation is only 1 cm, which would provide an extra rejection factor of 100. In this case the rate of fake-electron triggers from overlaps would drop to only 10 Hz.

Dalitz decays and γ-Conversions in Matter

The branching fraction for the decay $\pi^0 \rightarrow \gamma e^+ e^-$ is 0.015, as if the vacuum is 0.007 of a radiation length thick. Electrons from conversions of γ's in material will be more numerous than those from Dalitz decay if the photon has traversed

more than 0.007 radiation lengths. For example, with a beam pipe whose wall is 400-μm-thick Be, or 0.001 of a radiation length, photons at angles of less than 1/7 to the beam are more likely to convert in the pipe than during the π^0 decay.

Figure 22 shows that the rate of electrons from Dalitz decay with $P_T > 1$ GeV/c is about 10 kHz at a luminosity of 10^{32} cm^{-2}sec^{-1}. The rate of electrons from γ-conversions in matter will be higher. Thus a rejection factor of order 100 is needed against these conversions.

Conversions outside the beam pipe can be suppressed by fast tracking all the way to the first silicon plane. Conversions in the pipe and Dalitz decays could be suppresed by a dE/dx measurement in the first silicon plane. These factors could only be obtained via algorithms running on the numeric processors.

Electron Detection Efficiency

The process of electron identification inevitably causes some real electrons to be lost. Rough estimates of the various detection efficiencies are:

- Fast tracking: 0.95
- E/P cut: 0.95
- TRD cut: 0.90
- RICH counter cut: 0.95
- Electron shower overlapped by another particle: 0.95
- Photon-conversion cuts: 0.90

The overall efficiency of electron identification might then be 0.62.

7.3 Data Acquisition

7.3.1 Basic Architecture of the Data-Acquisition System

The architecture of the Data Acquisition system takes advantage of several new approaches, in particular:

- Digital transmission via fiber optic cables.
- Numeric processors, especially suited to physics problems, are used for the second-level triggers employing in some cases full reconstruction algorithms.
- Simple barrel shifter for online event building.

A block diagram of the proposed data-acquisition system is shown in Figure 23. Data flow is from top to bottom. Prompt triggers will first reduce the data rate by a factor of 20-50 (subset of detector elements A-Z in figure 23). From this point on in the system there is no other specially built logic for triggering. If the event is accepted by the first-level trigger, fragments are transmitted over fiber-optic cable to the Event-Builder Switch. There can be any number of data sources from each detector element.

The Event-Builder Switch receives event fragments from the detector elements and transmits unformatted total-event streams as its outputs, one total-event stream per output. There are no data-flow bottle necks in this system. Data rates of tens to a few hundreds of GigaBytes/second are possible.

The Receiver/Formatters receive total-event streams, buffer a small number of events, format the data into data structures suitable for higher-level-language applications programs, smooth out data flow and transmit formatted events to banks of processors. A block diagram of an example of a Receiver/Formatter is shown in figure 24.

The Receiver/Formatters pass the data to a farm of numeric processors. Industry-available numeric processors especially suited for solving $AX + B$ problems and capable of 100 Megaflops are used in this farm. Software triggers implemented in these processors reduce the data by a factor of 100-200 permitting the remaining events to be written to tape. These same processors can be used for offline data processing.

More details on the individual components follow.

7.3.2 The Event-Building Process

The Event-Builder Switch is intended to provide the usual event-building function, but at a bandwidth which makes it possible to work with total-event data at an earlier point in the system hierarchy. Together the Transmitters, Receiver/Formatters and the Event-Builder Switch form a communication network which is similar to a standard telephone switching system. Front-end data is buffered in the Transmitters. From there the data is time-division multiplexed on high-speed serial channels through the Event-Builder Switch. Receiver/Formatters at the Switch outputs serve to reassemble and buffer the total-event data.

The Switch is a simple barrel shifter requiring no significant control logic. The serial-line speeds are much higher than is typically used in local telephone systems but lower than in many long-distance trunks. The Transmitters and Receivers/Formatters are basically data buffers with enough control logic to break the data into packets and then reassemble it. Like a telephone network, this system provides a transparent connection from every possible data source to every possible destination with a limited number of wires.

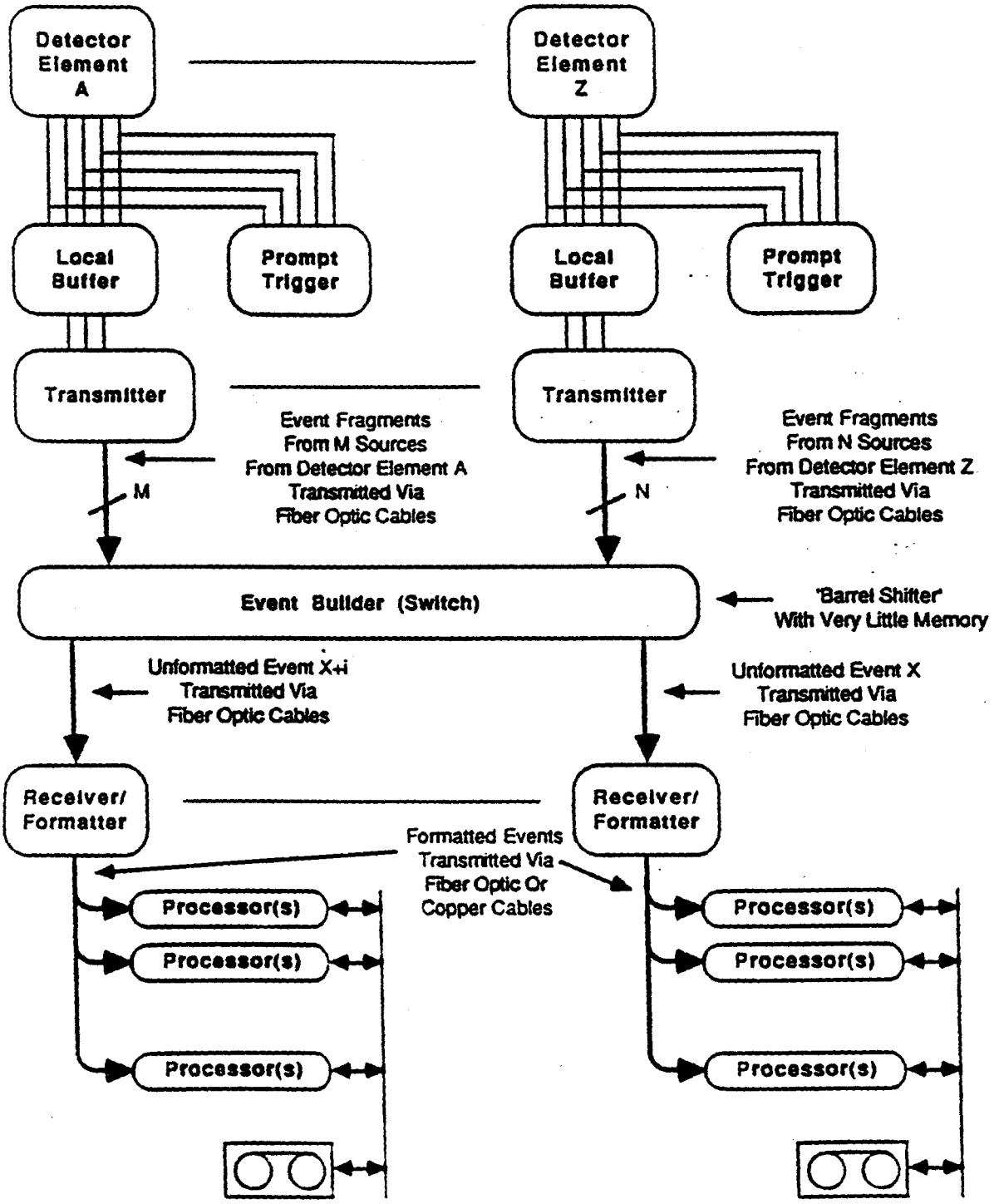

Figure 23: Block diagram of the proposed data-acquisition system.

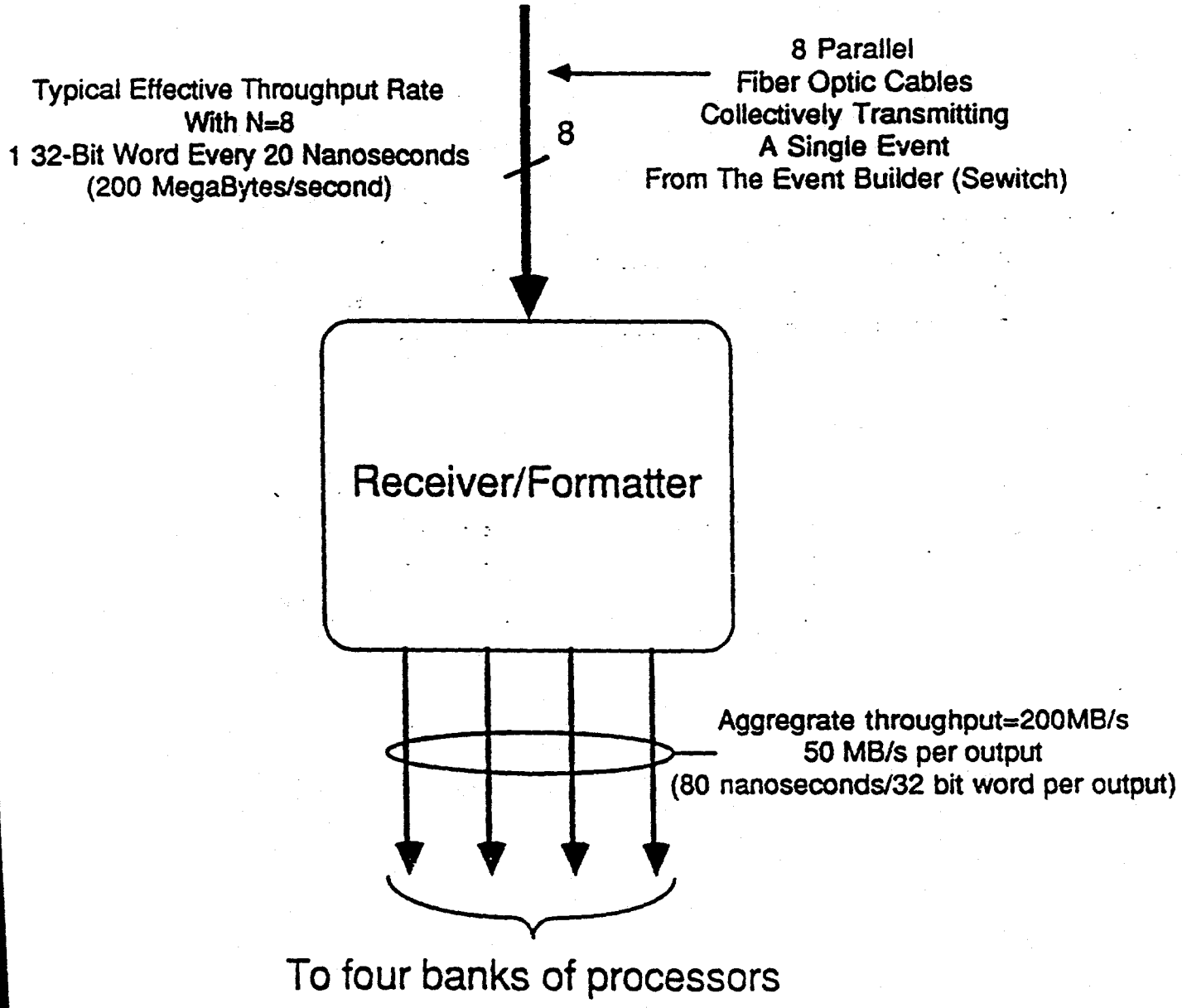

Figure 24: Block diagram of an example implementation of a Receiver/Formatter.

Use of the serial data channels reduces the number of cables leaving the detector while also eliminating many of the synchronization problems associated with parallel busses. It also moves data directly into the processor modules at rates 10 to 20 higher than possible using standard backplanes.

7.3.3 Processors

Microprocessors with on-chip floating point units in the 20 VAX-equivalent range are available now at reasonable cost. Soon-to-be-announced devices will provide an estimated 30 to 35 VAX-equivalents and by 1993 this number will be about 50 VAX-equivalents. We intend to replace much of the specialized electronics used in second-level triggers with programmable processors.

Digital signal processors and RISC processors which have been optimized for graphics applications have many features that would be useful in event reconstruction. For example, these new processors are able to perform fixed- or floating-point $Ax + B$ operations in a single cycle.

7.3.4 Fiber-Optic Digital-Data Transmission

Present fiber-optic data-transmission technology supports rates from less than 1 Megabit per second to higher than 10 Gigabits per second. These rates are achieved by using LED diodes at low frequencies and laser-diode optical transmitters coupled with light-sensitive receiving diodes connected to automatic-gain-controlled amplifiers at high frequencies. Costs vary between $200 for the slow devices to over $10,000 per pair for the fast devices.

There are existing communication chips that can be used in an optical-link design. Allowing for transmission overhead, these chips transmit at 12.5 MegaBytes per second. These chips are called TAXI chips and are available from Advanced Micro Devices. These chips accept parallel data, serialize and encode the data, and transmit the data, with the addition of optical components, over fiber-optic cable. At the receiving TAXI chip the data is decoded and converted into parallel form. These rates allow the use of relatively inexpensive LED components. Present estimates are that optical components can be designed for a short link (up to 500 meters) that will cost about $100 for a transmitter/receiver pair. For single source transmission rates higher than 12.5 MegaBytes per second, several fiber-optic cables can be used in parallel.

8 Machine Issues for Tevatron

8.1 Detector and Collision Hall Issues

The accelerator-related requirements for the Bottom Collider Detector are derived from the performance needed to achieve the physics goals in section 1. The central detector has a dipole magnet with a 1-Tesla field transverse to the beam axis, and a field volume of roughly four by four square meters by four meters along the beam axis. Compensation must be made for the transverse deflection of the beams by the dipole magnet.

The detection of the $B\bar{B}$ decay products requires that a sophisticated solid-state vertex detector and electronics, which may be prone to radiation damage, be located within 1/2" of the beamline. There will also be a forward/backward detector that extends several meters up- and downstream from the central detector.

The space required in an experimental hall is roughly determined by the overall dimensions of the detector. As presently envisioned, the detector occupies a volume of about ten by fourteen meters in cross section and 15 meters in length. The dimensions of the spectrometer magnet are comparable to those of the Chicago Cyclotron Magnet but with 4 times larger gap.

There are two ideas for a location for this experiment. The first is to use the $B0$ intersection region. This assumes that CDF no longer occupies this region. The region is ideal for the B collider experiment. The second option is to build a new collision hall, shown in figure 25, that would be available if the proposed Main Ring Injector, part of the Tevatron Upgrade, is constructed. By removing the main ring from the Tevatron tunnel, a third intesection region could be added. Estimates for the cost and downtime are included. The construction for the collision hall will take place during the shutdown for removing the Main Ring Injector and would take 6–10 months.

8.2 Beam Energy

The present detector is designed for the 1 × 1 TeV beams of the Tevatron. The $B\bar{B}$ production cross section varies approximately linearly with collider beam energy, so an option to run with 1.5-TeV beams would yield 50% more B's at the same luminosity.

8.3 Luminosity

As discussed in section 1, systematic exploration of CP violation in the $B\bar{B}$ system becomes possible for luminosities of order 10^{32} $cm^{-2}sec^{-1}$. The large investment in the Bottom Collider Detector would be problematic if the average luminosity were

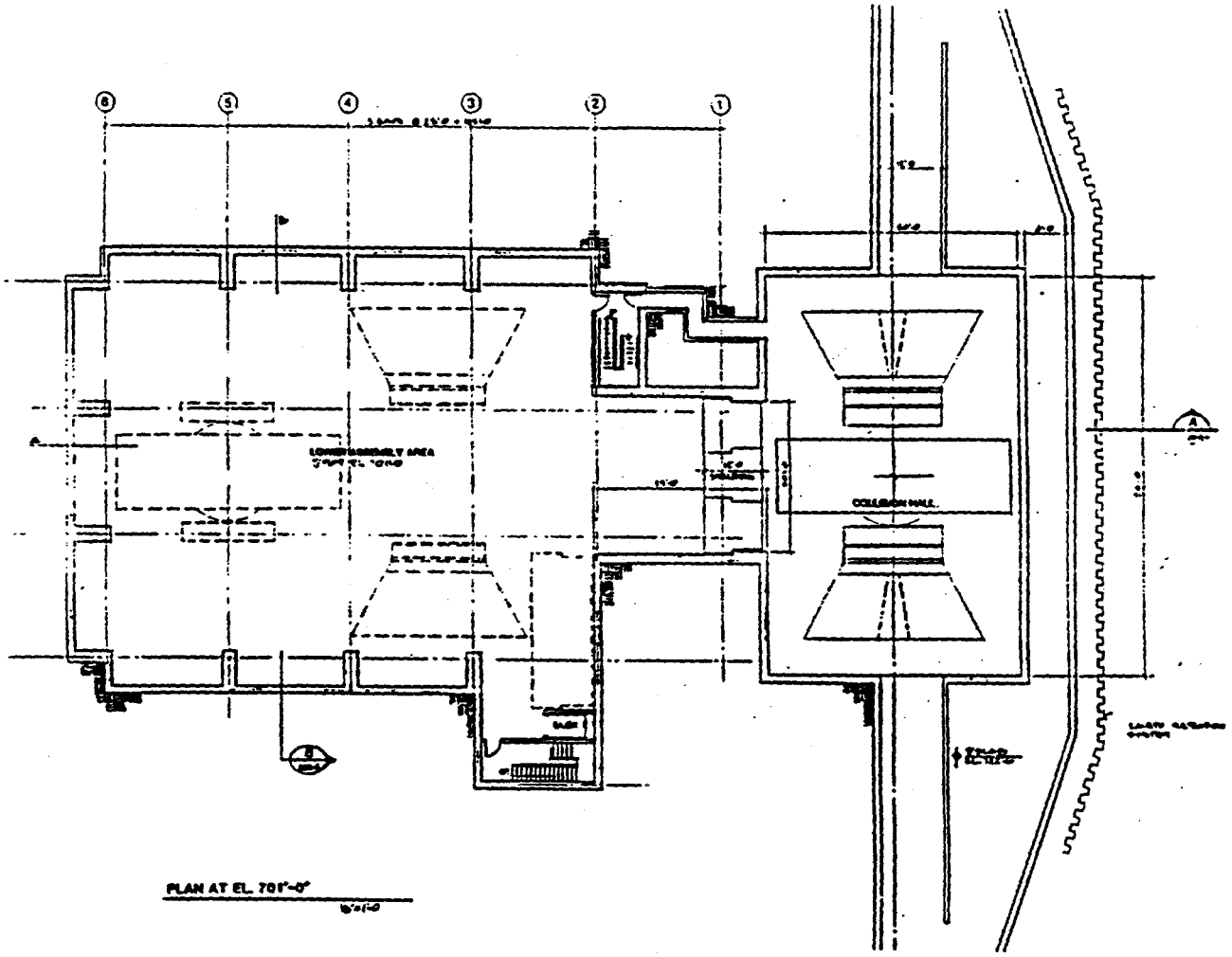

Figure 25: Layout of a new collision hall for the Bottom Collider Detector.

only 10^{30} cm^{-2}sec^{-1}. We recommend an average luminosity of 10^{32}cm^{-2}sec^{-1} be the accelerator goal. The higher luminosity and greater reliability of a p-p collider make this option extremely desirable for B physics.

8.4 Length of the Interaction Region

The length of the interaction region determines the length of the vertex detector. At the present Tevatron the interaction region has a σ of 35 cm. A vertex detector for this region would have to be at least one meter long, with several 10^5 readout channels and unwanted material close to the beam pipe. Current discussions for a Tevatron Upgrade include the possibility of a higher frequency rf system to bunch

the accelerated beam, yielding a shorter interaction region with a σ of 10 cm. The reduction in σ_z would greatly simplify the vertex detector design, lead to a significant reduction in the cost of the vertex detector, and eliminate much undesirable material intercepted by small-angle tracks.

Although all current versions of the Upgrade make provision for a reduced interaction-region length, the p-p option offers the greatest flexibility in that a crossing angle is part of the machine design. By increasing the size of the crossing angle, the length of the interaction region can be proportionately reduced at the expense of luminosity.

8.5 Beam Size

A small transverse beam size is desirable for several reasons. An important signature of B decays is the detection of their decay vertex some few-hundred μm from the primary interaction point. If the beam size is small compared to 100 μm then we gain the considerable advantage of regarding the beam as 1-dimensional. The diameter of the beam pipe, and therefore the vertex detector, is determined by the beam size. The motion of the beams within the beam pipe when the spectrometer dipole is turned on, which also affects the size of the beam pipe, is minimized when the beam size is smallest. And, of course, one achieves higher luminosity with a smaller beam cross section as well.

8.6 Beam Pipe

Conversions of photons in the beam pipe and multiple Coulomb scattering must be minimized in this experiment. A suitable beam pipe could be made of 400-μm-thick beryllium and should be roughly 1/2" in radius.

8.7 Beam Halo

Halo associated with the beams will contribute to the radiation exposure of the vertex detector and thereby shorten its lifetime. Present data indicate that the silicon detector can survive 10^5 rads and the micro-electronics withstand about 10^4 rads. It is clear that catastrophic beam loss must not occur near the detector. The beam-loss level for abort may need to be lowered compared to present operation.

8.8 Compensation for the Dipole Field

The presence of a spectrometer dipole in the Tevatron would alter the beam trajectory unless compensating measures are taken. The scheme that has been chosen for compensation uses two dogleg bends, one at each end of the straight section and each

20 feet from the center of the interaction region, just downstream of the low-beta quads. The two magnets are both of opposite polarity relative to the spectrometer dipole, and run in series with it (that is, the currents run up together). The spectrometer dipole and compensating magnets are energized only after coasting beam has been established. The beams at the crossing region then move laterally a few mm as the magnets are energized.

8.9 The Detector Hall and Support Facilities

The Detector Hall required for this facility will be comparable in size to that at D0. The detector itself will fill about one half the space available in a straight section at the Tevatron. The compensating dipoles are placed at the outer ends of the straight section. The need for electron detection, calorimetry and particle identification will require the use of special gasses and liquids. The detector may use ethane, TMAE, or TEA. Additional cryogenic support may be necessary to service the main dipole magnet. The detector will require a substantial signal processing area. The Detector Building must also provide for a control room, office and technician space and shop support.

An initial design of a new collision hall has been prepared by Nestander's Engineering Services Group.

8.10 Summary and Status of Accelerator Issues

The broadest issues associated with the accelerator have been successfully worked out. The installation of the spectrometer dipole magnet in the Tevatron seems eminently feasible. The detector size (except perhaps for the magnet yoke) is relatively modest compared to present collider detectors. The magnet parameters are well understood. The location of a vertex detector around the beam pipe is a main feature of this detector and presents special considerations for the accelerator.

The issues that remain to be solved are those that interface with the accelerator beam optics. While the field nonuniformity of the spectrometer dipole is not thought to pose a serious problem it must be studied in more detail. Methods must be developed to insure that a catastrophic loss of beam into the vertex detector does not occur.

Finally, although interesting physics can be performed with an average luminosity of 10^{31} $cm^{-2}sec^{-1}$, the detector will operate at 10^{32} $cm^{-2}sec^{-1}$, and we urge that a concentrated effort be exerted to meet this goal. With this higher luminosity the physics capability will be greatly expanded.

9 Prototyping and Test-Beam Efforts

A Yale/Fermilab group[59] has begun evaluation of the existing VLSI silicon readout chips using a test setup at Fermilab modeled after the one developed for CDF. We have obtained samples of all three available CMOS chips: CAMEX, SVX, and MXI. The noise performance of these chips has typically been evaluated for sampling and readout speeds unique to a particular experiment. Generally, the measurements relevant for the B-detector have not been made. We will measure the levels of signal and noise as a function of sampling rate, readout rate, number of samples, and power dissipation.

Whereas extensive radiation damage measurements have been made for silicon microstrip detectors using intense minimum ionizing beams and neutron sources, the VLSI readout chips have typically been subjected only to radioactive sources for the CMOS chips and synchrotron radiation for the SLAC microplex chip. To study the effect of minimum ionizing radiation we will place the chip directly in a test beam. To study the effect of heavy ionizing radiation we will place the readout chip downstream of various targets of substantial interaction and radiation lengths. This will be a realistic test of "albedo" encountered in a collider experiment from interactions in the beam pipe and detector material. We will make these measurements over a broad range of beam energies to simulate those encountered in colliding beam interactions.

A key feature of these measurements will be use of readout chips wire bonded to a silicon microstrip dectector to enable evaluation of the *system performance* and not just the readout chip alone. Thus the problems of channel-to-channel variation, RF shielding, cooling, and mechanical mounting will be addressed. In addition, we will develop the practical expertise necessary to mount an experiment with these devices.

Other prototyping efforts associated with this proposal include evaluations of double-sided silicon detectors at the U. of Oklahoma,[60] studies of scintillating fibers for forward tracking and/or calorimetry at Northeastern U., studies of silicon drift chambers at Princeton U.,[61] and studies of new-technology numeric processors at Fermilab and U. Penn.[35]

10 Cost

The estimated costs are quoted in thousands of dollars. Items 4-8 are for mechanical components of the detectors; the cost of the front-end electronics is quoted separately.

1. Magnet

   New magnet coils 3,000
   or, use MFTF coils 500
   Cryogenics 2,000
   Iron 1,500
   Assembly 1,000

2. Be Beam pipe 200

3. Compensating magnets 200

4. Silicon vertex detector

   400 wafers @ \$1k/wafer 400
   Engineering: 4 FTE's × 2 years @ 60k 480

5. Straw-tube chambers

   2×10^5 channels @ \$2 per straw 400
   Engineering: 3 FTE's × 2 years @ 60k 360
   Test equipment 100

6. TRD 1,000

7. RICH 3,000

8. EM calorimeter 3,000

9. Time-of-Flight Counters 200

10. Prompt trigger 400

11. Data acquisition

    Processor farm 3,200
    100 Exabyte tape drives 400

Host VAX, disk drives and workstations.....1,000

Engineering: 8 FTE's × 3 years @ 75k.....1,800

6 FTE's × 3 years @ 50k.....900

12. Front-end electronics

Silicon vertex detector: 500k channels @ $1.....500

Straw-tubes: 2×10^5 @ $6 per channel.....1,200

TRD: 10^6 pads @ $1 per channel.....1,000

RICH: 10^6 pads @ $1 per channel.....1,000

EM calorimeter: 50k channels @ $6.....300

13. Chip development

6 analog chips: each 1 FTE × 2 years @ 75k.....900

Foundry costs: 6 chips × 2 runs × 25k.....300

3 digital chips: 2 runs × 40k.....240

Test equipment.....500

Total.....27,980

Acknowledgements

We thank the laboratory management, Leon Lederman, John Peoples, Helen Edwards and Ken Stanfield for general support in this continuing effort. James Bjorken has continuously stressed the importance of bottom physics for several years now, and has contributed greatly to our enthusiasm and understanding of this subject. We also thank Bob Wands, Alan Wehmann, Ron Fast and Thorton Murphy for help with the beginnings of a magnet design. Finally we thank Rick Van Berg for help with the Front End Electronics section and Wayne Nestander for help with the collision hall study.

11 References

[1] P. Karchin, N. S. Lockyer, *et al.*, *Proposal for a Bottom Collider Detector* **BCD**, (March 1987).

[2] N. Reay, *et al.*, *Letter of Intent for a Tevatron Beauty Factory*, (March 1987).

[3] N. S. Lockyer, *Issues for a Bottom Collider Detector at Fermilab*, Proceedings of the High Sensitivity Beauty Physics Workshop held at Fermilab (Nov. 1987), Editors. J. Slaughter, N. S. Lockyer, M. Schmidt.

[4] Neville W. Reay *et al.*, *Summary of the Collider Architecture Working Group*, Proceedings of the High Sensitivity Beauty Physics Workshop held at Fermilab (Nov. 1987).

[5] K. Foley *et al.*, *A Beauty Spectrometer for the SSC*, Proceedings of the Workshop on Experiments, Detectors and Experimental Areas for the Supercollider, (Berkeley 1987) R. Donaldson and G. Gilchriese editors.

[6] BCD Study Group, *Status Report of the Fermilab B Collider Study Group*, Princeton University preprint DOE/ER/3072-45 (June 1988).

[7] E. Berger, *Benchmark Cross Sections for Bottom Quark Production*, Proceedings of the High Sensitivity Beauty Physics Workshop held at Fermilab (Nov. 1987); and private communication, Ed Berger.

[8] E. Berger, *Heavy Flavor Production*, ANL-HEP-PR 88-26

[9] P.Nason, S. Dawson, R.K. Ellis, *The total cross section for the production of heavy quarks in hadronic collisions*, Fermilab 87-222-T; and private communication, Keith Ellis.

[10] M. Schmidt, J. L. Rosner, A. I. Sanda, *Physics Group Summary*, Proceedings of the High Sensitivity Beauty Physics Workshop held at Fermilab (Nov. 1987).

[11] I. I. Bigi and A. I. Sanda, *CP Violation in Heavy Flavor Decays*, Nucl. Phys. **B281** (1987) 41-71.

[12] F. Gilman, *B Physics*, to appear in the proceedings of Les Rencontres de Physique de la Vallee d'Aoste (La Thuile, Italy, Feb. 1988).

[13] H. Harari, *B Physics*, to appear in the Proceedings of Les Rencontres de Physique de la Vallee d'Aoste (La Thuile, Italy, Feb. 1988).

[14] C. Hamzaoui, J. L. Rosner, A. I. Sanda, *B Meson Decay Asymmetry and $B\bar{B}$ Mixing*, Proceedings of the High Sensitivity Beauty Physics Workshop held at Fermilab (Nov. 1987).

[15] K.J. Foley *et al.*, *Bottom and Top Physics*, Proceedings of the Workshop on Experiments, Detectors and Experimental Areas for the SSC (Berkeley, 1987).

[16] I. Dunietz, *Measurement of the Mass and Lifetime Differences between the Heavy and Light B_s Eigenstates*, Proceedings of the High Sensitivity Beauty Physics Workshop held at Fermilab (Nov. 1987).

[17] I. I. Bigi and B. Stech, *Future Lessons from Two-Prong Two Body decays of Beauty*, Proceedings of the High Sensitivity Beauty Physics Workshop held at Fermilab (Nov. 1987).

[18] Ling-Lie Chau and Hai-Yang Cheng, *In Search of V_{ub} in Nonleptonic Decays from the Quark Diagram Scheme*, Physics Letters **B197** (1987).

[19] A. Soni. and G. Hou, *Loop Induced Rare B Decays*, Proceedings of the U.C.L.A. Workshop, Linear Collider $B\bar{B}$ Factory Conceptual Design, Editor Donald Stork (Jan. 1987).

[20] A. Ali, *$B\bar{B}$ Mixing - A Reappraisal*, Proceedings of the U.C.L.A. Workshop, Linear Collider $B\bar{B}$ Factory Conceptual Design, Editor Donald Stork (Jan. 1987).

[21] H. Albrecht *et al.*, (Argus Collaboration), Phys. Lett. **B192** (1987) 245.

[22] J. Bjorken, *Prospects for Future Fixed-Target B Physics at Fermilab*, Proceedings of the High Sensitivity Beauty Physics Workshop held at Fermilab (Nov. 1987).

[23] J. Sandweiss and B. Cox, *Summary of Fixed Target Working Group*, Proceedings of the High Sensitivity Beauty Physics Workshop held at Fermilab (Nov. 1987).

[24] P. Garbincius, *Review of Fixed-Target B Physics at Fermilab*, Proceedings of the High Sensitivity Beauty Physics Workshop held at Fermilab (Nov. 1987).

[25] F. Olness and W.-K. Tung, *Small-x Physics at the SSC and the Tevatron*, Int. Jour. Mod. Phys. **A2** (1987) 1413.

[26] A. J. Lankford and M. Johnson, *et al.*, *Summary of the Trigger and Data Acquisition Group*, Proceedings of the High Sensitivity Beauty Physics Workshop held at Fermilab (Nov. 1987).

[27] E.Barsotti,M.Bowden,H. Gonzalez, and C. Swoboda, *Digital Triggers & Data Acquisition Using New Microplex & Data Compaction ICs. Many Parallel Math Processors, & Fiber Optics to Fast Digital Triggers & Higher Level Farms*, Proceedings of the Workshop on High Sensitivity Beauty Physics at Fermilab (Nov. 11-14, 1987) Editors. J. Slaughter, N. S. Lockyer, M.Schmidt.

[28] R. Van Berg, *Front-End Architectures for New Beauty Detectors*, Proceedings of the High Sensitivity Beauty Physics Workshop held at Fermilab (Nov. 1987).

[29] V. Ashford *et al.*, *RICH for SLD*, IEEE Trans Nucl. Sci. **NS-34** (1987) 499.

[30] J. Sequinot, *RICH for DELPHI*, Second Hellinic School on Elementary Particle Physics, 61 (1985).

[31] G. Bassompierre, *et al.*, *JETSET Proposal*, CERN PSCC86-23 This is an effort to trigger on a Liquid Rich Counter in LEAR. We have talked to Y. Onel and J. Kirkby and will continue dialog in the future.

[32] O. Botner, *et al.*, Nucl. Instr and Meth. **A257** (1987) 580.

[33] G. Hallewell, *et al.*, *Progress Report on the SLD Cerenkov Ring Imaging Detector System*, SLAC-PUB-4405 (September, 1987).

[34] P. Beltran, *et al.*, *Design of the Forward RICH counter in DELPHI and Results from the Operation of a Full-Scale Prototype*, CERN-EP/88-80 (1 July 1988).

[35] N. Lockyer, *et al.*, *Proposal for Generic Detector R&D for the SSC*, (September, 1988).

[36] T. Ypsilantis, *RICH/CRID for Future Hadron Collider Experiments*, Talk given at Snowmass '88 (July, 1988).

[37] J Va'Vra, IEEE Trans. Nucl. Scvi. **NS-34** (1987) 486.

[38] T. Ludlam, *Summary of the Particle Identification Group*, Proceedings of the High Sensitivity Beauty Physics Workshop held at Fermilab (Nov. 1987).

[39] M. Strovinck, D0 Collaboration Internal Note.

[40] U. Amaldi and G. Coignet, *Conceptual Design of A Multipurpose Beauty Factory Based on Superconducting Cavities*, CERN-EP/86-211 (Dec. 16, 1986).

[41] D. Cline, *Conceptual Design for a High Luminosity Linear Collider $B\bar{B}$ Factory*, Proceedings of the U.C.L.A. Workshop, Linear Collider $B\bar{B}$ Factory Conceptual Design, Editor Donald Stork (Jan. 1987).

[42] R. Eichler, T. Nakada, K. R. Schubert, S. Weseler, and K. Wille, *Proposal for a Double Storage Ring*, SIN Report PR-86-13 (Nov. 1986).

[43] H. Aihara, *B Factory at KEK*, Proceedings of the U.C.L.A. Workshop, Linear Collider $B\bar{B}$ Factory Conceptual Design, Editor Donald Stork (Jan. 1987).

[44] E. Bloom, *N-PEP $B\bar{B}$ Factory*, Proceedings of the U.C.L.A. Workshop, Linear Collider $B\bar{B}$ Factory Conceptual Design, Editor Donald Stork (Jan. 1987),

[45] F. Paige and S. Protopopescu, *Isajet Monte Carlo.*

[46] P. Holl *et al.*, *Strip Detectors with Capacitive Readout and a New Method of Integrated Bias Coupling*, Contributed paper to the XXIV International Conference on High Energy Physics (Munich, Aug. 4-10, 1988).

[47] T. Kondo, *Radiation Damage of Silicon Devices*, from Future Directions in Detector Research and Development for Experiments at PP Colliders (Snowmass, Colorado, July 5-7, 1988).

[48] G. Lutz *et al.*, *Low Noise Monolithic CMOS Front End Electronics*, Nucl. Instr. Meth. **A263** (1988) 163-173.

[49] W. Buttler *et al.*, *Noise Performance and Radiation Hardness of the CAMEX64 Analog Multiplexing Readout Chip*, Contribution to the XXIV International Conference on High Energy Physics (M,unich, August, 1988).

[50] S. Kleinfelder *et al.*, *A Flexible 128 Channel Silicon Strip Detector Instrumentation Integrated Circuit with Sparse Data Readout*, IEEE 1987 Nucl. Sci. Symposiu, (San Francisco).

[51] P.P. Allport, P. Seller and M. Tyndal, *A Low Power CMOS VLSI Multiplexed Amplifier for Silicon Strip Detectors*, London Conference on Position Sensitive Detectors (Sept., 1987).

[52] J. T. Walker *et al.*, *Development of High Density Readout for Diode Strip Detectors*, Nucl. Instr. Meth. **226** (1984) 200.

[53] S.K. Dhawan *et al.*, *A RICH MWPC Pad Readout by Using Custom Microplex I.C.*, IEEE Trans. Nucl. Sci. 35 (1988) 436.

[54] P. Baringer et al., Nuc. Instr. and Meth. **A254** (1987) 542.

[55] S.L. Shapiro *et al.*, *Silicon PIN Diode Array Hybrids for Charged Particle Detectors*, SLAC-PUB-4701 (September 1988).

[56] R. DeSalvo, *A Proposal for an SSC Central Tracking Detector*, Cornell University preprint CLNS87/52 (1987).

[57] R. Thun, *Prospects for Wire Chambers at High Luminosity*, presented at Future Directions in Detector R&D for Experiments at pp Colliders (Snowmass, 1988).

[58] D. Groom, *Radiation Levels in SSC Experiments*, presented at Future Directions in Detector R&D for Experiments at pp Colliders (Snowmass, 1988).

[59] S.K. Dhawan *et al.*, *Performance Limits of Silicon Strip Front-End Electronics for the SSC B Detector*, Yale U. proposal for SSC Detector Development (1988).

[60] G.R. Kalbfleisch and P. Skubic, *Considerations Regarding Double-Sided Solid State Detectors*, U. Of Oklahoma preprint (Feb. 1988); G.R. Kalbfleisch, P.L. Skubic and M.A. Lambrecht, *Results on Signal Correlations from a 'Micron' Doubled-Sided Mini-Strip Detector*, U. of Oklahoma preprint (Aug. 1988).

[61] K.T. McDonald and M.V. Purohit, *Proposal for Generic Detector Development*, Princeton U. preprint DOE/ER/3072-46 (Aug. 1988).

December 9, 1987

Professor L. Lederman
Director
Fermilab
Batavia, Illinois

Dear Leon,

This letter is in response to your suggestion that we outline the basic requests of those people actively pursuing the design of a bottom collider detector for the Tevatron.

The Beauty Workshop held at Fermilab Nov.11-14 was, in our opinion, both successful in that it attracted over 215 participants, and encouraging to us in that a positive endorsement of a collider approach was evident. There was general agreement among people at the workshop that a design based around a dipole magnet was a positive step. As a consequence, we (the undersigned) are working together as a group on the feasibility of this design. The stated goal of this group is to produce a unified, realistic proposal in about a year from now.

A large effort by this group is required to address and answer the many questions associated with low pt triggering and the full reconstruction of bottom events in the collider. There is of course no existing experiment at CERN or Fermilab to emulate. Therefore the simulation effort needs to be very detailed and thorough, and only then will the full scope of the physics objectives be realistically assessed.

We need encouragement from the laboratory and the P.A.C. before embarking on this year long design study. In particular we request:

1) To be officially recognized by the laboratory as the Bottom Collider Detector Design Group. We understand of course this does not imply a commitment to an experiment.

2) To have assigned to us an accelerator physicist who can work on such questions as simultaneous low beta in A0, D0, and B0, the effect of the dipole on the lattice, the prospects for luminosity in A0 if the machine contains many bunches etc.

3) Desk space, computer accounts, and terminals be made available to us temporarily.

4) The continued support of the computer department through the participation of Lee Roberts, a programmer.

5) Fermilab support and help to provide resources to perform a systematic study of available integrated circuits for use with double sided silicon. We envision this as enlarging and complementing the present laboratory effort being pursued by CDF and E-771. We would provide several physicists and clearly strengthen this important effort. We of course plan more ambitious tests later if these early exercises prove successful.

We held an ad hoc meeting at Fermilab, Dec. 8, where we tried to get at least one person from each institution that expressed interest in the collider experiment at the workshop to attend. Several institutions could not make the meeting date, but 10 institutions were represented. At this meeting new work since the workshop was presented and this letter was discussed.

Much progress has been made recently and support from the laboratory will be very important if a realistic assessment of this physics program is to be made.

Yours sincerely,

N. Lockyer	U. of Pennsylvania
N. Reay	Ohio State U.
S. Frederiksen	Ohio State U.
K. Reibel	Ohio State U.
R. Sidwell	Ohio State U.
N. Stanton	Ohio State U.
K. McDonald	Princeton U.
M. Schmidt	Yale U.
P. Karchin	Yale U.
J. Slaughter	Yale U.
P. Avery	U. of Florida
G. Kalbfleisch	Oklahoma U.
J. Snow	Oklahoma U.
P. Skubic	Oklahoma U.
P. Yager	U.C. Davis
R. Burnstein	I.I.T.
S. Reucroft	Northeastern U.
R. Stefanski	Fermilab
J. Butler	Fermilab
L. Roberts	Fermilab
B. Lundberg	Fermilab

Fermilab

Fermi National Accelerator Laboratory
P.O. Box 500 • Batavia, Illinois • 60510
312-840-3211 FTS 370-3211

Directors Office

December 14, 1987

Prof. Nigel Lockyer
Department of Physics
University of Pennsylvania
Philadelphia, Pennsylvania 19104

Dear Nigel,

The PAC discussed your proposal to do a year-long study of the collider approach to B-physics at Fermilab. They were in fact enthusiastic but had several caveats. Clearly there is no commitment to the group to fund a detector. The Lab must reserve the right to receive a proposal from any other group for the same kind of research and if it is clearly better, we must be free to accept that one. Also, we must feel free to decide to do only fixed-target B-physics or, no B-physics at all. For these reasons, we can't designate you as THE Collider design group. I prefer to call you a Collider B-Physics Study Group. As such we'll try to find desk space, meeting rooms, secretarial help (modest) and a computer account. Ken Stanfield will be your interface. We will try to give you accelerator advice as is needed, but you must realize that that group is very busy and has very little manpower to spare. I hope all this isn't too negative sounding. The year's study and simulation is just what is needed and we'll help as much as we can.

Sincerely,

Leon M. Lederman

Princeton University
DOE/ER/3072-45
June 20, 1988

Status Report of the Fermilab B Collider Study Group[1]

Participating Institutions[2]

U. of California (Davis), Fermilab, U. of Florida, Illinois Institute of Tech., U. of Iowa, Northeastern U., Ohio State U., U. of Oklahoma, U. of Pennsylvania, Princeton U., and Yale U.

Abstract

The motivation, size and scope of a B-$\bar{B}$ CP-violation experiment, called here the Bottom Collider Detector, at an upgraded Tevatron Collider is indicated. Preliminary results from detector and event simulation studies by the Bottom Collider Study Group are presented. No detector design details are discussed though some overviews are given. Where appropriate, discussions on what further study is required is given. The need for an upgraded Tevatron is absolutely clear. A factor of 200 increase over the present design luminosity of 1×10^{30} $cm^{-2}sec^{-1}$ is highly desirable. This report is not intended as a proposal nor as a finished study but merely represents the status of our thinking at this time: the Bottom Collider Detector is challenging but doable; it is the most agressive pursuit of CP-violation physics possible in the near future, and would be a vital step in the development of the high-rate, 4π instrumentation needed for the SSC era.

Introduction

The goal of the Bottom Collider Detector is to produce 10^{11} B-$\bar{B}$ events for which an efficient single-lepton trigger tags one B and permits detailed study of the few-particle decay modes of the other B. The trigger efficiency should be at least 5%, and the combined acceptance and vertex reconstruction efficiency for the other B should be above 20%, so that a sample of 100,000 reconstructed events would be obtained for a mode with a 10^{-4} branching fraction. A sample of this size in each of several few-body decay channels will permit a detailed study of CP nonconservation in the B-$\bar{B}$ system. A decay mode with a 10^{-6} branching fraction would still yield 10 events, so the study of rare processes is an obvious byproduct.

The very large B-$\bar{B}$ cross section at 2 TeV ($\sim 45\ \mu$b),[3] the relatively favorable ratio of bottom to total cross section ($\sim 10^{-3}$), combined with an average luminosity of 10^{32} $cm^{-2}sec^{-1}$ makes the upgraded Tevatron Collider a unique B facility that will produce important and fundamental physics results on a time scale of approximately 5 years from now.

Similar ambitious physics goals are being considered in the e^+e^- community; the B-$\bar{B}$ cross section at the $\Upsilon(4S)$ is about 1 nb, while the trigger efficiency might be close to 100%. No credible plan exists for a new e^+e^- machine that could reach the luminosity of 10^{34} cm^{-2}sec^{-1} with asymmetric beam energies as needed to compete with the hadron collider option.

The Bottom Collider Study Group was formed to follow up on ideas developed at the Workshop on High Sensitivity Beauty Physics at Fermilab, Nov. 1987, which in turn was prompted by two letters of intent submitted to Fermilab for consideration in 1987.[4,5] The group has taken a very broad and ambitious approach to defining the experimental goals and parameters associated with performing a high-statistics B experiment in the upgraded Tevatron collider. The organization set up for studying the issues was to divide the study group into several sections, each addressing one aspect of the experimental design, and then meeting roughly once a month to present the work to date.

The starting design parameters used as guidelines are listed below:

- pp or $\bar{p}p$ collisions at $\sqrt{s} = 2$ TeV;
- An average luminosity of about 10^{32} cm^{-2}sec^{-1} ;
- Interaction rate of 5 MHz ($\sigma_t = 50$ mb);
- $\sigma_{B\bar{B}} = 45$ μb, or 4500 B-$\bar{B}$ events/sec;
- An average event multiplicity of 60 charged pions and 30 π^0's;
- A magnetic detector with acceptance from 2° to 178°, or roughly ± 4 units of rapidity;
- A semileptonic trigger efficient for electrons of 1 GeV/c P_T and above;
- At a hadron collider the B-decay modes useful for study of CP violation are those which permit reconstruction of the B mass;
- Charged tracks from B decay are fully reconstructed including a μ-vertex measurement and particle identification;
- A B-mass resolution of 25 MeV/c^2 is needed to suppress combinatoric backgrounds, and to separate B_d from B_s;
- Only B-decay modes containing all charged tracks will be reconstructed; π^0 reconstruction is not required;
- An hermetic hadron calorimeter is not required as missing-E_T is not an important quantity for B-$\bar{B}$ physics.

The main issues are discussed in the following sections:

1. Bottom Physics Goals

The major physics goal of this experiment is to observe and study CP nonconservation in the neutral and charged bottom-meson systems. The B-$\bar{B}$ system provides a detailed test of the standard model in that the parameters of the K-M matrix may be overdetermined by measurement of CP violation in several different modes. The opportunity for systematic study is much greater than in the K-$\bar{K}$ or D-$\bar{D}$ systems, with the corresponding prospect for greatly increased understanding of the quark mass matrix. Deviations from present expectations would give important clues about the Higgs sector and possible new generations of quarks. Exploration of the B-$\bar{B}$ system is vital for a better understanding of the sources of CP violation beyond the parametrization that we have now.[6]

The proposed experiment is concerned with the systematic investigation of CP violation in several channels of B-$\bar{B}$ decay, rather than merely providing low-statistics evidence that CP violation exists. The technique which appears of most general utility in a collider experiment is a search for asymmetries of the type

$$A = \frac{\Gamma(B \to f) - \Gamma(\bar{B} \to \bar{f})}{\Gamma(B \to f) + \Gamma(\bar{B} \to \bar{f})}.$$

When final state f is the same as $\bar{f}$, as in many potentially favorable cases, the decaying B must be identified as a B or $\bar{B}$ (which is complicated in an interesting manner by bottom oscillations). This identification is made by determining the flavor of the other B of the B-$\bar{B}$ pair. In a hadron-collider experiment this is necessary anyway for trigger purposes, in that the sign of the electron in the triggering decay $B \to eX$ identifies the flavor. Decay modes of the B^0 such as $D^+\pi^-$ are 'self tagging' and would not require a trigger on the other B. Likewise, analysis of asymmetries of charged-B decays does not require flavor identification of the other B. While these modes will be explored in the Bottom Collider Detector we are unlikely to profit from the freedom to ignore the second B.

We would concentrate on few-particle final states f such as $\pi^+\pi^-$, K^+K^-, $p\bar{p}$, $D^+\pi^-$, ψK_S, $\psi\pi^+\pi^-$, *etc.*, which yield only charged particles in the detector. Estimates of the asymmetry parameter A for such decays are of order 0.1, while the branching fractions are expected to lie in the range 10^{-4}-10^{-5}.

To reach a statistical significance of S standard deviations in a measurement of asymmetry A the total number N of tagged and reconstructed decays required is

$$N = \left(\frac{1}{A^2} - 1\right) S^2 \sim \frac{S^2}{A^2}.$$

Thus a 5σ signal requires $N = 2500$ for $A = 0.1$, but $N = 250{,}000$ for $A = 0.01$. Clearly the experiment must have the flexibility to profit from those decay modes with $A \sim 0.1$, but it is not known at present which modes these are.

It may well be a tradeoff of Nature that modes with large asymmetries, A, have small branching fractions. If we then take 10^{-5} as the more likely branching fraction for the interesting modes with $A \sim 0.1$, we would need 2.5×10^8 tagged B's for a significant study.

Supposing the tagging efficiency (times reconstruction efficiency) can be maintained at 1% in the hadron-collider environment, a total of 2.5×10^{10} B-$\bar{B}$ pairs is required for a serious investigation. This sets the scale of effort required in the proposed experiment.

2. Detector Overview

The physics goals of the B-$\bar{B}$ experiment at a hadron collider mandate two major capabilities of the detector:

- Tagging of one member of a B-$\bar{B}$ pair;
- Full reconstruction of charged decay modes of the other B.

Geometric Coverage: $2° < \theta < 178°$

An initial sense of the geometry of the B-$\bar{B}$ events can be gained from fig. 1 which shows the pseudorapidity, $\eta = -\ln\tan\theta/2$, for pions for the decay $B_d^0 \to \pi^+\pi^-$ for B's produced in $p\bar{p}$ collsions at $\sqrt{s} = 2$ TeV. This is taken from a simulation[7] using the Monte Carlo program *PYTHIA*.[8] About 95% of the tracks from a B decay lie within the range $-4 < \eta < 4$ corresponding to angles of $2° < \theta < 178°$ with respect to the beam axis. We then desire particle detection at all azimuthal angles over this range in polar angles.

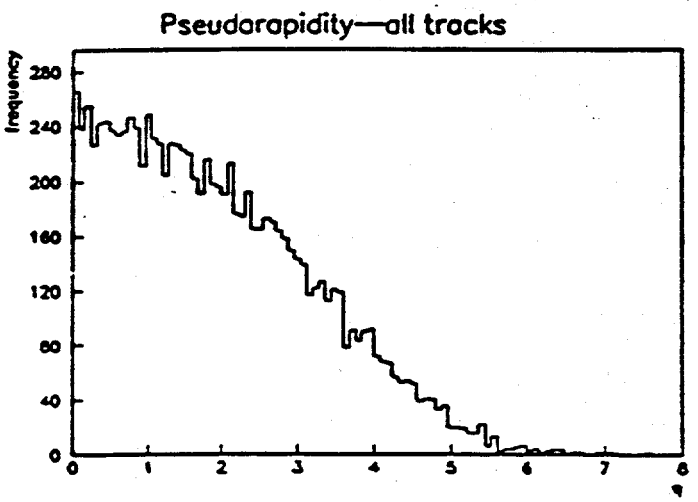

Fig. 1. Pseudorapidity distribution for decay products from $B_d^0 \to \pi^+\pi^-$ from a *PYTHIA* simulation at $\sqrt{s} = 2$ TeV.[7]

The basic character of the detector should thus be 'central,' but with greater emphasis on the angular region $2° < \theta < 30°$ than in present detectors designed for W and Z physics.

> At the SSC, with $\sqrt{s} = 40$ TeV, the corresponding range of pseudorapidity for B-decay products is about $-6 < \eta < 6$. The angular range corresponding to $|\eta| > 4$ is at very small angles to the beams, and would require detectors[9] resembling those in fixed-target experiments.[10] The present Bottom Collider Detector is, however, a prototype of that needed to cover the central rapidity range at the SSC.

The typical transverse momentum of the B-decay products is 1 GeV/c, corresponding to total momenta in the range of 1-50 GeV/c, at $\sqrt{s} = 2$ TeV (see fig. 2). The exciting B physics occurs in rather 'soft' events at collider energies.

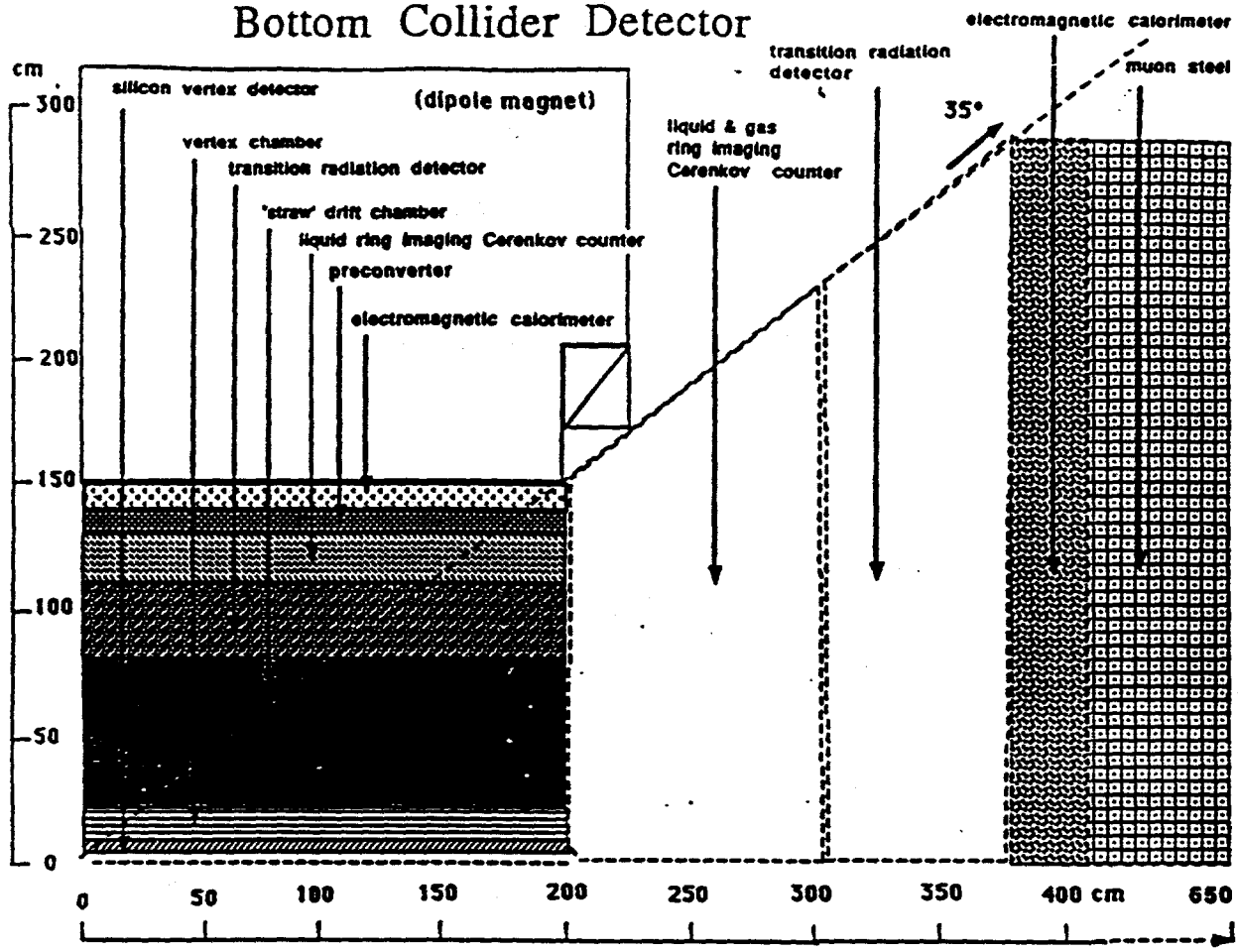

Fig. 4. View of the detector with the beam (z) axis horizontal and the dipole magnetic field along the vertical (y) axis.

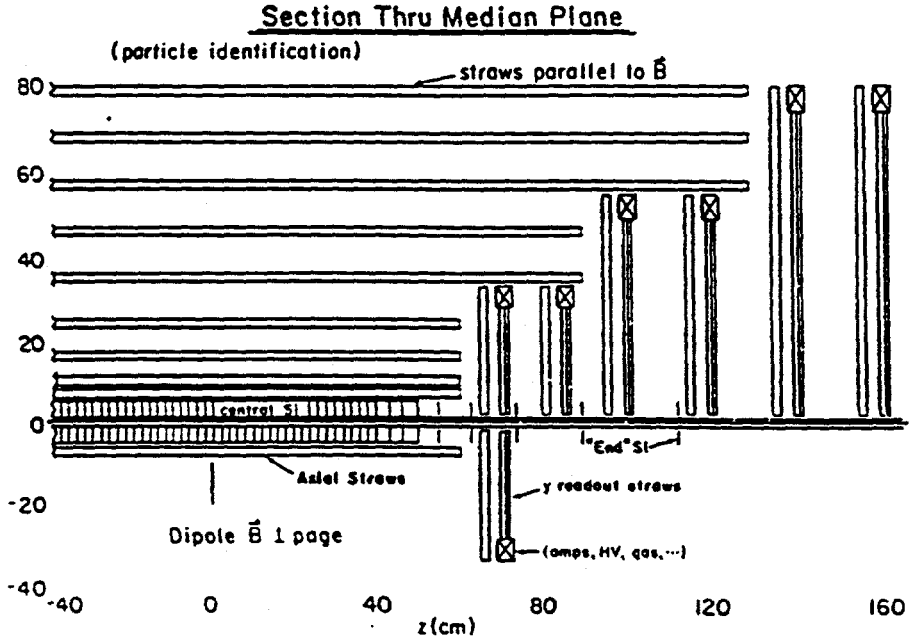

Fig. 5. A section through the median (x-z) plane of the silicon vertex detector and the straw tracking chamber.

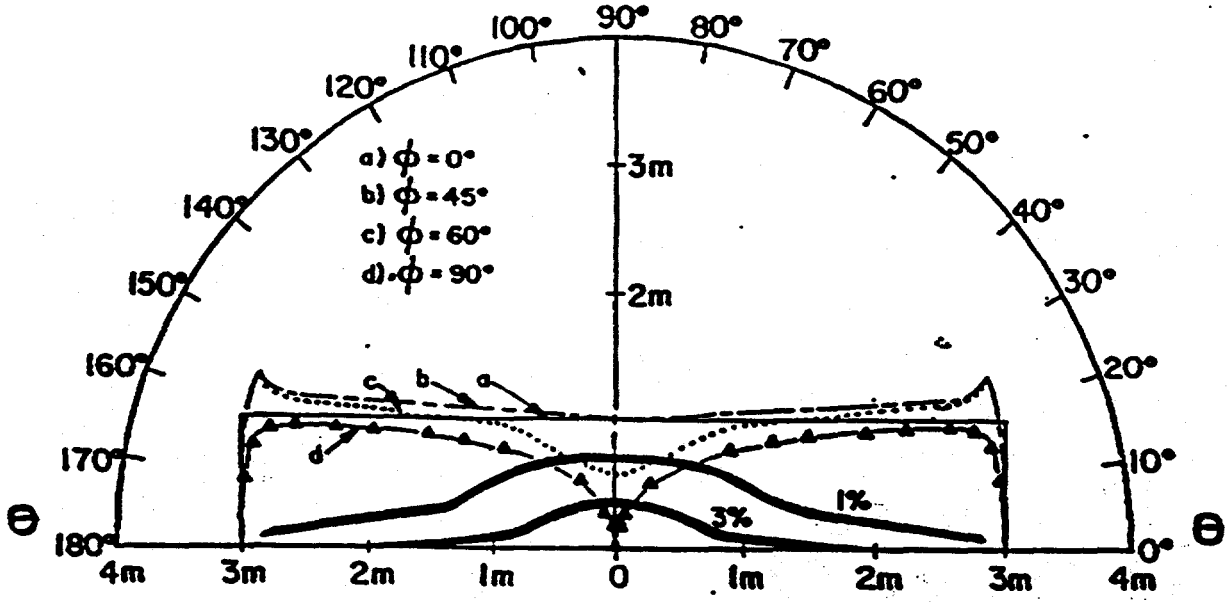

Fig. 3. The Reay plot illustrating the momentum resolution attainable with a 1-Tesla dipole magnet in the Bottom Collider Detector. The interaction point is at the origin and the beams lie along the horizontal (z) axis. The magnetic field is perpendicular to the paper (x-z plane) and is taken to be uniform within the rectangle which represents the top view of one half of the 2 m × 2 m × 6 m field volume. The curves labelled a) through d) show the path length, projected onto the x-z plane, of a track emerging from the origin with a given (θ, ϕ) direction. This path length is represented as the distance from the origin of the plot. The momentum resolution of the detector varies as Bl^2 where l is the path length shown on the plot. The countours labelled 1% and 3% show the required path length to achieve a momentum resolution of 1% and 3%, respectively, for tracks of transverse-momentum $P_T = 3.5$ GeV/c, supposing the measurement accuracy in the sagitta is 40 μm. For example, at $\phi = 90°$ a momentum resolution of better than 3% can be obtained at all polar angles except $75° < \theta < 105°$. For $\phi < 55°$ a momentum resolution of better than 1% is obtained at all polar angles.

Broad Requirements for Tracking and Particle Identification

To accomplish a full reconstruction of charged tracks from B decays in a high-multiplicity environment we shall need

- A 3D microvertex detector with a worst-case impact-parameter resolution of 20-μm.
- A magnetic field integral of 2-3 Tesla-m for small-angle tracks.
- A tracking chamber with 50-100 of samples per track for pattern recognition and momentum measurement of accuracy $\Delta P/P = 0.01$ for tracks with $P_T < 3$ GeV/c;
- Identification of π, K, p, e, and if possible μ. However, reconstruction of $\pi^0 \rightarrow \gamma\gamma$ and hadron calorimetry may not be necessary.

Figures 4 and 5 sketch a detector which incorporates these features. We briefly introduce the various detector elements in the remainder of this section, from the intersection regions outwards. Greater detail is presented in the subsequent sections.

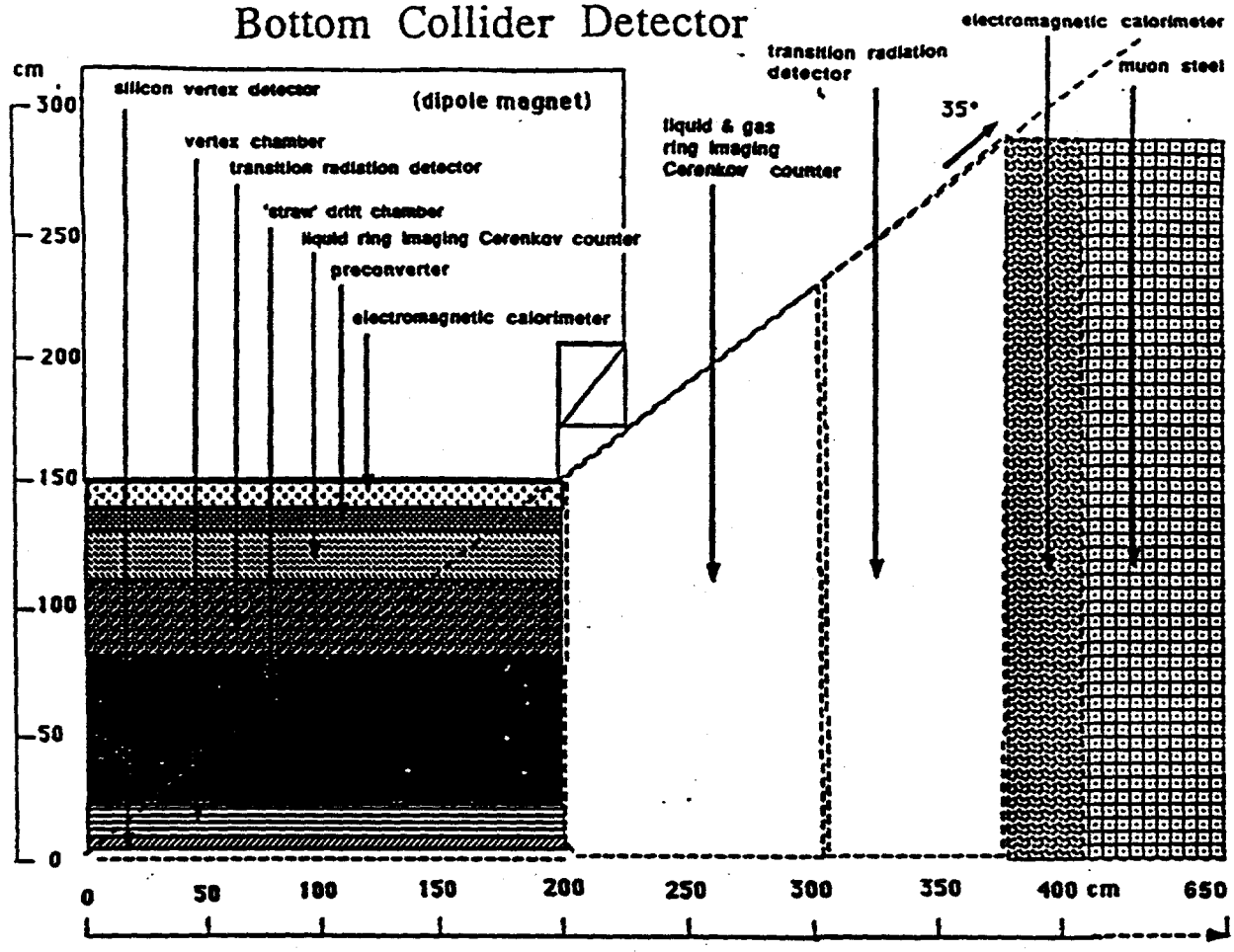

Fig. 4. View of the detector with the beam (z) axis horizontal and the dipole magnetic field along the vertical (y) axis.

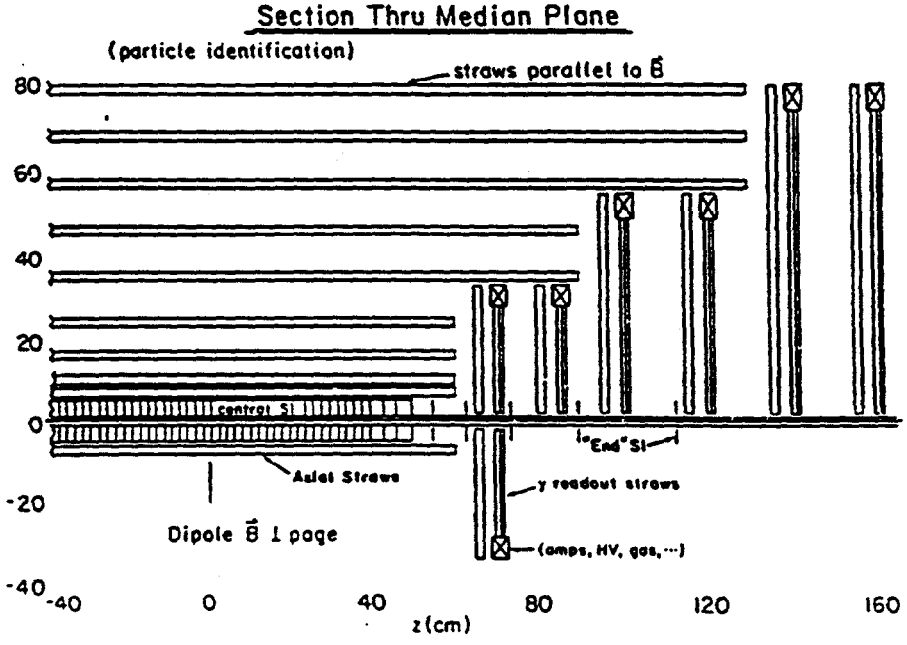

Fig. 5. A section through the median (z-z) plane of the silicon vertex detector and the straw tracking chamber.

Beam Pipe

The beam pipe must not only be thin to minimize secondary particle interactions but also must have a very small radius to permit high accuracy in the vertex reconstruction. We propose to use a beryllium pipe about 1 inch in diameter with a 400-μm-thick wall.

Microvertex detector

The lifetime, $c\tau$, of bottom mesons is about 360 μm. Secondary vertices must be reconstructable when their separation from the primary vertex is of this scale. We propose a microvertex detector based on silicon-strip detectors. Alternative vertex detectors utilizing pixel devices are also under consideration.

The novel difficulty for precision vertexing in a collider experiment is that the secondary tracks emerge into the full 4π laboratory solid angle (see fig. 6) At present, tracking with silicon-strip detectors has been implemented only in geometries with near-normal-incidence tracks. However, because the interaction region in a hadron collider is spatially extended there is no plausible geometrical arrangement of silicon planes which does not have some tracks at 45° incidence.

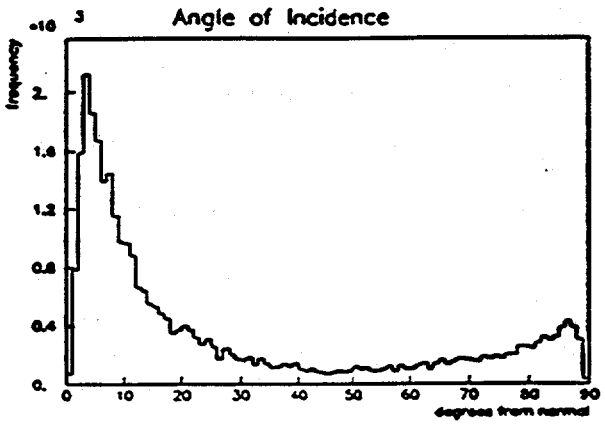

Fig. 6. Angle of incidence (degrees from normal) on the silicon vertex detector for decay products of bottom mesons.

We anticipate that development of silicon detector technology will permit its use for 45°-incident tracks. We plan to use 50-μm strip width, so that a 45° track would cross 70 μm of silicon per strip. The signal is then 70 μm × 80 electron-hole pairs/μm = 5600 electrons. It appears likely that VLSI readout chips for the silicon-strip detectors will achieve noise figures of 1000 electrons, which is entirely adequate. Indeed, if this noise level can be maintained even with $\sim$ 0° incidence should be detectable, as these would yield about 4000 electrons.

Multiple scattering of charged particles and conversion of photons in the silicon detectors is a non-neglible problem. As a consequence we plan to use 200-μm-thick silicon, with double-sided readout.

The number of channels required in the vertex detector is very large. If the interaction region is roughly 1-m long, as in the present $p\bar{p}$ running at the Tevatron, approximately 10^6 strips are needed. Furthermore, there must be an inner 'barrel' of silicon 1-m long

and concentric with the beam pipe in order to collect the large-angle tracks which emerge along the entire interaction region. This places considerable material just after the beam pipe which will be traversed by most small-angle tracks, leading to severe backgrounds of converted photons.

It would be much more favorable if a short interaction region were available, of order 10 cm. The inner barrel need only extend the length of the interaction region, so the number of silicon channels could be reduced by a factor of four, and γ-conversions would be greatly reduced. For this reason the Bottom Collider Detector is much more suited to a pp machine with a finite beam-crossing angle and correspondingly short interaction region.

Tracking Chamber

The silicon vertex chamber will provide typically only two measurements per track (in each of two coordinates) as the cost of, and multiple scattering in, additional planes is prohibitive. Therefore the inner vertex chamber must be surrounded by a tracking chamber capable of excellent pattern recognition in high-multiplicity events. The position resolution of and material traversed in crossing this chamber should permit a 25-MeV/c^2 resolution at the B-meson mass to distiguish B_d from B_s.

As we also wish particle identification for tracks in all 4π solid angle it is useful to have a tracking chamber which does not have massive end plates. The self-supporting 'straw' chambers are very appealing for this reason. In addition they offer high-rate capability and rather good position resolution.

A straw chamber for the Bottom Collider Detector might have about 10^5 channels of 3-mm-diameter tubes operating at 3-atmospheres pressure. Each track would cross approximately 80 tubes. The resolution transverse to the wire would be about 40 μm. Charge-division, or a pad readout, could be used to measure the longitudinal coordinate to a few mm accuracy. Development work is needed on thin-wall tubes to minimize the multiple scattering in the chamber.

RICH Counters

Separation of π, K and p will be accomplished with Ring Imaging Čerenkov Counters, with a liquid radiator for production angles above 30° and liquid plus gaseous radiators at smaller angles. Time-of-flight counters in the central region will help identify very soft tracks.

Transition Radiation Counters (TRD's)

Separation of e's from charged pions will be aided by multiple layers of TRD's, about 20 cm each. The combination of tracking information with the transition radiation signal should permit a pion rejection factor of 20 in the TRD. The utility of the TRD's at small production angles needs further study.[11]

Electromagnetic Calorimeter

The calorimeter functions primarily to aid in electron identification, rather than providing a precision energy measurement. As such position resolution is more critical. We thus have the option to use a sampling calorimeter (as opposed to total absorption in BGO or lead glass, *etc.*), with a tracking chamber after two radiation lengths. The first two radiation lengths can then serve as a preconverter to aid in rejection of $\pi^+ \rightarrow \pi^0$ charge exchange. The particular form of the electromagnetic calorimeter is not specified at this time.

Where space permits the electromagnetic calorimeter should be followed by a post-calorimeter of 1-2 hadron interaction lengths to help identify hadron showers which simulate electrons in the earlier detectors. The post-calorimeters could be located in the forward and backward detectors, and to the sides of the magnet aperture.

3. Accelerator Issues, Collision Hall, and Magnet

General Characteristics of the Detector and Collision Hall

The accelerator-related requirements for the Bottom Collider Detector are derived from the performance needed to achieve the physics goals sketched above in sec. 1. In order to study CP violation in the B-$\bar{B}$ system, the experiment should produce about 10^{11} bottom events per running year. The detector (see figs. 4 and 5 of sec. 2 above) will cover nearly 4π steradians. The central detector has a dipole magnet with a 1-Tesla field transverse to the beam axis, and a field volume of (at least) three by three square meters by four meters along the beam axis. Compensation must be made for the transverse deflection of the beams by the dipole magnet.

The detection of the B-$\bar{B}$ decay products requires that a sophisticated solid-state vertex detector, which may be prone to radiation damage, be located within 1/2" of the beamline. There will also be a forward/backward detector that extends several meters up- and downstream from the central detector.

The space required in an experimental hall is roughly determined by the overall dimensions of the detector. As presently envisioned, the detector occupies a volume of about six meters square in cross section and 12 meters in length. The dimensions of the spectrometer magnet will be comparable to those of the Chicago Cyclotron Magnet.

Beam Energy

The present detector is designed for the 1 × 1 TeV beams of the Tevatron. The B-$\bar{B}$ production cross section varies approximately linearly with collider beam energy so an accelerator with 500-GeV beams is still a serious contender for the B-physics experiment. For beam energies considerably above 1 Tev a substantial fraction of B-decay products emerge at extremely small angles to the beam, which likely requires a detector with multiple magnets. The Tevatron energy is perhaps the largest for which a detector based on a single central magnet will suffice.

Luminosity

As discussed in section 1, systematic exploration of CP violation in the B-$\bar{B}$ system becomes possible for luminosities of order 10^{32} $\text{cm}^{-2}\text{sec}^{-1}$. The large investment in the Bottom Collider Detector would be problematic if the average luminosity were only 10^{31} $\text{cm}^{-2}\text{sec}^{-1}$. We recommend an average luminosity of 10^{32} $\text{cm}^{-2}\text{sec}^{-1}$ be the accelerator goal. The higher luminosity and greater reliability of a pp collider make this option extremely desirable for B physics.

Length of the Interaction Region

The length of the interaction region determines the length of the vertex detector. At the present Tevatron the interaction region has a σ of 35 cm. A vertex detector for this region would have to be at least one meter long, with 10^6 readout channels and unwanted material close to the beam pipe. Current discussions for a Tevatron Upgrade include the possibility of a shorter interaction region with a σ of 10 cm. The reduction in σ would greatly simplify the vertex detector design.

Although all current versions of the Upgrade make provision for a reduced interaction-region length, the *pp* option offers the greatest flexibility in that a crossing angle is part of the machine design. By increasing the size of the crossing angle, the length of the interaction region can be proportionately reduced at the expense of luminosity. Because high luminosity can best be achieved in the *pp* option, the experiment would have the best chance of achieving an intersection-region length of about 5 cm at a luminosity of 10^{32} $cm^{-2}sec^{-1}$.

Beam Size

A small transverse beam size is desirable for several reasons. An important signature of B decays is the detection of their decay vertex some few-hundred μm from the primary interaction point. If the beam size is small compared to 100 μm then we gain the considerable advantage of regarding the beam as 1-dimensional. The diameter of the beam pipe, and therefore the vertex detector, is determined by the beam size. The motion of the beams within the beam pipe when the spectrometer dipole is turned on, which also affects the size of the beam pipe, is minimized when the beam size is smallest. And, of course, one achieves higher luminosity with a smaller beam cross section as well.

Beam Pipe

Conversions of photons in the beam pipe and multiple Coulomb scattering must be minimized in this experiment. A suitable beam pipe could be made of 400-μm-thick beryllium and should be roughly 1/2" in radius.

Beam Halo

Halo associated with the beams will contribute to the radiation exposure of the vertex detector and thereby shorten its lifetime. Present data indicate that the silicon detector can survive 10^5 rads and the micro-electronics withstand about 10^4 rads. It is clear that catastrophic beam loss must not occur near the detector. The beam-loss level for abort may need to be lowered compared to present operation.

The Spectrometer Dipole Magnet

The dipole magnet should be rather like the Chicago Cyclotron Magnet, but with its gap increased to 3 m in height. Such a magnet will weigh about 2500 tons, and will determine the transverse size of the detector hall. The cost of powering conventional coils for such a large magnet favors the use of superconducting coils. The cost of construction of a new magnet might be \$1.25M for the steel at \$500/ton, plus \$1M for the superconducting coils, plus cryogenics, plus installation.

A Comparison of Existing Magnets

A comparison has been made with existing magnets that might be available on a time scale adequate for the Bottom Collider Detector. The magnets that have been studied are the CCM (Chicago Cyclotron Magnet), the NFTF (Nuclear Fusion Test Facility), the Fifteen Foot Bubble Chamber Magnet, and the Berkeley 184" Cyclotron magnet.

The CCM would be an ideal magnet for the B Collider, if its gap were opened from the present 1 m to the needed 3 m. It will be tied up in the muon program for several years. If it should become available, the cost of moving it to a new facility would be around $750,000.

The NFTF has been turned on only once so this is a virtually new magnet. Only the superconducting coils of the NFTF magnet would be of use at the Bottom Collider Detector. The project would have to pay the cost of building the magnet yoke. A rough design shows that four of the existing ten coils could be used to achieve a 1-Tesla field. The cost of transport and installation are not known.

The Fifteen Foot Bubble Chamber Magnet has not been considered seriously for this project because it is being sought for an experiment at Gran Sasso. As for the NFTF magnet, a steel yoke would have to be built to incorporate the existing coils. No cost estimates are available.

An attempt had been made to acquire the Berkeley 184" Cyclotron Magnet for the Bottom Collider Detector. This was not possible because the magnet plates are only two inches thick (too many plates, too much rigging cost), they are mildly radioactive, and they are welded together into a yoke that also supports the crane at the Berkeley Cyclotron Building. The estimated costs of the procurement of this steel exceeds $1M, and was considered excessive. The magnet coils from the cyclotron are not considered useful because they are oil cooled and radioactive.

Compensation for the Dipole Field

The presence of a spectrometer dipole in the Tevatron would alter the beam trajectory unless compensating measures are taken. The scheme that has been chosen for compensation uses two dogleg bends, one at each end of the straight section and each 20 feet from the center of the interaction region, just downstream of the low-beta quads. The two magnets are both of opposite polarity relative to the spectrometer dipole, and run in series with it (that is, the currents run up together). The spectrometer dipole and compensating magnets are energized only after coasting beam has been established. The beams at the crossing region then move laterally a few mm as the magnets are energized.

The Detector Hall and Support Facilities

The Detector Hall required for this facility will be comparable in size to that at D0. The detector itself will fill about one half the space available in a straight section at the Tevatron. The compensating dipoles are placed at the outer ends of the straight section. The need for electron detection and calorimetry will require the use of special gasses and liquids. The detector may use ethane, TMAE, TEA, or liquid argon. The detector will require a substantial signal processing area. The Detector Building must also provide for a control room, office and technician space and shop support.

Summary and Status of Accelerator Issues

The broadest issues associated with the accelerator have been successfully worked out. The installation of the spectrometer dipole magnet in the Tevatron seems eminently feasible. The detector size (except perhaps for the magnet yoke) is relatively modest compared to present collider detectors. The magnet parameters are well understood. The location of a vertex detector around the beam pipe is a main feature of this detector and presents special considerations for the accelerator.

The issues that remain to be solved are those that interface with the accelerator beam optics. While the field nonuniformity of the spectrometer dipole is not thought to pose a serious problem it must be studied in more detail. Methods must be developed to insure that a catastrophic loss of beam into the vertex detector does not occur.

4. Silicon Vertex Detector

Overview

During the past year, the B Collider Study Group has specified the basic geometrical layout of a silicon-microstrip vertex detector suitable for the long interaction region of the present Fermilab $p\bar{p}$ collider.† In brief, this design consists of mosaics of silicon wafers of 200-μm thickness and 50-μm strip width, and double-sided readout arranged as in fig. 7 to form:

1) 2 cylindrical shells around the beam pipe with length 80 cm and radii of 1.5 and 5 cm, and
2) 27 annular disks of radius 10 cm oriented perpendicular to the beam and outside the beam pipe, with a total extent of 210 cm along the beam.

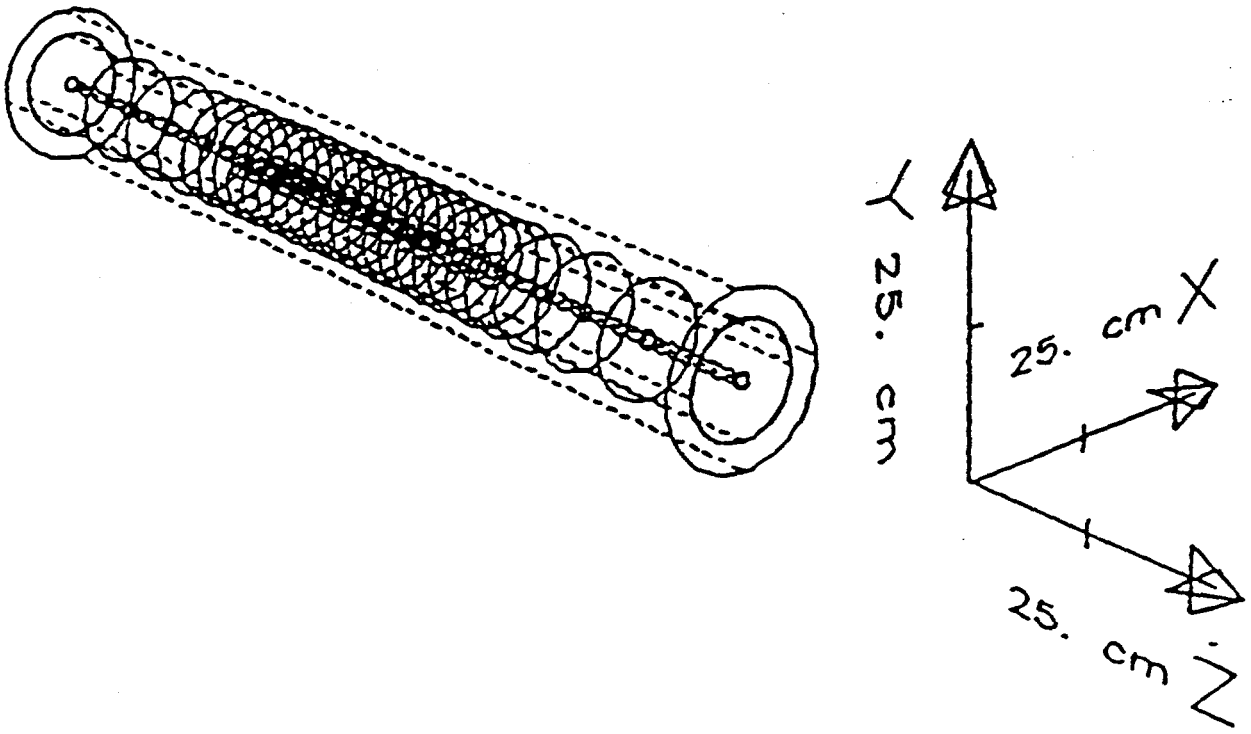

Fig. 7. Layout of the silicon vertex detector

This design is described in detail in ref. 7 along with a description of a Monte Carlo simulation of the decays $B \to \pi^+\pi^-$ and $B \to \psi K_S$, $(\psi \to e^+e^-)$. The simulation shows that efficiencies (per B-decay) of 45% are possible with a vertex cut of $S/\Delta S > 5$ (see fig. 8), where S is the distance from the primary interaction vertex to the measured secondary

† As noted in sec. 2 it is extremely advantageous to have an interaction region of < 10 cm to simplify the vertex detector. The vertex reconstruction efficiencies associated with a short interaction region are, however, only slightly larger than those reported here.

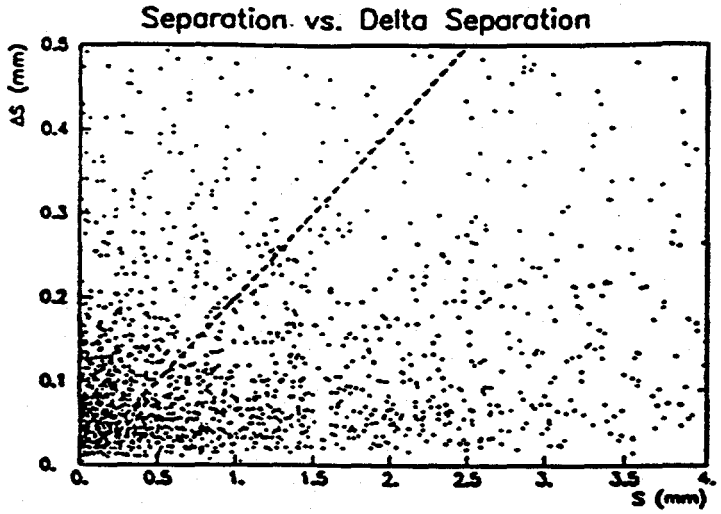

Fig. 8. Scatterplot of separation S vs delta separation ΔS for simulated $B \rightarrow \psi K_S$ events. The region below the dashed line contains events that satisfy the cut $S/\Delta S > 5$. Events with small S are predominantly produced in the central region, where the lower B momentum leads to a lower fraction of events surviving the cut.

vertex, and ΔS is the error in S (taken here as the distance between the reconstructed decay vertex and the Monte-Carlo-generated decay vertex).

Hardware Development

Although some optimization of plane spacings and sizes is no doubt possible, it would be prudent to assess the realization of this design in actual hardware devices. Fortunately, the basic hardware devices already exist. Double-sided silicon wafers have been successfully fabricated and low-power CMOS readout chips ("microplex chips") have been developed.[12]

However, a number of crucial operating parameters remain to be established:

a) The amount of material in mechanical mounting, cooling, and signal fanout. The simulation, so far, has included only the effects of the 200-μm-thick silicon-detector wafers and the 400-μm-thick Be beam pipe. The additional material must be included.
b) The noise rate for a given detection efficiency and the effect of efficiency and noise on pattern recognition. So far, the simulation has not considered the efficiency of detectors or the effects of errors in pattern recognition.
c) The detection efficiency for large angle of incidence, above 45°. Silicon detectors have not been used in the past to detect particles at large angle of incidence.
d) The effect of radiation damage in a hadron environment for *specific* devices. Devices could be tested in fixed-target beams or near the beam pipe of the collider. It is well known that radiation tolerance varies with manufacturing techniques.

To address these problems, members of the B Collider Study Group have expressed interest in a number of future projects. We will obtain and evaluate a double-sided silicon wafer from a commercial vendor (MBB-Messerschmidt, FRG) and study the large angle of incidence problem, and other characteristics of these devices. This work, and construction of a mechanical model of the silicon mosaic will be pursued at the U. of Oklahoma.

Physicists from Yale U. will obtain a variety of available microplex chips and evaluate the efficiency and noise as a function of gating time. Simulation efforts, building on the existing work, will focus on the effects of realistic material estimates, pattern recognition problems, and more sophisticated vertex fitting.

Detector Geometry

The silicon vertex detector under consideration is logically segmented into two regions. The central region covers most of the interaction region with a combined geometry of equally-spaced silicon planes and two segmented barrels. The rapidity-spaced region covers the outer limits of the interaction region with silicon planes at equal density in pseudorapidity. All silicon elements lie outside the beryllium beam pipe. Figure 7 presents a *GEANT3*[13] picture of the detector geometry.

The beryllium beam pipe has radius 1.3 cm and thickness 400 μm. All (double-sided) silicon elements are of 200-μm thickness and have a strip pitch of 50 μm. Each disk has an inner radius of 1.5 cm and an outer radius of 10 cm. The detector consists of 27 parallel silicon disks and two segmented silicon barrels. The barrels have strips in z and ϕ directions, while the planes have strips in the x and y directions. The total length of the vertex detector is approximately 210 cm.

The central region of the vertex detector contains 17 planes with an interdisk spacing of 5 cm. The barrel segments are placed in the interdisk volumes and extend to the disk edges of the neighboring planes. The inner barrel radius is 1.5 cm; the outer silicon barrel radius is 5.0 cm. The central region extends from the center of the interaction region to $z = \pm 40$ cm.

The rapidity-spaced region is abutted to the central region and covers the outer limits of the interaction region. Silicon planes are placed every one-third unit of pseudorapidity, with the $\eta = 3$ planes equivalenced to the outer planes of the central region. Five rapidity-spaced planes extend from the ends of the central region.

This detector combines the features of the planar and barrel silicon geometries. Planes provide effective detector surfaces for particles traveling into the forward and backward regions, while barrels provide effective detector surfaces for radially moving particles. The outer radius of the silicon planes has been chosen to be twice the interplane distance to guarantee two hits for all particles in the central region. The silicon thickness has been adjusted to 200 μm to guarantee satisfaction of the cluster cut parameter for tracks incident on detectors up to 45° from normal incidence. Since the planes and barrels present relatively perpendicular surfaces to the particle tracks, this provides that all tracks that pass through the body of the detector will have two acceptable hits.

Event Simulation

PYTHIA 4.8 was used as the event generator for this simulation. Bottom-meson events were generated for a $p\bar{p}$ collider with 2-TeV center-of-mass energy. The minimum invariant mass of the hard-scattering parton subsystem was set at 10.5 GeV; the minimum allowed transverse momentum was 0.2 GeV/c. Decays of secondary particles were prohibited in the *PYTHIA* event generation—all particle decays were handled by *GEANT3*.

Bottom mesons only were selected from among the full *PYTHIA*-generated event for entry into *GEANT3*. Our objective was to determine whether reconstruction of bottom

mesons would be possible using this vertex detector—one should first check that reconstruction is possible without any extraneous particles. Simulations were run using one of two decay modes: $B_d^0 \to \pi^+\pi^-$ and $B_d^0 \to \psi K_S$, $(\psi \to e^+e^-)$. No magnetic field was present in the simulations, this being a preliminary design study. (Current Bottom Collider Detector designs include a 1.0-1.5 Tesla dipole field.)

Analysis was performed using *GEANT3*'s knowledge of the particle decay. No pattern recognition was used; the *GEANT3* particle decay chain was followed to identify descendants of each bottom meson. Both of the chosen decay modes allow a simple trigger—both provide two prompt, charged particles. Bottom meson events were accepted if both charged particle tracks had at least two hits in the silicon detectors.

A cluster size cut was imposed on the particle hits in the silicon detectors. The cluster size is defined to be the number of adjacent silicon strips which are fired by the passage of a single particle track. Large cluster sizes present possible problems with signal size, hit location and pattern recognition. Hits with cluster sizes greater than four strips were rejected in this class of simulations.

Particle tracks were defined by the first two (valid) hits on the track. Cuts on the vertex resolution were imposed on the quantity $S/\Delta S$, where S represents the distance of flight of the bottom meson and ΔS represents the three-dimensional distance between the reconstructed decay vertex and the true (Monte Carlo) decay vertex. $S/\Delta S > 5$ was the imposed cut.

Results

Simulations were performed using a realistic model of the Tevatron interaction region—a normal (Gaussian) distribution of events with $\sigma = 35\,\text{cm}$. Vertex detector acceptance as a function of the applied cuts can be seen in Table 1 below. Results are shown for both of the decay modes $B_d \to \pi^+\pi^-$ and $B_d \to \psi K_S^0$. Application of cuts is cumulative down through the rows of the table.

Table 1. Vertex-detector acceptance for an interaction region with a normal (Gaussian) distribution, $\sigma_z = 35\,\text{cm}$, of primary vertices.

cuts	$B_d \to \pi^+\pi^-$	$B_d \to \psi K_S$
geometry cut	0.768	0.775
cluster cut	0.751	0.763
vertex cut	0.466	0.449

Figure 9 presents the accepted pseudorapidity distribution for bottom mesons in the BCD silicon vertex detector. All cuts (geometry, cluster size, and vertex) have been imposed on this distribution. The distribution is for the decay mode $B_d \to \pi^+\pi^-$; the distribution for the decay mode $B_d \to \psi K_S$ is virtually identical.

Computer simulations of the vertex chamber are presently being extended to include the problems of pattern recognition in the presence of non-B-decay tracks, noise hits, δ-rays, sampling fluctuations, and the curvature of low-momentum tracks.

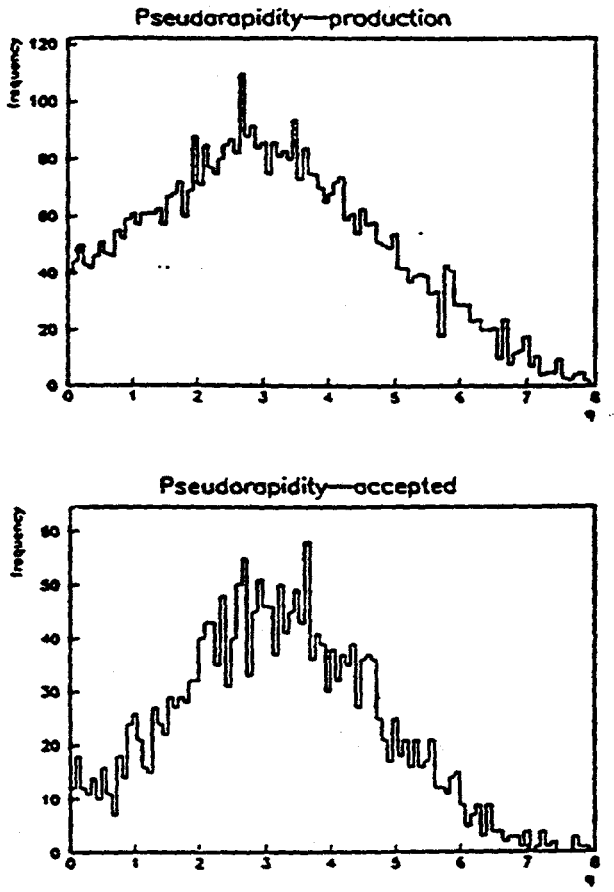

Fig. 9. Pseudorapidity distribution of generated B mesons (top) and accepted B mesons (bottom).

5. Tracking

Tracking Requirements

Multiple scattering and instrumentation costs in the silicon microstrip vertex detectors do not allow a sufficient number of planes to reconstruct tracks in three-dimensional space. The vertex detector must therefore be regarded as a precise vernier to improve the pointing accuracy of tracks reconstructed in three dimensions by an outer tracking system of wire chambers.

The outer tracking system must also measure the momentum of tracks with $P_T <$ 3 GeV/c to an accuracy of $\Delta P/P < \pm 1\%$ in the dipole magnetic field, and be able to reconstruct curved tracks coming from anywhere along the interaction region. This reconstruction problem is more difficult than that for detectors having a solenoidal field, in which the tracks in the azimuthal view are circles coming from a well-defined point (the beam intersection). The outer tracking system must operate at interaction rates of 5–10 MHz, and cannot have massive support structures such as end plates which would interfere with the 4π electron trigger which will surround it.

General Approach

There are two traditional approaches to tracking. One such approach (commonly used in collider experiments) is to have one strong view with 50 to 200 sampling points in the magnetic bend plane, and a weaker orthogonal view with subsidiary information such as small-angle stereo or resistive charge division to resolve the stereo ambiguity. The opposite approach (commonly used in fixed-target experiments) is to have at least three independent views with approximately the same number of samples in each view. This is necessary when the track density is high, as it will be at small angles in this experiment, and when resolving the stereo ambiguities is not trivial. If the total number of samples is limited (by multiple scattering considerations, for example) this means fewer samples per view.

The Bottom Collider Detector must have higher quality tracking at small angles to the beam than in most present collider experiments. Therefore we are pursuing a tracking configuration with precision measurements in both x and y, and with the large number of samples required for pattern recognition in high-multiplicity events. The proposed tracking chamber is based on 'straw-tube' technology.

Straw Tubes

Tracking chambers based on straw tubes have several advantages for this experiment:

- no massive mechanical supports are required;
- the small drift distance allows high rates;
- resolutions of better than 40 μm can be achieved with pressurized straws;
- the damage due to a broken wire is confined to its own tube.

However, the support for the wire tension is distributed in the walls of the straws, which are a potentially large source of multiple scattering. The wall thickness must be reduced

substantially below that now in common use. For example, one published design[14] uses one-atmosphere straws 7.0 mm in diameter with 85-μm aluminized-mylar walls. The multiple scattering from a double row of such tubes is approximately equivalent to that from a silicon wafer, and 40 such double rows (0.08 radiation lengths) uniformly distributed in 0.75 m of 10-kG field would degrade momentum resolution to greater than 1%.

DeSalvo[15] has proposed a design for an SSC central-tracking detector which is based on a large number of straws of 3.0-mm diameter and 30-μm wall thickness, pressurized to 3–4 atm. In addition to improving the resolution of the straws to 30–40 μm, the pressurization adds to the rigidity and allows the reduction in diameter which leads to thinner walls. A "superlayer" of 8 rows of such tubes (fig. 10) contains only 3.4×10^{-3} radiation lengths, resolves left-right ambiguities locally, and provides both a vector with 2-mrad pointing accuracy and an estimate of curvature. Eight such superlayers in 0.75 m of 10-kG field contribute only 0.6% to the momentum resolution due to multiple scattering.

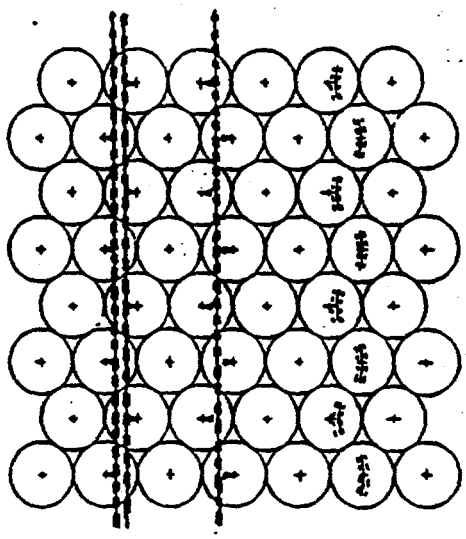

Fig. 10. A 'superlayer' of 8 rows of straw tubes.

A conceptual design for the outer tracking chamber using such superlayers of straws is shown in figs. 5 (sec. 2) and 11. The silicon vertex detector is immediately surrounded by a superlayer of straws aligned parallel to the beam (z) axis. In the central region (in which the track density is relatively low) nearly all straws are parallel to the magnetic field, taken to be along the y axis. The coordinate (y) in the non-bend plane is obtained from the superlayer of axial straws surrounding the silicon detector, and from resistive charge division in the wires. It is likely that at least one additional superlayer of straws measuring the coordinate in the non-bend plane will be required to ensure unambiguous extrapolation into the silicon vertex detector. In the forward and backward directions (where track densities are higher) there are alternating superlayers measuring coordinates in the bend (x-z) and nonbend (y-z) planes. Resolution of the stereo ambiguity would

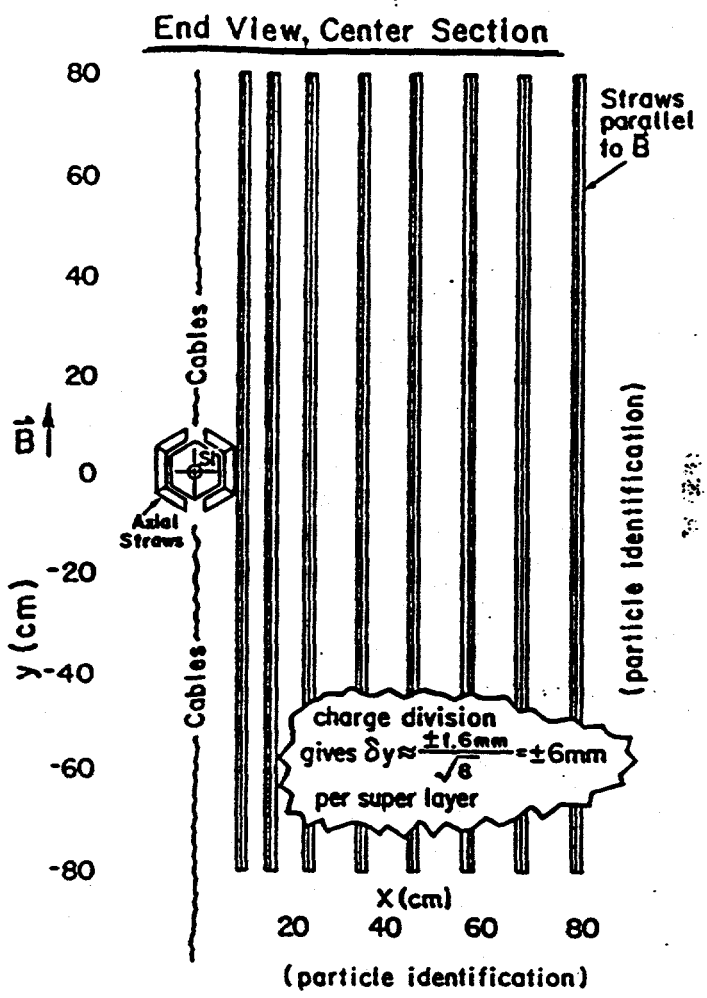

Fig. 11. View along the beam through the center section of the straw-tube tracking system.

be accomplished by rotating a few of the non-bend superlayers to an intermediate stereo angle.

Tracking Simulation

The next step in designing the tracking system is to confront realistic simulated events in the detector with an actual track-finding algorithm. We must determine the number of samples and the number and kind of stereo information needed to establish unambiguous three-dimensional tracks, and to extrapolate reliably into the silicon vertex detector. Work on such a "generic" trackfinder is underway at Ohio State, and will form the basis for studies at Snowmass. This program is designed to deal with configurations of N superlayers of M samples each, provided only that all detectors in a view are in the same rectangular coordinate system; it can find tracks of uniform curvature from an unspecified origin. On a longer timescale, a prototyping effort must be established to show that these very delicate straws can actually be built with the expected mechanical and electrical properties.

6. Trigger

Goals

The signature of a B meson which appears most suitable as a trigger for the Bottom Collider Detector is a moderate-transverse-momentum electron from a semileptonic decay. As indicated in fig. 12 (based on an *ISAJET*[16] calculation) about 50% of semileptonic B decays yield an electron with $P_T > 1$ GeV/c. The semileptonic branching fraction is 12%, and either B of a B-$\bar{B}$ pair is suitable for triggering. Thus a trigger cut of $P_T > 1$ on electrons could yield a 12% triggering efficiency for B-$\bar{B}$ pairs. If the efficiency of electron identification, including eventual offline reconstruction of a secondary vertex for the $B \rightarrow eX$ decay, is 40% an overall trigger efficiency of 5% could be achieved.

This is a formidable goal, as the electrons must be identified amidst a 5-MHz interaction rate yielding a 500-MHz total rate of particles in the detector. The triggering scheme will be implemented in a multilevel processor. If we anticipate a trigger rate as high as 1 kHz the dead-time associated with the highest level should not be much more that 10 μs. The difficulty in achieving this suggests that, as an alternative, B-candidate events be pipelined for the duration of the highest-level processor.

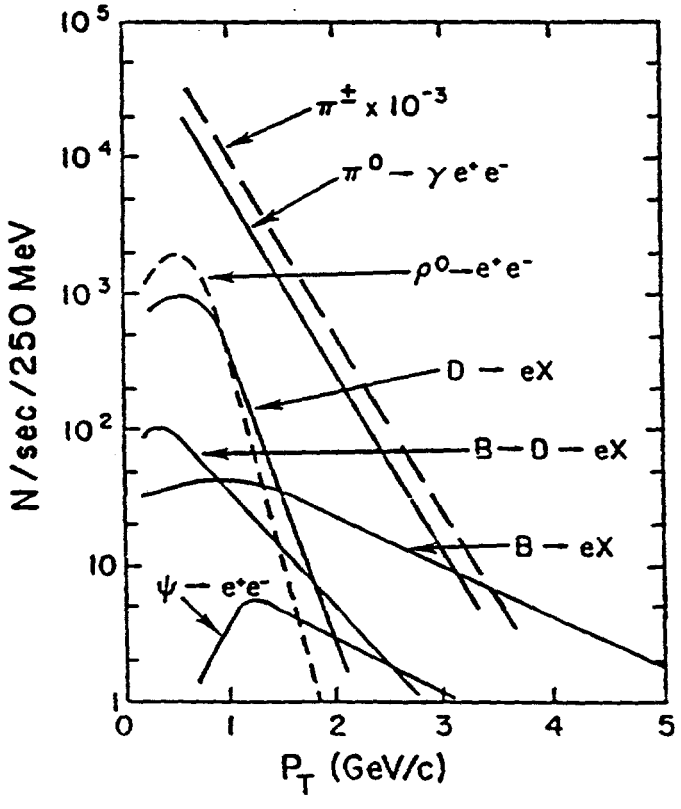

Fig. 12. The rate of electrons per 250-MeV/c bin from various sources in $p\bar{p}$ collisions at $\sqrt{s} = 2$ TeV and luminosity 10^{32} cm^{-2}sec^{-1}.

Sources of Electrons

A summary of the rate of electrons from various sources as a function of transverse momentum is given in fig. 12. Prompt electrons derive from direct electronic bottom and charm decay, e^+e^- decays of vector mesons, and Dalitz decays of pseudoscalar mesons. Fake electron triggers will derive from misidentified $\pi^{\pm}$'s, including $\pi^{\pm}$-π^0 overlaps. A hint of the severity of the fake-electron problem is given by the spectrum for $\pi^{\pm}$, also sketched in fig. 12.

The present philosophy is to pass all prompt electrons to the software-event-processing stage (supposing the fake electron triggers can be sufficiently suppressed). With a trigger cut of $P_T > 1$ GeV/c a substantial fraction of the prompt electrons are from B decay, and there is no need to distinguish among the various sources of prompt electrons in the trigger.

Misidentified Hadrons

The rate of charged π's into the detector is about 300 MHz: 60 charged pions per event times the 5-MHz interaction rate. Of these about 15 MHz have transverse momentum above 1 GeV/c and so are potential fake triggers if misidentified as electrons. The online π-e rejection must be greater than 10^4 to reduce fake electron triggers to a 'mere' 1 kHz. Such rejection factors have been achieved in offline analyses but not yet at the trigger level.

Three types of detectors will contribute to π-e separation: the transition radiation detectors, the RICH counters, and the electromagnetic calorimeter. We suppose that a two-layer system of tracking TRD's can yield a rejection factor of 20 online, and that the RICH counter yields a factor of 5.

The electromagnetic calorimeter is configured with its first two radiation lengths as an active preconverter, in which a 'shower' of three charged particles must be detected for an electron candidate. If the calorimeter is made with tungsten plates the two radiation lengths correspond to 0.04 of an interaction length, providing an immediate rejection factor of 25. A comparison of the shower energy with the charged-track's momentum will be made; only interactions leading to $\pi^{\pm}$-π^0 charge exchange will survive this E/P cut. As such interactions comprise less than 5% of the total, the overall rejection factor from the electromagnetic calorimeter is greater than 500.

The combined rejection factor from the three detector will then be 5×10^4, corresponding to a trigger rate of 300/sec from misidentified hadrons. As mentioned above, the difficulty is to obtain this rejection factor online.

Overlaps of $\pi^{\pm}$ and γ's from π^0's

A fake electron trigger is generated if the momentum of a charged pion matches the energy of a π^0 whose shower overlaps the charged-pion track in the electron calorimeter. The TRD and RICH detector still provide rejection of the charged pion, so the rate of dangerous charged pions is 0.01×15 MHz $= 150$ kHz. Further rejection is obtained by spatially resolving the charged track from the π^0 shower in the electron calorimeter.

A study of the overlap problem was made with the *ISAJET* Monte Carlo program. Initially, an 'overlap' was defined as a charged pion whose separation from a neutral pion

was $|\Delta\eta| < 0.1$ and $|\Delta\phi| < 0.2$. It was found that about 7% of charged pions with $P_T > 1$ GeV/c had such an overlap. These overlaps are dangerous only if the E/P cut is also satisfied. Assuming the electron calorimeter has energy resolution for photons of $\sigma_E = 0.15\sqrt{E}$ the statistical significance of the E/P cut in standard deviations is

$$S.D. = \frac{|E-P|}{0.15\sqrt{E}}.$$

A cut requiring a 2σ separation of E of the π^0 from the P of the $\pi^\pm$ yields a rejection factor of 15. The rate of overlaps satisfying the combined trigger cuts is then less than 1 kHz.

The definition of overlap used above is satisfied by a pair of pions whose separation is less than 10 cm at 1-m radius from the beamline. However, two particles should be resolvable in the electron calorimeter if their separation is only 1 cm, which would provide an extra rejection factor of 100. In this case the rate of fake electron triggers from overlaps would drop to only 10 Hz.

Dalitz decays and γ-Conversions in Matter

The branching fraction for the decay $\pi^0 \rightarrow \gamma e^+ e^-$ is 0.015, as if the vacuum is 0.007 of a radiation length thick. Electrons from conversions of γ's in material will be more numerous than those from Dalitz decay if the photon has traversed more than 0.007 radiation lengths. For example, with a beam pipe whose wall is 400-μm-thick Be, or 0.001 of a radiation length, photons at angles of less than 1/7 to the beam are more likely to convert in the pipe than during the π^0 decay.

Figure 12 shows that the rate of electrons from Dalitz decay with $P_T > 1$ GeV/c is about 10 kHz at a luminosity of 10^{32} cm^{-2}sec^{-1} . The rate of electrons from γ-conversions in matter will be higher. Thus a rejection factor of order 100 is needed against these conversions.

More study is needed as to how this rejection will be achieved. Conversions outside the beam pipe can be suppressed by fast tracking all the way to the first silicon plane. Conversions in the pipe and Dalitz decays could be suppresed by a dE/dx measurement in the first silicon plane, but very large numbers of channels are involved.

Electron Detection Efficiency

The process of electron identification inevitably causes some real electrons to be lost. Rough estimates of the various detection efficiencies are:

- Fast tracking: 0.95
- Preconvertor cut at 2 radiation lengths: 0.90
- E/P cut: 0.95
- TRD cut: 0.90
- RICH counter cut: 0.95
- electron shower overlapped by another particle: 0.95

The overall efficiency of electron identification might then be 0.62. Great care will be needed to achieve an efficiency this high!

7. Signal to Noise

Here we consider three issues related to signal strength: flavor tagging, combinatoric backgrounds, and reconstruction efficiency

Flavor Tagging

Even when the electron trigger has successfully identified a B-$\bar{B}$ event there remains the question as to whether the flavor of the B's can be properly determined. This is critical when the 'other' B decays to a mode accessible both to a B and $\bar{B}$, as the flavor of the 'trigger' B must be identified before the 'other' B can be used in the measurement of the CP-violating asymmetry, as discussed in sec. 1.

If the trigger electron is from a direct decay of the form $B \rightarrow eX$ the sign of the electron determines the flavor of the B. But if the electron is from a D decay in the cascade $B \rightarrow DX$, $D \rightarrow eY$, the sign of the electron anticorrelates with the flavor of the B. In the direct decays, $B \rightarrow eX$, X includes a D or D^* most of the time. Hence the question of flavor tagging of the 'trigger' B is largely equivalent to that of associating the trigger electron with the secondary B-decay vertex or with the tertiary D-decay vertex. We estimate that the electron can be properly associated with its vertex only 40% of the time, based on the studies described in sec. 5. This factor has been included in the estimates of overall trigger efficiency given elsewhere in this report.

In the case of the 'self-tagging' modes, $B \rightarrow f$, where $f \neq \bar{f}$, the trigger efficiency will thus be 2.5 times higher.

Combinatoric Backgrounds

A B-mass peak could not be identified against the continuum due to combinatoric backgrounds without the requirement that B-decay products have a significantly nonzero impact parameter with respect to the primary vertex. However, a small fraction of non-B-decay tracks will appear to come from secondary vertices due to measurement errors. This problem is certainly most severe when attempting to find the decay $B^0 \rightarrow \pi^+\pi^-$.

A study of minimum-bias events collected by CDF at $\sqrt{s} = 1.8$ TeV indicates that the number of events in the $\pi^+\pi^-$ continuum mass spectrum in a 120-MeV/c^2 interval around the B mass is roughly 10^3 times the number of $B \rightarrow \pi^+\pi^-$ decays, assuming a branching fraction of 10^{-4} for this decay. Thus to obtain a 10:1 signal to noise in the mass spectrum after applying the impact parameter cut, each pion track must have less than 0.01 probability of being wrongly associated with a secondary vertex. Existing fixed-target experiments have achieved better rejection of tracks from the primary vertex than this. We anticipate that the demonstrated noise rejection of the silicon vertex detector will be available to the Bottom Collider Detector.

Reconstruction Efficiency

- Geometrical acceptance = 0.9
- Track reconstruction efficiency = 0.95
- Vertex reconstruction efficiency = 0.4
- Particle identification efficiency = 0.9
- Overall B-decay reconstruction efficiency = 0.32

8. Data Acquisition

Overview

In order to harvest the 10^{11} B-$\bar{B}$ pairs produced in the Bottom Collider Detector all events that satisfy the electron trigger should continue through the data acquisition system for further analysis. System architectures appropriate for data acquisition in this experiment have been considered in detail at the Workshop on High Sensitivity Beauty Physics at Fermilab.[17,18]

We anticipate an event size commensurate with the size and complexity of this detector. Due to the large number of detector elements and channels, zero suppression will be required and thus the recording of addresses as well as hit information will be necessary. An estimate of the event record size is 10^5 bytes per event, supposing each of the 100 particles per typical event is sampled by 100 detector element with 10 bytes of information per sample. The total trigger rate of events emerging from the online processors is about 1-2 kHz, including the expected rate of 500 B-$\bar{B}$ pairs per second and about 1 kHz from other prompt electron sources. This gives a net information transfer rate of up to 200 Mbytes per second.

Recording Devices

Contemporary data-acquisition systems using parallel transfer to multiple video cassettes, such as that proposed in E-791 at Fermilab, will record about 8 Mbytes/sec to this permanent medium. Based on this, recording 100-200 Mbytes/sec to a permanent storage medium is not an unreasonable goal for an experiment planned for 5 years from now. Steve Bracker has pointed out that tape systems developed and in use by the Haystack Observatory of the astronomy department at MIT presently record 100 MBytes/sec. This custom system is several years from being useful for high-energy-physics experiments but nevertheless indicates the state of the art. In addition, we are considering the viability of rejecting the other sources of prompt electrons using software filters as a further reduction in rate to permanent storage.

For the near future, it will be necessary for this group to become involved with laboratory efforts to develop high-rate data-acquisition systems. Discussions with such experts as E. Barsotti, C. Swoboda, and S. Bracker are underway. We anticipate that this experiment will benefit greatly from the rapid evolution presently occuring in data-acquistion technology. In addition, the introduction of RISC processors suggest that large increases in online computing can be expected in the next several years.

We conclude that although the needs of the Bottom Collider Detector are very demanding, the data-acquisition system can be designed and built in the next few years.

9. Summary

We summarize here the accomplishments of the B Collider Study Group towards a realistic proposal for an experiment to study CP violation in the B-$\bar{B}$ system at a hadron collider, and sketch the directions for continuing study.

Accomplishments

- Merging of the two earlier proposals for B collider detectors[4,5] into a single concept based on a central dipole magnet.
- Setting of overall goals of the experiment:
  - Production of 10^{11} B-$\bar{B}$ pairs;
  - Reconstruction and particle identification only of charged tracks from B decay;
  - 10^5 reconstructed decays for charged-particle modes with a branching fraction of 10^{-4};
  - 5σ evidence for a CP-violating asymmetry of 0.1 in such a decay mode.
- Identification of accelerator performance goals vital to the success of the B-collider experiment:
  - An average luminosity of order 10^{32} cm^{-2}sec^{-1} ;
  - A short (< 10 cm) interaction region;
  - Compensation magnets to counteract the effect of the dipole magnet on the beams.
- Specification of the overall architecture of the experiment;
  - Central detector inside the gap of the dipole magnet, plus forward and backward arms for tracks below 35°
  - Silicon vertex chamber
  - Straw-tube tracking system
  - Particle identification via liquid and gas RICH counters, TRD's and electron calorimetry, with muon identification in the forward/backward arms
- Identification of performance goals for a silicon vertex chamber:
  - Innermost detector elements at a radius of 1.5 cm from the beam;
  - Use of double-side, 200-μm-thick silicon to minimize multiple scattering;
  - Need to measure tracks with 45° incidence to the detector plane;
  - Need for reliable noise performance of 1000 electrons.
- Scenario of a tracking chamber system based on straw-tube technology.
- Statement of a triggering scheme based on electrons of $P_T > 1$ GeV/c from the decay $B \to eX$.

Work to Do

Topics which will be under consideration at the Snowmass Workshop include:

- Experimental Signal
  - Flavor tagging
  - Self tagged modes
  - Time development of mixing
- Accelerator Liaison
- Design of the dipole magnet
- Simulation of the vertex detector
  - Effect of high event multiplicity
  - Use of large clusters of hits
  - Effects of noise, signal fluctuations, δ-rays
- Hardware design of the vertex detector
  - Silicon-strip architecture
  - Readout electronics, cabling
  - Alternatives based on pixel devices
- Design of the central tracking system
  - Charge division vs pad readout
  - Development of very thin-wall tubes
  - Effect of scattering in the tube-end material
- Pattern recognition in the tracking system
  - Vertex-finding
  - Track-finding
  - Overlapping events
  - Fast tracking algorithm at trigger level
- RICH counters, liquid vs solid
  - π-K-p separation offline
  - e-π separation online
- Transition radiation detectors
  - 3D tracking in the trigger
  - backgrounds at small angles
- Electromagnetic calorimeter
  - Type: warm vs cold; total absorption vs sampling
  - Segmentation: preconverter, post-calorimeter
- Forward muon detection
- Triggering
  - Electron trigger scenario, efficiency, background, hardware implementation
  - Other triggers: μ, K, secondary vertex, *etc.*
- Front-end electronics
- Data acquisition
- Online processing
- Staging and time scale of the experiment

Acknowledgements

We thank Fermilab for providing the encouragement to pursue these very interesting questions and for providing support in the form of office space and secretarial help.

References

1. This report was edited by N.S. Lockyer and K.T. McDonald from textual contributions by P. Karchin, P. Lebrun, N.S. Lockyer, K.T. McDonald, L.A. Roberts, N. Stanton, and R. Stefanski.
2. Persons participating in the *B* Collider Study Group include:
P. Yager, *U.C. Davis*;
E. Barsotti, J. Butler, S. Childress, R. Coleman, S. Holmes, P. Lebrun, B. Lundberg, J. Morfin, R. Rameika, L.A. Roberts, H. Schellman, R. Stefanski, L. Stutte, C. Swoboda, H. Venkataramania, A. Wehmann, *Fermilab*;
P. Avery, A. White, J. Yelton, *U. of Florida*;
R. Burnstein, H. Rubin *I.I.T.*;
E. McCliment, *U. of Iowa*;
D.B. MacFarlane, *McGill U.*;
S. Reucroft, *Northeastern U.*;
S. Fredricksen, N.W. Reay, C. Rush, R.A. Sidwell, N. Stanton , *Ohio State U.*;
G.R. Kalbfleisch, P. Skubic, J. Snow, S.E. Willis, *U. of Oklahoma*;
N.S. Lockyer, *U. of Pennsylvania*;
K.T. McDonald, *Princeton U.*;
P Karchin, M. Mannelli, M. Schmidt, A.J. Slaughter, *Yale U.*.
Invited speakers include J.D. Bjorken *Fermilab*; S. Palestini *INFN Torino*, R. Van Berg *U. Pennsylvania*. Minutes of the meetings can be obtained from R. Stefanski, *Fermilab*.
3 E.L. Berger, private communication, and *Benchmark Cross Sections for Bottom-Quark Production*, Proceedings of the Workshop on High Sensitivity Beauty Physics at Fermilab (Nov. 11-14, 1987), p. 185.
4. P. Karchin, N. S. Lockyer *et al.*, *Proposal for a Bottom Collider Detector* BCD (March 1987).
5. N.W. Reay *et al.*, *Letter of Intent for a Tevatron Beauty Factory* (March 1987).
6. Useful reviews of *B* physics include I.I Bigi and A.I. Sanda, Nucl. Phys. **B281**, 41 (1987);
J.L Rosner, Proceedings of the Salt Lake City Meeting, ed. by C DeTar and J. Bell (World Press, Singapore, 1987), p59;
F.J. Gilman, *B Physics*, Proceedings of the Workshop on High Sensitivity Beauty Physics at Fermilab (Nov. 11-14, 1987), p. 1;
J.L. Rosner, A.I. Sanda, and M.P. Schmidt, *B-Physics Working Group Summary*, Proceedings of the Workshop on High Sensitivity Beauty Physics at Fermilab (Nov. 11-14, 1987), p. 165;
I. Dunietz, *Measurement of the Mass and Lifetime Differences Between the Heavy and Light B_s Eigenstates*, Proceedings of the Workshop on High Sensitivity Beauty Physics at Fermilab (Nov. 11-14, 1987), p. 229, and references therein;
H. Harari, *Introduction to B Physics Round Table Discussion*, to appear in the Proceedings of Les Rencontres de Physique de la Vallee d'Aoste (La Thuille, Italy, Feb. 1988);
A. Soni and G. Hou, *Loop-Induced Rare B Decays*, Proceedings of the UCLA Workshop, Linear Collider B-$\bar{B}$ Factory Conceptual Design, ed. by D. Stork (Jan. 1987);
L.-L. Chau and H.-Y. Cheng, *In Search of V_{ub} in Nonleptonic Decays from the Quark Diagram Scheme*, Phys. Lett. **B197**, 244 (1987);
A. Ali, *B-$\bar{B}$ Mixing–A Reappraisal*, Proceedings of the UCLA Workshop, Linear Collider B-$\bar{B}$ Factory Conceptual Design, ed. by D. Stork (Jan. 1987);
C.H. Albright, C. Jarlskog and B.-Å. Lindholm, *Three Family Fritzsch and Stech Models with Minimal and Two doublet Higgs Structure*, Fermilab-PUB-88/23-T (Feb. 1988).

7. Lee Roberts, *Monte Carlo Simulation of Silicon Vertex Detector for Bottom Collider Detector*, Fermilab preprint FN-488 (June, 1988).
8. H.-U. Bengtsson and T. Sjöstrand, Comp. Phys. Comm. 46, 43 (1987).
9. K. Foley *et al.*, *A Beauty Spectrometer for the SSC*, to appear in the Proceedings of the Workshop on Experiments, Detectors and Experimental Areas for the SSC, (Berkeley, 1987).
10. J. Sandweiss and B. Cox, *Summary of the Fixed-Target Architecture Working Group*, Proceedings of the Workshop on High Sensitivity Beauty Physics at Fermilab (Nov. 11-14, 1987), p. 273.
11. M. Strovink, D0 Collaboration Internal Note.
12 P. Karchin and M. Ogg, *Summary: Tracking and Vertex Detection Group*, Proceedings of the Workshop on High Sensitivity Beauty Physics at Fermilab (Nov. 11-14, 1987), p. 309.
13. R. Brun *et al.*, *GEANT3 User's Guide*, CERN DD/EE/84-1 (May 1986).
14. P. Baringer *et al.*, Nucl. Instr. and Meth. A254, 542 (1987).
15. R. DeSalvo, *A Proposal for an SSC Central Tracking Detector*, Cornell University preprint CLNS87/52.
16. F.E. Paige and S.D. Protopopescu, *ISAJET*, BNL preprint.
17. A.J. Lankford, M. Johnson *et al.*, *Summary of the Triggers and Data Acquisition Group*, Proceedings of the Workshop on High Sensitivity Beauty Physics at Fermilab (Nov. 11-14, 1987), p. 343.
18. E.Barsotti *et al.*, *B Physics–Digital Triggers and Data Acquisition...*, Proceedings of the Workshop on High Sensitivity Beauty Physics at Fermilab (Nov. 11-14, 1987), p. 383;
R. Van Berg, *Front-End Architectures for New Beauty Detectors*, Proceedings of the Workshop on High Sensitivity Beauty Physics at Fermilab (Nov. 11-14, 1987), p. 387.

APPENDIX D

BCD Proposal (E784)

Proposal for Research & Development: Vertexing, Tracking, and Data Acquisition for the Bottom Collider Detector

H. Castro, B. Gomez, F. Rivera, J.-C. Sanabria, *Universidad de los Andes*
P. Yager, *University of California, Davis*
E. Barsotti, M. Bowden, S. Childress, P. Lebrun, J. Morfin, L.A. Roberts, R. Stefanski, L. Stutte, C. Swoboda, *Fermilab*
P. Avery, J. Yelton, *University of Florida*
K. Lau, *University of Houston*
R. Burnstein, H. Rubin, *Illinois Institute of Technology*
E. McCliment, Y. Onel, *University of Iowa*
G. Alverson, W. Faissler, D. Garelick, M. Glaubman, I. Leedom, S. Reucroft, D. Kaplan, *Northeastern University*
S. E. Willis, *Northern Illinois University*
S. Fredricksen, N. W. Reay, C. Rush, R. A. Sidwell, N. Stanton, *Ohio State University*
G. R. Kalbfleisch, P. Skubic, J. Snow, *University of Oklahoma*
N. S. Lockyer, R. Van Berg, *University of Pennsylvania*
D. Judd, D. Wagoner, *Prairie View A&M University*
D. R. Marlow, K. T. McDonald, M.V. Purohit, *Princeton University*
A. Lopez, *Universidad de Puerto Rico*
B. Hoeneisen, *Universidad San Francisco de Quito*
S. Dhawan, P. E. Karchin, W. Ross, A. J. Slaughter, *Yale University*

(January 2, 1989)

Abstract

We propose a program of research and development into the detector systems needed for a B-physics experiment at the Fermilab p-$\bar{p}$ Collider. The initial emphasis is on the critical issues of vertexing, tracking, and data acquisition in the high-multiplicity, high-rate collider environment. R&D for the particle-identification systems (RICH counters, TRD's, and EM calorimeter) will be covered in a subsequent proposal. To help focus our efforts in a timely manner, we propose the first phase of the R&D should culminate in a system test at the C0 collider intersect during the 1990-1991 run: a small fraction of the eventual vertex detector would be used to demonstrate that secondary-decay vertices can be found at a hadron collider. The proposed budget for the R&D program is \$800k in 1989, \$1.5M in 1990, and \$1.6M in 1991.

Contents

List of Figures

List of Tables

1 Introduction

We have recently submitted a Letter of Intent[1] to inaugurate a study of B physics at the Tevatron collider with the goal of observing the strongest signals for CP violation in the B-$\bar{B}$ system. This experiment combines a rich physics program for the 1990's with the opportunity for development of detector technology needed in the SSC era. The program is ambitious and is not a direct extension of any existing experiment. We propose here to begin research and development of several critical detector systems as a means of dedicating our efforts towards the B-physics program prior to the approval of the full experiment.

One B-$\bar{B}$ pair is produced in every 1000 interactions at the Tevatron collider,[2,3] while each interaction produces about 60 'background' particles. To extract the B mesons from this background we will employ two techniques: reconstruction of a secondary decay vertex for the B's (whose lifetime, $c\tau$, is 360 μm[4]), and reconstruction of the invariant mass of the products of B decay into all-charged final states. In recent years, the development of silicon vertex detectors has permitted hadronic fixed-target experiments to compete favorably with e^+e^- colliders in the study of charmed mesons. We propose to demonstrate that silicon vertex detectors are also appropriate for a hadron collider.

CP violation is expected to manifest itself prominently only in rare ($\Gamma \sim 10^{-5}$) decay modes of the B mesons; some 10^8 reconstructible B's will be needed to establish the effect clearly.[5] Hence the experiment must be performed with a reasonably high collision rate, and we adopt $\mathcal{L} = 6 \times 10^{31}$ cm^{-2}sec^{-1} as the detector-design luminosity. This corresponds to an event rate of 2.5 MHz, and requires the experiment to have a very high rate data-acqusition system by present standards. We propose to develop a data-acquisition architecture based around a 'barrel switch' that can build 10^5 complete events per second, which events are then processed in a large 'farm' of numeric processors before archival storage of at most 10^3 events per second.

The issues of vertex detection and data acquisition are the most critical for B physics at a hadron collider, and are emphasized in the present R&D proposal. A discussion of the technical issues to be studied is given in section 2, which includes a number of secondary items to be covered by the present proposal, as well as important items beyond the scope of the initial effort. Schedules and costs are presented in section 3, with the rough scenario that 1989 is devoted primarily to bench tests with a budget of \$0.8M, leading to tests of individual devices in an external beam in 1990 with a budget of \$1.5M, followed by a system test in 1991 at the C0 intersect with a budget of \$1.6M.

2 Issues for Research and Development

The current vision of the Bottom Collider Detector is shown in fig. 1. The detector is comprised of 5 detector systems, plus the electronics for data acquisition. In this section we outline the technical issues related to these systems that require study, as well as several issues of the impact of the experiment on the accelerator operation.

While some discussion is given of R&D for the particle-identification systems (the RICH counters, the TRD's, and the EM calorimeter), work on this is not part of the initial proposal detailed in section 3. Our plans in this area should become much more well-defined following the upcoming Symposium on Particle Identification at High Luminosity Hadron Colliders, organized by J. Morfin and to be held at Fermilab on April 5-7, 1989.

The present detector design is based on the assumption that the Tevatron collider will operate with 44 bunches with a spacing of 21 rf buckets, so the time between bunch crossings is 400 nsec.

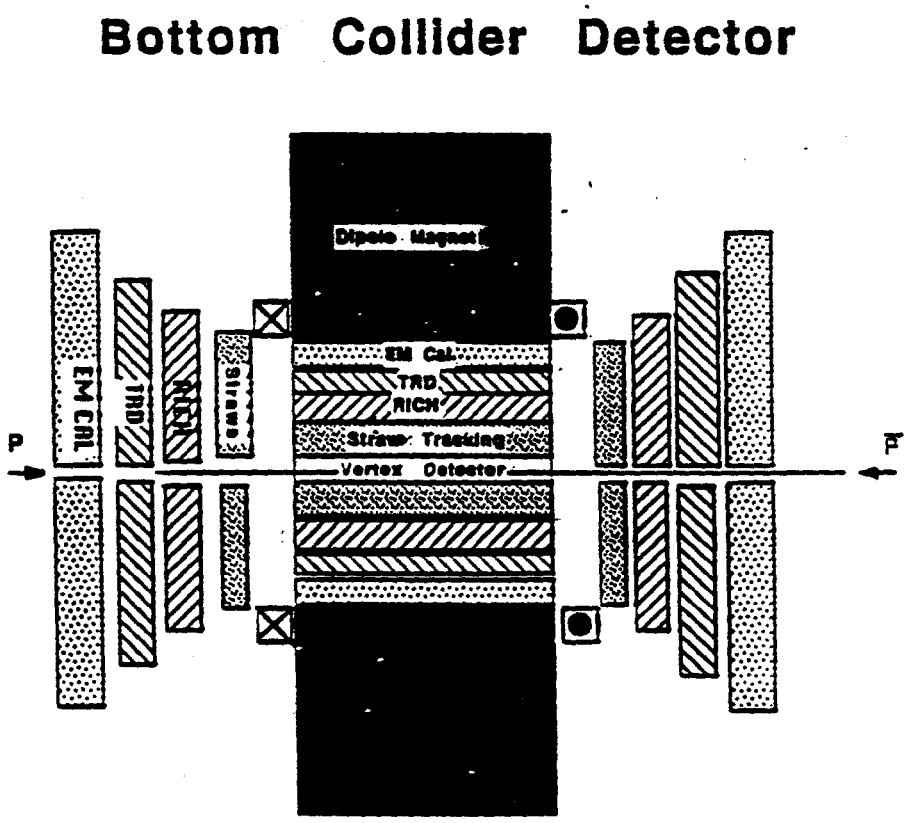

Figure 1: Overview of the Bottom Collider Detector.

2.1 Dipole Magnet

Reconstruction of B-decays requires magnetic analysis. The kinematics of B production and decay at the Tevatron collider indicate the need for coverage for particles primarily

with $P_T < 5$ GeV/c and pseudorapidity $-4 < \eta < 4$ (lab angles $2° < \theta < 178°$). A dipole magnet with field transverse to the colliding beams is the best configuration, and provides good accuracy for high-momentum tracks in the forward and backward directions, at the expense of a small loss in useful solid angle around the direction of the magnetic field. This 'dead' region will be useful for cable paths out from the interior of the detector.

The magnet should have a field integral of $\int Bdl \approx 3$ Tesla-m out from the interaction point along the beam direction, and an integral of 0.6 Tesla-m outwards transversely to the beams. The central-detector systems should be entirely within the magnet (there is no hadron calorimeter), while in the forward/backward directions the particle-identification systems can be outside the field volume.

A magnet with circular pole tips (such as a cyclotron magnet) meets these requirements, while providing a field with circular symmetry to simplify the track-finding algorthm. Such a magnet is relatively open in both the forward and sideways directions, permitting great flexibility in configuring the detectors.

Design studies for such a magnet have been initiated at Fermilab by R. Wands and A. Wehmann, and should be continued. A magnet with pole tips 4 m in diameter and with a 4-m gap would weigh 2500 tons. With a central field of about 1 Tesla the stored energy is 100 mJoule. Superconducting coils are needed to keep the operational cost down, and represent the major design issue. A scenario to recycle the Livermore Magnetic Fusion Test Facility coils could be pursued, but an engineering study is needed to determine whether this option would be cost effective.

2.2 Silicon Vertex Detector

At a hadron collider, the intersection region is typically tens of centimeters long, and tracks of interest emanate in all directions from this line source. Thus the geometry of tracking is much more complicated than in a fixed-target experiment, where most tracks of interest have near-normal incidence on detector planes in the forward direction. Further, to obtain good reliability for finding secondary vertices, the vertex detector must provide all three coordinates of each intercept of a track with a detector plane. In the future this may be best accomplished with pixel detectors, but at present we are exploring the use of silicon strip detectors each with two strip orientations.

Because the collider intersection region is extended, the only practical arrangements of silicon detector planes are those in which some particles must be observed at angles up to 45° incidence. This leads to mechanical and electronic specifications somewhat beyond presently achieved values. The present proposal is to develop the technology to meet these specifications.

Silicon detectors have reduced sensitivity for tracks with large angles of incidence. We currently plan to use silicon strip detectors with 50-μm strip width, 200-μm thickness, and double-sided readout (a.c. coupled). A minimun-ionizing particle creates 80 electron-hole pairs per μm of silicon traversed, so the signal is 16,000 electrons at normal incidence, 5600 electrons per strip at 45° incidence, and only 4000 electrons at grazing incidence. We are setting a goal of an r.m.s. noise level of 600 electrons in the preamplifier, so that tracks

of less than 45° incidence will have better than 9:1 signal-to-noise. The preamplifiers are to be implemented in VLSI technology and bonded directly to the silicon detectors. The R&D program to produce such amplifiers is already underway, and is elaborated upon in section 2.9 below.

The mechanical configuration of the silicon planes is sketched in fig. 2. Tracks with angles less than 45° to the beams are to be observed in detectors oriented perpendicular to the beams, which are called disks. Tracks with angles between 45° and 135° to the beams are to be observed in detectors arranged in barrels around the beams.

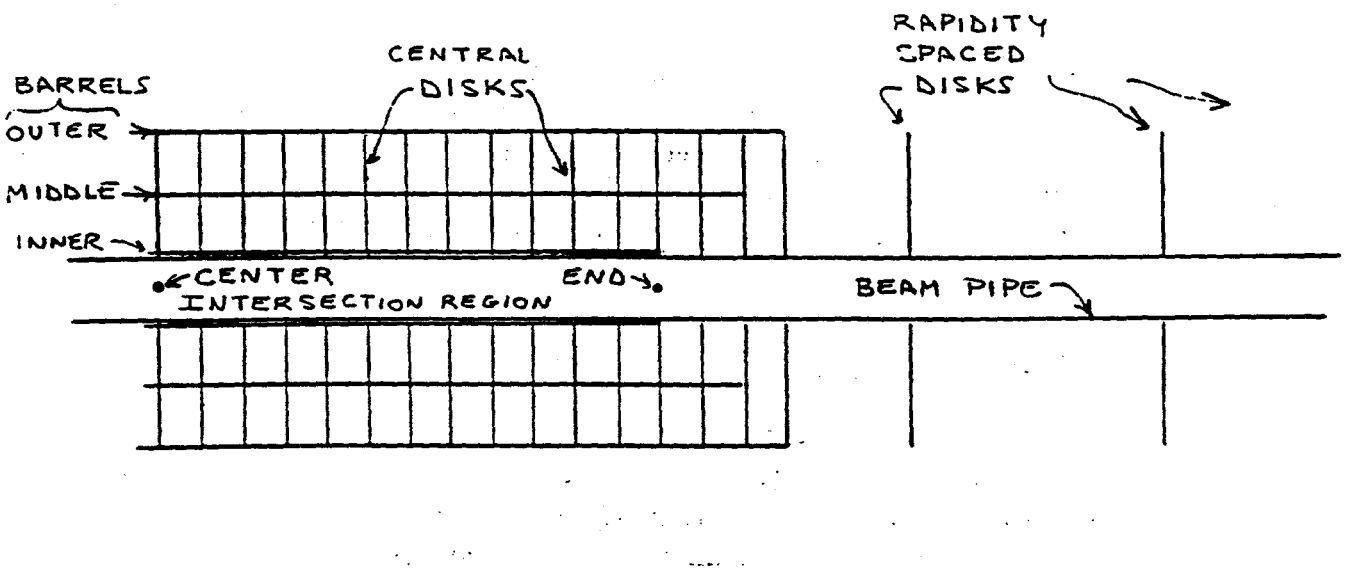

Figure 2: A section through the silicon vertex detector including the beam axis. In this view the disks are vertical and the barrels are horizontal.

If the intersection region were a point, there would be no overlap in the solid angle covered by the disks and barrels. But for a finite interaction length these two detector types must be interspersed, leading to significant mechanical complexity, especially for the cooling of the preamplifiers mounted on the silicon detectors.

In principle, each particle might pass through so many silicon detectors that the entire task of tracking could be accomplished with the resulting signals (although multiple scattering in the silicon would limit the accuracy). However, the cost of this is deemed prohibitive at present, and we plan for a configuration in which each particle penetrates at least 3 silicon detectors (each providing an x-y-z space point) at an angle of incidence less

than 45°. Even so the number of silicon strips is roughly $2 \times 10^5 + (10^6 \times$ interaction length in meters). The task of pattern recognition of the tracks must be accomplished in the tracking system described in the next section; the silicon detectors provided an accurate measurement of the track segments in the vicinity of the beams.

Double-sided silicon detectors only 200-μm thick are used to reduce the multiple scattering in the detectors. The barrel detectors intermingle with the central disks to form a closed, layered structure. Penetrations must be provided for signal readout, and for cooling of the preamplifiers. This leads to a nontrivial mechanical structure which requires immediate study.

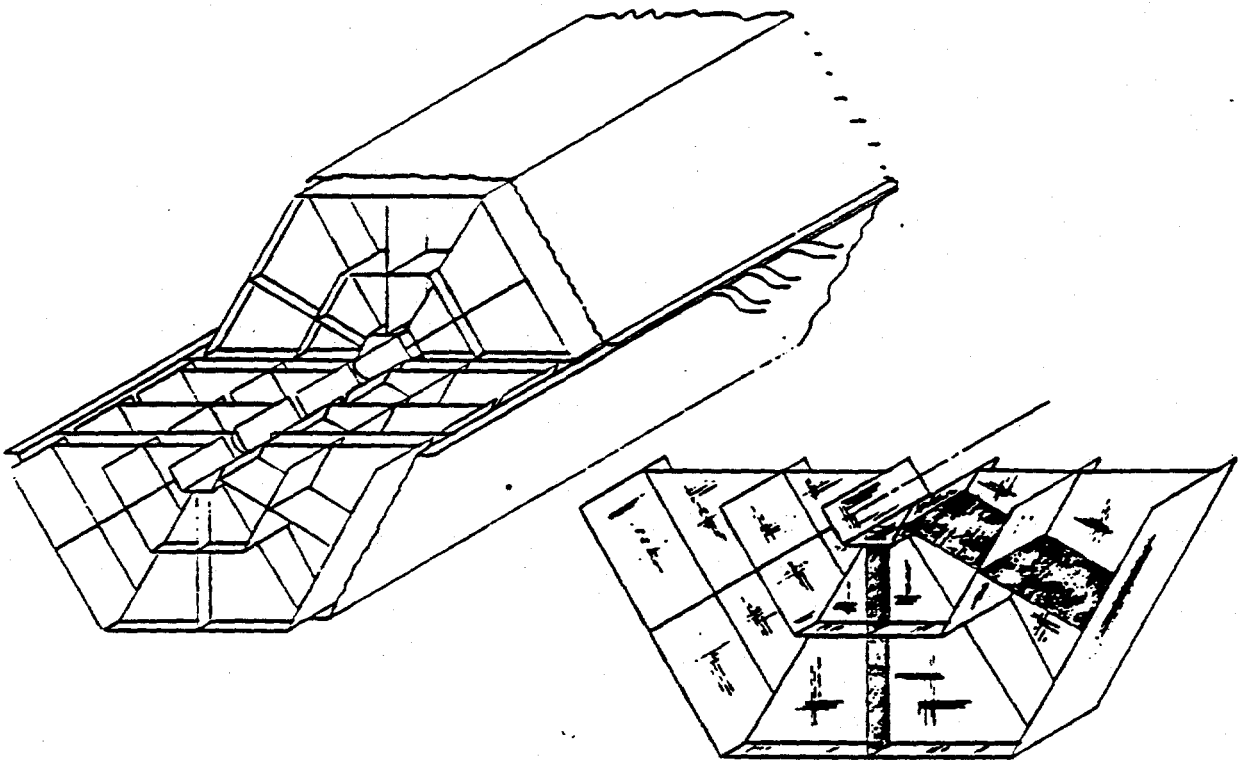

Figure 3: Sketch of a model built to study the assembly of the silicon vertex detector.

Two sets of models have been built to help characterize a suitable arrangement of the detectors into a largely self-supporting structure. These first steps must now be followed by more realistic models, eventually made of silicon, which include heat sources simulating the anticipated load of 2 mWatt per strip (about 2000 Watt for the whole silicon vertex detector).

If the detector is to be gas cooled a flow of order 100 cfm is needed, which flow must be channeled into the inaccessible interior of the detector without inducing vibrations. A scheme in which the disks of the central silicon detector are only partially implemented in azimuth is under study. An alternative scheme involving local cooling of the preamplifiers

by liquid in small tubes is also under consideration.

The individual silicon detectors will be assembled into the overall structure via small channels of beryllium or kevlar, machined to a few μm accuracy, and glued to the silicon at a minimum number of points. The detectors may need to be cradled in an exterior trough to counteract sagging over its 1-m length, and to provided means of alignment of the vertex detector with the exterior tracking system. Figure 3 shows a preliminary conception of the assembly that was the basis for one of the models, and which revealed the need for continued evolution of the design.

The silicon vertex detector will be operated in the 1-Telsa dipole magnetic field. The effect of the Lorentz force on the drift of the signal electrons must be characterized for each of the several orientation of strips relative to the magnetic field.

2.3 Straw-Tube Tracking System

The outer tracking system must reconstruct charged-particle tracks unambiguously in three-dimensional space and extrapolate them into the silicon vertex detector, which functions as a vernier. The tracking system must measure the particles' momenta to $\pm 1\%$ in the dipole field of about 1 Tesla, and cannot have massive support structures such as end plates that would interfere with the particle identification systems which surround it. The tracking system should be configured so that a fast measure of the particles' P_T could be obtained for triggering.

The requirements of low-mass devices with high spatial resolution seem well met with straw-tube technology. A possible layout of some 2×10^5 pressurized straws is shown in fig. 4. The tubes are configured in 'superlayer' modules comprised of 8 layers of tubes each. Each track should pass through at least 8 superlayers, yielding a minimum of 64 measurements per track. With a tube diameter of 3 mm and a gas pressure of 4 atmospheres, a spatial resolution of 50 μm per hit should be achieved. To minimize multiple scattering in the walls of the tubes it is advantageous to use tubes of only 30-μm thickness, half of that achieved to date.

The straw-tube systems will bear the primary burden of pattern recognition for particle tracks. Further study is needed to confirm that our configuration of the straws has sufficient stereo-matching capability. We are exploring the possibility that 'neural-net' hardware processors might be developed which associate vector track segments with the patterns in each superlayer for use in the trigger. The front-end electronics for the straw tubes are relatively modest extrapolations of present designs, as discussed more in section 2.9.2 below.

A hardware R&D program for straw tubes should be initiated in the near future. We must determine whether thin-walled straws can be manufactured, and determine their mechanical stability under presssurized operation. Low-mass end plug must be developed with gas and electrical feed throughs. Spacers may need to be inserted into the longest straws, whose length might be 2 m. The effect of high radiation dose on the chamber gas must be studied along with the more usual aspects of optimizing the gas mixture. Assembly and alignment schemes are to be specified and tested. A lengthy scenario for

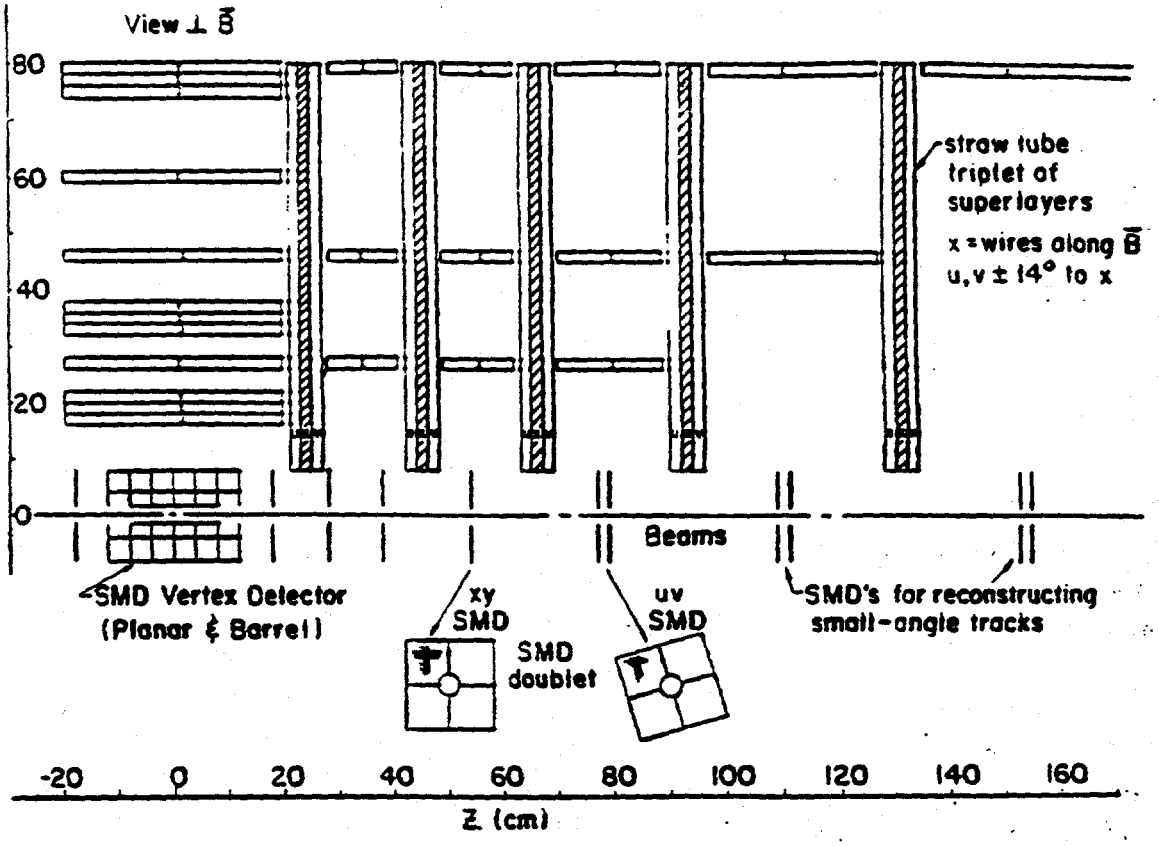

Figure 4: Plan view through the median plane of one quadrant of the tracking system, showing the configuration of the straw-tube 'superlayers' and the silicon strip detectors. The dipole-magnet field and the wires in the x straws are perpendicular to the page.

straw-tube development has been given by DeSalvo.[6]

2.4 Ring Imaging Čerenkov Counters

Identification of hadrons in the Bottom Collider Detector will be accomplished primarily with RICH counters, supplemented by a time-of-flight system in the central region. The goal is to provide flavor tagging for all hadrons of transverse momenta less than 5 GeV/c. This could be done with RICH counters with a liquid radiator in the central region, and gas + liquid radiators in the forward/backward directions. The desired ranges of momentum coverage are summarized in table 1.

The space available for the RICH counters permits a thickness of approximately 25 cm for the liquid-radiator counters, and 1 m for the gas-radiator counters. Complete coverage of the momentum ranges given in table 1 would require a position resolution of about 1 mm for detection of the Čerenkov photons. This implies the need for about 10^7 detector pixel elements. Readout electronics suitable for such large-scale implementation are currently being designed at the Rutherford Laboratory.[7]

	P (GeV/c) at $\gamma_t = 2$	γ at $P = 8$ GeV/c	P'(GeV/c) at $\gamma_t = 17$	γ at $P = 120$ GeV/c
π	0.3	56	2.5	840
K	1	16	8.5	240
p	2	8	17	120

Table 1: Ranges of momenta and γ which should be covered by the RICH counters. $\gamma_t = 2$ for liquid C_6F_{14}, and $\gamma_t = 17$ for gaseous C_5F_{12}.

The detector for the UV Čerenkov photons needs R&D. The issue is complicated by the use of a liquid radiator, which absorbs photons of energy greater than 7 eV. These photons are to be detected in a photosensitive gas, such as TMAE, and the ionization electrons observed via the signals induced on cathode pads of a multiwire chamber. The drift velocity for the photoelectron is about 15 nsec/mm, so if the signal width is desired to be, say, at most 200 nsec, the active depth of the photodetector must be only 6 mm. However, the absorption depth for TMAE at room temperature is about 2 cm, so only 30% efficiency could be achieved within the desired time window, unless the TMAE is heated. There is a clear need for a 'designer molecule' whose photoionization properties are better matched to the experimental requirements. Some progress in this direction has been recently achieved by Ypsilantis in colloboration with a chemist, Alan Katzrik of the U. of Florida.[8]

Another problem which must be faced in a collider experiment is the large signals due to charged particles passing through the detector gas. The partial pressure of the photosensitive gas is only a few Torr, so operation at atmospheric pressure is obtained by adding a buffer-gas mixture such as argon-isobutane-methane. About ten times as many electrons are ionized directly by a charged particle as are ionized by the Čerenkov photons. With a high gas gain to observe the Čerenkov signal, there is risk of discharges due to the minimum-ionizing 'background.' A possible solution is to operate the photodetector at only a few-Torr pressure, which nearly eliminates the signal from minimum-ionizing particles, and actually improves the gas gain. However, considerable developement is needed on the mechanical configuration of a large-area, low-pressure detector.

2.5 Transition Radiation Detectors

While evidence for CP violation in B decays will likely come primarily from measurement of asymmetries in all-charged decay modes, it is important to tag semileptonic modes, $B \to e\nu X$, as well. The best modes for observation of CP violation are those where the final state f is a CP eigenstate, so the particle/antiparticle character of the parent B cannot be determined from measurement of this decay alone; the second B of the produced B-$\bar{B}$ pair must be tagged. This leads to the need for electron identification systems, comprised of TRD's and electromagnetic calorimeter.

Of all the technologies to be used in the BCD, the TRD's are the most well-developed at present.[9] However, it will be advantageous to use next-generation thin-sampling detectors,[10] in which some 30 detectors each 1.5-cm thick yield better pion rejection than the 15-cm-thick devices currently in use. An online rejection of 100:1 against pions should be achievable, presuming some processing of the 30 samples per track.

The BCD requires about 60 m^2 of TRD's. If the size of the cathode readout pad is taken as 1 cm^2, there are 6×10^5 pads per layer of TRD. Thus a 30 layer system of this granularity has about 2×10^7 readout elements. While the cost of VLSI electronics in such numbers is not excessive, the question of mechanical costs of mounting these chips on a low-density board must be explored.

2.6 Electromagnetic Calorimeter

The calorimeter functions primarily to aid in electron identification, rather than providing a precision energy measurement. As such, position resolution is more critical. We thus have the option to use a sampling calorimeter (as opposed to total absorption in BGO or lead glass, *etc.*).

The calorimeter should have tower geometry, with three longitudinal samplings per tower. This feature should permit an online rejection factor of several hundred for charged π's. The transverse size of the towers should be sufficient that the energy measurement is of only a single particle with 99% probability, leading to a tower count of 10^4 given an average multiplicity of 100. A position-sensitive detector will be placed between the first and second layers of each tower to reject overlaps of a charged pion with a photon from π^0 decay. For this a two-track resolution of about 1 cm is desirable.

Of the technologies available for calorimetry, liquid argon appears the most satisfactory in terms of performance, but is cumbersome to implement in a 4π experiment. A warm-liquid system could be advantageous if perfected. A calorimeter with scintillator as the sampling medium is adequate, if the difficulty of an optical readout in a magnetic field can be solved.

A speculative option is to read out the scintillating fibers of a 'spaghetti' calorimeter with to-be-developed devices called 'silicon phototubes.' In these, a small photodiode has a silicon pixel detector as its anode, which is bonded to a low-noise amplifier inside the vacuum. About 300 electrons would be liberated per photoelectron per 1000 volts across the diode. For a small pixel size the noise could be held to perhaps 500 electrons, so with a 3-keV voltage, the noise level is 0.5 photoelectrons. The silicon phototubes might have cathode areas of 1 cm^2, matched to a 2×2 cm^2 segment of the spahghetti calorimeter, assuming 25% coverage by area with the scintillating fibers. Because they are photodiodes with a small gap, the silicon phototubes are relatively insensitive to magnetic fields. A possible drawback is that the anode is sensitive to charged particles which pass through it, each such giving a signal equivalent to one photoelectron. It would require a large R&D program in cooperation with an interested vendor, perhaps Burle Industries, to develop the silicon phototube.

2.7 Signal-Processing Architecture

Because the B experiment is based on reconstruction of all soft charged tracks, a large amount of data is produced by each event. Each of 60 tracks will be sampled approximately 100 times for a total of about 6000 words per event. A word will typically consist of 4 address bytes and one data byte, for a total of 30,000 bytes per event. The detector is to operate at event rates of up to 2.5 MHz, so the potential data rate is 75 gigabytes/sec.

By utilizing the technology of modern telephone switches we can process this high data rate in 3 levels, as illustrated in fig. 5:

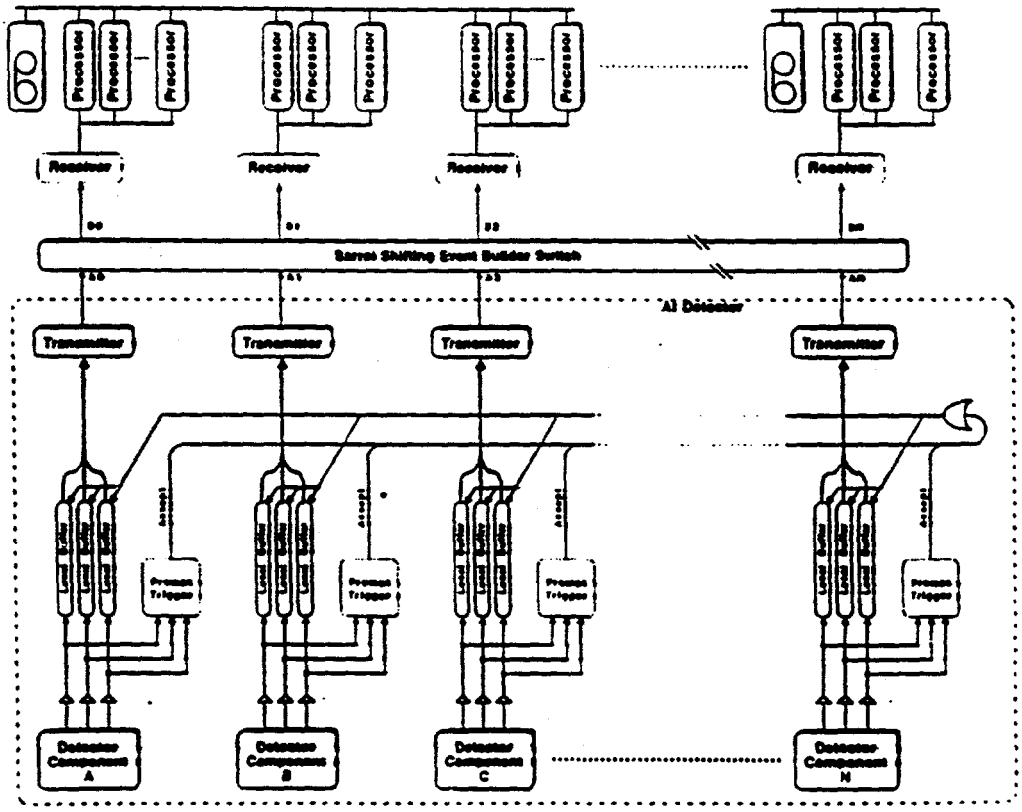

Figure 5: Schematic of the signal-processing architecture.

- A fast trigger reduces the event rate by a factor of 25, for a maximum of 100 kHz of surviving events. The fast trigger is based on analog signal processing; all trigger decisions based on numerical calculations are to be deferred to the second level.
- A 'barrel switch' organizes that data from up to 10^5 events/sec into individual event records, which are fed to a farm of perhaps 10,000 numeric processors. Each processor is about 50 VAX-780 equivalents, and must make a second-level trigger decision in 0.1 sec, with a desired reduction in the event rate of 100.
- The remaining event rate of up to 1 kHz is archived to some storage medium such as video cassette, or perhaps the new technology of 'digital paper.' The archival data

rate is then about 30 Mbytes/sec, which would require 120 present-day Exabyte cassette drives. The archived events would later be analyzed on the processor farm, whose combined processing power is about 0.5 TIPs (0.5×10^{12} instructions per second).

In the next three subsections we discuss issues relating to the fast trigger, the front-end electronics, and the data-acquisition system.

2.8 Fast Trigger

As discussed in our Letter of Intent,[1] two kinds of fast triggers are under consideration for the Bottom Collider Detector:

- A **topology** trigger which is satisfied whenever n or more tracks in an event have P_T above a cut value. For $n = 1$ the cut might be 3 GeV/c, while for $n = 2$ the cut could be at 2 GeV/c. Either could yield a factor of 25 reduction in the event rate according to preliminary Monte Carlo simulations. This trigger would be based on fast tracking, and could use coarse-grained position information from pad chambers (*i.e.*, the first and last pad layers of the TRD's) as well as signals from the straw-tube tracking system.
  - In addition, the fast-tracking system must have precise ($\sim \pm 1$ cm) z-coordinate information within a few hundred nsec after a collision. This component of the fast trigger would be provided by a scintillating-fiber tracking system located several meters upstream and downstream of the interaction region. One encouraging design consists of 4 identical 9-plane arrays of fibers positioned to cover the rapidity range from 4 to 6. Each detector plane consists of 200 fibers oriented in the nonbend plane.
- An **electron** trigger with a minimum-P_T cut of about 1 GeV/c. Since each event will have about three charged pions with $P_T > 1$ GeV/c, an online pion rejection of greater than 75:1 is needed to reduce the event rate by the desired factor of 25. This should be achievable using signals from the TRD's, and from the longitudinally segmented electromagnetic calorimeter.

Thus the fast trigger will be derived primarily from signals in the outer layers of the detector, but the design should preserve an option to incorporate signals from the inner tracking systems as well. This may be particularly important for rejection of electrons from photon conversions.

Continued study of the trigger scheme is needed, with emphasis in the near term on computer simulations.

2.9 Front-End Electronics

The front-end electronics will be in the form of custom, very-large-scale integrated (VLSI) circuits, permitting low-cost and low-power readout of the large number of detector elements of the Bottom Collider Detector. All of the various chips proposed here are straightforward extrapolations or reconfigurations of presently available devices, although they will necessarily be 'state-of-the-art' devices.

The experience of a number of high-energy-physics groups has shown that such chips can be successfully developed by a small number of people, but that turn-around times with the silicon foundries dictates a time scale of perhaps two years per chip. Resistance to radiation damage is of particular interest to us, and will require additional studies best performed once the chips are electronically operational.

For running of the Bottom Collider Detector at the Tevatron collider we take the bunch crossing time to be 400 nsec (compared to 16 nsec at the SSC). Hence any signals not requiring a fast timing pulse can be shaped to a full width of 400 nsec. This permits the use of low-power CMOS technology for most chips. The notable exception is the preamplifier for the straw tubes, which must use Bipolar technology to provide a time resolution of 0.5 nsec, corresponding to the desired 50-μm spatial resolution.

While the detector will have a channel count in excess of 10^7, only about 10^4 channels will be struck during an event of interest. The front-end electronics must include functions to sparsify the data, outputting only addresses and digitized data for the struck channels. Further, the data must be stored at its source until the fast trigger is formed, perhaps as long as 6 μsec, before passing it on to the data-acquisition system.

The flow of data out of the detector should be on fiber-optic cables whose higher rate capability will minimize the number of physical cables. This requires a class of data-collection chips on the detector which format and buffer the data before transmission off the detector.

The front-end electronics for the various detector systems will be designed with the maximum of commonality. Efforts will begin on chips for the silicon strip detectors. Only the straw-tube chambers will require electronics with considerably different features.

2.9.1 Silicon Strip Front-End Electronics

From the considerations outlined in section 2.2, we have arrived at the following specifications for the front-end chip (designated the BVX) for the silicon strip detectors:

- 1.25-μm CMOS technology.
- Power consumption: 1 mWatt/channel.
- R.m.s. noise $<$ 600 electrons.
- Signal shaped to 400-nsec full width at base.
- Adjustable discriminator threshold in the range 3000-6000 electrons, with option for a second discriminator threshold.

- On-chip storage of the analog signals for about .6 μsec = 16 bunch crossings.
- Six-bit ADC for signals above threshold, with digitization beginning only if the fast trigger is satisfied.
- Sparsified readout of the 128 channels which make up a physical BVX chip.
- Individual channel electronics sized for the 50-μm strip pitch of the silicon detectors.
- Radiation hardness to 100 krad, the expected yearly dose at 1 cm from the beam at a luminosity of 10^{31} cm^{-2}sec^{-1}.

These specifications are slightly beyond those met by the current generation of chips, such as the MPI CAMEX,[11,12] the LBL SVX[13] and the RAL MXI.[14] However, the relatively long bunch crossing time at the Tevatron, 400 nsec, should permit the stringent noise requirement to be met. Also, we plan to use a.c. coupling to the amplifiers, which renders them largely immune to leakage current, and eliminates the need for quadruple-correlated sampling.

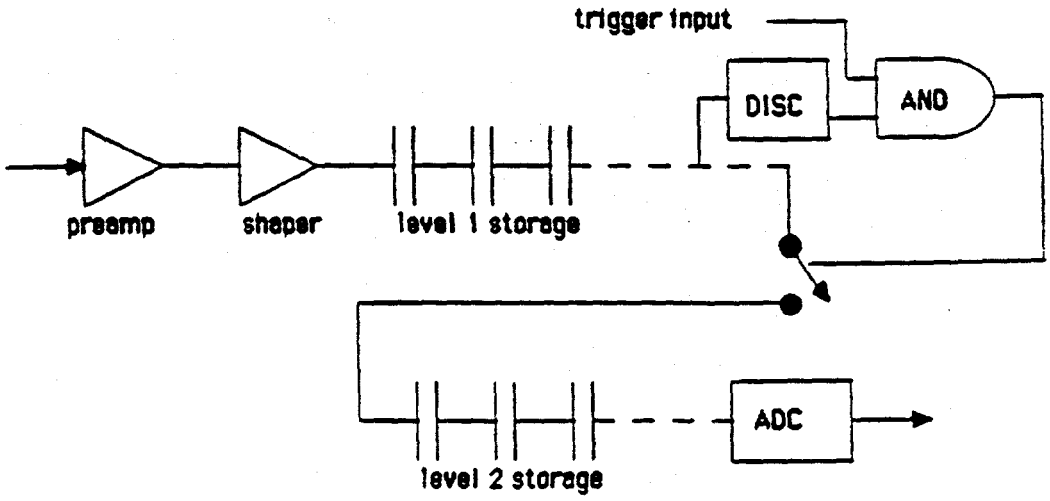

Figure 6: Block diagram of one channel of the BVX readout chip for the silicon strip detectors.

A block diagram of one channel on the BVX chip is shown in fig. 6.

Tracks with angle of incidence greater than 45° present an additional problem for the readout. Such tracks may deposit signals of greater than 4000 electrons into a large number of contiguous strips, called here a cluster. It is not necessary that these signals be processed further, because the silicon is arranged so that all tracks strike at least three detector at angles of incidence less than 45°. However, signals as low as 5600 electrons, due to tracks at exactly 45° incidence, must be kept. Because the r.m.s. noise is a substantial fraction of the difference between 5600 and 4000 electrons, it is dangerous to set a threshold in this region; because of noise fluctuactions the cluster of struck strips would be processed as a number of isolated hits, filling the event records with useless data.

If would be preferable if there were an on-chip capability to sense the number of contiguous struck strips above a threshold of, say, 4000 electrons, and suppress the readout of the entire cluster (or entire chip!) if more than 6 contiguous strips were struck.

The BVX chips are to be bonded directly to the silicon wafers, without requiring a dead space near the readout end of the wafer. Figure 7 sketches how this might be accomplished with a tab-bonding technique.

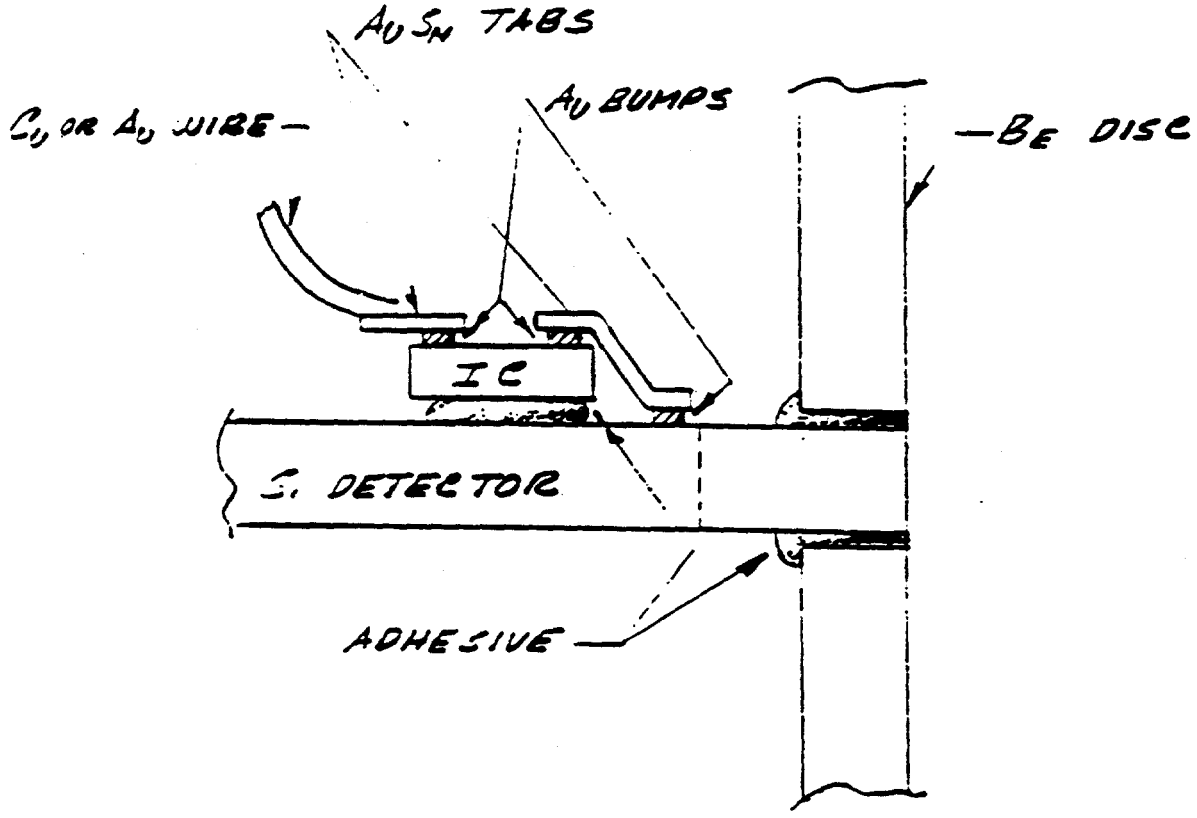

Figure 7: Possible scheme for bonding the BVX readout chips to the silicon strip detectors.

If there are 10^6 silicon strips serviced by the 128-channel BVX chips, then about 10^4 of the latter are required. If separate data lines emerge to the outside world from each BVX chip the cabling problem would be severe. However, the average occupancy of a BVX

chip should be less than one channel per event (if clusters of greater than six strips can be suppressed). It will be advantageous to route the signals from 10 to 100 neighboring BVX chips into a 'data collection' chip, which further buffers the data until the data-acquisition system is ready to receive it. Details of the data-collection architecture need further specification; this architecture should be suitable for collection of signals from all systems of the Bottom Collider Detector.

2.9.2 Straw-Tube Electronics

The high spatial resolution of the straw tubes is obtained by measuring the time of arrival of the first ionization electron. A resolution of 50 μm requires a timing accuracy of 0.5 nsec. Hence the preamplifiers for the straw tubes must be fast devices even though the event rate is at most 2.5 MHz. The speed requirement dicates the use of Bipolar technology for the integrated circuits, at the expense of a heat load of about 15 mWatt per channel. Cooling the low density of straw-tube preamps is, however, a straigthforward matter. Once the electron-arrival time has been converted to a voltage, the rest of the signal processing (trigger delay and digitization) can be performed in CMOS circuitry very similar to that on the BVX chip

The block diagram of the proposed Bipolar/CMOS chip is shown in fig. 8, which closely follows the so-called TVC chip set developed at U. Penn for the SSC.[15] The Bipolar amplifier/shaper/discriminator of the TVC could be used directly, and the CMOS analog store could be used but with a slower clock, typically 5-10 MHz.

The system would consist of the Bipolar preamp/shaper/discriminator followed by the CMOS analog-store/ADC/readout-control chip. The Bipolar chip will have four channels and the CMOS chip will have 8 channels. In addition the system would need a data-collection chip (digital CMOS), similar to that for the silicon strip electronics, for every 8-32 front-end chips. Total power costs would be about 20 mW per channel.

A possible arrangement would have a thin printed-circuit board mounted on the ends of a group of 128 straws, with 32 Bipolar chips, 16 CMOS TVC chips, and one data-collection chip, in addition to discharge protection and bypass and coupling capacitors for the straws. The cost would be about \$2-3 for the Bipolar chip/channel, \$1-2 for CMOS, \$0.25 for the data chip and \$0.50 for mounting, for a total of $<$ \$6/channel.

It will be useful to include segment-finding electronics for some of the straw-tube superlayers. This should be possible by adding a CMOS digital-logic chip in parallel to the CMOS TVC chip. Found segments would then be shipped to the trigger system. The increase in power cost should be only about 10% assuming a high level of multiplexing. An intriguing alternative possibility for the segment-finding chip is an anolog processor based on 'neural-net' concepts. This option is currently being explored for the Bottom Collider Detector by Bruce Denby.[16]

2.9.3 RICH-Counter and TRD Electronics

Both the RICH counters and the TRD's will have pad sensors whose signals will be similar in magnitude and shape to the signals from silicon strips. Thus we have the option that

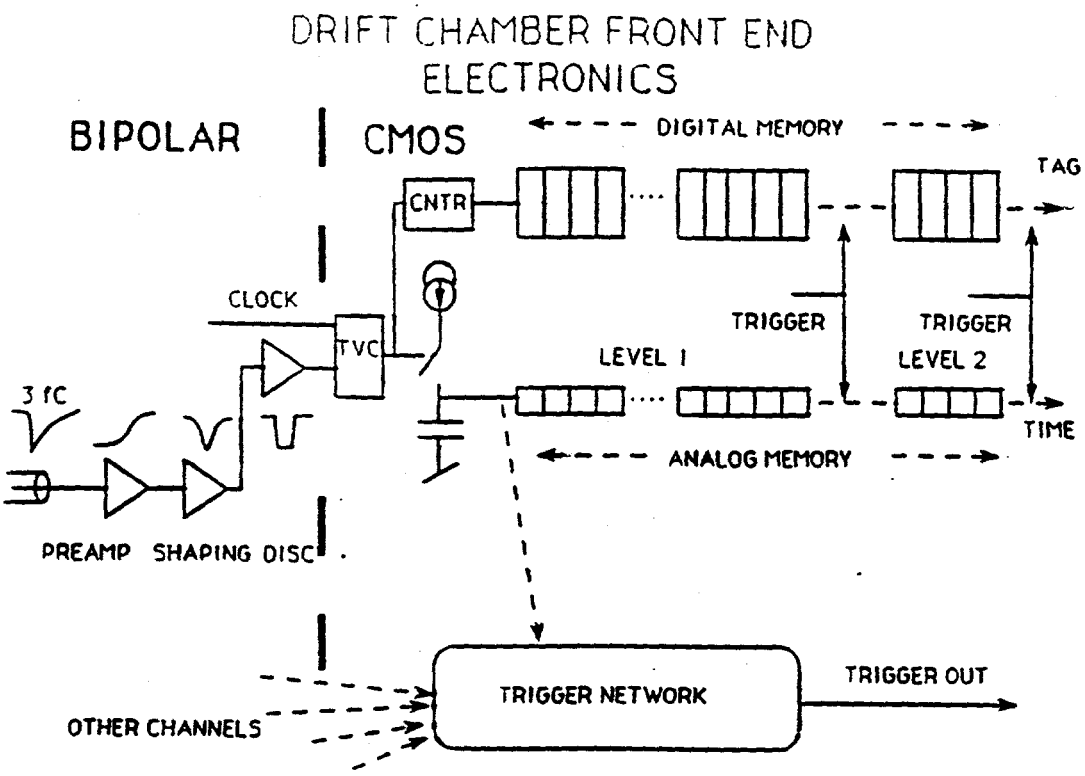

Figure 8: Block Diagram of the Bipolar/CMOS readout chip set for the straw-tubes.

the BVX chips may be used for these devices as well. However, the number of channels in the RICH counters and TRD is greater by at least an order of magnitude compared to the silicon vertex detector, so the major cost of electronics for the entire detector is likely that of the pad readout. Hence the pad readout may deserve a specifically optimized solution.

It should be possible to design pad-readout chips with rate capabilties significantly higher than those required at the Tevatron, but which could be suitable for the SSC. Very recently we have made contact with an electronics group at Rutherford Appleton Laboratory,[7] who may be interested in a collaboration towards this end.

In any case, the low density, large channel count, and large physical size of the pad readout mandates a large R&D program addressing cost-effective methods of chip mounting and signal routing, in additional to the development of the readout chips themselves.

2.9.4 Electromagnetic Calorimeter

The calorimeter could use a readout system similar to that of the straw tubes in the sense that a Bipolar front end would feed a CMOS delay-and-encode section. However, the calorimeter requires charge measurement over a large dynamic range and may or may not require an acurate time measurement. Thus the Bipolar chip will necessarily require rather more power (for the dynamic range) and the CMOS chip will require more area for storage capacitors (high- and low-charge ranges).

In addition the calorimeter will serve as one of the primary triggering detectors and

must provide fast signals out of the detector to the central triggering system. These signals will require > 40 mW per output, but the trigger outputs will be sums of local channels so that the total power burden is not greatly increased. If a suitable clustering algorithm can be defined and tested, we could ship only cluster-position and -size information to the trigger system, greatly reducing the burden on and increasing the power of the trigger.

We estimate that the total power requirement per channel would be about 30 mW and the cost per channel would rise slightly to < \$7. Mounting and cooling is least restrictive in this region and we anticipate no major problems for the calorimeter system.

2.10 Data-Acquisition System

The overall signal-processing architecture for the Bottom Collider Detector has been introduced in section 2.7 and illustrated in fig. 5. The data-acquisition system incorporates three new technologies which require an R&D program:

- Fiber optics for digital-data transmission.
- Barrel-switch event builder.
- Industry-supported numeric processors for the second-level trigger.

The design goal for the data-acquisition system is an input of 10^5 events/sec containing about 5 gigabytes/sec of data, and an output of 1000 events/sec to archival storage. A design to meet this goal has been prepared by the group of Ed Barsotti at Fermilab as part of the present proposal.[17,18]

2.10.1 Local Buffers and Transmitters

Figure 9 shows a portion of the data-acquisition system between the front-end electronics on the detector and the event-builder switch. The block labeled 'local buffer' resides on the CMOS data collection chips described in section 2.9.1. A fiber-optic link connects the local buffers to a smaller number of transmitters. The latter must organize the data from each event into units, called 'fragments,' whose format is suitable for processing by the event builder switch. A transmitter would receive data from the local buffers in parallel streams at a rate of 1 Mbyte/sec, and send out a serial data stream at a rate of 10 Mbyte/sec. About 512 transmitters will be required to accomodate the expected total data rate of 5 Gbyte/sec.

2.10.2 Barrel-Shifting Event-Builder Switch

The key section of the data path is the event-builder switch. This should organize the 512 event fragments from the transmitters into individual events at a rate of 10^5 events/sec (compared to 10/sec presently achieved in the CDF detector). This can be accomplished via the barrel-shifting technique used in the telephone industry.

A barrel-shifting event-builder switch is an N-input, N-output device with only N possible interconnects at any given moment (in contrast to a crossbar switch that has $N!$

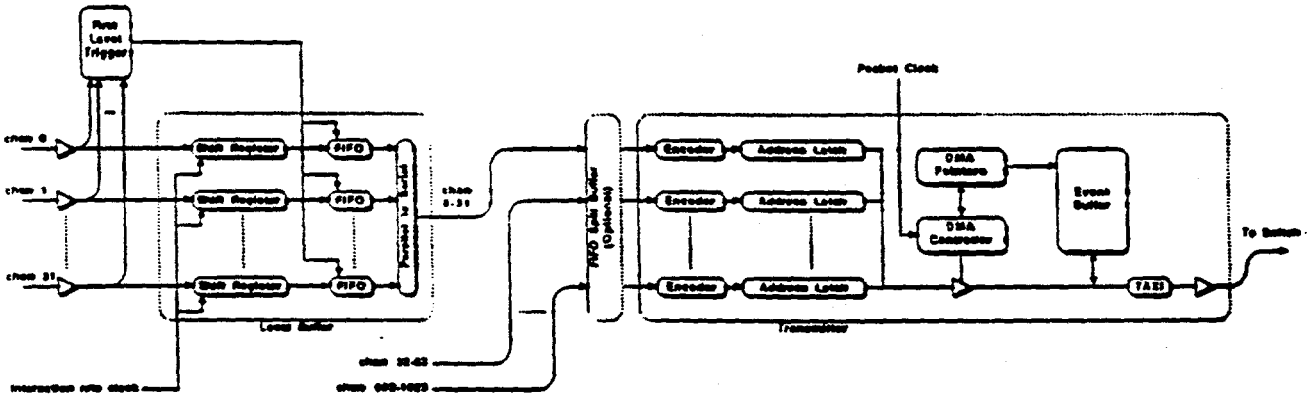

Figure 9: Block diagram of local buffers (data collection chips), 'event-fragment' transmitters, and their fiber-optic interconnections.

interconnections). The pattern of the N interconnections is altered at every cycle of a clock, so after N clock cycles all inputs have been connected to all outputs once. Since there are exactly as many interconnects as inputs, the switch can transmit the full input bandwidth.

To illustrate how the barrel switch organizes data fragments into whole events, consider a simple example in fig. 10. Fixed-length event fragments pass through the system with each input channel delayed by one clock cycle relative to the adjacent channel. With the switch-control word set to 00 (fig. 10a), the first fragment of event 1 (labeled 1A) passes directly through the switch along with three empty fragments. The switch-control word is the incremented by one (fig. 10b) and the second fragment of the first event (1B) and the first fragment of the second event (2A) are transmitted; because the pattern of the interconnects has changed, fragment 1B now follows 1A. During the next cycle of the switch (fig. 10c), fragments 1C, 2B, and 3A are transmitted. After one full rotation of the switch control, the system reaches a steady-state condition, shown in figs. 10e and 10f. Parallel event fragments are converted to assembled event streams with no low of bandwidth.

As a first step in the development of the barrel-shifter technique, a 16-channel demonstration system will be constucted, shown in fig. 11.

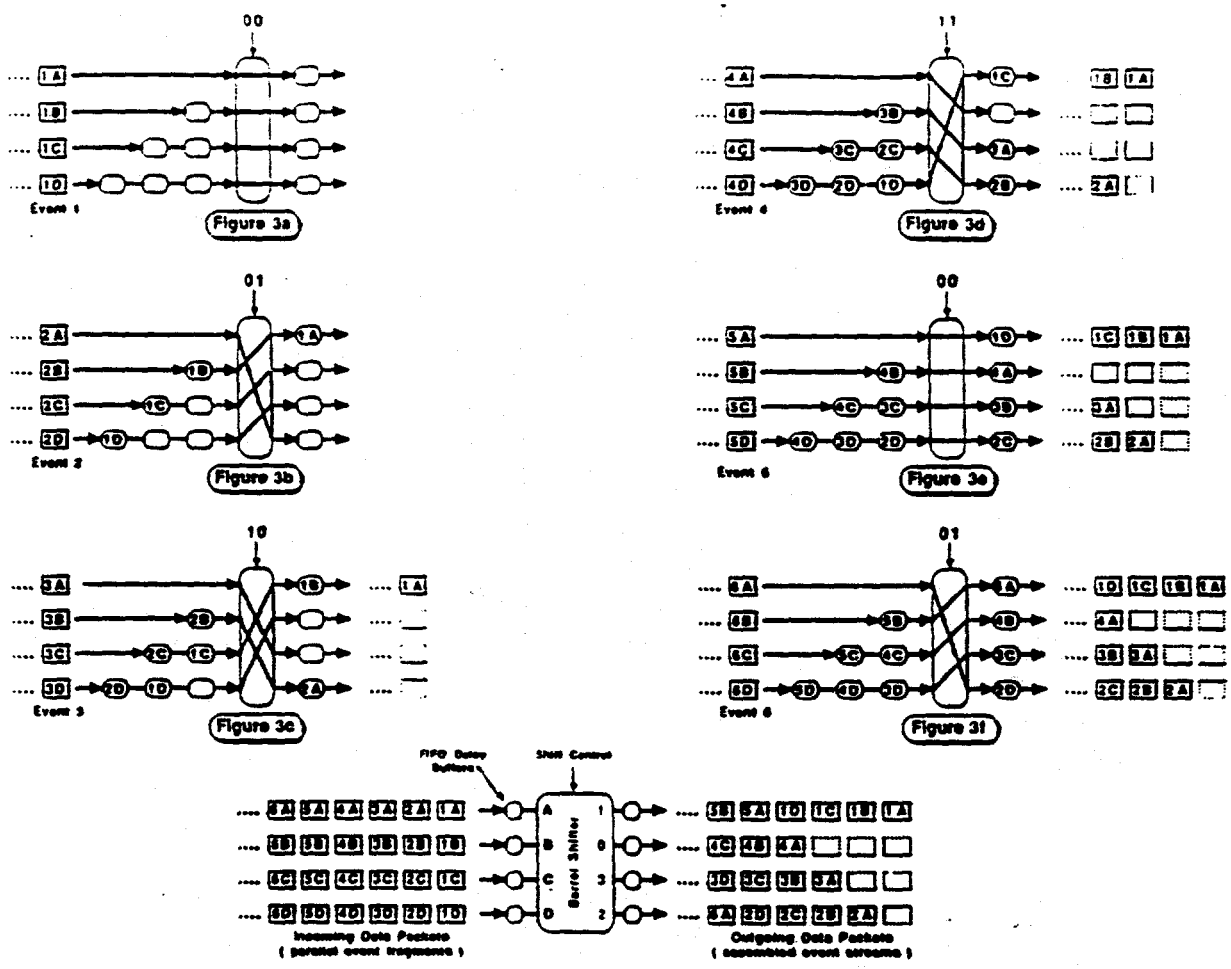

Figure 10: Principle of operation of a 4-input, 4-output barrel-shifting event-builder switch.

2.10.3 Numeric Processors and Archival Storage

The assembled events emerging from the event-builder switch are fed to a farm of numeric processors in which the level-2 trigger calculations are performed. No special-purpose numerical processors will be built; we propose to take maximum advantage of industry support of high-speed processors optimized for numerical calculations. Prototypes of 30-MIP processors will become available in Spring 1989, which we plan to incorporate them in the 16-channel demonstration system.

We anticipate the need for 5000-10000 processors in the eventual configuration of the Bottom Collider Detector. Then each processor would have about 0.1 second to make the level-2 trigger decision, with the goal of a factor of 100 reduction in the event rate.

The total archival data rate is expected to be 1000 events/sec, or 30 Mbyte/sec. This could be handled by an array of 120 Exabyte drives. Options for the use of fewer devices will emerge in the next few years. In 1989 the so-called 'digital paper' devices should become available from Creo.[19] In this, one terabyte can be stored on a 2400' reel of write-only optical tape, with a data rate of 3 Mbyte/sec. A more virtual device is the Haystack drive, being developed for the radio-astronomy community, in which a magnetic drive with 100 heads should eventually be capable of writing 100 Mbytes/sec.

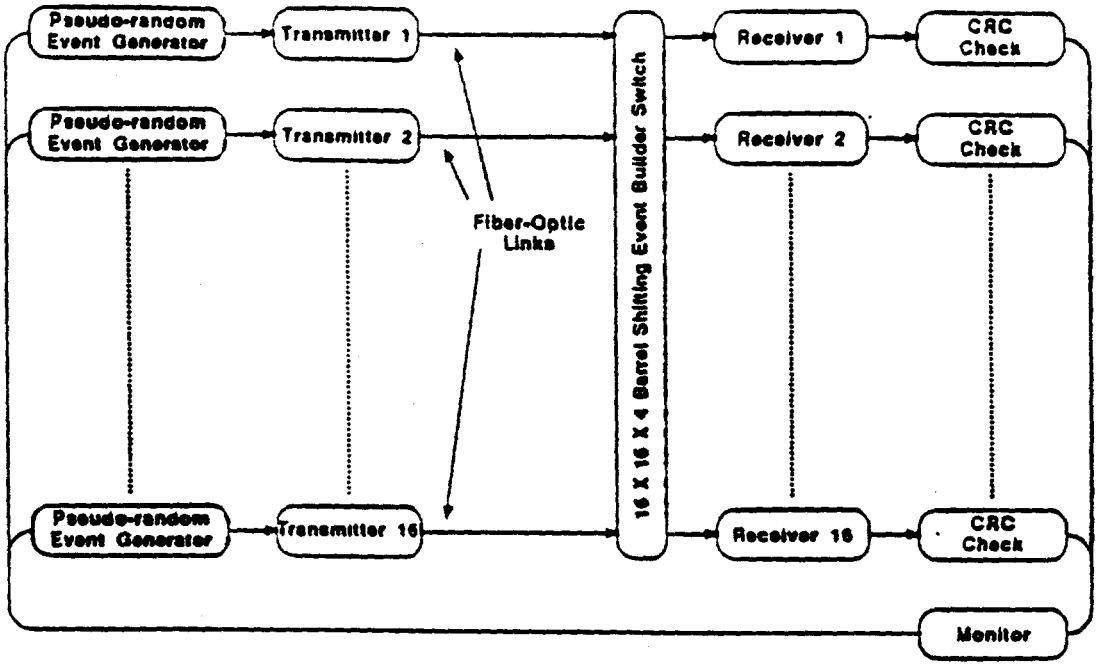

Figure 11: Proposed demonstration of a 16-channel barrel-shifting event-builder switch.

2.11 Accelerator Physics Issues

2.11.1 Luminosity

The window of opportunity for observation of CP violation in the B meson system at the Tevatron collider opens for luminosities above 10^{31} cm^{-2}sec^{-1}. We strongly support the Tevatron upgrade programs which would make this possible.

2.11.2 Beam Pipe

The resolution of a silicon vertex detector improves when the innermost detector is closer to the beam. We plan to use a beam pipe 1 inch in diameter with walls of 400-μm-thick beryllium.

2.11.3 Length of the Interaction Region

Most of the mechanical complexity of the silicon vertex detector arises because of the finite length of the interaction region which it must cover. We wish to explore the possibility of reducing the luminous region to a σ of 10 cm, down from the value of 35 cm in present running. Following discussions with Dave Finley, this might be accomplished in two ways:

- Reduce the β^* at the intersect with stronger quads. This might be possible because the 1-inch beam pipe would permit a smaller bore for the quads, and the experimental

configuration might permit the quads to be closer than 7.5 m from the intersect. Of course, a lower β^* is also useful in raising the luminosity.

- Add a higher-harmonic rf system to bunch the beams more tightly. This has the bad effect of increasing the intrabeam scattering, leading to a shorter luminosity lifetime. Calculations should be made to judge whether this option can produce a net gain in useful luminosity for a shorter interaction region.

2.11.4 Bunch Crossing Rate

The time between neighboring bunch crossing sets the time scale for all readout electronics. We now assume that this time will be 400 nsec, which is well matched to the stated goal of a luminosity of several times 10^{31} of the p-$\bar{p}$ upgrade program.

2.11.5 Beam Halo

Halo associated with the beams will contribute to the radiation exposure of the vertex detector and thereby shorten its lifetime. Present data indicate that the silicon detector can su[Brvive about 10^5 rads. It is clear that catastrophic beam loss must not occur near the detector. The beam-loss level for abort may need to be lowered compared to present operation.

2.11.6 Compensation for the Dipole Field

The presence of a spectrometer dipole in the Tevatron would alter the beam trajectory unless compensating measures are taken. The scheme that has been chosen for compensation uses two dogleg bends, one at each end of the straight section and each 20 feet from the center of the interaction region, just downstream of the low-beta quads. The two magnets are both of opposite polarity relative to the spectrometer dipole, and run in series with it (that is, the currents run up together). The spectrometer dipole and compensating magnets are energized only after coasting beam has been established. The beams at the crossing region then move laterally a few mm as the magnets are energized.

2.11.7 The Detector Hall and Support Facilities

The Detector Hall required for this facility will be comparable in size to that at D0. The detector itself will fill about one half the space available in a straight section at the Tevatron. The compensating dipoles are placed at the outer ends of the straight section. The need for electron detection, calorimetry and particle identification will require the use of special gasses and liquids. The detector may use ethane, TMAE, or TEA. Additional cryogenic support may be necessary to service the main dipole magnet. The detector will require a substantial signal-processing area. The Detector Building must also provide for a control room, office and technician space and shop support.

An initial design of a new collision hall is shown in fig. 12, as prepared by Nestander's Engineering Services Group.

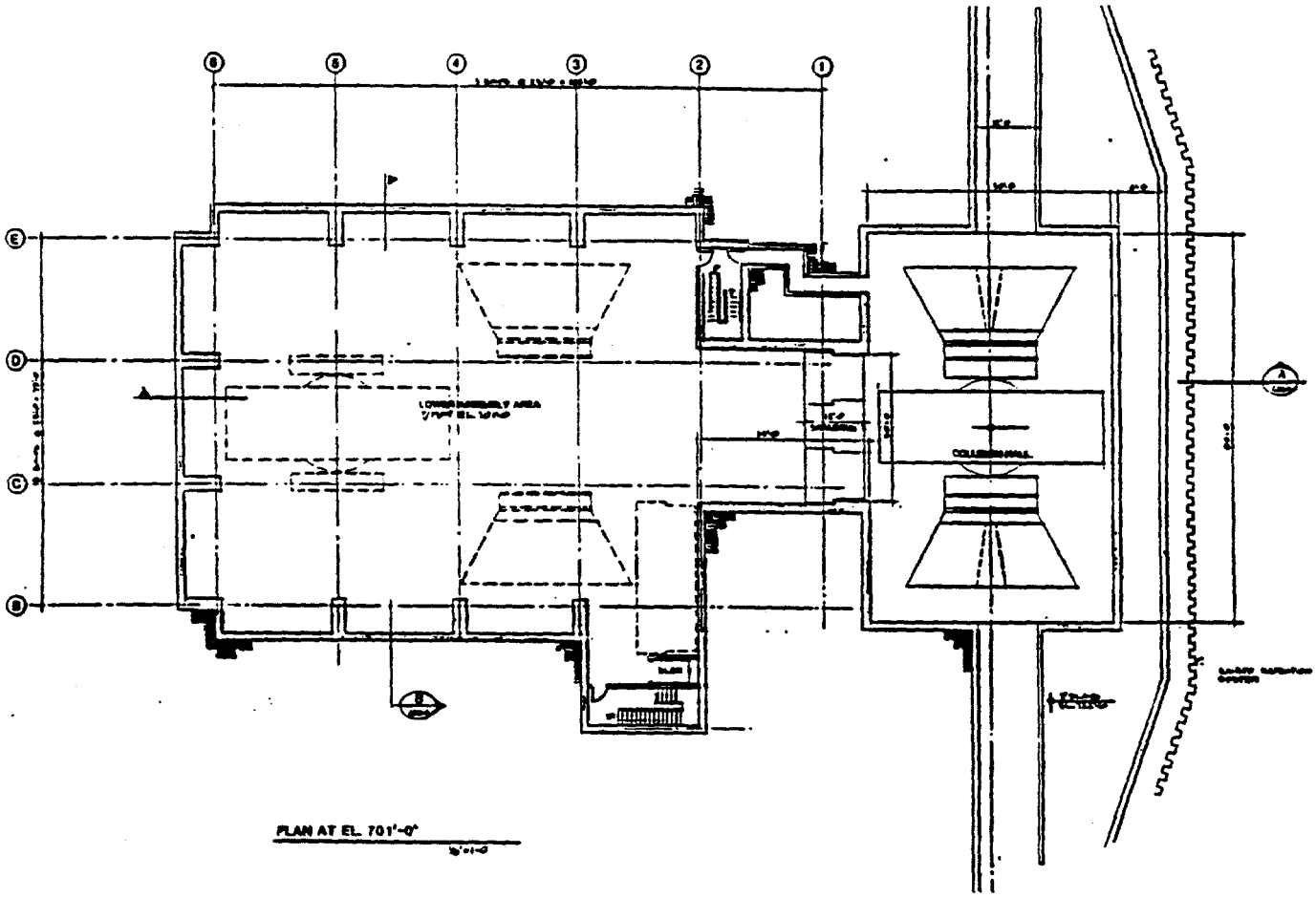

Figure 12: Layout of a new collision hall for the Bottom Collider Detector.

2.11.8 System Test at the C0 Intersect

We propose to test prototype versions of the silicon vertex detector, straw-tube chambers, and scintillating-fiber detector at the C0 intersect during the 1990-1991 collider run. This test will provide crucial evidence that secondary-decay vertices can be found at a hadron collider, and will also serve to focus the R&D efforts towards a timely measurement.

We can run at C0 in a parasitic mode in the sense that we would not require retuning of the beam for higher luminosity. But when we run, the electrostatic separators must be turned off so beams actually collide at C0.

In a run of 10^6 seconds at a luminosity of 10^{28} cm^{-2}sec^{-1}, about 100 $K^0_S \to \pi^+\pi^-$ decays would be observed (in the prototype apparatus) per each 100 μm of decay path. A study would then be made as to how close to the primary vertex the K-decay vertex can be reconstructed. This, of course, presumes the primary vertex can be located by the detector as well. A sample of about 50 decays $D^0 \to K^+\pi^-$ would also be observed in the

test run.

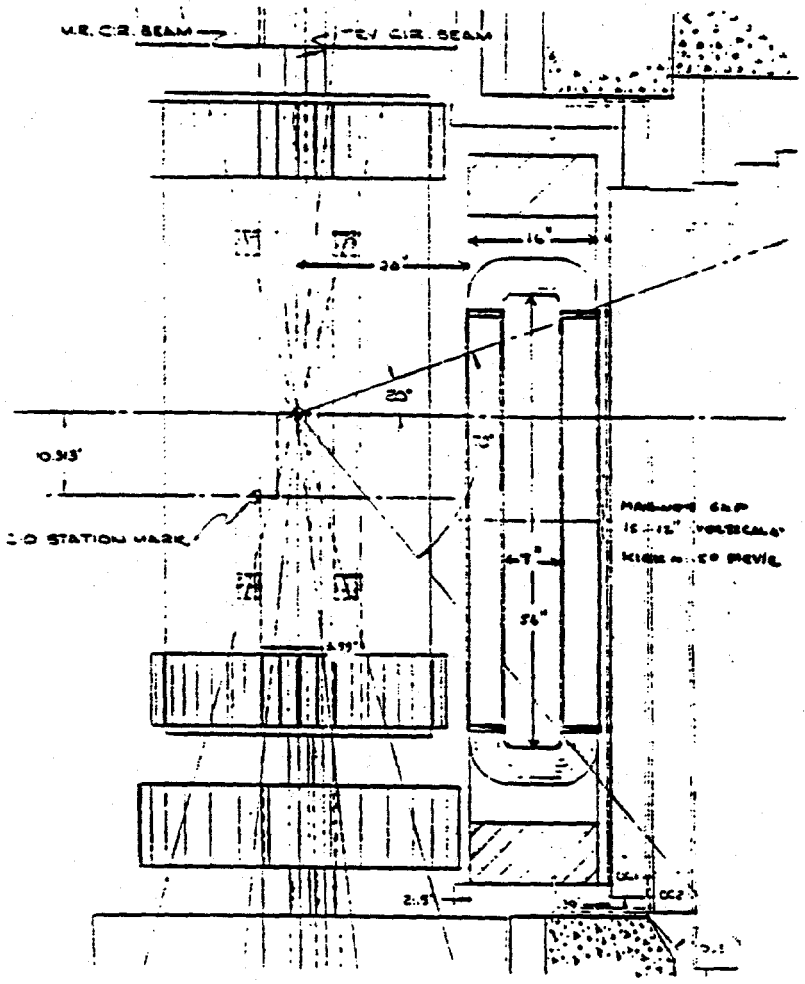

Figure 13: The existing layout of E-735 at the C0 intersect.

The existing configuration of E-735 in C0 is shown in fig. 13. We would need to replace the present central detector with our silicon vertex detector and straw tubes. A factor of about four in acceptance could be gained if the window-frame magnet were moved closer to the beams until it abuts the abort line of the 150-GeV ring. As mentioned in section 2.11.2, it is advantageous to have a small-diameter beam pipe for better resolution in the vertex reconstruction. The β^* is large in C0, so the pipe cannot be 1 inch in diameter. However, we would like the smallest pipe size compatible with the Tevatron beams.

3 Research & Development Program

The proposed research and development program for the Bottom Collider Detector is divided into three phases that overlap three fiscal years, 1989 through 1991.

- Phase I takes place in fiscal 1989 and consists of what might be called bench tests for each of the systems under consideration.
- Phase II takes place during fiscal 1990 and utilizes the fixed-target test beams available at the laboratory.
- Phase III takes place in fiscal 1991 and uses the C0 intersection region in a parasitic mode to perform system tests in the collider environment during the next collider run.

The three major systems addressed in this proposal are

1. The silicon vertex detector.
2. The tracking system.
3. The data-acquisition system.

The R&D issues for the silicon detector and straw-tube tracker are logically subdivided into mechanical and electrical parts, *i.e.*, construction and front-end electronics. The DAQ system includes everything after the front-end electronics including the fast trigger.

We outline below the R&D tasks and costs for each of the three systems, also breaking these down into the three phases.

3.1 Silicon Vertex Detector

3.1.1 Silicon: Mechanical & Electrical Tasks - Phase I

- Construct models of the silicon detector out of plastic and G-10 to explore assembly techniques.
- Continue modelling of the silicon cells and the supporting gutter structure using 'junk' (unprocessed) silicon and aluminum for the gutter. Survey various adhesives for resistance to creep, and for coefficients of thermal expansion matched to silicon. Add resistors to simulate the overall 2 kWatt heat load.
- Study the cable-plant issues with the silicon models. Develop techniques to cut slots in the silicon for cables (and cooling, possibly).
- Study the cooling requirements.
  - Can the device be cooled with a modest nitrogen gas flow?
  - Is liquid cooling an option?

- Is better electronic noise performance obtained at temperatures below ambient?

- Study alignment issues.
  - How accurately can the disks and barrels be assembled?
  - What is the long term stability?
  - How stable is the detector against thermal gradients?
  - Use the CORDAX (optical) measurement machine and proximity sensors for bench tests.

- Study the various techniques for bonding VLSI chips to silicon wafers now used by industry: bump bonding, tab bonding, and wire bonding.
  - Does the more robust procedure of tab bonding cause cracking of the silicon during heating?
  - Does the adhesive chemically damage the high-resistivity silicon near the bond?

- Test the performance of the double-sided silicon strip wafers. Obtain the a.c.-coupled detectors from Messerschmitt-Bölkow-Blohm GmbH, Munich and Senter for Industriforskning, Olso and test them.

- Design, build and test a VLSI readout chip set that permits a low cost, low power, and low noise readout system for the roughly 500,000 silicon strips.
  - Begin the front-end (BVX) chip design immediately.
    * Define the specifications and overall architecture for the chips.
    * Design the first chip in three parallel efforts: the amplifier/discriminator, the storage/delay array, and the digitization.
    * The hardest part of the design is the amplifier and this will determine the schedule.
    * Existing VLSI amplifier designs are excellent starting points.
    * Goal is to have a first version sometime during the summer.
  - Start the collection-chip design in February.
    * Specify the data-collection architecture for the whole detector, maintaining compatibility with the input formats for the data-acquisition system.
    * The actual chip design will be relatively straightforward digital CMOS.
    * Have first run back from MOSIS by summer 1989.

3.1.2 Silicon: Costs - Phase I

The mechanical costs and electrical costs are listed separately. An estimate of the salary costs are given for each category.

- Electronics: equipment/operating

- Chip-processing costs using MOSIS, 4 runs @ $15k $60k
- Test equipment $30k
- Travel to conferences and workshops on VLSI $10k

- Electronics: salaries
  - 1.5 FTE electrical engineer @ $45k $68k
  - 0.5 FTE electrical technician @ $25k $13k

- Mechanical: equipment/operating
  - Build gutter and alignment jigs using inside and outside shops $10k
  - Use of outside companies to test bonding techniques, glueing, welding and cutting of silicon. Purchase of junk silicon for mechanical studies and of silicon strip detectors for bonding studies $15k
  - Purchase power supplies and miscellaneous parts for thermal studies on junk-silicon model $5k
  - Lab-D clean-room space for this work $5k

- Mechanical: salaries
  - 0.5 FTE mechanical engineer @ $45k $23k

3.1.3 Silicon: Mechanical & Electrical Tasks - Phase II

This work will require the use of a test beam. Discussions with the laboratory are taking place on where (M-Test, M-Bottom or Lab-D) we could be located. We need a place where we can leave equipment set up over the period of the next fixed-target run. We require a low-intensity beam for single-track studies.

- Phase II of the silicon test involves the construction of two cells using junk silicon for alignment studies using the beam. This will require a support structure or jig that rotates and moves in such a way that alignment studies can be performed economically.

- We may need to build a partial beryllium support for the cells in order to study multiple-scattering effects.

- Some of the mechanical questions are:
  - How well is the silicon internally aligned?
  - How well is the silicon aligned with respect to the straws?
  - How large are the dead regions?
  - How robust are the bonds?

- We need to instrument (bond chips to and readout) about 10 double-sided wafers with 50-μm pitch or roughly 5,000 channels. This will allow several studies of detector performance, as well as alignment. We hope to use an early version of the BVX chip for this work.
- Measure the resolution of the device as a function of momentum with and without the use of pulse-height information. Compare this to the Monte Carlo predictions.
- Perform signal-to-noise, efficiency and pulse-height-correlation studies using the double-sided detectors.
- Correlate tracks in the silicon and the straws.
- Study the issues associated with radiation damage. It is believed that a radiation-hard process can be specified once the desired electrical performance has been achieved in a possibly soft process.

3.1.4 Silicon: Costs - Phase II

- Electronics: equipment/operating
  - Purchase 10 doubled-sided silicon detectors @ \$1k each **\$10k**
- Electronics: salaries
  - 1.5 FTE electrical engineer @ \$45k **\$68k**
  - 1 FTE electrical technician **\$25k**
- Mechanical: equipment/operating
  - Glueing, cutting and bonding the chips to the wafers **\$15k**
  - Beryllium mechanical work **\$8k**
  - Miscellaneous supplies **\$20k**
- Mechanical: salaries
  - Mechanical engineer: 4 months @ \$45k **\$15k**
  - Mechanical technician: 1 year @ \$25k **\$25k**

3.1.5 Silicon: Mechanical & Electrical Tasks - Phase III

- Design and assemble a portion of a full 4π vertex detector, using about 20 wafers or roughly 5000 channels.
- Instrument this detector for operation at the C0 intersect.
- Readout every beam crossing (as a test of the data-acquisition system).

- Study the multi-track environment, including effects due to dipped tracks and closely spaced tracks.
- Determine impact-parameter resolution in 2 and 3 dimensions for both the disk and barrel configuration together and separately.
- Determine vertex resolution of the system in the multi-particle environment.
- Reconstruct a sample of $K_S \rightarrow \pi^+\pi^-$.

3.1.6 Silicon: Costs - Phase III

- Electronics: equipment/operating
  - 48 silicon detectors (2 cells) **$50k**
  - BVX chips, data collection chips for above..... **$50k**
- Electronics: salaries
  - 1 FTE electrical engineer..... **$45k**
  - 2 FTE technician @ $25k **$50k**
- Mechanical: equipment/operating
  - Assembly of 2-cell prototype detector..... **$50k**
  - Mounting of prototype in C0 intersect **$25k**
  - Cooling, cabling for prototype detector **$25k**
- Mechanical: salaries
  - Mechanical engineer: 4 months @ $45k **$15k**
  - Mechanical technician: 1 year @ $25k **$25k**

3.2 Tracking System

3.2.1 Tracking: Mechanical & Electrical Tasks - Phase I

The goal of this phase is build an instrumented superlayer of straw-tube chambers and perform a cosmic-ray test. In addition, we will start a program of R&D for a plastic scintillating fiber detector whose role would be to provide a fast measue of the z coordinate of the primary interaction vertex.

- Compare samples of straws from two vendors.
- Study different sizes of tubes. First try the 3-mm-diameter tube.
- Study both a short- and long-straw design, the latter with spacers inside the straw.

- Study the mechanical properties such as roundness, sag, and the adherence of the mylar to the aluminum as a function of temperature and pressure.
- Design and test the feedthroughs electrically and as gas seals.
- Make drift-velocity measurments as a function of high voltage, pressure, gas composition and magnetic field.
- Study the mechanical mounting and glueing techniques for assembling a superlayer.
- Measure the resolution as a function of all variables, including the orientation in the magnetic field.
- Study radiation damage.
- Study the feasibility of small pads on the straws as a means of obtaining fast z-coordinate information.
- Construct a sample of test straws.
- Design a readout system.
- Perform studies to see how well one can align and calibrate the system, and maintain optimal position resolution over time.
- Develop the readout chip set (3 chips):
    1. Bipolar amplifier/discrimator. Begin with the Penn-Louven design underway for SSC Generic R&D.
    2. CMOS time-to-voltage converter, analog storage/delay, and ADC.
    3. Data collection chip. Might be the same as for the silicon vertex detector.
    4. Study options for a fourth chip–for segment finding. This might be an analog processor implementing a neural-net algorithm, or a more conventional digital design.

Some of the group are interested in the development of plastic scintillating fibers. We are considering the application for both small-angle tracking and calorimetry. We discuss the need below as it pertains to the prompt trigger envisioned for the DAQ system. Because of the dipole field, the fast-tracking trigger needs the z coordinate within a few hundred nanoseconds after the collision.

- Develop a plastic scintillating fiber optic system that separates a beam-beam collision from a beam-gas collision. The system would subtend the rapidity range 4-6 units and is located several meters downstream and upstream of the collision point.
- Also use this system to determine the z-coordinate of the beam-beam interaction to 1-cm accuracy by tracing the low-angle tracks back to a common vertex.
- Design a fast readout system that can provide this information to the trigger.

3.2.2 Tracking: Costs - Phase I

- Electronics: equipment/operating
  - Chip development: 3 MOSIS runs @ $15k **$45k**
  - Studies of pad readout of straw tubes **$10k**
- Electronics: salaries
  - 1.5 FTE electrical engineer @ $45k **$68k**
- Mechanical: equipment/operating
  - Purchase straws, travel to vendors **$10k**
  - HV supply, wire, and gas system **$15k**
  - Prototype feedthroughs **$5k**
  - Test fixtures, cables, jigs and supplies **$40k**
- Mechanical: salaries
  - 1 FTE mechanical engineer **$45k**
  - 1 FTE technician for the mechanical straw work **$25k**
  - 1 FTE technician for the gas studies **$25k**
  - 1 FTE technician for alignment studies **$25k**
- Fibers: equipment/operating
  - Scintillating fibers, and readout tubes **$50k**
- Fibers: salaries
  - 1 FTE technician **$25k**

3.2.3 Tracking: Mechanical & Electrical Tasks - Phase II

Phase II of the straw-tube development requires constructing a two-superlayer system to be tested in a test beam (M-Test, M-Bottom or Lab-D Test Beam). The scintillating-fiber detector will be tested in the beam also.

- Straw-tube studies
  - Perform pattern recognition and track fitting for tracks traversing several superlayers.
  - Measure the single-hit, single-track and two-track resolution.
  - Study the alignment issues associated with the assembly procedure of an octant of a 4π tracking system.

- Correlate tracks in the straw tubes with the tracks in the silicon.
- Study multiple-scattering effects.
- Test the readout system.

- Fiber studies
  - Build and test prototype fiber-array system.

3.2.4 Tracking: Costs - Phase II

- Electronics: equipment/operating
  - 6 MOSIS runs @ $15k **$90k**
  - Readout chips at $7 per chip and 4 channels/chip **$13k**
  - Test equipment such as digital scopes, and logic analysers **$50k**
- Electronics: salaries
  - 2 FTE electrical engineer @ $45k **$90k**
- Mechanical: equipment/operating
  - Build 7000 straws with feedthroughs @ $5 each **$35k**
  - Cables, mounting boards, epoxies, and supplies **$20k**
  - Bonding of readout chips to straws **$5k**
- Mechanical: salaries
  - 1 FTE mechanical engineer @ $45k **$45k**
  - 2 FTE technicians @ $25k **$50k**
- Fibers: equipment/operating
  - Scintillating fibers **$20k**
  - Test equipment **$30k**
- Fibers: salaries
  - 1 FTE technician **$25k**

3.2.5 Tracking: Production R&D - Phase III

A four superlayer straw-tube system would be used in the system test in C0 during Phase III, along with a prototype scintillating fiber detector.

A separate but parallel effort is needed to pursue the techniques for producing the very large number of straws that any major system will contain.

- Design overall layout for the C0 test.
- Reconstruct K_S's in the straw-tube tracker.
- Devise tools and techniques for stringing the sense wires.
- Devise superlayer-alignment techniques.
- Design pressure-testing and voltage-testing devices and procedures.
- Design the assembly-line techniques in preparation for mass-production personnel.
- Design the overall electronics mounting scheme for the full system including the cooling.

3.2.6 Tracking: Costs - Phase III

- Electronics: equipment/operating
  - Test equipment such as digital scopes, and logic analysers **$50k**
- Electronics: salaries
  - 1 FTE electrical engineer @ $45k **$45k**
- Mechanical: equipment/operating
  - Prototype fixtures for large-scale production **$100k**
  - Mounting of prototype straw-tube system in C0 ..... **$20k**
- Mechanical: salaries
  - 1 FTE mechanical engineer @ $45k **$45k**
  - 3 FTE technicians @ $25k **$75k**
- Fibers: equipment/operating
  - Prototype detector for the C0 test **$50k**
- Fibers: salaries
  - 1 FTE technician **$25k**

3.3 Data-Acquisition System

3.3.1 Data Acquisition: Tasks - Phase I

- Specify in detail the overall architecture of the DAQ system including the interface between front-end electronics and the DAQ system.
- Build the following nine modules to test this architecture:
  - 2 transmitter boards
  - 2 receiver boards
  - 2 barrel-switch boards
  - 1 optical link
  - 2 boards with 4 numeric processors each

3.3.2 Data Acquisition: Costs - Phase I

- Development: equipment/operating
  - 9 prototype boards at roughly \$6k each **\$54k**
  - Terminals and workstations **\$50k**
- Development: salaries
  - 1.5 FTE electrical engineers @ \$45k **\$68k**
  - 1 FTE programmer **\$45k**

3.3.3 Data Acquisition: Tasks - Phase II

- Bring up system in test-beam area and connect to online system.
- Readout the silicon vertex detector through to the processors.
- Readout the straw-tube system.
- Develop the necessary performance and debugging tools for the system.

3.3.4 Data Acquisition: Costs - Phase II

- Development: equipment/operating
  - Simple clock system for readout in test beam \$10k
  - Alarms, crates, racks, power supplies \$100k
  - Host computer system for numeric processors \$30k
  - Terminals and workstations \$50k

- Development: salaries
  - 1 FTE electrical engineer **$45k**
  - 1 FTE electrical technician **$25k**
  - 1 FTE programmer **$45k**
- Prototypes: equipment/operating
  - Board production **$300k**
- Prototypes: salaries
  - 3 FTE electrical engineer @ $45k **$135k**
  - 3 FTE electrical technician @ $25k **$75k**
  - 1 FTE programmer **$45k**

3.3.5 Data Acquisition: Tasks - Phase III

- Build up processor farm. Add racks and power supplies.
- Install hardware-protection system.
- Install network between racks and crates of processors.
- Develop downloading procedures for a large farm.

3.3.6 Data Acquisition: Costs - Phase III

- Development: equipment/operating
  - Terminals and workstations **$100k**
- Prototypes: equipment/operating
  - 25 numeric processors **$400k**
  - Racks, alarms **$50k**
  - Exabyte tape drives (18) **$66k**
- Prototypes: salaries
  - 3 FTE electrical engineers @ $45k $135k
  - 3 FTE technicians @ $25k $75k
  - 1 FTE programmer $45k

4 Cost Summary

	FY89 Phase I (Bench Tests)		FY90 Phase II (Beam Tests)		FY91 Phase III (C0 System Test)	
	Equipment/ Operating	Salaries	Equipment/ Operating	Salaries	Equipment/ Operating	Salaries
	Silicon Vertex Detector (FNAL)					
Electronics	$100k	$81k	$10k	$93k	$100k	$95k
Mechanical	35k	22k	43k	40k	100k	40k
	135k	103k	53k	133k	200k	135k
	Tracking System (Universities)					
Electronics	55k	68k	153k	90k	50k	45k
Mechanical	70k	120k	60k	95k	120k	120k
Fibers	50k	25k	50k	25k	50k	25k
	175k	213k	263k	210k	220k	190k
	Data-Acquisition System (FNAL)					
Development	104k	113k	190k	115k	100k	
Prototypes			300k	255k	516k	255k
	104k	113k	490k	370k	616k	255k
Total	**414k**	**429k**	**806k**	**713k**	**1036k**	**580k**

Table 2: Summary of costs of the proposed 3-year R&D program. Benefits, overhead, contingency, and escalation are not included.

5 References

[1] H. Castro *et al.*, *Letter of Intent for the BCD, A Bottom Collider Detector for the Fermilab Tevatron*, October 7, 1988.

[2] P.Nason, S. Dawson and R.K. Ellis, *The total cross section for the production of heavy quarks in hadronic collisions*, Fermilab 87-222-T; and private communication, Keith Ellis.

[3] E. Berger, *Heavy Flavor Production*, ANL-HEP-PR 88-26.

[4] N.S. Lockyer *et al.*, *Measurement of the Lifetime of Bottom Hadrons*, Phys. Rev. Lett. **51**, 1316 (1983); R. Ong, Ph.D thesis, Stanford Univ., SLAC-Report-320,1987; W.W. Ash *et al.*, Phys. Rev. Lett. **58**, 640 (1987); J. M. Brom *et al.*, Phys. Lett. **B195**, 301 (1987); D. Klem *et al.*, Phys. Rev. **D37**, 41 (1988).

[5] See, for example, I. I. Bigi and A. I. Sanda, *CP Violation in Heavy Flavor Decays*, Nucl. Phys. **B281**, 41 (1987).

[6] R. DeSalvo, *A Proposal for an SSC Central Tracking Detector*, Cornell University preprint CLNS87/52 (1987).

[7] P. Sharp, private communication.

[8] T. Ypsilantis, private communication.

[9] T. Ludlam, *Summary of the Particle Identification Group*, Proceedings of the Workshop on High Sensitivity Beauty Physics at Fermilab, ed. by A.J. Slaughter, N.S. Lockyer and M. Schmidt (Nov. 1987) p. 447.

[10] T. Åkesson *et al.*, *Estimate of a TRD's Performance as Part of an Electron Identification Scheme*, Proceedings of the LHC High Luminosity Study, ed. by J. Mulvey (1987).

[11] G. Lutz *et al.*, *Low Noise Monolithic CMOS Front End Electronics*, Nucl. Instr. Meth. **A263**, 163 (1988).

[12] W. Buttler *et al.*, *Noise Performance and Radiation Hardness of the CAMEX64 Analog Multiplexing Readout Chip*, Contribution to the XXIV International Conference on High Energy Physics (Munich, August, 1988).

[13] S. Kleinfelder *et al.*, *A Flexible 128 Channel Silicon Strip Detector Instrumentation Integrated Circuit with Sparse Data Readout*, IEEE 1987 Nucl. Sci. Symposium, (San Francisco).

[14] P.P. Allport, P. Seller and M. Tyndal, *A Low Power CMOS VLSI Multiplexed Amplifier for Silicon Strip Detectors*. London Conference on Position Sensitive Detectors (Sept., 1987).

[15] L. Callewaert *et al.*, *Front End and Signal Processing Electronics for Detectors at High Luminosity Colliders*, U. Penn preprint UPR-162E, submitted to IEEE Trans. Nuc. Sci, 1988 Nuclear Science Symposium.

[16] B. Denby, *Neural Networks and Cellular Automata in Experimental High Energy Physics*, Orsay preprint (Nov. 1987).

[17] M. Bowden *et al.*, *A High-Throughput Data Acquisitiion Architecture Based on Serial Interconnects*, Fermilab preprint (Nov. 1988).

[18] E. Barsotti *et al.*, *Proposal for Generic Detector R&D for the SSC*, (Nov. 1988).

[19] K. Spencer, *The 60-second terabyte*, Can. Res. (June, 1988); M.S. Fisher, Digital Paper Promises Cost, Storage Gains for Optical Media, Datamation (May 15, 1988).

Professor P. Yager

Fermilab

Fermi National Accelerator Laboratory
P.O. Box 500 • Batavia, Illinois • 60510
312-840-3211 FTS 370-3211

Directors Office

January 30, 1989

Dr. Nigel Lockyer
Department of Physics
University of Pennsylvania
Philadelphia, Pennsylvania 19104

Dear Nigel,

At its January meeting, the PAC discussed your presentation of P-784 and phased proposal for R&D leading toward possible construction of a Bottom Collider Detector (BCD).

The Committee recommended approval of Phase I (bench tests) and Phase II (beam tests). They recommended that Phase III (C0 run at the Tevatron collider) be deferred until results of simulation studies (i.e. to show that tracking and vertexing will lead to B physics) and bench tests are available.

The Committee had some concerns regarding the data acquisition part of P-784. This is a major development exercise requiring considerable support from the Laboratory. In particular, the processor hardware and software efforts need evaluation by the Laboratory before proceeding. Development of components of the data acquisition system up through the event builder seems reasonable. They recommended that other activities toward the development of a complete system should not start yet. They looked forward to negotiations between the BCD collaboration and the Laboratory over the issue of support for these activities.

The PAC also asked me to emphasize that there are long-term uncertainties (still!) in the Fermilab program. In doing this I remind you that approval for the R&D proposal is not necessarily an assurance that approval of a complete proposal is forthcoming.

There was considerable discussion of the silicon vertex detector. The PAC would like to hear a discussion on the relative merits of silicon strips versus pixel devices. They would like to know whether simulations show that the proposed silicon strips work effectively for B physics in the Tevatron environment.

It seems clear that presentations will be required at the next (April 28-29) PAC meeting. We hope to be able to act on these recommendations to implement Phase I and II and to have a possible Phase III in mind for the next fiscal year. However, the FY 89 budget is in deep trouble so that it is highly unlikely to do more than the $50,000 you have been granted.

Sincerely,

Leon

Leon M. Lederman

Task F

This task was created in 1989 with an allotment of approximately $5000.00 out of a request of $89,203.00 to participate in the TPC/Two Gamma experiment at high luminosity PEP. The experiment had a brief test in the fall of 1988. During 1989, the initial effort will be to establish efficient SLAC Linac switching between PEP filling and SLC running. Once rapid switching has been established, high luminosity PEP running should begin.

The TPC-Two Gamma experiment has been modified to run in a new one-fold minibeta configuration.[1] The rebuilding of the LINAC control system for SLC plus improved instrumentation in the PEP injection line has greatly increased the efficiency of PEP filling and operation. The result has been an increase in peak luminosity to 0.7×10^{32} $cm^{-2}sec^{-1}$.

Modifications to the detector which have been completed for high luminosity running include the installation of a "straw" vertex chamber for B studies and the removal of much of the equipment from the former Two Gamma experiment to accommodate the minibeta quads. The first drift chamber and the NaI tagger array remain from that experiment with the NaI array in a new position much closer to the interaction point.

The modified apparatus was tested in a run during the Fall 1988 cycle during which PEP delivered 42.5 pb^{-1}. The most serious problem, overheating of the vertex chamber at high beam currents, has required installation of a special cooling system. This is expected to correct the problem, allowing PEP to run at even higher peak luminosity.

Sufficient events were accumulated for a detailed understanding of vertex chamber operation and to develop combined TPC–vertex chamber tracking. The experimental resolution for impact parameter measurement was checked with Bhabhas and found to be under 100 μ.

We are working with David Nygren's group on the development of finely segmented two-dimensional arrays of solid state detectors (so-called *pixel devices*). This effort could find application in an improved vertex detector for a future PEP upgrade.

Our analysis of the existing data from the TPC/Two Gamma experiment has concentrated recently on the measurement of the single tagged $\gamma\gamma$ total cross section, photon structure functions and two photon jets, as well as certain excusive processes such as $\gamma\gamma \rightarrow p\bar{p}$. We will continue these efforts with the new data.

In the past, this work has largely utilized the Monte Carlo system of the former Two Gamma experiment. In the two photon jet analysis, a start has been made to work in the context of the standard TPC Monte Carlo. There is a further goal of integrating the entire Monte Carlo effort into a GEANT-based structure. We will take responsibility for integrating the rest of our Two Gamma Monte Carlo generators into the TPC system.

We will also take responsibility for the Monte Carlo simulation of the TPC muon system. This will include monitoring its performance so that efficiencies are understood for the B and τ analyses, in which we will participate.

In addition, we will continue Monte Carlo studies of vertex detector upgrades involving pixel devices.

These efforts will be facilitated by our proximity to LBL and SLAC, by our computer system at UCD with its high speed link to LBL (recently upgraded to 56 Kbaud) and by our connection to the SLAC computers.

The concluding work by UCD on the PEP-9 experiment was being carried out by D. Pellett, J. Smith and C. Zeitlin. Zeitlin, however, finished his dissertation in the summer of 1988 and immediately accepted a position at the University of Oregon.

THEORETICAL TASKS

Task B - Theory, Particle Physics
Task E - Theory, Particle Physics

PROGRESS REPORT FOR TASK B: JUNE 1990

Publications, Preprints and Activities: Task B

The publications and preprints produced by the members of the Task B theory effort are listed. In addition, the seminars given, organizational and adminstrative contributions, conferences and workshops participated in, and other major collaborative activities are outlined.

J.F. Gunion: Publications/Preprints June 1, 1989—June 1, 1990

1. J.F. Gunion, H.E. Haber, G. Kane and S. Dawson, "The Higgs Hunters Guide", Addison and Wesley (1990), Frontiers in Physics Series.
2. S. Dawson, J.F. Gunion, and H.E. Haber, "Are Light Higgs Bosons Allowed?" *Phys. Rev.* **D41** (1990) 2844.
3. J.F. Gunion, "Probing Higgs Bosons/Electroweak Symmetry Breaking in Purely Leptonic Channels at Hadron Colliders", UCD-89-24, to appear in Proceedings of "Higgs Particles: Physics Issues and Experimental Searches in High Energy Collisions", 8th Erice Workshop, Erice, Italy, July 15-26, 1989.
4. J.F. Gunion, "The SSC: Status and Physics Update", UCD-89-27, to appear in Proceedings of the 1989 European Physical Society Meeting, Madrid, Spain, September 1989.
5. J.F. Gunion and B. Grzadkowski, "Limits on the Top Quark and on the Charged Higgs Boson of a Two-Doublet Model from $\overline{K^0} - K^0$ mixing, $B_d - \overline{B_d}$ mixing, and $b \to u$ Decays", UCD-89-30, to appear in *Phys. Lett.* **B**.
6. S. Dawson, J.F. Gunion, H.E. Haber, A. Seiden, and G. Kane, "The Search for Higgs Bosons of Any Mass", *Comm. Nucl. Part. Phys.* **14** (1990) 259.
7. J.F. Gunion, R. Vega, and J. Wudka, "Higgs Triplets in the Standard Model", UCD-89-13, to appear in *Phys. Rev.* **D**.
8. N. Deshpande, J.F. Gunion, B. Kayser, and F. Olness, "Left-Right Symmetric Electroweak Models with Higgs Triplets", NSF-ITP-90-69, submitted to *Phys. Rev.* **D**.

J.F. Gunion: Invited Talks and Seminars June 1, 1989—June 1, 1990

1. "Triggering on Crucial Physics Signatures at the SSC", SSC Trigger Workshop on Trigger Algorithms, LBL, June, 1989.
2. Two Talks: "Higgs Boson Cross Sections and Event Rates — A Comparative Study of LHC/SSC/Eloisatro Colliders", **and** "Exotic Higgs Sectors: Theory and Experiment", INFN Eloisatron Project, 8th Workshop: Higgs Particles - Physics Issues, Ettore Majorana Centre for Scientific Culture, Erice, Italy, July, 1989.
3. Two Talks: "SSC Physics and Status" **and** "Higgs Bosons: Standard Model and Beyond", 1989 European Physical Society Meeting, Madrid, Spain, September, 1989.
4. "Non-Minimal Higgs Bosons", Univ. Autonoma, Barcelon, Spain, September, 1989.
5. "Higgs Hunting", DESY Theory Workshop, October, 1989.
6. "Probing New Physics at the SSC", Colloquium at University of Southern California, October, 1989.
7. "The Top Quark and the Charged Higgs Boson: Limits from Weak Decays and Impact on Future Searches", NSF-ITP Meeting on "Thinking about the Top Quark", U.C. Santa Barbara, February, 1990.

8. "New Results for the old Left-Right Symmetric Model", Institute for Theoretical Physics, U.C. Santa Barbara, April, 1990.

J.F. Gunion: Additional Activities *etc.*., June 1, 1989—June 1, 1990

1. Elected to APS Fellowship, December 1989.
2. Member of SSC Adhoc Committee on Energy/Luminosity Reassessment, SSC Laboratory, Nov. 30 - Dec. 1, 1989.
3. Participant in "Physics Below the Planck Scale", Institute for Theoretical Physics, UCSB, February-May, 1990.
4. Extensive organization of lobbying for the SSC within California. As I did last year, I again orchestrated the contacting of most of the California House and Senate members by individuals from their own districts, February-April, 1990.
5. Session chair, "New Topics in Electroweak Physics", SSC Laboratory, May 30 - June 1, 1990.
6. Organizer, "Intermediate Mass Higgs Bosons", Snowmass, 1990.

J.F. Gunion: Meetings and Workshops June 1, 1989—June 1, 1990

1. SSC Trigger Workshop, Lawrence Berkeley Laboratory, June, 1989.
2. 8th INFN Eloisatron Project Workshop on "Higgs Particles, ...", July, 1989.
3. 1989 Symposium on Lepton-Photon Interactions, Stanford Linear Accelerator Center, Stanford, CA, August, 1989.
4. 1989 European Physical Society Meeting, Madrid, Spain, September, 1989.
5. DESY Theory Workshop, DESY, Hamburg, West Germany, October, 1989.
6. NSF-ITP Workshop on "Thinking About the Top Quark", Institute for Theoretical Physics, UCSB, February, 1990.
7. NSF-ITP Workshop on "Heavy Quark Physics", Institute for Theoretical Physics, UCSB, May, 1990.

J.E. Kiskis, R. Narayanan, and P. Vranas: Publications/Preprints June 1, 1989—June 1, 1990

1. J. Kiskis, R. Narayanan and P. Vranas, "Random Walks, Critical Behavior, and Finite Temperature, SU(2) Lattice Gauge Theory", submitted to *Phys. Rev.* **D**.
2. R. Narayanan and R.R.P. Singh, "A Finite Lattice Expansion for Quantum Spin-Chains", submitted to *Phys. Rev.* **B**.
3. R.R.P. Singh and R. Narayanan, "Dimer versus Twist Order in the J_1-J_2 model", submitted to *Phys. Rev. Lett.*
4. R. Narayanan and C. Tracy, "Holonomic Quantum Field Theory of Bosons in the Poincaré Disk and the Zero Curvature Limit", to appear in *Nucl. Phys.* **B**.
5. J. Kiskis, "Behavior of Higher Representation Wilson lines in Finite-Temperature, SU(2), Lattice Gauge Theory", *Phys. Rev.* **D41**, 3204, (1990).

J.E. Kiskis, R. Narayanan, and P. Vranas: Invited Talks and Seminars June 1, 1989—June 1, 1990

1. J. Kiskis, "Behavior of Higher Representation Wilson Lines in Finite Temperature, SU(2), Lattice Gauge Theory", DPF90, Houston, January 1990.

2. R. Narayanan, "Flux Tube Model for the $SU(2)$ Deconfining Phase Transition", DPF90, Houston, January 1990.

3. P. Vranas, "A Technique for Analytical Calculation of Observables in Lattice Gauge Theories", LATTICE '89 Capri, Italy, September 1989.

J. Wudka: Publications/Preprints June 1, 1989—June 1, 1990

1. "Higgs triplets in the standard model" (with J.F. Gunion and R. Vega) *Phys. Rev.* **D42** (1990)

2. "Adiabatic evolution of quantum mechanical systems" (with J. Vidal), Univ. of Calif. at Davis preprint UCD–89–22, submitted to *Nucl. Phys.* **B**.

3. "Screening of heavy Higgs radiative corrections", contributed paper to the International Europhysics Conference on High Energy Physics, Madrid (Spain), Sept 6–13 (1989).

4. "A comment on the Born–Oppenheimer approximation", *Phys. Rev.* **D41** (1990) 712.

J. Wudka: Invited Talks and Seminars June 1, 1989—June 1, 1990

1. "Solar neutrinos and the Sun's magnetic field ", Univ. of California, Riverside, Jan. 1990.

2. "On the adiabatic approximation", Universitat de València, València, Spain, Sept. 1989.

3. "Screening of heavy Higgs radiative effects", Univ. Autónoma de Barcelona, Barcelona, Spain, Sept. 1989.

4. "Introduction to Berry's phase", Instituto de Física, Universidad Nacional Autónoma de México, México, D.F., June 1989.

Progress Report (J. Gunion)

1. J.F. Gunion, H.E. Haber, G. Kane and S. Dawson, "The Higgs Hunters Guide", Addison and Wesley (1990) Frontiers in Physics Series.

The physics of Higgs bosons, whether that of the Standard Model or those of extended models, and their detection has become an extremely involved and extensive subject over the last few years. As a result, a group of us decided to write a Physics Report on the subject containing a systematic study and survey of all the accumulated knowledge, including a full detailing of existing experimental constraints on and future probes of the Higgs boson sectors of all attractive models considered in the literature to date. The material eventually reached such a length that we decided to turn it into a book. We hope that this book will become a standard reference for this type of physics. It includes a complete listing of all relevant Feynman rules, branching ratios, and so forth. Along the way we encountered several areas where we felt old results could be improved or required correction, and have included much of this material in the book. We have done nearly everything with far greater thoroughness and perspective than any previous such survey. In addition, it contains much original material not available anywhere in the literature.

2. S. Dawson, J.F. Gunion, and H.E. Haber, "Are Light Higgs Bosons Allowed?" *Phys. Rev.* **D41** (1990) 2844.

The purpose of this paper was to survey the limitations on Higgs bosons deriving from relatively low-energy, pre-LEP, experiments. There had been several papers along this line prior to ours, all of which we felt to be inadequate or misleading in a variety of ways. Our survey included a detailed reassessment of predictions (using low-energy theorems and the like) for Kaon and B-meson rare decays to Higgs bosons, as well as the decays of the Higgs boson itself. A number of experiments were reanalyzed, either by us, or at our request by spokesmen for the experiments themselves, resulting in considerable clarification, and often substantial improvement on the bounds that could be placed on the Higgs boson. Our final conclusion was that the Standard Model Higgs boson could be ruled out for masses up to about $2m_\tau$, a result now confirmed by ALEPH and other experiments at LEP. For non-standard model Higgs bosons, the results of our analysis of low-energy experiments and the restrictions from the LEP experiments are in many ways complementary. In particular, the low-energy experiments are largely sensitive to Higgs bosons with fermionic couplings, while the LEP experiments are essentially only sensitive to Higgs bosons with couplings to vector bosons. Our analysis shows that Higgs bosons with SM-like fermionic couplings and mass up to and of order $2m_\tau$ are pretty much ruled out, barring certain "fine-tuned" cancellations between different amplitudes contributing to the rare K and B decays.

3. J.F. Gunion, "Probing Higgs Bosons/Electroweak Symmetry Breaking in Purely Leptonic Channels at Hadron Colliders", UCD-89-24, to appear in Proceedings of "Higgs Particles: Physics Issues and Experimental Searches in High Energy Collisions", 8th Erice Workshop, Erice, Italy, July 15-26, 1989.

It has long been recognized that the cleanest channels in which to search for the Standard Model Higgs boson at a hadron collider are those where the Higgs boson decays entirely to leptons. Such channels are free of hadronic backgrounds deriving from quark jets and the like. The extent to which such channels can be employed for the Standard Model Higgs boson has been the subject of numerous Snowmass studies, and other published work. In contrast, prior to this workshop study which I performed, almost no attention had been paid to the question of sensitivity to non-standard Higgs bosons in purely leptonic channels. Considerations, such as production rates and decay branching ratios, for neutral Higgs bosons are often very different from those appropriate to the Standard Model scenario. And, of course, charged Higgs bosons (singly or doubly charged were examined) are entirely without a Standard Model analogue. In this workshop article I present the results of extensive calculations of event rates and relevant backgrounds for a variety of non-standard Higgs sector scenarios. The results are surprisingly encouraging for the SSC (though quite discouraging for the LHC); substantial

sensitivity to non-standard Higgs bosons, even those with reduced vector boson-vector boson couplings, exists. Charged Higgs bosons in triplet and higher representation models yield often dramatic signals in the purely leptonic final state channels.

4. J.F. Gunion, "The SSC: Status and Physics Update", UCD-89-27, to appear in Proceedings of the 1989 European Physical Society Meeting, Madrid, Spain, September 1989.

This article was divided into two distinct parts. In the first, I reviewed the status of the SSC program and funding, and high-lighted the short time scale (as of the time of the article) for 'letter-of-intent' type proposals and the like. My primary goal was to make the European experimental community fully cognizant of the fact that the SSC had become a reality, and that if they were to participate in its program they should get moving. The second part of the article was devoted to a review of recent progress in developing techniques for isolating the physics signals likely to be of importance at the SSC. The subjects considered included: the like-sign dimuon signatures for supersymmetry developed by myself, Barnett and Haber;[1] the use of hadronic multiplicity to isolate the signal for a heavy $\sim 1\ TeV$ Standard Model Higgs boson as developed by me and a number of collaborators;[2] the status of the intermediate mass Higgs boson search modes (pointing out, in particular, the inadequacies and necessary improvements in several of the studies performed at Snowmass 1988 claiming large backgrounds — these I claimed could be eliminated by various cuts I outlined); and, finally, the techniques developed by Hinchliffe[3] for isolating a signal for a heavy lepton. In general, I hope I succeeded in high-lighting the enormous physics potential for the SSC that has emerged as a result of detailed studies of signals for new physics. The talk itself was very well received at the meeting, and made many of the European physicists acutely aware of some of the short comings of the LHC — most of the techniques and signals mentioned above would not be viable there.

5. J.F. Gunion and B. Grzadkowski, "Limits on the Top Quark and on the Charged Higgs Boson of a Two-Doublet Model from $\overline{K^0} - K^0$ mixing, $B_d - \overline{B_d}$ mixing, and $b \to u$ Decays", UCD-89-30, to appear in Physics Letters.

Two very interesting types of new physics are intimately connected — namely the physics of the top quark and the physics of a charged Higgs boson. For instance, a top quark can decay into a charged Higgs boson for $m_t \gtrsim m_{H^+} + m_b$, while the charged Higgs decay modes are dominated by $t\bar{b}$ if $m_{H^+} \gtrsim m_t + m_b$. Less obvious, but equally important, are the interconnections between a charged Higgs and the top quark in the area of rare K and B decays, and $\overline{K} - K$ and $\overline{B} - B$ mixing. For instance, in the latter, Feynman graphs involving the H^+ are at least as important as the standard box diagrams involving the W^+. In this paper, we combine the existing results for such mixing with limits from $b \to u$ decays on the crucial V_{bu} entry of the Cabibbo-Kobayashi-Maskawa matrix to place limits, both on the top quark and on the two crucial parameters of a two-doublet Higgs sector — the mass of the H^+ and the ratio of vacuum expectation values for the two Higgs doublets, normally called $\tan\beta$. Among other things we demonstrated that there is an m_t-dependent boundary in $m_{H^+} - \tan\beta$ parameter space that separates the domain of allowed from that of disallowed solutions. Roughly, the larger $\cot\beta$ is (*i.e.* the larger the H^+ coupling to the $t\bar{b}$) the heavier the Higgs boson must be. These bounds are quite significant and will play an important role in suggesting the most reasonable ranges of parameter space in which to search for a charged Higgs boson. In the paper, we also demonstrate that the weak-mixing and $b \to u$ results combine (in the absence of a charged Higgs boson) to exclude a range of m_t that depends upon the so-called bag parameters B_K and B_B describing the hadronic expectation value of the relevant quark-level matrix elements. Thus, discovery of the top quark at a particular mass, in combination with a fairly reliable lattice computation of B_K and B_B (something to be expected in the not too distant future) could easily imply that a charged Higgs boson (or other new physics that influences mixing) is required, and would place a strong constraint on its mass and the value of $\tan\beta$. A number of other issues of a similar nature are also considered in this paper.

6. S. Dawson, J.F. Gunion, H.E. Haber, A. Seiden, and G. Kane, "The Search for Higgs Bosons of Any Mass", *Comm. Nucl. Part. Phys.* **14** (1990) 259.

In this paper, we summarize and review the techniques required to discover the Standard Model Higgs boson at the SSC throughout the entire mass range from $\sim m_Z$ (the highest value that will be probed by LEP-II) up to $\sim 1\ TeV$. Our primary emphasis was upon the fact that at the SSC there are no mass regions where discovery is not possible, so long as appropriate detectors are constructed, whereas at the LHC there are regions of Higgs mass (in the intermediate mass region and in the TeV region) that simply cannot be probed for any conceivably realistic detector design. The level of presentation was that appropriate to a large audience of general physicists and experimentalists who have not been active in SSC studies. In part, our goal was to make it clear that the SSC design really will allow our first true probe of Electroweak Symmetry breaking, regardless of the mass at which the important signals appear.

7. J.F. Gunion, R. Vega, and J. Wudka, "Higgs Triplets in the Standard Model", UCD-89-13, to appear in *Phys. Rev.* **D**.

Relatively little attention has been devoted to the subtleties associated with probing a Higgs sector that contains Higgs representations higher than doublets. In part this is because Higgs sectors with triplets and higher representations must be rather carefully constructed in order to avoid conflicting with the observed value of $\rho \equiv m_W/(m_Z c_W) \simeq 1$. Nonetheless, models can be easily constructed containing triplet Higgs representations (usually in combination with doublet representations in order to give fermions mass) which exhibit a custodial $SU(2)$ symmetry at tree-level that preserves $\rho = 1$ even when the neutral members of the triplet representations acquire a non-zero vacuum expectation value. An example of such a model is that discussed by Georgi and collaborators.[4] In this paper, we explore the rather intricate and subtle structure of the signatures for the Higgs bosons of this model. In particular, we demonstrate that decays of one Higgs boson into several others will often dominate over the more standard decays of a Higgs boson into vector boson pairs. Indeed, unless the triplet Higgs fields are given an overwhelming share of the vacuum expectation value required to give the W and Z their observed mass, the former decays are likely to be dominant. This leads to many unexpected signals, unusually long lifetimes, *etc.* for the Higgs bosons of the model. Production cross sections are also significantly dependent upon the amount of vacuum expectation value given to the triplet fields. All these issues are explored at some depth in the paper, and appropriate strategies for the detection of the Higgs bosons of such a triplet model outlined. Also presented are all the Feynman rules and couplings required for these and future calculations within this type of model, including the critical Higgs self-couplings.

8. N. Deshpande, J.F. Gunion, B. Kayser, and F. Olness, "Left-Right Symmetric Electroweak Models with Higgs Triplets", NSF-ITP-90-69, submitted to *Phys. Rev.* **D**.

In an extensive series of papers, I, Boris Kayser, and Fred Olness, along with assorted collaborators have explored the physics of left-right symmetric gauge models and the potential of the SSC for probing such physics.[5] Aside from the production cross sections and phenomenology as a function of Higgs boson mass scale pursued in these early studies, the most crucial issue is the mass scale itself. In this paper, we use the full structure of the most general Higgs potential for such a model, along with a full analytic minimization of this potential, in order to completely implement all the constraints on the model. We demonstrate that 'see-saw' relations among the vacuum expectation values for the different neutral Higgs fields emerge. In combination with the mass see-saw relation responsible for determining the masses of the charged leptons and neutrinos, the VEV see-saw relations yield extraordinarily powerful constraints upon the parameters of the model. In particular, we conclude that the natural mass scale for all new gauge bosons and Higgs bosons is of order $10^3\ TeV$ (or higher), *i.e.* not accessible at the SSC, unless certain terms in the Higgs potential are either absent (perhaps by virtue of symmetries from a higher GUT scheme — we demonstrate that obvious phase and other symmetries are not adequate) or else fine-tuned at a level of 10^{-6} (at least) relative to their natural

order of magnitude. Even if a GUT symmetry does indeed eliminate these terms in the Higgs potential, we enumerate many other severe difficulties (which are only apparent after complete minimization of the Higgs potential) that must be circumvented. Such circumvention is certainly possible, but the resultant phenomenology is rather more strongly constrained than one might have supposed. The most easily discoverable Higgs bosons, and their signatures, are enumerated.

Progress Report (J. Kiskis, R. Narayanan, S. Staniford-Chen, and P. Vranas)

Introduction

The general goal of this research is to further the understanding of non-Abelian gauge fields in non-perturbative regions. We are particularly interested in the interplay of gauge symmetry and vacuum structure.

Some research has also been carried out in the areas of massive field theories in two dimensions and quantum statistical models in one and two dimensions.

Non-Abelian gauge theories are the foundation of the Standard Model. In particular, it is generally accepted that the $SU(3)$ gauge theory of quarks and gluons describes the strong interactions. For those physical processes that are controlled by short-distance interactions and that are relatively insensitive to large-distance effects, the results of perturbative calculations and experiments can be compared quantitatively. For most reactions, this is not the case, because large-distance, nonperturbative effects are important. Confinement is only the most dramatic example; hadronization and strong interaction corrections to weak decays are important, practical issues.

The perturbative calculations that are valid at short distance where the effective coupling is weak require a gauge fixing that obscures to some considerable extent the fundamental role of gauge symmetry. Lattice gauge theory is an approximation that is complementary to continuum perturbation theory in that it maintains manifest gauge invariance while sacrificing Poincaré symmetry. The space-time symmetry is restored as the correlation length for lattice fields diverges (as measured in lattice units) and the lattice spacing approaches zero (as measured in physical units). This occurs at a second order phase transition. The long-distance, nonperturbative effects are more accessible in the lattice approximation.

Within the framework of lattice gauge theory, one can employ either approximate, analytical methods or a direct attack by numerical simulation. Our work exploits both approaches.

The zero-temperature pure gauge theory has no adjustable parameters. This is part of the reason that it is so difficult to approximate. A study of the theory at finite temperature introduces a parameter T that can be varied in a controlled way so as to probe different aspects of the theory. In particular, confinement, which is apparently present at low temperature, is absent at sufficiently high temperature. A study of the theory as the temperature is changed can yield useful information about the features that distinguish these two phases and thus contribute to an understanding of the vacuum state. Two completed works and several active projects deal with the finite-temperature theory.

The first completed work is concerned with the screening of static quarks in representations higher than the fundamental. This gives information on the behavior of the gauge field both above and below T_c that is more detailed than that obtained by restricting oneself to the fundamental representation. This work relies heavily on numerical experiments.

The second completed project models the finite-temperature flux tube as a self-interacting random walk. This simple model seems to incorporate some of the nontrivial features of the critical behavior of the gauge theory as $T \rightarrow T_c$ from below.

Three active projects are concerned with $SU(2)$ gauge fields near the finite-temperature phase transition. The first is an analytical approximation developed to give a physical understanding of the value

of the adjoint Wilson line at $T = T_c$ that was computed numerically in the first completed project. The second is a numerical study of the critical properties of a flux model that can be used *above* T_c. The third will check for universality of amplitude ratios associated with the $SU(2)$, finite-temperature phase transition.

The next two sets of projects study models that share many problems and properties with the field theories that are directly related to high energy physics.

One project was completed in the area of exactly solvable massive field theories in two dimensions. A closely related work is now in progress. The goal is to understand conformal field theories away from criticality.

Two projects were completed in the area of quantum statistical mechanics. They deal with the anti-ferromagnetic Heisenberg model in one and two dimensions. The aim is to understand the ground state properties of this model and possibly shed some light into the area of high temperature superconductivity.

1. J. Kiskis, "Behavior of Higher Representation Wilson Lines in Finite-Temperature, $SU(2)$, Lattice Gauge Theory", *Phys. Rev.* **D41** (1990) 3204.

This project was a Monte Carlo numerical simulation of finite-temperature, $SU(2)$, pure gauge theory. The response of the gauge field to static color sources in representations $J = \frac{1}{2}$, 1, and $\frac{3}{2}$ was studied.

First P. Damgaard and then K. Redlich and H. Satz reported the intriguing numerical result that the expectation value of a source (Wilson line) in representation J is proportional to the expectation value of the fundamental line ($J = \frac{1}{2}$) raised to the power $2J$:

$$\langle L_J \rangle \propto \left\langle L_{\frac{1}{2}} \right\rangle^{2J} . \tag{1}$$

Although Damgaard showed that a mean field approximation can give this result, it is very difficult to understand how it can hold in the critical region where mean field theory is certainly not valid.

The relation (1) says that the gauge theory in the deconfined phase responds to a J source as if it were $2J$ sources with $J = \frac{1}{2}$. This would be a surprising result since it is believed that the confined phase system responds very differently to $J = \frac{1}{2}$ sources which are confined ($\left\langle L_{\frac{1}{2}} \right\rangle = 0$) and adjoint sources which can be screened by the field ($\langle L_1 \rangle \neq 0$).

My work adds to previous results in two ways. First, there are some theoretical predictions. One approach is based on a flux tube model of the deconfined phase. It leads to $\langle L_1 \rangle \rightarrow$constant and $\langle L_{3/2} \rangle \propto \langle L_{1/2} \rangle$ as $T \rightarrow T_c^+$. The other approach exploits the connection through universality with $(\phi^4)_3$ field theory and gives these predictions with additional corrections.

Then some Monte Carlo results are presented. The data are consistent with my theoretical predictions while the mean field result is excluded close to T_c. These data differ from previous results in that they were taken at smaller values of $(T - T_c)/T_c$.

In summary, this work indicates that even above T_c one can understand the $T \rightarrow T_c^+$ gauge field in simple terms. The dynamical field screens higher representation static color sources so that integer representations are completely screened while half-integer representations are screened to behave like $J = 1/2$ fundamental sources.

The numerical work was done on a VAXstation II at UCD and on the CRAY-2's at NMFECC. All are supported by DOE.

2. J. Kiskis, R. Narayanan and P. Vranas, "Random Walks, Critical Behavior, and Finite-Temperature, $SU(2)$, Lattice Gauge Theory", submitted to *Phys. Rev.* **D**.

We develop a flux tube model to improve upon the physical understanding of the $SU(2)$, finite-temperature phase transiton and its associated universality class. In this model, a color flux tube is formed between a static quark and an anti-quark. The flux tube is thought of as a thin string with a certain zero-temperature string tension which is a parameter of the model. The string connecting the two static sources can be of any length and is expected to fluctuate at any finite temperature. Different configurations of the string are weighted with a Boltzmann factor which is proportional to the length of the string.

Previous work in this area neglected the interactions of the string with itself and reduced the problem to that of an unconditional random walk. The result is a second order phase transition with gaussian exponents. This is not quantitatively correct because the lattice $SU(2)$ gauge theory has the nongaussian exponents of the Ising universality class. On the other hand, the flux tube formed between the static sources does have repulsive self interactions.

Model studies of random walks with interactions suggest that the exponent ν describing the vanishing of the string tension at the critical temperature is a product of two exponents ν_p and ν_θ. ν_p is altered by the non-Markov behavior coming from interactions of the walk with itself at intersections. ν_θ is altered by interactions of the walk with a background of loops. In the approximation where all spacelike plaquettes are neglected, a random walk representation is developed for the $SU(2)$ lattice gauge theory and it is shown that the walk has both types of interactions.

3. R. Narayanan and C.A. Tracy, "Holonomic Quantum Field Theory of Bosons on a Poincaré Disk and the Zero Curvature Limit", to appear in *Nucl. Phys.* **B**.

Conformal field theory tells us a great deal about correlation functions of critical, or equivalently massless, 2D quantum field theories. On the other hand, progress in correlation functions for *massive* 2D quantum field theories has been restricted to a smaller class of models. The most general methods presently available are those coming from the theory developed by Sato, Miwa, and Jimbo (SMJ) called *Holonomic Quantum Fields*. The most important special case of their theory is the massive Ising field theory on $\mathbf{R}^2$. One direction to pursue to enlarge the class of solvable, massive 2D quantum field theories, is to construct holonomic quantum field theories on two-dimensional manifolds other that $\mathbf{R}^2$. Since the hyperbolic plane is the universal covering space for Riemann surfaces of genus greater than one, it is natural to first extend the SMJ analysis to massive Klein-Gordon and Dirac operators on the hyperbolic plane. It is the purpose of this project to establish a detailed connection between the Euclidean results of SMJ and the hyperbolic results for the Klein-Gordon equation. The corresponding results for the Dirac case is currently under study.

The hyperbolic plane can also be modeled by the Poincaré disk of radius R, $\mathbf{D}_R$. In this model the curvature of the manifold is $-(2/R)^2$. This then is a convenient model to analyze the limit of zero curvature, or equivalently, $R \to \infty$. We show that the results associated with monodromy preserving deformation of the Klein-Gordon equation found in the work of SMJ can be obtained as the limiting case of the corresponding results on $\mathbf{D}_R$. It is interesting to note that the analysis on $\mathbf{D}_R$ is in some sense nicer than the Euclidean case, i.e. irregular singularities in $\mathbf{R}^2$ get replaced with regular singularities in $\mathbf{D}_R$, and the irregular singularities arise as a confluence of regular singularities as $R \to \infty$. This point was also observed by Atiyah while working on the problem of monopoles. The closed one form ω associated with the deformation equations is discussed. The importance of ω is that locally it is $d \log \tau$ where the τ function is precisely the n point function for certain interacting bosons defined on $\mathbf{D}_R$. The results are carefully analyzed and it is shown in detail that the theory developed by Sato, Miwa and Jimbo on the Euclidean plane is a limiting case of the corresponding theory on the Poincaré disk. The limiting procedure actually turns out to be quite subtle.

4. R.R.P. Singh and R. Narayanan, "Dimer versus Twist Order in the J_1-J_2 Model", submitted to *Phys. Rev. Lett.* .

Motivated by the discovery of antiferromagnetism in the insulating phase of high T_c materials and the suggestion that magnetic fluctuations may be central to a microscopic understanding of the high T_c phenomena, there have been several theoretical studies of ground state properties of frustrated square lattice Heisenberg models. Perhaps the simplest of these models is the J_1-J_2 model, with nearest neighbor antiferromagnetic exchange J_1 and the second neighbor exchange J_2. In the classical limit ($S \to \infty$), this model has a 2 sublattice Néel ground state for $J_2/J_1 < 1/2$ and a 4 sublattice Néel

ground state for $J_2/J_1 > 1/2$. At $J_2/J_1 = 1/2$ various states ordered at wave vectors (π, q), or (q, π), become degenerate. Expansion in powers of $1/S$ reveals that the magnetically ordered phases are pushed away from $J_2/J_1 = 1/2$ leaving an intermediate phase with no long range magnetic order. The nature of the ground state in this intermediate phase has been of considerable interest.

Earlier studies of the $1/S$ expansion suggested that the ground state in the intermediate phase was a resonating valence bond state with no long range order. On the other hand stuides based on a large N expansion suggested that the magnetically disordered phase obtained by quantum fluctuations may have long range dimer order, where the nearest neighbor spin correlations alternate in a column pattern. Other suggestions have included twist order as well as chiral order.

In this project we study the 4×4 periodic system at finite temperatures by a complete diagonalization. We study the specific heat, the static structure factors, as well as the squares of dimer and twist order parameters. We find that in the intermediate region around $J_2/J_1 = 1/2$ the specific heat of the system has a peak around a temperature of $0.27J_1$. Near this temperature the square of the bond order parameter, ψ, increases sharply as the temperature is lowered. Between a temperature of $0.5J_1$ and $0.1J_1$ it increases by roughly a factor of 2.5. The zero temperature value of ψ is roughly 0.4 times that of a fully dimerized state. This is a clear evidence for enhancement of dimer order. In contrast, the square of the twist order parameter, ϕ, does not show any significant enhancement with respect to the infinite temperature value. The only structure is a maximum increase of about twenty percent between $T = \infty$ and $T \approx 0.27J_1$, which is followed by a decrease as the temperature is further lowered. Hence, there is no indication of twist order at $T = 0$.

5. R. Narayanan and R.R.P. Singh "Thermodynamic Properties of Spin-Chains as a Sum Over Contributions from Different Finite Chains", submitted to *Phys. Rev.* **B**.

Finite size studies of quantum spin Hamiltonians have proven very valuable in extracting the thermodynamic properties of the system. At $T = 0$, they have been used to determine the ground state energy, the excitation spectra and various correlation functions of the spin chains, while at finite temperatures they have led to estimates for the internal energy, the specific heat and other thermodynamic quantities. Much of the extrapolation has relied on the assumption that an extensive quantity P_l, for a chain of length l, takes the form $P_l = lp + q$, where p is the bulk density in the thermodynamic limit and q is the contribution from the boundary. A plot of P_l versus l was used to estimate p. In this extrapolation scheme the effects of correlations are ignored. Hence the extrapolation becomes unreliable when the correlation length is comparable to the size of the largest system considered.

In this project we consider a different scheme to obtain the thermodynamic quantities of interest by studying finite chains. It is based on a technique developed orginally for lattice gauge theories. The idea behind this scheme is to express the various thermodynamic quantities for the infinite chain as a sum over contributions associated with increasing length scales. The contribution to a given length scale l, is obtained from the thermodynamic properties for chains with free boundary conditions up to length l ($l + 1$ spins) and it accounts for correlations of that length in the infinite system. This method enables a systematic study of the convergence of various thermodynamic quantities and also in extracting the correlation length.

Progress Report (José Wudka)

1. "Higgs triplets in the standard model" (with J.F. Gunion and R. Vega) *Phys. Rev.* **D42** (1990).

The possibility of spontaneous symmetry breaking being produced by "exotic" Higgs representations was investigated in detail for the case of a model originally proposed by Georgi and Machacek (*Nucl. Phys.* **B262** (1985) 463). This model is constructed in such a way that the tree level value of the ρ parameter ($= m_W/(m_Z c_W)$) is equal to one; moreover the structure of the scalar sector is such that some of the scalars do not couple to fermions. These properties, together with the possible phenomenological relevance of this model, are studied in detail in our paper. We consider as well the possibility of detection of the new scalars present in this model and the expected discrepancies with respect to the standard model. The question of the naturalness (in the technical sense) of the model is also discussed.

2. "Adiabatic evolution of quantum mechanical systems" (with J. Vidal), U.C. Davis preprint UCD-89-22, submitted to *Nucl. Phys.* **B**.

In recent years, with the important remarks of Berry (*Proc. Roy. Soc., London* **A392** (1984) 45), the relevance of the adiabatic phases in a variety of fields of physics has been clarified. In this paper we present a discussion of the exact time evolution operator within the adiabatic approximation. Next we study the corrections to this approximation. While these cannot be evaluated in general, for the case of a quantum system interacting with rapidly varying external (classical) fields of arbitrary amplitude, we are able to calculate, to a very good approximation, all these corrections. Moreover, whereas in the case were the amplitude of the external fields is small the effects are irrelevant, in the case were the external fields are strong the effects are important and in fact will induce transitions which would otherwise be strongly suppressed.

3. "Screening of heavy Higgs radiative corrections", contributed paper to the International Europhysics Conference on High Energy Physics, Madrid (Spain), Sept 6–13 (1989).

In this paper I report the results of a collaboration, with M. Einhorn, where we studied the radiative effects of a heavy Higgs on low energy measurements. Our aim was to generalize Veltman's screening theorem for the standard model. We were able to state precisely such a theorem and to identify it as a renormalization effect; we provided also a proof to all orders in perturbation theory. As a spinoff of the calculation, we devised gauge–fixing conditions which have proved useful in other areas, such as detailed studies of the equivalence theorem.

4. "A comment on the Born–Oppenheimer approximation", *Phys. Rev.* **D41** (1990) 712.

In this brief note I have studied the applications of Berry's ideas to the concrete problem of the Born–Oppenheimer approximation. This approximation is not directly related to the definition of the adiabatic approximation used in connection with the topological phases. In fact, to relate the two approximations, a higher order correction must be calculated in the adiabatic approximation; as another product of the calculation I was able to quantify the accuracy of the Born–Oppenheimer approximation.

TASK E

Ling-Lie Chau

I.a. Analysis of Two-Body Charm Meson Decays

Recently several new experimental data of exclusive two-body decays of charmed mesons were reported. The Mark III collaboration have revised their analysis of exclusive charm decays and obtained branching fractions, some of which are reduced by 21–24% compared to their previously reported results. Several new measurements of the D_s^+ lifetime indicate that lifetimes of D_s^+ and D^0 are very close. In addition, a few new experimental results on two-body D_s^+ decays were obtained. Using different techniques many other experimental groups, including CLEO, ARGUS, HRS, TASSO, E691, LEBC–EHS collaborations, have also studied the exclusive decay modes of charmed mesons and supplied cross checks on Mark III data and provide some new data.

The experimental data can be understood in the general framework of the quark-diagram scheme. All meson decays can be expressed in terms of six quark diagrams (Fig. 1): $\mathcal{A}$, the external W-emission diagram; $\mathcal{B}$, the internal W-emission diagram; $\mathcal{C}$, the W-exchange diagram; $\mathcal{D}$, the W-annihilation diagram; $\mathcal{E}$, the horizontal W-loop diagram; and $\mathcal{F}$, the vertical W-loop diagram. These quark diagrams are specific and well-defined physical quantities. They are classified according to the topology of first-order weak interactions, but all QCD strong-interaction effects are included. Such a general scheme is useful in analyzing experimental data and extracting their theoretical implications as well as pointing out future interesting experiments. For charm decays, the quark-diagram amplitudes of exclusive two-body modes are listed in Tables I and II.

$D \to VP$ Decays: By analyzing the data of charm meson to vector pseudoscalar $D \to VP$ decays, using the quark diagram scheme as given in Table I, we reach the following conclusions. For details, see Chau's publications.

1. To satisfactorily describe $D \to \bar{K}^*\pi$ decays, the consideration of final-state interactions is inevitable. Without such effects the prediction of $D \to \bar{K}^*\pi$ rates will be off by at least two standard deviations.

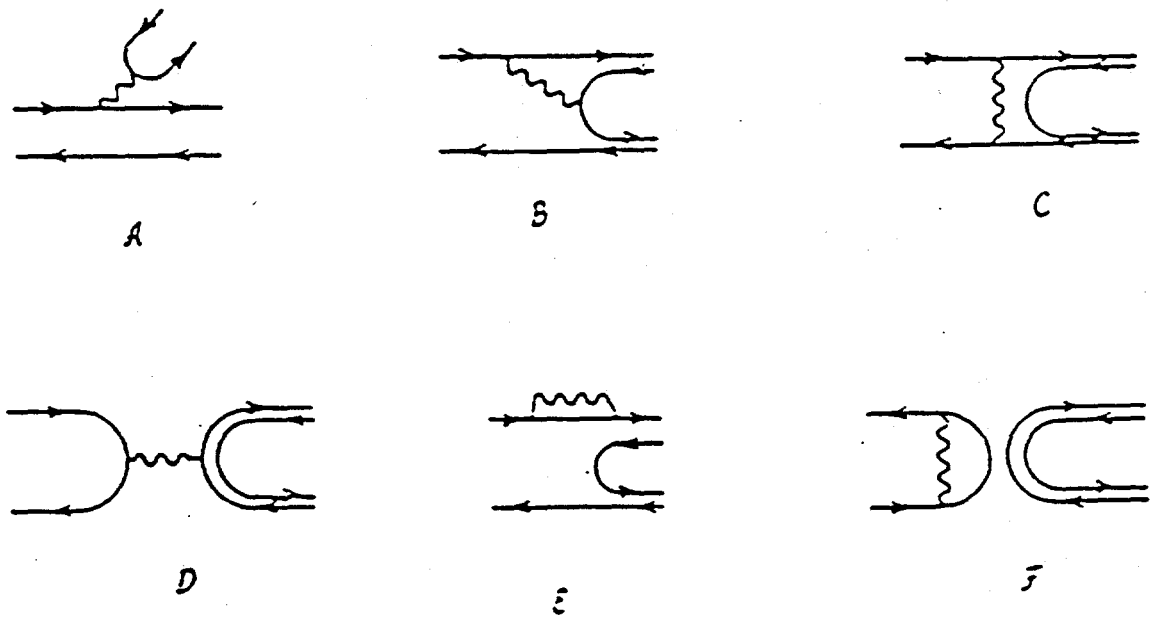

Figure 1. The six quark diagrams for a meson → two mesons.

2. The data also implies the importance of W-annihilation in $D_s^+ \to VP$.

3. Perturbative QCD calculations always give $|\mathcal{A}'| > |\mathcal{B}'|$ due to the color suppression in the internal W-emission diagram $\mathcal{B}'$. The experimental fact that $|\mathcal{A}'| < |\mathcal{B}'|$ clearly indicates the importance of nonperturbative effects (e.g., soft-gluon exchange). The decay rates of some color-mismatched channels, e.g., $D^0 \to \omega\bar{K}^0$, $\phi\bar{K}^0$, $\pi^0\bar{K}^0$, $D_s \to \bar{K}^{*0}K^+$ are not suppressed relative to that of color-matched modes. From the quark-diagram scheme we can predict that

$$Br(D^0 \to \phi\pi^0) = \frac{1}{2}(0.05)\,\frac{\Gamma(D^0)}{\Gamma(D^+)}\,Br(D^+ \to \phi\pi^+).$$

$D \to PP$ **Decays:** After analyzing the data of charm-meson decay into two pseudoscalars $D \to PP$, as given in Table II, we reach the following conclusions:

1. The penguin diagram contribution is expected to be very small in charm decay because of the good approximation $V_{us}V_{cs}^* \simeq -V_{ud}V_{cd}^*$. Indeed, the new measurement of $D_s \to \bar{K}^0K^+$ together with $D^+ \to \pi^+\bar{K}^0$ and $D^+ \to \bar{K}^0K^+$ implies that the penguin contribution in charm decay is negligible.

2. The *W-exchange and/or the W-annihilation diagrams play an essential role in* $D \to PP$ *decays.*

3. There are possible hairpin-diagram contributions to $D^0 \to \bar{K}^0\eta_0$ and $D_s \to \pi\eta_0$. If they are small we can make the following possible predictions

$$Br\,(D_s \to \pi\eta') \sim 1\% \qquad Br\,(D^0 \to \bar{K}^0\eta') \sim 1\%;$$

or

$$Br(D_s^+ \to \pi^+\eta') \sim 0.2\%, \quad Br(D^0 \to \bar{K}^0\eta') \sim 7\%$$

Any deviation from the above prediction might signal the importance of hairpin diagrams. A large branching ratio of about 19% for $D_s^+ \to \pi^+\eta'$ measured recently by Mark II indicates that hairpin diagrams may play an essential role in $D \to PP$ decays.

Non-resonant 3-body decays of charmed mesons are first studied in the approach of effective $SU(4) \times SU(4)$ chiral Lagrangians. It is pointed out that the predictions of the branching ratios in chiral perturbation theory are in general too small when compared with experiment. However, the experimental results are comprehensible in the general framework of the quark-diagram scheme. The existence of a sizable W-annihilation amplitude, which is evidenced by the observation $D_3^+ \to (\pi^+\pi^+\pi^-)_{NR}$, is the key towards an understanding of the 3-body non-resonant decays of D^+ and D_3^+. The measurement of $D^0 \to \bar{K}^0K^+K^-$ and $D^0 \to \bar{K}^0\pi^+\pi^-$ indicates that color suppression is not effective in the 3-body decay. Based on the quark-diagram analysis, predictions for some other non-resonant modes are given.

Table I. Doubly-Suppressed Charm Meson Decays into a Vector Boson and a Pseudoscalar Meson

Channels	Predicted Branching Ratios	Amplitudes with SU(3) Symmetry and no final-state Interactions	Amplitudes with SU(3) breaking and final-state interactions
$\mathcal{D}^+ \to \phi K^+$	0.5×10^{-4}	$-(s_1)^2 \times \{\mathcal{L} + \mathcal{D}_h\}$	$\to \{\mathcal{L} + \mathcal{D}_h\} e^{i\delta^{\phi K}}$
$\to \omega K^+$	2.5×10^{-4}	$-(1/\sqrt{2})(s_1)^2 \times \{\mathcal{A}' + \mathcal{D}' + 2\mathcal{D}_h\}$	$\to \{\mathcal{A}' + \mathcal{D}' + 2\mathcal{D}_h\} e^{i\delta^{\omega K}}$
$\to K^{*+}\eta_8$		$-(1/\sqrt{6})(s_1)^2 \times \{\mathcal{A} + \mathcal{D} - 2\mathcal{D}'\}$	$\to \{\mathcal{A} + \mathcal{D} - 2\mathcal{D}' + 2\mathcal{D}'_h - 2\mathcal{D}'_{\underline{h}}\} e^{i\delta^{K^*\eta_8}}$
$\to K^{*+}\eta_0$		$-(1/\sqrt{3})(s_1)^2 \times \{\mathcal{A} + \mathcal{D} + \mathcal{D}' + 3\mathcal{D}'_h\}$	$\to \{\mathcal{A} + \mathcal{D} + \mathcal{D}' + 2\mathcal{D}'_h + \mathcal{D}'_{\underline{h}}\} e^{i\delta^{K^*\eta_0}}$
$\to K^{*+}\eta$	1.7×10^{-4}	$\eta = \eta_8 \cos\theta + \eta_0 \sin\theta;\ \eta' = -\eta_8 \sin\theta + \eta_0 \cos\theta;\ \theta \approx 20^\circ$	
$\to \rho^+ K^0$	2.0×10^{-4}	$-(s_1)^2 \times \{\mathcal{B} + \mathcal{D}'\}$	$\to \{(\mathcal{B} + \mathcal{D}') + (\mathcal{A}' - \mathcal{B} - 2\mathcal{D}')(1/3)(1 - e^{-i\Delta_{\rho K}})\} e^{i\delta^{\rho K}_{3/2}}$
$\to \rho^0 K^+$	1.0×10^{-4}	$(1/\sqrt{2})(s_1)^2 \times \{\mathcal{A}' - \mathcal{D}'\}$	$\to \{(\mathcal{A}' - \mathcal{D}') - (\mathcal{A}' - \mathcal{B} - 2\mathcal{D}')(2/3)(1 - e^{-i\Delta_{\rho K}})\} e^{i\delta^{\rho K}_{3/2}}$
$\to K^{*0}\pi^+$	1.1×10^{-4}	$-(s_1)^2 \times \{\mathcal{B}' + \mathcal{D}\}$	$\to \{(\mathcal{B}' + \mathcal{D}) + \frac{1}{3}(\mathcal{A} - \mathcal{B}' - 2\mathcal{D})(1 - e^{-i\Delta_{K^*\pi}})\} e^{i\delta^{K^*\pi}_{1/2}}$
$\to K^{*+}\pi^0$	2.2×10^{-4}	$(1/\sqrt{2})(s_1)^2 \times \{\mathcal{A} - \mathcal{D}\}$	$\to \{(\mathcal{A} - \mathcal{D}) - \frac{2}{3}(\mathcal{A} - \mathcal{B}' - 2\mathcal{D})(1 - e^{-i\Delta_{K^*\pi}})\} e^{i\delta^{K^*\pi}_{1/2}}$
$\mathcal{D}^0 \to \phi K^0$	0.2×10^{-4}	$-(s_1)^2 \times \{\mathcal{L} + \mathcal{C}_h\}$	$\to \{\mathcal{L} + \mathcal{C}_h\} e^{i\delta^{\phi K}}$
$\to \omega K^0$	0.9×10^{-4}	$-(1/\sqrt{2})(s_1)^2 \times \{\mathcal{B} + \mathcal{C}' + 2\mathcal{C}_h\}$	$\to \{\mathcal{B} + \mathcal{C}' + 2\mathcal{C}_h\} e^{i\delta^{\omega K}}$
$\to K^{*+}\pi^-$	1.9×10^{-4}	$-(s_1)^2 \times \{\mathcal{A} + \mathcal{C}\}$	$\to \{(\mathcal{A} + \mathcal{C}) - \frac{1}{3}(\mathcal{A} + \mathcal{B})(1 - e^{-i\Delta_{K^*\pi}})\} e^{i\delta^{K^*\pi}_{1/2}}$
$\to K^{*0}\pi^0$	1.2×10^{-4}	$-(1/\sqrt{2})(s_1)^2 \times \{\mathcal{B} - \mathcal{C}\}$	$\to \{(\mathcal{B} - \mathcal{C}) - \frac{2}{3}(\mathcal{A} + \mathcal{B})(1 - e^{-i\Delta_{K^*\pi}})\} e^{i\delta^{K^*\pi}_{1/2}}$
$\to K^{*0}\eta_8$		$-(1/\sqrt{6})(s_1)^2 \times \{\mathcal{B}' + \mathcal{C} - 2\mathcal{L}'\}$	$\to \{\mathcal{B}' + \mathcal{C} - 2\mathcal{L}' + 2\mathcal{C}'_h - 2\mathcal{C}'_{\underline{h}}\} e^{i\delta^{K^*\eta_8}_{1/2}}$
$\to K^{*0}\eta_0$		$-(1/\sqrt{3})(s_1)^2 \times \{\mathcal{B}' + \mathcal{C} + \mathcal{L}' + 3\mathcal{C}'_h\}$	$\to \{\mathcal{B}' + \mathcal{C} + \mathcal{L}' + 2\mathcal{C}'_h + \mathcal{C}'_{\underline{h}}\} e^{i\delta^{K^*\eta_0}}$
$\to K^{*}\eta$	0.2×10^{-4}	$\eta = \eta_8 \cos\theta + \eta_0 \sin\theta;\ \eta' = -\eta_8 \sin\theta + \eta_0 \cos\theta;\ \theta \approx 20^\circ$	
$\to \rho^- K^+$	0.9×10^{-4}	$-(s_1)^2 \times \{\mathcal{A}' + \mathcal{C}'\}$	$\to (\mathcal{A}' + \mathcal{C}') - 2/3(\mathcal{A}' + \mathcal{B})(1 - e^{i\Delta_{\rho K}})\} e^{i\delta^{\rho K}_{1/2}}$
$\to \rho^0 K^0$	0.4×10^{-4}	$-(1/\sqrt{2})(s_1)^2 \times \{\mathcal{B} - \mathcal{C}'\}$	$\to \{(\mathcal{B} - \mathcal{C}') - 1/3(\mathcal{A}' + \mathcal{B})(1 - e^{i\Delta_{\rho K}})\} e^{i\delta^{\rho K}_{1/2}}$
$\mathcal{D}_s^+ \to K^{*+}K^0$	0.7×10^{-4}	$-(s_1)^2 \times \{\mathcal{A} + \mathcal{B}\}$	$\to \{(\mathcal{A} + \mathcal{B}) + \frac{1}{2}(\mathcal{A}' + \mathcal{B}' - \mathcal{A} - \mathcal{B})(1 - e^{-i\Delta_{K^*K}})\} e^{i\delta_1^{K^*K}}$
$\to K^{*0}K^+$	0.6×10^{-4}	$-(s_1)^2 \times \{\mathcal{A}' + \mathcal{B}'\}$	$\to \{(\mathcal{A}' + \mathcal{B}') - \frac{1}{2}(\mathcal{A}' + \mathcal{B}' - \mathcal{A} - \mathcal{B})(1 - e^{-i\Delta_{K^*K}})\} e^{i\delta_1^{K^*K}}$

Table II. Doubly-Suppressed Charm Meson Decays to Two Pseudoscalars

Channels	Predicted Branching Ratios	Amplitudes with SU(3) Symmetry and no final-state Interactions	Amplitudes with SU(3) breaking and final-state interactions
$\mathcal{D}^+ \to K^0\pi^+$	2.1×10^{-4}	$-(s_1)^2 \times \{\mathcal{B}+\mathcal{D}\}$	$\to \{(\mathcal{B}+\mathcal{D}) + (\mathcal{A}-\mathcal{B}-2\mathcal{D})(1/3)(1-e^{-i\Delta_{K\pi}})\}e^{i\delta_{3/2}^{K\pi}}$
$\to K^+\pi^0$	3.7×10^{-4}	$(1/\sqrt{2})(s_1)^2 \times \{\mathcal{A}-\mathcal{D}\}$	$\to \{(\mathcal{A}-\mathcal{D}) - (\mathcal{A}-\mathcal{B}-2\mathcal{D})(2/3)(1-e^{-i\Delta_{K\pi}})\}e^{i\delta_{3/2}^{K\pi}}$
$\to K^+\eta_8$		$-(1/\sqrt{6})(s_1)^2 \times \{\mathcal{A}-\mathcal{D}\}$	$\to \{\mathcal{A}-\mathcal{D}+2\mathcal{D}_h-2\mathcal{D}_h\}e^{i\delta^{K\eta_8}}$
$\to K^+\eta_0$		$-(1/\sqrt{3})(s_1)^2 \times \{\mathcal{A}+2\mathcal{D}+3\mathcal{D}_h\}$	$\to \{\mathcal{A}+2\mathcal{D}+2\mathcal{D}_h+\mathcal{D}_h\}e^{i\delta^{K\eta_0}}$
$\to K^+\eta$	1.5×10^{-4}	$\eta = \eta_8\cos\theta + \eta_0\sin\theta$	
$\to K^+\eta'$	0.1×10^{-5}	$\eta' = -\eta_8\sin\theta + \eta_0\cos\theta;\ \theta \approx 20^\circ$	
$\mathcal{D}^0 \to K^+\pi^-$	1.2×10^{-4}	$-(s_1)^2 \times \{\mathcal{A}+\mathcal{C}\}$	$\to$ same as for $K^-\pi^+$
$\to K^0\pi^0$	0.6×10^{-4}	$-(1/\sqrt{2})(s_1)^2 \times \{\mathcal{B}-\mathcal{C}\}$	$\to$ same as for $\bar{K}^0\pi^0$
$\to K^0\eta_8$		$-(1/\sqrt{6})(s_1)^2 \times \{\mathcal{B}-\mathcal{C}\}$	$\to$ same as for $\bar{K}^0\eta_8$
$\to K^0\eta_0$		$-(1/\sqrt{3})(s_1)^2 \times \{\mathcal{B}+2\mathcal{C}+3\mathcal{C}_h\}$	$\to$ same as for $\bar{K}^0\eta_0$
$\to K^0\eta$	0.4×10^{-4}	$\eta = \eta_8\cos\theta + \eta_0\sin\theta$	
$\to K^0\eta'$	0.6×10^{-4}	$\eta' = -\eta_8\sin\theta + \eta_0\cos\theta;\ \theta \approx 20^\circ$	
$\mathcal{D}_s^+ \to K^+K^0$	0.3×10^{-4}	$-(s_1)^2 \times \{\mathcal{A}+\mathcal{B}\}$	$\to \{(\mathcal{A}+\mathcal{B})\}e^{i\delta_1^{KK}}$

Table III. Doubly-Suppressed Charm Meson Decays into Two Vector Bosons

Channels	Predicted Branching Ratios	Amplitudes with SU(3) Symmetry and no final-state Interactions		Amplitudes with SU(3) breaking and final-state interactions
$\mathcal{D}^+ \to \phi K^{*+}$		$-(s_1)^2 \times \{\mathcal{L}+\mathcal{D}_h\}$	$\to$	$\{\mathcal{L}+\mathcal{D}_h\}e^{i\delta^{\phi K^*}}$
$\to \omega K^{*+}$		$-(1/\sqrt{2})(s_1)^2 \times \{\mathcal{A}+\mathcal{D}+2\mathcal{D}_h\}$	$\to$	$\{\mathcal{A}+\mathcal{D}+2\mathcal{D}_h\}e^{i\delta^{\omega K^*}}$
$\to \rho^+ K^{*0}$		$-(s_1)^2 \times \{\mathcal{B}+\mathcal{D}\}$	$\to$	$\{(\mathcal{B}+\mathcal{D})+(\mathcal{A}-\mathcal{B}-2\mathcal{D})(1/3)(1-e^{-i\Delta_{\rho K^*}})\}e^{i\delta_{3/2}^{\rho K^*}}$
$\to \rho^0 K^{*+}$		$(1/\sqrt{2})(s_1)^2 \times \{\mathcal{A}-\mathcal{D}\}$	$\to$	$\{(\mathcal{A}-\mathcal{D})-(\mathcal{A}-\mathcal{B}-2\mathcal{D})(2/3)(1-e^{-i\Delta_{\rho K^*}})\}e^{i\delta_{3/2}^{\rho K^*}}$
$\mathcal{D}^0 \to \phi\ K^{*0}$		$-(s_1)^2 \times \{\mathcal{L}+\mathcal{C}_h\}$	$\to$	$\{\mathcal{L}+\mathcal{C}_h\}e^{i\delta^{\phi K^*}}$
$\to \omega\ K^{*0}$	6×10^{-5}	$-(1/\sqrt{2})(s_1)^2 \times \{\mathcal{B}+\mathcal{C}+2\mathcal{C}_h\}$	$\to$	$\{\mathcal{B}+\mathcal{C}'+2\mathcal{C}_h\}e^{i\delta^{\omega K^*}}$
$\to \rho^- K^{*+}$		$-(s_1)^2 \times \{\mathcal{A}+\mathcal{C}\}$	$\to$	$\{(\mathcal{A}+\mathcal{C})-2/3(\mathcal{A}+\mathcal{B})(1-e^{i\Delta_{\rho K^*}})\}e^{i\delta_{1/2}^{\rho K^*}}$
$\to \rho^0 K^{*0}$		$-(1/\sqrt{2})(s_1)^2 \times \{\mathcal{B}-\mathcal{C}\}$	$\to$	$\{(\mathcal{B}-\mathcal{C})-1/3(\mathcal{A}+\mathcal{B})(1-e^{i\Delta_{\rho K^*}})\}e^{i\delta_{1/2}^{\rho K^*}}$
$\mathcal{D}_s^+ \to K^{*+}K^{*0}$		$-(s_1)^2 \times \{\mathcal{A}+\mathcal{B}\}$	$\to$	$\{(\mathcal{A}+\mathcal{B})\}e^{i\delta_1^{K^*K^*}}$

The possible presence of hairpin diagrams is analyzed in the model-independent quark-diagram scheme for two-body decays of charmed mesons. Current experimental data do not necessarily require the presence of hairpin diagrams in $D \to VP$ (V: vector meson, P: pseudoscalar meson), in accordance with the *OZI* rule. However, there is a possible indication that they are important in the decay of $D \to PP$. The measurement of $D_3^+ \to \pi^+\eta'$ is crucial to test the mechanism of hairpin diagrams.

I.b. Interesting Physics in B Decays and CP Noninvariance

Recently, experimental limits on some rare exclusive decays of B mesons have been given by Avery et al. (CLEO collaboration). We have studied their implications, as well as future calculations and measurements. For such discussions, we have used the model-independent quark-diagram scheme. Results are given in Table IV.

The salient feature of charmless rare B decays is that they can proceed either through the W-loop diagrams $\mathcal{E}$ and $\mathcal{F}$ without Kobayashi-Maskawa (KM) mixing suppression, or through the W-tree diagrams $\mathcal{A}, \mathcal{B}, \mathcal{C}$, and $\mathcal{D}$ with KM-mixing double suppression (see Table IV). There are also some decays which can occur solely via the W-loop diagrams, e.g., $B_d^0(\equiv \bar{b}d) \to \phi K^0$, ϕK^{*0}; $B_s^0 \to \overline{K}^0\phi$, $\overline{K}^{*0}\phi$, $B_{d,s}^0 \to \phi\phi$, $K^0\overline{K}^0$, $K^{*0}\overline{K}^0$, $K^0\overline{K}^{*0}$, $K^{*0}\overline{K}^{*0}$. In any case, W-loop diagrams play an essential role in rare B decays, and the measurements of these decays will provide the test of the mechanism of the W-loop diagrams (or their one gluon-exchange approximation, the penguin diagram) and give some insight of QCD calculations.

A general convenient way to search for decay-amplitude CP noninvariance is to measure the partial-decay-rate differences between a particle and its antiparticle. It was shown that the quark-diagram scheme can provide a model-independent general survey of whether decay-amplitude CP noninvariance can exist in a particular exclusive decay in the KM model of CP noninvariance. A general picture has emerged that the partial-decay-rate differences can be very large, tens of percent b-flavored particle decays. Such large partial-decay-rate differences are very encouraging. The decays of $B_d^0 \to K^+\pi^-$ and $K^\pm\rho^0$, $\overline{K}^{*0}\pi^\pm$, $K^\pm\pi^+\pi^-$ discussed by us have the particular advantage in the simplicity in detecting its final particles which are all charged.

(1) To determine how important the W-loop diagrams are, measurements of

$$B_d^0 \to \phi K^0,\ \phi K^{*0};\ B_s^0 \to \overline{K}^0\phi,\ \overline{K}^{*0}\phi;\ \text{and}$$
$$B_{d,s}^0 \to \phi\phi,\ K^0\overline{K}^0,\ K^{*0}\overline{K}^0,\ K^0\overline{K}^{*0},\ K^{*0}\overline{K}^{*0};$$

are important, since these decays can only arise from the W-loop diagrams. It is interesting to note that $B_d \to \phi\phi$ comes only from the vertical W-loop diagram $\mathcal{F}$; and $B_d \to K^0\phi$, $K^{*0}\phi$, $B_s^0 \to \overline{K}^0\phi$, $\overline{K}^{*0}\phi$ comes only from the horizontal loop diagram $\mathcal{E}$.

(2) Theoretical calculations of the nonleptonic decays are still very rudimentary. Here we give a qualitative discussion on the current estimates. The branching ratios of rare B decays are $\simeq 10^{-4} \sim 10^{-6}$. The theoretical uncertainties lie in the estimates of the spacelike penguin diagram. We estimate that the inclusion of this amplitude will change our results by a factor of 3 in either direction. Most rare decay modes are primarily or exclusively dominated by the W-loop diagrams. However, for decays which can proceed via the external W-emission mechanism $\mathcal{A}$, the contribution of the amplitude $\mathcal{A}$ is comparable to that of the W-loop amplitude $\mathcal{E}$. For instance, we find $|V_{cs}V_{cb}^*\mathcal{E}/V_{us}V_{ub}^*\mathcal{A}| = 0.44$, 2.0, 1.3, respectively, for $B_u^+ \to K^+\pi^0$, $K^+\rho^0$, $K^{+*}\pi^0$.

(3) The size of the Penguin diagram (one gluon-exchange approximation of the W-loop diagram) had been estimated to be very small. Here we can obtain further understanding by comparing our theoretical calculation $B_r(B_d^0 \to k^+\pi^-) = 1 \times 10^{-4}$, including both the $\mathcal{A}$ and $\mathcal{E}$ amplitudes in the general formulation, with the new experimental data of $B_r(B_d^0 \to k^+\pi^-) \leq 3.2 \times 10^{-4}$. We obtain $|\mathcal{E}/\mathcal{A}| \sim 10^{-2}$, i.e. the W-loop graph is negligibly small compared to the W-emission diagram. This may cast further doubt on Penguin mechanics for the origin of the $\Delta I = 1/2$ rule in K decays.

(4) For KM-mixing-favored B or charm decays, e.g., $B_u^+ \to F^+\overline{D}^0$, it is known that whenever one of the pseudoscalar mesons is replaced by the corresponding vector meson, e.g., $B_u^+ \to F^{*+}\overline{D}^0$, the branching ratio is enhanced because of the large coupling of the vector meson. This is no longer true for rare B decays. From Table IV, we find the pattern $Br(B \to P_1P_2) \approx Br(B \to P_1V_2) > Br(B \to V_1P_2)$ where V_1 is the vector meson which comes directly from the b-quark decay, whereas V_2 comes from other parts of the diagrams.

This pattern can be traced back to the differences in the penguin-diagram contribution. For $B \to V_1 P_2$, the interference between $(V-A)(V-A)$ and $(S+P)(S-P)$ parts is destructive, while such interference is constructive in $B \to P_1 P_2$ decays. For $B \to P_1 V_2$ there is no $(S+P)(S-P)$ contribution since the matrix element $< V|\bar{q}'_L q_R|0 >= 0$.

(5) Large purely decay-amplitude CP-violating effects of order 0.2-0.5 can exhibit in decay modes which proceed via the W-tree graphs with doubly suppressed KM mixing coefficients and via the W-loop diagram with favored KM mixing coefficients: e.g. $B_u^+ \to K^+\rho^0$, $K^{*+}\pi^0$; $B_d^0 \to K^+\rho^-$, $K^{*+}\pi^-$, $\pi^+\pi^-$, $K^+\pi^-$; $B_s^0 \to K^+K^-$, $K^0\pi^0$. For $B_u^+ \to K^0\pi^+$, $K^0\rho^+$, $K^{*0}\pi^+$, $K^+\phi$, $K^+\omega$, the CP-noninvariant partial-decay-rate differences arises from the interference between the annihilation diagrams $\mathcal{C}$ and $\mathcal{D}$ with the time-like penguin amplitude, and are suppressed by the smallness of these W-annihilation amplitude in most model calculations. The upper bound of the CP asymmetry in these decays is given in Table IV. If in nature these diagrams $\mathcal{C}$ and $\mathcal{D}$ are not suppressed comparing to diagram $\mathcal{A}$. The partial-decay-rate differences of these decays can also become tens of percent.

(6) Note that partial-decay-rate differences can exist only in mixing-matrix-suppressed channels. The large partial-decay-rate differences in these decays of B particles are a trade-off effect from the severe mixing matrix suppression (see Ref. 10 for a general discussion including the charm and top particles) which give small branching ratios of these decays $\sim 10^{-4} - 10^{-5}$. But this is a nice trade off because the number of events needed to see the effect is $\sim \Delta^{-2} Br^{-1}$. So to see a Δ of 50% a 100-event reconstruction out of $10^5 \sim 10^7$ B particles is sufficient.

(7) For detecting the partial-decay-difference effect, the decays of charge $B^\pm$ always have the advantage over neutral B^0, $\overline{B}^0$ decays since the latter exhibit the mixing effects in addition and experimental tagging is needed. Conceptually the partial-decay-rate differences in charged-B decays are also simpler. They are purely from decay-amplitude CP noninvariance effects. Some neutral B particle decays have similar advantages, e.g. as was pointed out in Ref. 9, the partial-decay-rate differences in neutral B^0 decays such as $B_d^0 \to K^+\pi^-$, D^-F^+, i.e. $B_d \to (s=1, c=0$ states), which are not CP self-conjugate states and into which only B^0 (not $\overline{B}^0$) can decay into them. are purely decay-amplitude type of CP noninvariance. There

are neither $B^0 \rightleftharpoons \overline{B}^0$ mixing effects, nor mass-matrix CP noninvariance is involved. Therefore the interpretations of any observations of such partial-decay-rate differences are straightforward. There are neutral channels into which both B^0, $\overline{B}^0$ can decay, e.g., $B_d^0 \to \pi^+\rho^-$, $\pi^-\rho^+$, $\pi^+\pi^-$, D^+D^- i.e. $s = 0$, $c = 0$ final states. Their time integrated partial-decay-rate differences are results of all three following distinct effects: decay-amplitude CP nonvariance, mass-matrix CP noninvariance, and $B^0 \rightleftharpoons \overline{B}^0$ mixing. Therefore the interpretations of observed results of partial-decay-rate differences in these channels are more complicated. To separate these three effects, two more different types of experiments measuring $B^0 \rightleftharpoons \overline{B}^0$ mixing and mass-matrix type of CP non-invariance are needed.

Branching ratios of nonleptonic exclusive two-body decays of charged B mesons without final-state charm particles are studied in detail. The technique used for evaluating the nonleptonic decay amplitudes is elucidated. Charmless decay channels, such as $B_u^+ \to K^+\eta', \pi^+\eta', p^+\pi^0, p^+\eta, p^+\eta', p^+w, B_d^0 \to K^0\eta', \eta\eta', \eta'\eta', K^{*+}\pi^-, p^+\pi^-, K^{*+}p^-, p^+p^-$, should be accessible experimentally in the near future. The implications of the quark-diagram scheme are also discussed. See results in Table.

In conclusion, the rare B decays provide valuable opportunities to advance our understanding on dynamics of nonleptonic decays, and to look for new CP-noninvariance effects.

TABLE II

	Reaction	Amplitude				$(Br)_{theory}$	*exp. limits from* ARGUS	CLEO
$B_d^\circ \to$	$K^+\pi^-$	$V_{us}V_{ub}^*$	$(\mathcal{A}+\mathcal{E}_{u-c})$	$+V_{ts}V_{tb}^*$	$(\mathcal{E}_{t-c})$	1.7×10^{-5}	1.8×10^{-4}	0.9×10^{-4}
$\to$	$K^\circ\bar{K}^\circ$	$V_{ud}V_{ub}^*$	$(\mathcal{E}_{u-c}+\mathcal{F}_{u-c})$	$+V_{td}V_{tb}^*$	$(\mathcal{E}_{t-c}+\mathcal{F}_{t-c})$	1.2×10^{-6}		
$\to$	$K^\circ\pi^\circ$	$V_{us}V_{ub}^*\frac{1}{\sqrt{2}}$	$(\mathcal{B}-\mathcal{E}_{u-c})$	$+V_{ts}V_{tb}^*\frac{1}{\sqrt{2}}$	$(-\mathcal{E}_{t-c})$	6.0×10^{-6}		
$\to$	$K^\circ\eta$	$V_{us}V_{ub}^*\frac{1}{\sqrt{3}}$	$(\mathcal{B}+\mathcal{E}_{u-c}-\mathcal{E}_{u-c})$	$+V_{ts}V_{tb}^*\frac{1}{\sqrt{3}}$	$(\mathcal{E}_{t-c}-\mathcal{E}_{t-c})$	1.7×10^{-6}		
$\to$	$K^\circ\eta'$	$V_{us}V_{ub}^*\frac{1}{\sqrt{6}}$	$(\mathcal{B}+\mathcal{E}_{u-c}+2\mathcal{E}_{u-c})$	$+V_{ts}V_{tb}^*\frac{1}{\sqrt{6}}$	$(\mathcal{E}_{t-c}+2\mathcal{E}_{t-c})$	2.9×10^{-5}		
$\to$	$\pi^+\pi^-$	$V_{ud}V_{ub}^*$	$(\mathcal{A}+\mathcal{C}+\mathcal{E}_{u-c}+\mathcal{F}_{u-c})$	$+V_{td}V_{tb}^*$	$(\mathcal{E}_{t-c}+\mathcal{F}_{t-c})$	1.3×10^{-5}	1.3×10^{-4}	0.9×10^{-4}
$\to$	$\pi^\circ\pi^\circ$	$V_{ud}V_{ub}^*\frac{1}{2}$	$(-\mathcal{B}+\mathcal{C}+\mathcal{E}_{u-c}+\mathcal{F}_{u-c})$	$+V_{td}V_{tb}^*\frac{1}{2}$	$(\mathcal{E}_{t-c}+\mathcal{F}_{t-c})$	1.0×10^{-6}		
$\to$	$\pi^\circ\eta$	$V_{ud}V_{ub}^*\frac{1}{\sqrt{6}}$	$(\underline{\mathcal{B}}-\mathcal{B}+\underline{\mathcal{C}}-\mathcal{C}-\mathcal{E}_{u-c}-\mathcal{E}_{u-c})$	$+V_{td}V_{tb}^*\frac{1}{\sqrt{6}}$	$(-\mathcal{E}_{t-c}-\mathcal{E}_{t-c})$	4.1×10^{-6}	1.8×10^{-3}	
$\to$	$\pi^\circ\eta'$	$V_{ud}V_{ub}^*\frac{1}{2\sqrt{3}}$	$(\underline{\mathcal{B}}-\mathcal{B}+\underline{\mathcal{C}}+\mathcal{C}-\mathcal{E}_{u-c}-\mathcal{E}_{u-c})$	$+V_{td}V_{tb}^*\frac{1}{2\sqrt{3}}$	$(-\mathcal{E}_{t-c}-\mathcal{E}_{t-c})$	1.3×10^{-5}		
$\to$	$\eta\eta$	$V_{ud}V_{ub}^*\frac{1}{3}$	$(\mathcal{B}+\mathcal{C}+\mathcal{E}_{u-c}+\mathcal{F}_{u-c})$	$+V_{td}V_{tb}^*\frac{1}{3}$	$(\mathcal{E}_{t-c}+\mathcal{F}_{t-c})$	1.4×10^{-5}		
$\to$	$\eta\eta'$	$V_{ud}V_{ub}^*\frac{1}{3\sqrt{2}}$	$(\mathcal{B}+\underline{\mathcal{B}}+\mathcal{C}+\underline{\mathcal{C}}+\mathcal{E}_{u-c}+\mathcal{E}_{u-c})$	$+V_{td}V_{tb}^*\frac{1}{3\sqrt{2}}$	$(\mathcal{E}_{t-c}+\mathcal{E}_{t-c})$	4.2×10^{-5}		
$\to$	$\eta'\eta'$	$V_{ud}V_{ub}^*\frac{1}{6}$	$(\mathcal{B}+\mathcal{C}+\mathcal{E}_{u-c}+6\mathcal{F}_{u-c})$	$+V_{td}V_{tb}^*\frac{1}{6}$	$(\mathcal{E}_{t-c}+6\mathcal{F}_{t-c})$	3.0×10^{-5}		
$B_u^+ \to$	$K^+\pi^\circ$	$V_{us}V_{ub}^*\frac{1}{\sqrt{2}}$	$(\mathcal{A}+\mathcal{B}+\mathcal{D}+\mathcal{E}_{u-c})$	$+V_{ts}V_{tb}^*\frac{1}{\sqrt{2}}$	$(\mathcal{E}_{t-c})$	8.1×10^{-6}		
$\to$	$K^\circ\pi^+$	$V_{us}V_{ub}^*$	$(\mathcal{D}+\mathcal{E}_{u-c})$	$+V_{ts}V_{tb}^*$	$(\mathcal{E}_{t-c})$	1.2×10^{-5}	1.0×10^{-4}	9.0×10^{-5}
$\to$	$K^+\bar{K}^\circ$	$V_{ud}V_{ub}^*$	$(\mathcal{D}+\mathcal{E}_{u-c})$	$+V_{td}V_{tb}^*$	$(\mathcal{E}_{t-c})$	1.0×10^{-6}		
$\to$	$K^+\eta$	$V_{us}V_{ub}^*\frac{1}{\sqrt{3}}$	$(\mathcal{A}+\mathcal{B}+\mathcal{D}-\underline{\mathcal{D}}+\mathcal{E}_{u-c}-\mathcal{E}_{u-c})$	$+V_{ts}V_{tb}^*\frac{1}{\sqrt{3}}$	$(\mathcal{E}_{t-c}-\mathcal{E}_{t-c})$	4.5×10^{-6}		
$\to$	$K^+\eta'$	$V_{us}V_{ub}^*\frac{1}{\sqrt{6}}$	$(\mathcal{A}+\mathcal{B}+\mathcal{D}-2\underline{\mathcal{D}}+\mathcal{E}_{u-c}+2\mathcal{E}_{u-c})$	$+V_{ts}V_{tb}^*\frac{1}{\sqrt{6}}$	$(\mathcal{E}_{t-c}+2\mathcal{E}_{t-c})$	3.6×10^{-5}		
$\to$	$\pi^+\pi^\circ$	$V_{ud}V_{ub}^*\frac{1}{\sqrt{2}}$	$(\mathcal{A}+\mathcal{B})$			6.0×10^{-6}	2.4×10^{-4}	
$\to$	$\pi^+\eta$	$V_{ud}V_{ub}^*\frac{1}{\sqrt{3}}$	$(\mathcal{A}+\mathcal{B}+2\mathcal{D}+\mathcal{E}_{u-c}+\mathcal{E}_{u-c})$	$+V_{td}V_{tb}^*\frac{1}{\sqrt{3}}$	$(\mathcal{E}_{t-c}+\mathcal{E}_{t-c})$	5.6×10^{-6}‡	7.0×10^{-4}	
$\to$	$\pi^+\eta'$	$V_{ud}V_{ub}^*\frac{1}{\sqrt{6}}$	$(\mathcal{A}+\mathcal{B}+2\mathcal{D}+\mathcal{E}_{u-c}+\mathcal{E}_{u-c})$	$+V_{td}V_{tb}^*\frac{1}{\sqrt{6}}$	$(\mathcal{E}_{t-c}+\mathcal{E}_{t-c})$	1.5×10^{-5}‡		

TABLE III

	Reaction	Amplitude				$(Br)_{theory}$	exp. limits from ARGUS	exp. limits from CLEO
$B_d^o \to$	$K^{*o}\bar{K}^o$	$V_{ud}V_{ub}^*$	$(\mathcal{E}_{u-c}+\mathcal{F}_{u-c})$	$+V_{td}V_{tb}^*$	$(\mathcal{E}_{t-c}+\mathcal{F}_{t-c})$	3.9×10^{-8}		
$\to$	$K^o\bar{K}^{*o}$	$V_{ud}V_{ub}^*$	$(\mathcal{E}'_{u-c}+\mathcal{F}_{u-c})$	$+V_{td}V_{tb}^*$	$(\mathcal{E}'_{t-c}+\mathcal{F}_{t-c})$	1.0×10^{-6}		
$\to$	$K^+\rho^-$	$V_{us}V_{ub}^*$	$(\mathcal{A}'+\mathcal{E}_{u-c})$	$+V_{ts}V_{tb}^*$	$(\mathcal{E}_{t-c})$	1.9×10^{-6}		
$\to$	$K^o\rho^o$	$V_{us}V_{ub}^*\frac{1}{\sqrt{2}}$	$(\mathcal{B}'-\mathcal{E}_{u-c})$	$+V_{ts}V_{tb}^*\frac{1}{\sqrt{2}}$	$(-\mathcal{E}_{t-c})$	3.5×10^{-7}	1.6×10^{-4}	5.8×10^{-4}
$\to$	$K^{*+}\pi^-$	$V_{us}V_{ub}^*$	$(\mathcal{A}+\mathcal{E}'_{u-c})$	$+V_{ts}V_{tb}^*$	$(\mathcal{E}'_{t-c})$	1.9×10^{-5}	6.2×10^{-4}	4.4×10^{-4}
$\to$	$K^{*o}\pi^o$	$V_{us}V_{ub}^*\frac{1}{\sqrt{2}}$	$(\mathcal{B}-\mathcal{E}'_{u-c})$	$+V_{ts}V_{tb}^*\frac{1}{\sqrt{2}}$	$(-\mathcal{E}'_{t-c})$	4.7×10^{-6}		
$\to$	$K^o\phi$	$V_{us}V_{ub}^*$	$(\mathcal{E}'_{u-c})$	$+V_{ts}V_{tb}^*$	$(\mathcal{E}'_{t-c})$	8.9×10^{-6}	3.6×10^{-4}	4.9×10^{-4}
$\to$	$K^o\omega$	$V_{us}V_{ub}^*\frac{1}{\sqrt{2}}$	$(\mathcal{B}'+\mathcal{E}_{u-c})$	$+V_{ts}V_{tb}^*\frac{1}{\sqrt{2}}$	$(\mathcal{E}_{t-c})$	1.1×10^{-7}		
$\to$	$K^{*o}\eta$	$V_{us}V_{ub}^*\frac{1}{\sqrt{3}}$	$(\mathcal{B}-\mathcal{E}_{u-c}+\mathcal{E}'_{u-c})$	$+V_{ts}V_{tb}^*\frac{1}{\sqrt{3}}$	$(-\mathcal{E}_{t-c}+\mathcal{E}'_{t-c})$	4.5×10^{-6}		
$\to$	$K^{*o}\eta'$	$V_{us}V_{ub}^*\frac{1}{\sqrt{6}}$	$(\mathcal{B}+2\mathcal{E}_{u-c}+\mathcal{E}'_{u-c})$	$+V_{ts}V_{tb}^*\frac{1}{\sqrt{6}}$	$(2\mathcal{E}_{t-c}+\mathcal{E}'_{t-c})$	3.4×10^{-6}		
$\to$	$\rho^+\pi^-$	$V_{ud}V_{ub}^*$	$(\mathcal{A}+\mathcal{C}+\mathcal{E}'_{u-c}+\mathcal{F}_{u-c})$	$+V_{td}V_{tb}^*$	$(\mathcal{E}'_{t-c}+\mathcal{F}_{t-c})$	3.9×10^{-5}	5.2×10^{-4}	
$\to$	$\rho^-\pi^+$	$V_{ud}V_{ub}^*$	$(\mathcal{A}'+\mathcal{C}'+\mathcal{E}_{u-c}+\mathcal{F}_{u-c})$	$+V_{td}V_{tb}^*$	$(\mathcal{E}_{t-c}+\mathcal{F}_{t-c})$	1.1×10^{-5}		
$\to$	$\rho^o\pi^o$	$V_{ud}V_{ub}^*\frac{1}{2}$	$(-\mathcal{B}-\mathcal{B}'+\mathcal{C}+\mathcal{C}'+\mathcal{E}_{u-c}+\mathcal{E}'_{u-c})$	$+V_{td}V_{tb}^*\frac{1}{2}$	$(\mathcal{E}_{t-c}+\mathcal{E}'_{t-c})$	2.3×10^{-6}	4.0×10^{-4}	
$\to$	$\rho^o\eta$	$V_{ud}V_{ub}^*\frac{1}{\sqrt{6}}$	$(\mathcal{B}'-\mathcal{B}+\mathcal{C}+\mathcal{C}'-\mathcal{E}_{u-c}-\mathcal{E}'_{u-c})$	$+V_{td}V_{tb}^*\frac{1}{\sqrt{6}}$	$(-\mathcal{E}_{t-c}-\mathcal{E}'_{t-c})$	7.3×10^{-6}		
$\to$	$\rho^o\eta'$	$V_{ud}V_{ub}^*\frac{1}{2\sqrt{3}}$	$(\mathcal{B}'-\mathcal{B}+\mathcal{C}+\mathcal{C}'-\mathcal{E}_{u-c}-\mathcal{E}'_{u-c})$	$+V_{td}V_{tb}^*\frac{1}{2\sqrt{3}}$	$(-\mathcal{E}_{t-c}-\mathcal{E}'_{t-c})$	1.2×10^{-5}		
$\to$	$\omega\pi^o$	$V_{ud}V_{ub}^*\frac{1}{2}$	$(\mathcal{B}-\mathcal{B}'+\mathcal{C}+\mathcal{C}'-\mathcal{E}_{u-c}-\mathcal{E}'_{u-c})$	$+V_{td}V_{tb}^*\frac{1}{2}$	$(-\mathcal{E}_{t-c}-\mathcal{E}'_{t-c})$	1.2×10^{-5}	4.6×10^{-4}	
$\to$	$\omega\eta$	$V_{ud}V_{ub}^*\frac{1}{\sqrt{6}}$	$(\mathcal{B}'+\mathcal{B}+\mathcal{C}+\mathcal{C}'+\mathcal{E}_{u-c}+\mathcal{E}'_{u-c})$	$+V_{td}V_{tb}^*\frac{1}{\sqrt{6}}$	$(\mathcal{E}_{t-c}+\mathcal{E}'_{t-c})$	4.7×10^{-6}		
$\to$	$\omega\eta'$	$V_{ud}V_{ub}^*\frac{1}{2\sqrt{3}}$	$(\mathcal{B}'+\mathcal{B}+\mathcal{C}+\mathcal{C}'+\mathcal{E}_{u-c}+\mathcal{E}'_{u-c})$	$+V_{td}V_{tb}^*\frac{1}{2\sqrt{3}}$	$(\mathcal{E}_{t-c}+\mathcal{E}'_{t-c})$	1.5×10^{-5}		
$\to$	$\phi\eta$	$V_{ud}V_{ub}^*\frac{1}{\sqrt{3}}$	$(-\mathcal{F}_{u-c})$	$+V_{td}V_{tb}^*\frac{1}{\sqrt{3}}$	$(-\mathcal{F}_{t-c})$	--		
$\to$	$\phi\eta'$	$V_{ud}V_{ub}^*\frac{1}{\sqrt{6}}$	$(2\mathcal{F}_{u-c})$	$+V_{td}V_{tb}^*\frac{1}{\sqrt{6}}$	$(2\mathcal{F}_{t-c})$	--		
$B_u^+ \to$	$K^+\rho^o$	$V_{us}V_{ub}^*\frac{1}{\sqrt{2}}$	$(\mathcal{A}'+\mathcal{B}'+\mathcal{D}'+\mathcal{E}_{u-c})$	$+V_{ts}V_{tb}^*\frac{1}{\sqrt{2}}$	$(\mathcal{E}_{t-c})$	6.0×10^{-7}	1.8×10^{-4}	7.0×10^{-5}
$\to$	$K^{*+}\pi^o$	$V_{us}V_{ub}^*\frac{1}{\sqrt{2}}$	$(\mathcal{A}+\mathcal{B}+\mathcal{D}+\mathcal{E}'_{u-c})$	$+V_{ts}V_{tb}^*\frac{1}{\sqrt{2}}$	$(\mathcal{E}'_{t-c})$	8.9×10^{-6}		
$\to$	$K^o\rho^+$	$V_{us}V_{ub}^*$	$(\mathcal{D}'+\mathcal{E}_{u-c})$	$+V_{ts}V_{tb}^*$	$(\mathcal{E}_{t-c})$	3.4×10^{-7}		
$\to$	$K^{*o}\pi^+$	$V_{us}V_{ub}^*$	$(\mathcal{D}+\mathcal{E}'_{u-c})$	$+V_{ts}V_{tb}^*$	$(\mathcal{E}'_{t-c})$	8.8×10^{-6}	1.7×10^{-4}	1.3×10^{-4}
$\to$	$K^+\phi$	$V_{us}V_{ub}^*$	$(\mathcal{D}+\mathcal{E}'_{u-c})$	$+V_{ts}V_{tb}^*$	$(\mathcal{E}'_{t-c})$	1.4×10^{-5}	1.8×10^{-4}	8.0×10^{-5}
$\to$	$K^+\omega$	$V_{us}V_{ub}^*\frac{1}{\sqrt{2}}$	$(\mathcal{A}'+\mathcal{B}'+\mathcal{D}'+\mathcal{E}_{u-c})$	$+V_{ts}V_{tb}^*\frac{1}{\sqrt{2}}$	$(\mathcal{E}_{t-c})$	1.4×10^{-6}		
$\to$	$\rho^+\pi^o$	$V_{ud}V_{ub}^*\frac{1}{\sqrt{2}}$	$(\mathcal{A}+\mathcal{B}-\mathcal{E}_{u-c}+\mathcal{E}'_{u-c})$	$+V_{td}V_{tb}^*\frac{1}{\sqrt{2}}$	$(-\mathcal{E}_{t-c}+\mathcal{E}'_{t-c})$	1.7×10^{-5}	5.5×10^{-4}	
$\to$	$\rho^o\pi^+$	$V_{ud}V_{ub}^*\frac{1}{\sqrt{2}}$	$(\mathcal{A}'+\mathcal{B}'+\mathcal{E}_{u-c}-\mathcal{E}'_{u-c})$	$+V_{td}V_{tb}^*\frac{1}{\sqrt{2}}$	$(\mathcal{E}_{t-c}-\mathcal{E}'_{t-c})$	3.7×10^{-6}	1.5×10^{-4}	1.5×10^{-4}
$\to$	$\omega\pi^+$	$V_{ud}V_{ub}^*\frac{1}{\sqrt{2}}$	$(\mathcal{A}'+\mathcal{B}'+2\mathcal{D}'+\mathcal{E}_{u-c}+\mathcal{E}'_{u-c})$	$+V_{td}V_{tb}^*\frac{1}{\sqrt{2}}$	$(\mathcal{E}_{t-c}+\mathcal{E}'_{t-c})$	4.7×10^{-6}	4.0×10^{-4}	
$\to$	$K^{*+}\bar{K}^o$	$V_{ud}V_{ub}^*$	$(\mathcal{D}'+\mathcal{E}_{u-c})$	$+V_{td}V_{tb}^*$	$(\mathcal{E}_{t-c})$	3.9×10^{-8}		
$\to$	$K^+\bar{K}^{*o}$	$V_{ud}V_{ub}^*$	$(\mathcal{D}+\mathcal{E}'_{u-c})$	$+V_{td}V_{tb}^*$	$(\mathcal{E}'_{t-c})$	1.0×10^{-6}		
$\to$	$K^{*+}\eta$	$V_{us}V_{ub}^*\frac{1}{\sqrt{3}}$	$(\mathcal{A}+\mathcal{B}-\mathcal{E}_{u-c}+\mathcal{E}'_{u-c})$	$+V_{ts}V_{tb}^*\frac{1}{\sqrt{3}}$	$(-\mathcal{E}_{t-c}+\mathcal{E}'_{t-c})$	1.2×10^{-5}		
$\to$	$K^{*+}\eta'$	$V_{us}V_{ub}^*\frac{1}{\sqrt{6}}$	$(\mathcal{A}+\mathcal{B}+3\mathcal{D}+2\mathcal{E}_{u-c}+\mathcal{E}'_{u-c})$	$+V_{ts}V_{tb}^*\frac{1}{\sqrt{6}}$	$(2\mathcal{E}_{t-c}+\mathcal{E}'_{t-c})$	8.1×10^{-6}		
$\to$	$\rho^+\eta$	$V_{ud}V_{ub}^*\frac{1}{\sqrt{3}}$	$(\mathcal{A}+\mathcal{B}+2\mathcal{D}+\mathcal{E}_{u-c}+\mathcal{E}'_{u-c})$	$+V_{td}V_{tb}^*\frac{1}{\sqrt{3}}$	$(\mathcal{E}_{t-c}+\mathcal{E}'_{t-c})$	4.3×10^{-5}		
$\to$	$\rho^+\eta'$	$V_{ud}V_{ub}^*\frac{1}{\sqrt{6}}$	$(\mathcal{A}+\mathcal{B}+2\mathcal{D}+\mathcal{E}_{u-c}+\mathcal{E}'_{u-c})$	$+V_{td}V_{tb}^*\frac{1}{\sqrt{6}}$	$(\mathcal{E}_{t-c}+\mathcal{E}'_{t-c})$	5.3×10^{-5}		

TABLE IV

	Reaction	Amplitude				$(Br)_{theory}$	*exp. limits from* ARGUS	CLEO
$B_d^o \to$	$K^{*+}\rho^-$	$V_{us}V_{ub}^*$	$(\mathcal{A}+\mathcal{E}_{u-c})$	$+V_{ts}V_{tb}^*$	$(\mathcal{E}_{t-c})$	1.8×10^{-5}		
$\to$	$K^{*o}\bar{K}^{*o}$	$V_{ud}V_{ub}^*$	$(\mathcal{E}_{u-c}+\mathcal{F}_{u-c})$	$+V_{td}V_{tb}^*$	$(\mathcal{E}_{t-c}+\mathcal{F}_{t-c})$	9.6×10^{-7}		
$\to$	$K^{*o}\rho^o$	$V_{us}V_{ub}^*\frac{1}{\sqrt{2}}$	$(\mathcal{B}-\mathcal{E}_{u-c})$	$+V_{ts}V_{tb}^*\frac{1}{\sqrt{2}}$	$(-\mathcal{E}_{t-c})$	4.7×10^{-6}	4.6×10^{-4}	6.7×10^{-4}
$\to$	$K^{*o}\phi$	$V_{us}V_{ub}^*$	$(\mathcal{E}_{u-c})$	$+V_{ts}V_{tb}^*$	$(\mathcal{E}_{t-c})$	9.0×10^{-6}	3.2×10^{-4}	4.4×10^{-4}
$\to$	$K^{*o}\omega$	$V_{us}V_{ub}^*\frac{1}{\sqrt{2}}$	$(\mathcal{B}+\mathcal{E}_{u-c})$	$+V_{ts}V_{tb}^*\frac{1}{\sqrt{2}}$	$(\mathcal{E}_{t-c})$	8.1×10^{-6}		
$\to$	$\rho^+\rho^-$	$V_{ud}V_{ub}^*$	$(\mathcal{A}+\mathcal{C}+\mathcal{E}_{u-c}+\mathcal{F}_{u-c})$	$+V_{td}V_{tb}^*$	$(\mathcal{E}_{t-c}+\mathcal{F}_{t-c})$	3.4×10^{-5}	2.2×10^{-3}	
$\to$	$\rho^o\rho^o$	$V_{ud}V_{ub}^*\frac{1}{2}$	$(-\mathcal{B}+\mathcal{C}+\mathcal{E}_{u-c}+\mathcal{F}_{u-c})$	$+V_{td}V_{tb}^*\frac{1}{2}$	$(\mathcal{E}_{t-c}+\mathcal{F}_{t-c})$	1.6×10^{-6}	2.8×10^{-4}	3.4×10^{-4}
$\to$	$\rho^o\omega$	$V_{ud}V_{ub}^*\frac{1}{2}$	$(-\mathcal{B}+\mathcal{B}'-\mathcal{E}_{u-c}-\mathcal{E}'_{u-c})$	$+V_{td}V_{tb}^*\frac{1}{2}$	$(-\mathcal{E}_{t-c}-\mathcal{E}'_{t-c})$	3.9×10^{-7}		
$\to$	$\omega\omega$	$V_{ud}V_{ub}^*\frac{1}{2}$	$(\mathcal{B}+\mathcal{C}+\mathcal{E}_{u-c}+\mathcal{F}_{u-c})$	$+V_{td}V_{tb}^*\frac{1}{2}$	$(\mathcal{E}_{t-c}+\mathcal{F}_{t-c})$	2.8×10^{-6}		
$\to$	$\phi\phi$	$V_{ud}V_{ub}^*$	$(\mathcal{F}_{u-c})$	$+V_{td}V_{tb}^*$	$(\mathcal{F}_{t-c})$	—		
$B_u^+ \to$	$K^{*+}\rho^o$	$V_{us}V_{ub}^*\frac{1}{\sqrt{2}}$	$(\mathcal{A}+\mathcal{B}+\mathcal{D}+\mathcal{E}_{u-c})$	$+V_{ts}V_{tb}^*\frac{1}{\sqrt{2}}$	$(\mathcal{E}_{t-c})$	7.6×10^{-6}		
$\to$	$K^{o*}\rho^+$	$V_{us}V_{ub}^*$	$(\mathcal{D}+\mathcal{E}_{u-c})$	$+V_{ts}V_{tb}^*$	$(\mathcal{E}_{t-c})$	8.0×10^{-6}	9.0×10^{-4}	
$\to$	$K^{*+}\phi$	$V_{us}V_{ub}^*$	$(\mathcal{D}+\mathcal{E}_{u-c})$	$+V_{ts}V_{tb}^*$	$(\mathcal{E}_{t-c})$	8.2×10^{-6}		
$\to$	$K^{*+}\omega$	$V_{us}V_{ub}^*\frac{1}{\sqrt{2}}$	$(\mathcal{A}+\mathcal{B}+\mathcal{D}+\mathcal{E}_{u-c})$	$+V_{ts}V_{tb}^*\frac{1}{\sqrt{2}}$	$(\mathcal{E}_{t-c})$	1.5×10^{-5}	1.3×10^{-4}	
$\to$	$K^{*+}\bar{K}^{*o}$	$V_{ud}V_{ub}^*$	$(\mathcal{D}+\mathcal{E}_{u-c})$	$+V_{td}V_{tb}^*$	$(\mathcal{E}_{t-c})$	1.0×10^{-6}		
$\to$	$\rho^+\rho^o$	$V_{ud}V_{ub}^*\frac{1}{\sqrt{2}}$	$(\mathcal{A}+\mathcal{B})$			1.4×10^{-5}	1.0×10^{-3}	
$\to$	$\rho^+\omega$	$V_{ud}V_{ub}^*\frac{1}{\sqrt{2}}$	$(\mathcal{A}+\mathcal{B}+2\mathcal{D}+\mathcal{E}_{u-c}+\mathcal{E}'_{u-c})$	$+V_{td}V_{tb}^*\frac{1}{\sqrt{2}}$	$(\mathcal{E}_{t-c}+\mathcal{E}'_{t-c})$	2.5×10^{-5}		

TABLE V

Reaction	Amplitude				$(Br)_{theory}$	*exp. limits from* ARGUS	CLEO
$B_d^o \to K^+ a_1^-$	$V_{us}V_{ub}^*$	$(\mathcal{A}+\mathcal{E}_{u-c})$	$+V_{ts}V_{tb}^*$	$(\mathcal{E}_{t-c})$			
$\to K^o a_1^o$	$V_{us}V_{ub}^* \frac{1}{\sqrt{2}}$	$(\mathcal{B}+\mathcal{E}_{u-c})$	$+V_{ts}V_{tb}^* \frac{1}{\sqrt{2}}$	$(\mathcal{E}_{t-c})$			
$\to \pi^+ a_1^-$	$V_{ud}V_{ub}^*$	$(\mathcal{A}+\mathcal{C}+\mathcal{E}_{u-c}+\mathcal{E}_{u-c}+\mathcal{F}_{u-c})$	$+V_{td}V_{tb}^*$	$(\mathcal{E}_{t-c}+\mathcal{E}_{t-c}+\mathcal{F}_{t-c})$		6.3×10^{-4}	5.7×10^{-4}
$\to \pi^- a_1^+$	$V_{ud}V_{ub}^*$	$(\mathcal{A}+\mathcal{C}+\mathcal{E}_{u-c}+\mathcal{E}_{u-c}+\mathcal{F}_{u-c})$	$+V_{td}V_{tb}^*$	$(\mathcal{E}_{t-c}+\mathcal{E}_{t-c}+\mathcal{F}_{t-c})$			5.7×10^{-4}
$\to \pi^o a_1^o$	$V_{ud}V_{ub}^* \frac{1}{2}$	$(-\mathcal{B}-\mathcal{B}+\mathcal{C}+\mathcal{E}_{u-c}+\mathcal{E}_{u-c}+\mathcal{F}_{u-c})$	$+V_{td}V_{tb}^* \frac{1}{2}$	$(\mathcal{E}_{t-c}+\mathcal{E}_{t-c}+\mathcal{F}_{t-c})$		1.1×10^{-3}	
$\to \eta a_1^o$	$V_{ud}V_{ub}^* \frac{1}{\sqrt{6}}$	$(-\mathcal{B}+\mathcal{B}+\mathcal{C}-\mathcal{E}_{u-c}-\mathcal{E}_{u-c})$	$+V_{td}V_{tb}^* \frac{1}{\sqrt{6}}$	$(-\mathcal{E}_{t-c}-\mathcal{E}_{t-c})$			
$\to \eta' a_1^o$	$V_{ud}V_{ub}^* \frac{1}{2\sqrt{3}}$	$(-\mathcal{B}+\mathcal{B}+\mathcal{C}-\mathcal{E}_{u-c}-\mathcal{E}_{u-c})$	$+V_{td}V_{tb}^* \frac{1}{2\sqrt{3}}$	$(-\mathcal{E}_{t-c}-\mathcal{E}_{t-c})$			
$B_u^+ \to \pi^o a_1^+$	$V_{ud}V_{ub}^* \frac{1}{\sqrt{2}}$	$(\mathcal{A}+\mathcal{B}-\mathcal{E}_{u-c}+\mathcal{E}'_{u-c})$	$+V_{td}V_{tb}^* \frac{1}{\sqrt{2}}$	$(-\mathcal{E}_{t-c}+\mathcal{E}'_{t-c})$		1.7×10^{-3}	
$\to \pi^+ a_1^o$	$V_{ud}V_{ub}^* \frac{1}{\sqrt{2}}$	$(\mathcal{A}'+\mathcal{B}'+\mathcal{E}_{u-c}-\mathcal{E}'_{u-c})$	$+V_{td}V_{tb}^* \frac{1}{\sqrt{2}}$	$(\mathcal{E}_{t-c}-\mathcal{E}'_{t-c})$		9.0×10^{-4}	
$\to K^o a_1^+$	$V_{us}V_{ub}^*$	$(\mathcal{D}+\mathcal{E}_{u-c})$	$+V_{ts}V_{tb}^*$	$(\mathcal{E}_{t-c})$			
$\to K^+ a_1^o$	$V_{us}V_{ub}^* \frac{1}{\sqrt{2}}$	$(\mathcal{A}+\mathcal{B}+\mathcal{D}+\mathcal{E}_{u-c})$	$+V_{ts}V_{tb}^* \frac{1}{\sqrt{2}}$	$(\mathcal{E}_{t-c})$			
$\to \eta a_1^+$	$V_{ud}V_{ub}^* \frac{1}{\sqrt{3}}$	$(\mathcal{A}+\mathcal{B}+2\mathcal{D}+\mathcal{E}_{u-c}+\mathcal{E}'_{u-c})$	$+V_{td}V_{tb}^* \frac{1}{\sqrt{3}}$	$(\mathcal{E}_{t-c}+\mathcal{E}'_{t-c})$			
$\to \eta' a_1^+$	$V_{ud}V_{ub}^* \frac{1}{\sqrt{6}}$	$(\mathcal{A}+\mathcal{B}+2\mathcal{D}+\mathcal{E}_{u-c}+\mathcal{E}'_{u-c})$	$+V_{td}V_{tb}^* \frac{1}{\sqrt{6}}$	$(\mathcal{E}_{t-c}+\mathcal{E}'_{t-c})$			

TABLE VI

	Reaction	Amplitude				$(Br)_{theory}$	exp. limits from ARGUS	exp. limits from CLEO
$B_d^o \to$	$K^{*+}a_1^-$	$V_{us}V_{ub}^*$	$(\mathcal{A}+\mathcal{E}_{u-c})$	$+V_{ts}V_{tb}^*$	$(\mathcal{E}_{t-c})$			
$\to$	$K^{*o}a_1^o$	$V_{us}V_{ub}^*\frac{1}{\sqrt{2}}$	$(\mathcal{B}+\mathcal{E}_{u-c})$	$+V_{ts}V_{tb}^*\frac{1}{\sqrt{2}}$	$(\mathcal{E}_{t-c})$			
$\to$	$\rho^+a_1^-$	$V_{ud}V_{ub}^*$	$(\mathcal{A}'+\mathcal{C}+\mathcal{E}_{u-c}+\mathcal{E}'_{u-c}+\mathcal{F}_{u-c})$	$+V_{td}V_{tb}^*$	$(\mathcal{E}_{t-c}+\mathcal{E}'_{t-c}+\mathcal{F}_{t-c})$			
$\to$	$\rho^-a_1^+$	$V_{ud}V_{ub}^*$	$(\mathcal{A}+\mathcal{C}'+\mathcal{E}_{u-c}+\mathcal{E}'_{u-c}+\mathcal{F}_{u-c})$	$+V_{td}V_{tb}^*$	$(\mathcal{E}_{t-c}+\mathcal{E}'_{t-c}+\mathcal{F}_{t-c})$		3.4×10^{-3}	
$\to$	$\rho^oa_1^o$	$V_{ud}V_{ub}^*\frac{1}{2}$	$(-\mathcal{B}'-\mathcal{B}+\mathcal{C}+\mathcal{E}_{u-c}+\mathcal{E}'_{u-c}+\mathcal{F}_{u-c})$	$+V_{td}V_{tb}^*\frac{1}{2}$	$(\mathcal{E}_{t-c}+\mathcal{E}'_{t-c}+\mathcal{F}_{t-c})$		2.4×10^{-3}	
$\to$	ωa_1^o	$V_{ud}V_{ub}^*\frac{1}{2}$	$(-\mathcal{B}'+\mathcal{B}+\mathcal{C}-\mathcal{E}_{u-c}-\mathcal{E}'_{u-c})$	$+V_{td}V_{tb}^*\frac{1}{2}$	$(-\mathcal{E}_{t-c}-\mathcal{E}'_{t-c})$			
$B_u^+ \to$	$\rho^oa_1^+$	$V_{ud}V_{ub}^*\frac{1}{\sqrt{2}}$	$(\mathcal{A}+\mathcal{B}+\mathcal{E}_{u-c}-\mathcal{E}'_{u-c})$	$+V_{td}V_{tb}^*\frac{1}{\sqrt{2}}$	$(\mathcal{E}_{t-c}-\mathcal{E}'_{t-c})$		6.0×10^{-4}	5.4×10^{-4}
$\to$	$\rho^+a_1^o$	$V_{ud}V_{ub}^*\frac{1}{\sqrt{2}}$	$(\mathcal{A}+\mathcal{B}+\mathcal{E}_{u-c})$	$+V_{td}V_{tb}^*\frac{1}{\sqrt{2}}$	$(\mathcal{E}_{t-c})$			
$\to$	ωa_1^+	$V_{ud}V_{ub}^*\frac{1}{\sqrt{2}}$	$(\mathcal{A}+\mathcal{B}+2\mathcal{D}+\mathcal{E}_{u-c}+\mathcal{E}'_{u-c})$	$+V_{td}V_{tb}^*\frac{1}{\sqrt{2}}$	$(\mathcal{E}_{t-c}+\mathcal{E}'_{t-c})$			
$\to$	$K^{*o}a_1^+$	$V_{us}V_{ub}^*$	$(\mathcal{D}+\mathcal{E}_{u-c})$	$+V_{ts}V_{tb}^*$	$(\mathcal{E}_{t-c})$			
$\to$	$K^{*+}a_1^o$	$V_{us}V_{ub}^*\frac{1}{\sqrt{2}}$	$(\mathcal{A}+\mathcal{B}+\mathcal{D}+\mathcal{E}_{u-c})$	$+V_{ts}V_{tb}^*\frac{1}{\sqrt{2}}$	$(\mathcal{E}_{t-c})$			

TABLE VII

Reaction	Amplitude				$(Br)_{theory}$	exp. limits from ARGUS	exp. limits from CLEO
$B_d^\circ \to a_1^\circ a_1^\circ$	$V_{ud}V_{ub}^* \frac{1}{2}$	$(-\mathcal{B}+\mathcal{C}+\mathcal{E}_{u-c}+\mathcal{F}_{u-c})$	$+V_{td}V_{tb}^* \frac{1}{2}$	$(\mathcal{E}_{t-c}+\mathcal{F}_{t-c})$			
$\to a_1^+ a_1^-$	$V_{ud}V_{ub}^*$	$(\mathcal{A}+\mathcal{C}+\mathcal{E}_{u-c}+\mathcal{F}_{u-c})$	$+V_{td}V_{tb}^*$	$(\mathcal{E}_{t-c}+\mathcal{F}_{t-c})$		6.0×10^{-3}	3.2×10^{-3}
$B_u^+ \to a_1^\circ a_1^+$	$V_{ud}V_{ub}^* \frac{1}{\sqrt{2}}$	$(\mathcal{A}+\mathcal{B})$					

I. Supergravity Theories

I.a. $\underline{D = 4}$: It has been shown that light–like integrability conditions for $n \geq 5, 6, 7, 8$ lead to conformal supergravity equations of motion.[85–7]

I.b. $\underline{D = 4}$: Linear systems have been constructed from all ($n = 1, ..., 8$) the light–like integrability conditions.[88–23] These linear systems help to solve the light–like constraints and thus equation of motion for $n = 5, 6, 7, 8$; and helps to solve the light–like constraints for $n = 1, 2, 3, 4$ for off–shell formulation.

I.c. $\underline{D = 10, n = 1}$: It has been shown that light–like integrability constraints lead to equations (Poincare) of motion only if an additional algebraic constraint is imposed.[87–8] Thus the light–like integrability constraints can allow an off–shell formulation of the theory.

I.d. $\underline{D = 10, n = 1}$: Linear systems and conservation laws can be constructed for the light–like integrability conditions,[89–3] and thus useful for the off–shell formulation of the $D = 10, n = 1$ supergravity theory. In the construction of the linear systems and conservation laws, it is essential to use the bi–spinor representation for the light–like vectors.

II. Supersymmetric Yang–Mills Theories

In addition to the similar developments[84–4] as mentioned in section I for $D = 4$, supergravity theories, our recent new addition is the construction of linear systems, and an infinite number of nonlocal conservation laws using the bi–spinor representation[87–6] for any light–like vector in $D = 6$ and 10. These will be certainly useful for constructing new solutions in $D = 6$ and 10, and then in $D = 4$ by dimensional reduction.

III. Progress Made For The $D = 4$, Self–Dual Yang–Mills Equation

III.a. Permutability property has been shown to be true for the Chau–Prasad–Sinha Bäcklund transformations (BT).[85–6,86–3]

III.b. The sequence, Parametric BT $\rightarrow$ Riccati $\rightarrow$ linear systems, has been constructed for the self–dual Yang–Mills equations.[86–4]

III.c. A generalized Bäcklund transformation, which is capable of generating instanton solutions has been constructed for the (supersymmetric) self–dual Yang–Mills equations.[89–2]

IV. The $D = 2$ Theories

IV.a. The Ernst equations which are reduced non–linear systems of static and axially symmetric Einstein, or Yang–Mills equations: linear systems, infinite–nonlocal conservation laws, finite Riemann–Hilbert transforms, and infinitesimal RH transform $\Rightarrow$ Kac–Moody algebra; Bäcklund transformations, etc. have been thoroughly discussed.[85–4]

IV.b. All the integrability properties as listed in IV.a. have been constructed for the super–chiral equations with Wess–Zumino term.[86–2]

IV.c. A general gauge covariant formulation, as well as all the integrability properties have been constructed for general symmetric–space chiral fields.[84–2]

IV.d. Using the special Riemann-problem technique of Zakharov et al., an explicit N-step Bäcklund transformation for a certain class of 2-d nonlinear evolution equations was derived and thus provided an alternative explicit expression of their N-soliton solutions.[90–5]

V. General Integrability Discussions

V.a. A unifying derivation of BT has been given from the point of view of finite Riemann–Hilbert transformation.

V.b. A general discussion of Kac–Moody algebra has been made from the point of view of infinitesimal Riemann–Hilbert transformation.[89–1]

Now we are ready to move forward in two fronts: first, finding solutions to the full Yang–Mills equations. The essential new feature in the search for classical solutions for the full Yang–Mills and supergravity equations is the use of superspace, and to develop two–complex–variable Riemann–Hilbert transforms, contrasting to the one–complex–variable Riemann–Hilbert transform used in two–dimensional systems and the self–dual Yang–Mills systems. And second, quantizing the super–Yang–Mills and supergravity fields from these new points of view.[87–20]

VI. Approach to Quantization

To approach quantum field theory from this geometrical–integrability point of view, the following work has been done:

VI. 1. We have studied the light–cone Hamiltonian formalism of the nonabelian chiral model with Wess–Zumino term in arbitrary coupling constant. The monodromy matrices and their bracket structure are derived explicitly and discussed.[90–4]

VI. 2. From an action for the self–dual Yang–Mills (SDYM) system, we have constructed a higher dimensional version of the Kac–Moody–Virasoro algebra which appears as the symmetry of this system. We have also constructed a SDYM hierarchy with using these algebras.[90–7]

VI. 3. We have studied a conformally invariant theory which consists of scalar fields on a Riemann surface Σ coupling to a Chern–Simons gauge filed on a three dimensional manifold B with boundary Σ. The presence of gauge fields introduces interesting phase factors given by the line integral of gauge potential in the correlation functions. After quantization to the gauge field, these phase factors are related to the Gauss linking number and the self–linking number for the $U(1)$ case, and the link polynomials for the nonabelian case.[90–6]

89–9 Physics of Doubly Cabbibo Suppressed Charm Decays
Invited talk, the Proceedings of International Tau-Charm Workshop,
May 23-27, Stanford
Ling-Lie Chau

89–10 CP Noninvariance in Charm Decays
Invited talk, the Proceedings of International Tau-Charm Workshop,
May 23-27, Stanford.
Ling-Lie Chau

89–11 Physics From Nonleptonic Charm Decays
Invited talk at and to appear in the Proceedings of the Workshop
on Weak Interactions and CP Violation
Institute of High Energy Physics, Beijing, China, Aug. 22-26, 1989
Ling-Lie Chau

89–12 Decay Amplitude CP Noninvariance: A Charm Possibility
Invited talk at and to appear in the Proceedings of the Workshop
on Weak Interactions and CP Violation
Institute of High Energy Physics, Beijing, China, Aug. 22-26, 1989
Ling-Lie Chau

89–13 Geometrical Integrability Properties of Gravitational
and Other Classical Field Theories in Physics
Invited talk at and to appear in the Proceedings of the Third Hungarian
Relativity Workshop, Budapest, Sept. 4-9, 1989
Ling-Lie Chau

89–14 In Search of CP Noninvariance in Heavy Quark Systems
In a book "CP Violation", publisher World Scientific, ed. by C. Jarlskog
Ling-Lie Chau

90–1 On the Non-Resonant Three-Body Decays of Charmed Meson
To appear in Phys. Rev.
Ling-Lie Chau, and H.Y. Cheng

90–2 Predictions for the Quark-Mixing Doubly Suppressed Decays of Charmed Mesons
to appear in Phys. Rev.
Ling-Lie Chau, and Hai-Yang Cheng

90–3 Ways to Measure the Hairpin Diagrams in Charmed Meson Decays
Submitted to Phys. Rev.
Ling-Lie Chau, H.Y. Cheng, and Tao Huang

90–4 Quantization of Chiral Model with Wess-Zumino term in the light-cone coordinate
Submitted to Phys. Rev.
Ling-Lie Chau and Itaru Yamanaka

90–5 An Alternative Explicit Construction of N-Soliton Solutions in Two Dimensions
Submitted to Jour. Math. Phys.
Ling-Lie Chau, J.C. Shaw and H.C. Yen

90–6 Chern-Simons Gauged Conformal Field Theories
Submitted to Phys. Rev.
Ling-Lie Chau and Yue Yu

90–7 A Virasoro Algebra in Self-Dual Yang-Mills System
Submitted to Phys. Rev.
Ling-Lie Chau and Itaru Yamanaka

90–8 Charmless Nonleptonic Rare Decays of B Mesons
Submitted to Phys. Rev.
Ling-Lie Chau, H.-Y. Cheng, W.K. Sze, H. Yao and B. Tseng.

90–9 Field Theory from Integrable-System Point of View
25th Int. Conf. on High Energy Physics,Singapore, August 2-8, 1990
Ling-Lie Chau

90–10 The Integrable-System Connection.
ibid.

90–11 Rare Nonleptonic Decays of Charm and Beauty Mesons
ibid.

In Preparation

I–1 Geometrical Integrability Nonlinear Systems in Physics—A Unified View
Physics Report in preparation
Chau, Ling-Lie

I–2 The Quest for CP Noninvariance
To be submitted to Comments on Nuclear and Particle Physics
Chau, Ling-Lie

I–3 I have been invited by the Cambridge University Press to write two books on the following two separate subjects: a) Weak Interaction; b) Integrability Properties of Nonlinear and Gauge Theories in Physics.

Proceedings

P–1 NATO Advanced Workshop, ARW;
XVIIIth International Conference on Differential Geometric Methods Methods in Theoretical Physics; **PHYSICS AND GEOMETRY**
Ling-Lie Chau and Werner Nahm, Editors
in preparation

P–2 NATO Advanced Study Institute, ASI;
The Fifth Annual UC Summer School on Nonlinear Science;
PHYSICS AND GEOMETRY
Ling-Lie Chau and Werner Nahm, Editors
in print.

a) Constrained systems and BRST-approach

The most powerful method of quantization of constrained systems is based on the use of BRST-operator. In particular, BRST-operator plays an important role in very general Batalin-Fradkin-Vilkovisky (BFV) approach to quantization. It is shown in [7] that the appearance of BRST-operator in the analysis of quantum systems with constraints can be understood very easily within the framework of Lie algebra cohomology. (It is important to note that in this approach BRST-operator arises directly in quantum case and is not connected with quantization of classical system.)

The treatment in [7] is restricted to the case when there is only a finite number of constraints. The case of infinite number of constraints can be analyzed by means of the notion of semi-infinite cohomology groups of Lie algebra (paper in preparation). It is well-known that in general the standard construction of BRST-operator Q gives an operator that does not satisfy $Q^2 = 0$ due to some kind of anomaly. (In other words, the standard construction of semi-infinite cohomology can be applied only under certain conditions. I am planning to analyze the anomalous case in collaboration with A. Voronov). This is important for physical applications (for example, for strings in non-critical dimensions). The analysis can be based on the recent paper by Voronov. Voronov gave a general definition of semi-infinite cohomology groups; it is plausible that this definition can be applied to the anomalous case and gives correct quantum theory.

The analysis given in [7] must be generalized also to the case of reducible constraints. (First consideration of classical system with reducible constraints was given in [56]. Later corresponding BRST-operator was constructed in BFV-approach. I am planning to analyze a quantum system with reducible constraints.)

There are also some important questions concerning BFV-approach to quantization of constrained systems. In this approach the gauge condition can be interpreted as a choice of Lagrangian submanifold in a certain supermanifold with an odd symplectic structure. It is well-known that the physical quantities do not change by the continuous variation gauge condition. I hope to prove that two gauge conditions lead to the same answer if corresponding Lagragian manifolds are connected by Lagrangian cobordism. (One can construct examples

showing that in general the answer depends on the choice of gauge condition).

b) Topological quantum field theories (TQFT)

This branch of QFT attracts great attention especially after Witten's paper [24] in which it is shown that topological invariants arising from Chern-Simons Lagrangian are related with Jones polynomials in Knot theory. (The construction of topological invariants by means of Chern-Simons Lagrangian was proposed earlier in [17], in the same paper I conjectured that these invariants are connected with Jones polynomials. The method permitting to obtain topological invariants from QFT and the first example of TQFT were given long ago in my papers [18] and [19].) Witten has shown that TQFT can be useful not only for mathematics but also for physics [24], [23]. (See also papers by Moore and Seiberg, etc.) I am planning to return to TQFT, in particular, I intend to analyze TQFT connected with the moduli space of superconformal manifolds. Witten's results [23] give a hint that this theory can be useful in the analysis of two-dimensional supergravity coupled with superconformal matter.

c)Transmutation of statistics

In [9], I studied the statistics of skyrmions (particles corresponding to topologically non-trivial fields in non-linear σ-model.) I intend to continue the analysis of this question. I would like to analyze also more general questions connected with transmutation of statistics. These questions are interesting from the general viewpoint, but they are especially important in connection with discovery of anyon superconductivity. To establish the connection with real properties of novel superconductors it is necessary to study more carefully how fractional statistics arises in the quantum theories with elementary particles obeying bose and fermi statistics.

String theory

I intend to continue my work in the string theory (see [8], [10]-[17]). My last results in this field were motivated by the wish to go beyond the framework of perturbation theory [10]. I constructed the extension of super-Mumford form (holomorphic square root from the string measure on the moduli space) to the universal moduli space and expressed it in the terms of superanalog of Sato's τ-function. The universal moduli space contains moduli spaces for all general genuses and therefore in some sense corresponds to all orders of perturbation theory. Recently, very interesting results were obtained for non-critical bosonic strings

(strings in dimension < 1=matter with central charge < 1 coupled with two-dimensional gravity.) These results are much stronger because they give non-perturbative expression of the partition function and correlation functions in terms of τ-functions. I will think about the generalization of these results to the case of non-critical superstrings; one can hope the superanalog of the τ-function construction in [8] will be useful for such a generalization.

The construction of extension of super-Mumford form to the universal moduli space led to discovery of hidden $N = 2$ superconformal symmetry of this form [8]. I am planning the further study of the role of $N = 2$ superconformal symmetry in the standard ($N = 1$) superstring.

Mathematical results obtained in [10] can be used also to anlayze $N = 2$ superstring. It was shown in [25] that $N = 2$ superstring has many very interesting features. The results of [10] permit to calculate the string measure on the moduli space of $N = 2$ superconformal manifolds (paper in preparation).

I studied also the string field theory. In collaboration with A. Sen, I proved that Witten's open string field theory can be generalized to the string in arbitrary conformal background with central charge $c = 26$ [4]. In connection with open string filed theory I considered appropriate 2-dimensional conformal field theories in axiomatic approach and the relation between conformal background, appropriate for open and closed strings. It is possible that I continue this consideration.

In connection with string theory I am planing to study some mathematical questions concerning the so called model spaces. The paper [2] devoted to Virasoro model space can be considered as the first step in this direction.

References

1. Schwarz A. Geometry of fermionic string. Invited lecture on the International Congress of Mathematicians, Proc. of ICM-90, Springer.

2. Schwarz A., HO Seong La, Nelson P. Virasoro model space IASSNS-HEP-90-25, to be published in CMP.

3. Schwarz A. Symplectic, contact and superconformal geometry, membranes and strings, IASSNS-HEP-90-12, lecture on Supermembrane conference, Trieste, 1989.

4. Schwarz A., Sen A., Glueing theorem, star product and integration in open string gield theory in arbitrary background fields IASSNS-HEP-90-5.

5. Schwarz A. Universal moduli space and string theory lecture on Spring School on Superstring. Trieste 1989.

6. Schwarz A. Dolgikh S., and Rosly A. Supermoduli spaces, ICTP preprint IC/89/210, to be published in CMP.

7. Schwarz A. Lefshetz trace formula and BRST, Mod. Phsy. Lett. A4 (1989) 1891-1898.

8. Schwarz A., Dolgikh S., Super Grassmannians, super τ-functions ans strings, V. Knizhnik memorial volume, L. Brink, A. Polyakov (ed.), 1990.

9. Schwarz A., Statistics of skyrmions, Mod. Phys. Lett. A (1989) 403.

10. Schwarz A., Fermionic string and universal moduli space. Nucl. Phys. B317:323-343 (1989).

11. Schwarz A., M. Baranov and I. Frolov. Geometry of superconformal moduli space. Teor. Mat. Fiz. 79:241-252 (1989).

12. Schwarz A., A. Rosly and A. Voronov. Superconformal geometry and string theory. Comm. Math. Phys. 119:129-152 (1988).

13. Schwarz A., M. Baranov, and I. Frolov. Geometry of two-dimensional superconformal field theories. Teor. Mat. Fiz. 70:92-103 (1987).

14. Schwarz A., S. Dolgikh and A. Rosly. Supermoduli spaces. ICTP preprint IC/89/210, submitted to Nucl. Phys. B.

15. Schwarz A., M. Baranov, Yu. Manin, and I. Frolov. A superanalog of the Selberg trace formula and multiloop contribution for fermionic strings. Comm. Math. Phys. 111:373-392 (1987).

16. Schwarz A., M. Baranov, Yu. Manin, I. Frolov. Multiloop contributions for fermionic string. Yad. Fiz. 43:1053-1058 (1986).

17. Schwarz A. New topological invariants arising in the theory of quantized fields. Baku International topological conference. Abstracts (Part II), 1987, Baku.

18. Schwarz A. Partition function of degenerate quadratic functional and Ray-Singer invariant. Lett. Math. Phys. 2:247-252 (1978).

19. Schwarz A. The partition function of a degenerate functional. Comm. Math. Phys. 67:1-16 (1979).

20. Brezin E., Kazakov V., Exactly solvable field theories of closed strings, ENS preprint (1989).

21. Gross D., Migdal A., Nonperturbative two dimensional quantum gravity, Phys. Rev. Lett. 64 (1990) 127.

22. Douglas M., Shenker S., Strings in less than one dimensin, Rugers preprint RUT-89-34 (1989).

23. Witten E. On the topological phase of two dimensional gravity IASSNS-HEP-89-66.

24. Witten E., Quantum field theory and the Jones Polynomial in Braid groups, Knot Theory and Statistical Mechanics, C. N. Yang, M.-L. Ge (ed) 1989.

25. Ooguri H., Vafa C. Self-duality and $N = 2$ String Magic HUTP-90/A024.